INVESTIGATING THE PHYSIOLOGICAL AND FUNCTIONAL ROLES OF THE NICOTINAMIDE RIBOSIDE KINASE PATHWAY IN SKELETAL MUSCLE

by

DAVID MICHAEL CARTWRIGHT

A thesis submitted to The University of Birmingham

for the degree of

DOCTOR OF PHILOSOPHY

Institute of Metabolism and Systems Research

College of Medical and Dental Sciences

University of Birmingham

June 2020

Abstract

Skeletal muscle is a major site of energy metabolism and critical to metabolic health. Bioavailability of the redox coenzyme nicotinamide adenine dinucleotide (NAD^+) is essential for metabolic function, which is also consumed by NAD^+ dependent signalling enzymes driving metabolic adaptation. Ageing and a sedentary lifestyle is accompanied by metabolic dysregulation partly attributable to a decline in skeletal muscle NAD^+ levels. The functional relevance of NAD^+ salvage from the dietary vitamin B3 precursor nicotinamide riboside (NR) via the rate limiting, muscle specific nicotinamide riboside kinase 2 (NRK2) enzyme is unclear, and could constitute an exploitable pathway for maintaining NAD^+ levels with age. Using a novel in vivo skeletal muscle NRK2 overexpressing (NRK2.Tg) mouse model, this thesis determined that NRK pathway augmentation does not affect development or young metabolic phenotype, with no significant changes to the NAD^+ metabolome or metabolic phenotype in aged animals with or without oral NR supplementation. These data further support evidence that the metabolic contribution of NRK mediated NAD^+ salvage is dispensable in skeletal muscle. However, aged NRK2.Tg quadriceps, gastrocnemius and soleus muscles were significantly enlarged, suggesting resistance to sarcopenia. Aged NRK2.Tg myofibres presented with historic regeneration and perturbed NAD^+ dependent cell-ECM adhesion processes, identifying the importance of localised NAD^+ salvage via NRK2 for in vivo mammalian skeletal muscle remodelling.

Dedication

For my Wife – Vikki,

who endured the best and worst of me and provided endless support throughout.

Acknowledgements

I would like to thank my supervisor Professor Gareth Lavery first and foremost for all of his knowledge, support and encouragement throughout my time as his technician and PhD student. He is a dedicated and excellent scientist who has always had time for me whilst also giving me the space to grow on my own. I would also regard him as a friend who has accommodated my needs and supported me through some very difficult times. His friendly demeanour, humour and approachability provided the narrative for my PhD, and I couldn't have asked for a better supervisor. I would also like to thank Professor David Hodson as my second supervisor, especially for being willing to get his hands dirty again to show me some mouse experimentation techniques!

I am indebted to all past, present and honorary members of the Molecular Metabolism Research Group for making my time with the group so enjoyable (Craig, Rachel, Lucy, Dean, Pete, Antje, Yasir, Silke, Stuart, Ali, Sam, Pete and Olivia). I have loved every minute of being part of the group and always enjoyed work however stressful it got at times. Craig, Rachel, and Lucy were fantastic at showing me the ropes when I was new to the group and providing assistance as I continued to develop, and towards the end I truly couldn't have done without Dean, Pete and Silke thanks to their incredible support. I'd also like to thank Antje for all of her assistance and the fun times we all had in at conferences. I know that Sam, Ali and Olivia will go on to write fantastic PhDs and become amazing scientists. I have had the pleasure to work with extremely capable colleagues and simultaneously made a lot of good friends and memories.

I would also like to thank everybody in the IMSR for their support and guidance, and feel privileged to belong of a group of peers within an institute that continues to grow and excel. I would equally like to thank the staff of the BMSU for all of their invaluable help, especially Diane for so diligently looking after my ageing mice for all these years!

I would also like to thank my parents for a lifetime of love and encouragement, and allowing me to make my own choices (whether good or bad)! My Mum sparked and encouraged my interest in science and the natural world, and my Dad gave me the work ethic required to undertake something as arduous and intimidating as a PhD. He saw me embark on this journey though was unfortunately unable to see me complete it. I love and miss him terribly but I know he would be proud of what I have achieved already.

Finally, I would like to thank my beautiful wife Vikki for her love and support throughout the entire experience. I started my PhD with a girlfriend and I have finished it with a wife and an extended family that I love very much, and I could not be happier. Her intelligence and thoughtfulness has gotten me through each and every day whether good or bad, and thinking about her makes my determination to succeed stronger than ever.

Table of Contents

Table of Figures

Table of Tables

Abbreviations

µl	Microlitre
µM	Micromole
µm	Micrometre
4EBP1	Eukaryotic translation initiation factor 4E-binding protein 1
ACAA	Acetyl-CoA acyltransferase
ACAC	Acetyl-CoA carboxylase
ACACB	Acetyl-CoA carboxylase 2
ACADM	Acyl-CoA dehydrogenase medium chain
ACADSB	Short/branched chain acyl-CoA dehydrogenase
AchR	Acetylcholine receptor
ACLY	ATP citrate lyase
ACMS	Amino-3-carboxymuconate semialdehyde
ACOT	Acyl-CoA thioesterase
ACS	Acetyl-CoA synthetase
ACSL	Long chain fatty acid CoA ligase
ACT	Actin
ACTA1	Actin alpha 1, skeletal muscle
ACTBL	Beta-actin like protein
ACTC	Alpha-actin cardiac muscle
ACVR2	Activin type II receptor
ADP	Adenosine diphosphate
ADPr	ADP ribose
AE	Acute Exercise
AFM	Arylformidase
AJ	Adhesive junction
AK	Adenosine kinase
AKT	Protein kinase B
AMP	Adenosine monophosphate
AMPK	AMP-activated protein kinase
ANCOVA	Analysis of covariance
ANOVA	Analysis of variance

ANXA	Annexin
APS	Ammonium Persulfate
AR	Androgen receptor
ARF	ADP-ribosylation factor
ARL	ADP-ribosylation factor like GTPase
ART	ADP-ribosyl transferase
ATP	Adenosine triphosphate
AUC	Area under curve
BCAA	Branched chain amino acid
bFGF	Basic fibroblast factor
BIOPS	Mitochondrial biopsy preservation solution
BMAL	Brain and muscle ARNT-like
bp	Base pair
BSA	Bovine serum albumin
BW	Body weight
Ca^{2+}	Calcium ion
CACT	Carnitine:acylcarnitine translocase
cADPR	Cyclic ADP ribose
CaMK	Ca^{2+}/calmodulin-dependent protein kinase
cAMP	Cyclic adenosine monophosphate
CAPZ	F-actin-capping protein
CAV	Caveolin
CC	Caloric consumption
CD	Cluster of differentiation
CDF	Common data format
cDNA	Complimentary DNA
CELSR	EGF LAG seven pass G-type receptor
Cl^-	Chloride ion
CLOCK	Circadian locomotor output cycles kaput
CMAC	Cell matrix adhesion complex
CO_2	Carbon dioxide
CoA	Coenzyme A
COL	Collagen

complex I	NADH dehydrogenase
complex II	Succinate dehydrogenase
complex III	Cytochrome c reductase
complex IV	Cytochrome c oxidase
CPT	carnitine palmitoyltransferase
CSA	Cross-sectional area
CSRP	Cysteine and glycine-rich protein
cT	Cycle threshold value
DAB	3,3'-Diaminobenzidine
ddH_2O	Double distilled water
DDIT	DNA damage inducible transcript
DEXA	Dual energy x-ray absorptiometer
DIA	Data independent acquisition
DLK1	Protein delta homolog 1
DMD	Duchenne muscular dystrophy/dystrophin
DNA	Deoxyribonucleic acid
dNTP	Deoxynucleotide triphosphate
dpc	Days post coitum
dpf	Days post fertilisation
dsDNA	Double stranded DNA
DTT	Dithiothreitol
DYNCH	Cytoplasmic dynein heavy chain
DYNLL	Dynein light chain LC8-type
ECL	Electrochemiluminescence
EDL	Extensor digitalis longus
ECM	Extracellular matrix
EDTA	Ethylenediaminetetraacetic acid
EE	Energy expenditure
EEF	Eukaryotic elongation factor
EGF	Epidermal growth factor
EGTA	Ethylene glycol-bis(ß-aminoethyl ether)-N,N,N',N'-tetraacetic acid
EI	Electron ionisation
eIF	Eukaryotic translation initiation factor

eNAMPT	Extracellular NAMPT
ENT	Equillibrative nucleoside transporters
ER	Endoplasmic reticulum
ERK	Extracellular signal-regulated kinase
ESI	Electrospray ionisation
ETC	Electron transport chain
EtOH	Ethanol
ETS	Electron transfer state
FABPpm	Plasma membrane fatty acid binding protein
FAD	Flavin adenine dinucleotide
$FADH_2$	Flavin adenine dinucleotide + 2 Hydrogen
FAK	Focal adhesion kinase
FAM	6-carboxy-fluorsciein
FAO	Fatty acid oxidation
FATP	Fatty acid transport protein
FCCP	Carbonyl cyanide-4-(trifluoromethoxy)phenylhydrazone
FFPE	Formalin fixed paraffin embedding
FMOD	Fibromodulin
FOX	Forkhead box
FRET	Fluorescence resonance energy transfer
FWHM	Full width at half maximum
g	Gram
G3P	Glyceraldehyde-3-phosphate
G3PD	Glucose-3-phosphate dehydrogenase
GCMS	Gas chromatography mass spectrometry
GDP	Guanosine diphosphate
GF	Growth factor
Gln	Glutamine
Glu	Glutamate
GLUT	Glucose transporter type
GO	Gene ontology
GPI	Glycosyl-phosphatidyl-inositol
GTP	Guanosine triphosphate

GUSB	Glucuronidase beta
h	Hour
H_2O_2	Hydrogen peroxide
H6PDH	Hexose-6-phosphate dehydrogenase
HACD	Very-long-chain (3R)-3-hydroxyacyl-CoA dehydratase
HAO	3-hydroxyanthranilate 3,4 dioxygenase
HAT	Histone acetyltransferase
HCl	Hydrochloric acid
HDAC	Histone deacetylase
HDL	High density lipoprotein
HFD	High fat diet
HGF	Hepatocyte growth factor
HIF1A	Hypoxia-inducible factor 1 alpha
HINT	Histidine triad nucleotide binding
HMDB	Human Metabolome Database
HPLC	High performance liquid chromatography
HRP	Horseradish peroxidase
HRR	High resolution respirometry
HSP	Heat shock protein
HUWE	HECT, UBA and WWE domain containing E3 ubiquitin protein ligase
ICaL	L-type calcium channel
ICaT	T-type calcium channel
IDA	Information dependent acquisition
IDO	Indoleamine 2,3-dioxygenase
IGF	Insulin growth factor
IGFR	Insulin growth factor receptor
IGTGB	Integrin beta
IL	Interleukin
IMS	Intra-membrane space
IMS	Industrial methylated spirits
IP	Intraperitoneal
IP_3	Inositol trisphoshate
IPGTT	Intraperitoneal glucose tolerance test

IR	Insulin receptor
IRS	Insulin receptor substrate
ITGA	Integrin alpha
IV	Intravenous
kDa	Kilodalton
KEGG	Kyoto Encyclopedia of Genes and Genomes
Kg	Kilogram
Km	Michaelis constant
KMO	Kynurenine 3-monooxygenase
KO	Knockout
KRT	Keratin
KYU	Kynureninase
l	Litre
LAMA	Laminin alpha
LBM	Lean body mass
LCEH	Long-chain enoyl-CoA hydratase
LCHAD	Long-chain (S)-3-hydroxyacyl-CoA dehydrogenase
LCKAT	Long-chain 3-ketoacyl-CoA thiolase
LCMS	Liquid chromatography mass spectrometry
LDL	Low density lipoprotein
LogFC	Log fold change
M	Mole
m/z	Mass -to-charge ratio
MAPK	Mitogen-activated protein kinase
MCAD	Medium-chain acyl-CoA dehydrogenase
MCKAT	Medium-chain 3-ketoacyl-CoA thiolase
MECH	Mechanoreceptor
MEK	Mitogen-Activated protein kinase kinase
MeNAM	N-methylnicotinamide
MES	2-(N – morpholino)ethanesulfonic acid
mg	Milligram
Mg^{2+}	Magnesium ion
MIBP	Muscle-specific integrin β1 binding protein

min	Minute
mL	Millilitre
mM	Millimole
MOPS	3-(N-morpholino)propanesulfonic acid/sodium acetate/sodium dehydrate
MPC	Mitochondrial pyruvate carrier
MRF	Myogenic regulatory factor
mRNA	Messenger ribonucleic acid
MRPL	Mitochondrial ribosomal protein L
MS	Mass spectrometry
MSTN	Myostatin
MTBSTFA	N-tertbutyldimethylsilyl-N-methyltrifluoroacetamide
MTJ	Myotendinous junction
mTOR	Mammalian target of rapamycin
mTORC	Mammalian target of rapamycin complex
MTP	Mitochondrial trifunctional protein
MuRF	Muscle RING-finger protein
MSDC	Muscle derived stem cell
MYC	Myocilin
MYF	Myogenic factor
MyHC	Myosin heavy chain
MyLC	Myosin light chain
MYOD	Myoblast determination protein
MYOG	Myogenin
MYOT	Myotilin
NA	Nicotinic acid
Na_3VO_4	Sodium orthovanadate
NAAD	Nicotinic acid adenine dinucleotide
NaCl	Sodium chloride
NAD^+	Nicotinamide adenine dinucleotide
NADH	Nicotinamide adenine dinucleotide hydride
NADK	NAD Kinase
$NADP^+$	Nicotinamide adenine dinucleotide phosphate
NADPH	Nicotinamide adenine dinucleotide phosphate hydride

NADSYN	Nicotinamide adenine dinucleotide synthetase
NaF	Sodium fluoride
NAFLD	Non alcoholic fatty liver disease
NAM	Nicotinamide
NAMN	Nicotinic acid mononucleotide
NAMPT	Nicotinamide phosphribosyltransferase
NaOH	Sodium hydroxide
NAPRT	NA phosphoribosyltransferase
NAR	Nicotinic acid riboside
NCAM	Neural cell adhesion molecule
Nfix	Nuclear factor 1 X-type
NFW	Nuclease free water
ng	Nanogram
nm	Nanometre
nmol	Nanomole
NMJ	Neuromuscular junction
NMN	Nicotinamide mononucleotide
NMNAT	Nicotinamide mononucleotide adenylyltransferase
NNMT	Nicotinamide N-methyltransferase
NNT	Nicotinamide nucleotide transhydrogenase
NR	Nicotinamide riboside
NRAP	Nebulin-related anchoring protein
NRF	Nuclear respiratory factors
NRH	1-[(2R,3R,4S,5R)-3,4-Dihydroxy-5-(hydroxymethyl)tetrahydrofuran-2-yl]-4H-pyridine-3-carboxamide
NRK	Nicotinamide riboside kinase
Nrk2b	Nicotinamide riboside kinase 2b
NuGEMP	Nuclear genes encoding mitochondrial proteins
O_2	Oxygen
O2K	OROBOROS Oxygraph-2k
OAADPr	O-acetyl-ADP-ribose
°C	Degree Celsius
OGG1	8-oxoguanine-DNA glycosylase 1

Opa	Mitochondrial dynamin like GTPase
p70S6K	Ribosomal protein S6 kinase
PARP	Poly-ADP ribose polymerase
PAX	Paired box
PBEF	Pre-B cell colony enhancing factor
PBMC	Peripheral blood monocyte
PBS	Phosphate buffered saline
PBS-T	Phosphate buffered saline-tween
PCR	Polymerase chain reaction
PDH	Pyruvate dehydrogenase
PDK	Phosphoinositide-dependent kinase
PFN	Profilin
PFTBA	Perfluorotributylamine
PGC	Peroxisome proliferator-activated receptor gamma co-activator
Pi	Phosphate group
PI3K	Phosphoinositide 3-kinase
PIP_3	Phosphatidylinositol (3,4,5)-trisphosphate
PKA	Protein kinase A
PLEC	Plectin
pmol	Picomole
POLR2A	RNA polymerase II
PPAR	Peroxisome proliferator-activated receptor
PPI	Pyrophosphate
PQP	Peptide query parameters
PRPP	5'-phosphoribosyl-1-pyrophosphate
PSMA	Proteasome subunit alpha
PSMB	Proteasome subunit beta
PSMC	Proteasome subunit gamma
PSMD	Proteasome subunit delta
PVDF	Polyvinylidene difluoride
PXN	Paxillin
QA	Quinolinic acid
QAPRT	Quinolinic acid phosphoribosyltransferase

qPCR	Quantitative realtime polymerase chain reaction
RAF	Rapidly accelerated fibrosarcoma
RAPTOR	Regulatory associated protein of mammalian target of rapamycin
RAS	Ras GTPase
RER	Respiratory exchange ratio
RIPA	Radioimmunoprecipitation assay
RNA	Ribonucleic acid
ROS	Reactive oxygen species
ROX	Residual oxygen consumption
RPL	Large ribosomal 60s subunit
rpm	Revolutions per minute
RPS	Small 40s ribosomal subunit
rpS6	Ribosomal protein S6
R-SMAD	Receptor mothers against decapentaplegic homolog
RT	Room temperature
RYR	Ryanodine receptor
s	Second
S6K1	Ribosomal protein S6 kinase 1
SCAD	Short-chain acyl-CoA dehydrogenase
SCHAD	Short-chain (S)-3-hydroxyacyl-CoA dehydrogenase
SDS	Sodium dodecyl sulfate
SEM	Standard error of the mean
Ser	Serine
SIRT	Sirtuin
SMAD	Mothers against decapentaplegic homolog
SNS	Somatic nervous system
SOD	Superoxide dismutase
SR	Sacroplasmic Reticulum
ssDNA	Single stranded DNA
SWATH-MS	Sequential window acquisition of all theoretical mass spectra
TA	Tibialis anterior
TAK	Transforming growth factor beta activated kinase
TAMRA	6-carboxylate-tetramethyl-rhodamine

TBDMSCl	Tertbutyldimethyl-chlorosilane
TBE	Tris-Borate EDTA
TBS-T	Tris buffered saline-tween
TCA	Tricarboxylic acid
TDO	Tryptophan 2,3-dioxygenase
TEMED	Tetramethylethylenediamine
TF	Transcription factor
TGFβ	Transforming growth factor beta
Thr	Threonine
TMOD	Tropomodulin
TNF	Tumour necrosis factor
TOFMS	Time-of-flight mass spectrometry
TRIM	Tripartate motif containing
TSC	Tuberous sclerosis complex
TβR	Transforming growth factor beta receptor
UBC	Ubiquitin-conjugating enzyme E2
UBE	Ubiquitin conjugating enzyme
UCK	Uridine/cytidine kinase
UPR	Unfolded protein response
V	Volt
VCAM	Vascular cell adhesion protein
VCO_2	Volume of carbon dioxide produced
VLCAD	Very long chain acyl-CoA dehydrogenase
VO_2	Volume of oxygen consumed
w/v	Weight/volume
WAT	White adipose tissue
WT	Wild type
x g	Times gravity
XIC	Extracted ion chromatogram
ZEB	Zinc finger E-box binding homeobox
ZT	Zeitgeber

CHAPTER 1 – INTRODUCTION

Due to recent healthcare advances, the global population is becoming increasingly aged (1). However, the rate of increase in human lifespan has not been matched by improvements to healthspan, significantly increasing pressure on healthcare services worldwide (2, 3). Skeletal muscle mass and function is progressively lost with age and disuse, significantly affecting healthspan due to its central importance to locomotion and overall metabolic health (4, 5). The clinical manifestation of skeletal muscle loss, termed sarcopenia, affects over 50 million people worldwide and is predicted to rise to 200 million over the next 40 years (6, 7). Sarcopenia is anticipated by perturbations to energy metabolism including reduced insulin sensitivity and mitochondrial health (8), and closely correlates with further chronic disease states including type II diabetes, osteoporosis and metabolic syndrome (9, 10). Improved knowledge of the molecular mechanisms responsible for aged skeletal muscle decline is therefore of paramount importance for establishing combative strategies.

The importance of the redox cofactor and metabolic signalling cosubstrate nicotinamide adenine dinucleotide (NAD^+) to skeletal muscle health has recently been described (11), the levels of which decline with age (12). Skeletal muscle NAD^+ repletion mechanisms may therefore constitute key therapeutic targets, but are not yet fully defined (13). Skeletal muscle NAD^+ is primarily salvaged through the vitamin B3 precursor nicotinamide (NAM), though enzymes which process the more recently discovered precursor nicotinamide riboside (NR) (14) are also active (15), including the skeletal muscle specific nicotinamide riboside kinase 2 (NRK2). Interest in this pathway has increased over recent years (13, 15-17), but the specific roles of NRK2 in skeletal muscle remain poorly defined. This thesis therefore aims to further elucidate the metabolic relevance of the NRK/NR salvage pathway with age through a novel NRK2 skeletal muscle exclusive overexpressing

mouse model, alongside any potential muscle specific cellular roles of the NRK2 enzyme itself.

This introduction will provide a general overview of skeletal muscle embryogenesis, structure and function alongside oxidative metabolism and the role of NAD^+ as a redox cofactor and metabolic signalling substrate. The importance of skeletal muscle to metabolic health will also be discussed in the context of ageing and NAD^+, with a thorough review of cellular NAD^+ salvage pathways and repletion strategies. Finally, current knowledge surrounding the nicotinamide riboside/nicotinamide riboside kinase (NR/NRK) pathway in skeletal muscle will be explored along with the specific roles of NRK2 in skeletal muscle, outlining the foundations of the specific aims of this thesis.

1.1 Skeletal muscle structure and function

Skeletal muscle is a contractile tissue that is essential for locomotion and metabolic homeostasis (18). It is the largest organ in the body, accounting for 40% of the total body mass of a healthy adult and 50-75% of all body proteins. Skeletal muscle is highly vascularised and innervated, and the maintenance of healthy skeletal muscle is essential for preserving systemic homeostasis and overall healthspan (18, 19).

1.1.1 Skeletal muscle structure

The mammalian body possesses three types of muscle – smooth muscle which forms organs such as the bladder and stomach and involuntarily contracts to facilitate organ function, cardiac muscle that contracts the heart enabling it to pump blood, and skeletal muscle which mediates voluntary movement and is mainly located proximally with bones (20). Skeletal

muscle is rigidly organised at both macro and microscopic level, and characterised by long, multinucleated cylindrical cells termed myofibres (18). Myofibres are coated in connective tissue, termed the endomysium, and held together in bundles, termed fascicles, by a further layer of connective tissue called the perimysium. An outer layer of connective tissue bundles the fascicles together to form the whole muscle (18) (Figure 1-1).

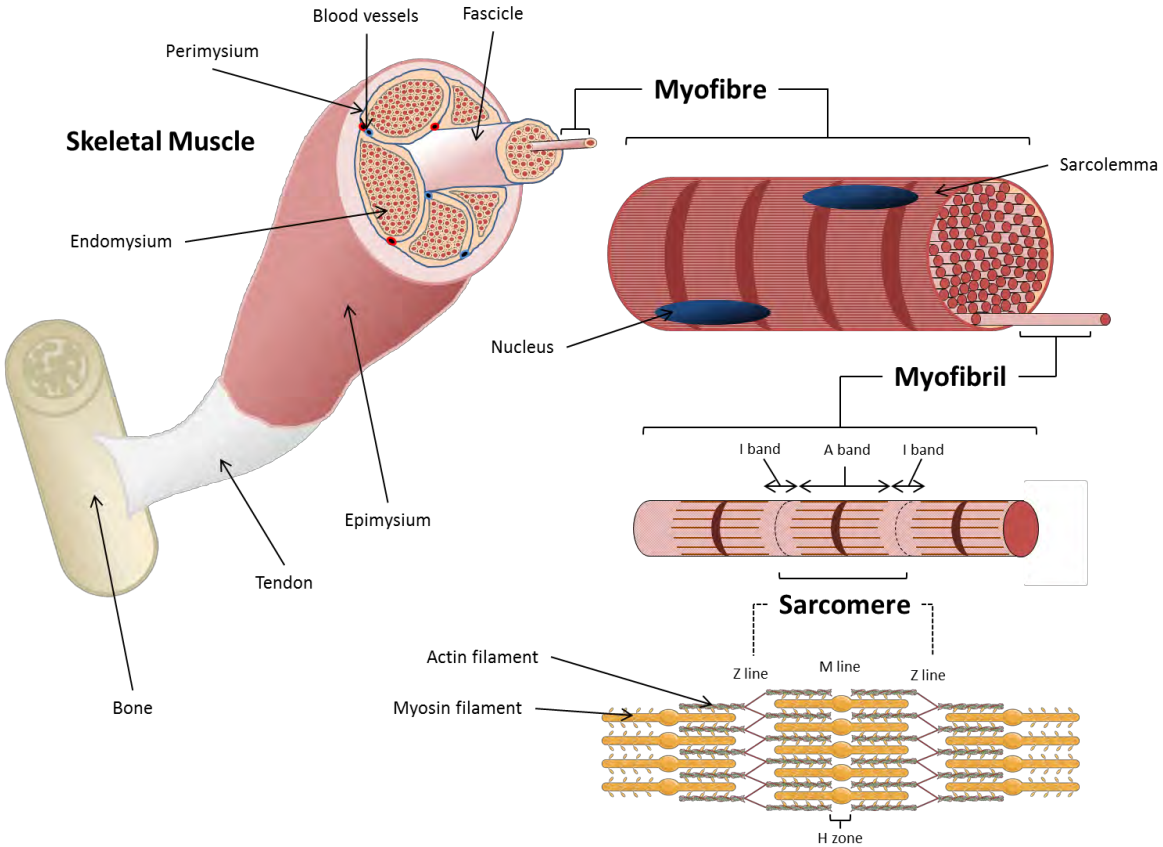

Figure 1-1 – Simplified overview of skeletal muscle macroscopic, microscopic and molecular contractile structure. Skeletal muscle structure is rigidly organised from macroscopic to molecular level and reflects its contractile function. The sarcolemma and sarcoplasmic reticulum (SR) are not depicted.

The microscopic structure of myofibres reveals their contractile function, being composed of filamentous myofibrils that are 1-2 µm in diameter and extend throughout the fibre (18). Individual myofibrils are surrounded by the sarcoplasmic reticulum (SR), an extensive membrane bound calcium ion (Ca^{2+}) storage organelle essential for skeletal muscle

contraction and signalling processes (21). Myofibrils are further subdivided by their appearance into thin and thick fibres, which differ in their composition of filamentous contractile proteins of which actin and myosin are the most important. Thin fibres are comprised mainly of actin filaments with other important proteins such as troponin, tropomyosin and titin, while thick fibres contain mainly myosin. Thick and thin filaments are orientated in parallel against each other within myofibrils forming the sarcomere, which bestows the characteristic striated appearance and is the essential basic unit for skeletal muscle contractility (18) (Figure 1-1). Sections that are rich in thick fibres are termed the A bands with thin filament rich areas termed I bands, and the Z lines in which thin filaments are bound to mark the boundary between individual sarcomere units (18) (Figure 1-1).

1.1.2 Contraction of skeletal muscle

The musculoskeletal system is essential for locomotion, posture, stability and movement of the chest wall for physiological respiration, all of which rely on skeletal muscle contraction. Voluntary contraction is coordinated by the somatic nervous system (SNS), whereby a process termed excitation-contraction coupling is induced through motor neuron signalling. An action potential is initiated, triggering a signalling cascade releasing Ca^{2+} ions from the peri-myofibrillar SR into the sarcoplasm which interact with the Ca^{2+} sensor troponin C (22). This removes troponin I/tropomyosin inhibition on the actin/myosin interaction by reforming the actin-troponin-tropomyosin complex and exposing the actin active site for interaction with myosin (23). The myosin head binds to actin in its high energy adenosine diphosphate (ADP) and phosphate group (Pi) bound state, forming a cross bridge between the thick and thin filaments. ADP + Pi then dissociates from myosin inducing a

conformational change, causing the myosin head to pivot and pull the actin filament towards the M line (22, 24). Adenosine triphosphate (ATP) then binds to the myosin head causing it to detach, before the ATP is hydrolysed to ADP + Pi "cocking" the head and preparing it for binding to the actin active site if available. This process repeats itself as more ATP attaches and is hydrolysed, shortening the I band and reducing the distance between Z discs and ultimately resulting in contraction of the skeletal muscle. This molecular mechanism, termed the "sliding filament theory", and is highly conserved across the animal kingdom (18) (Figure 1-2).

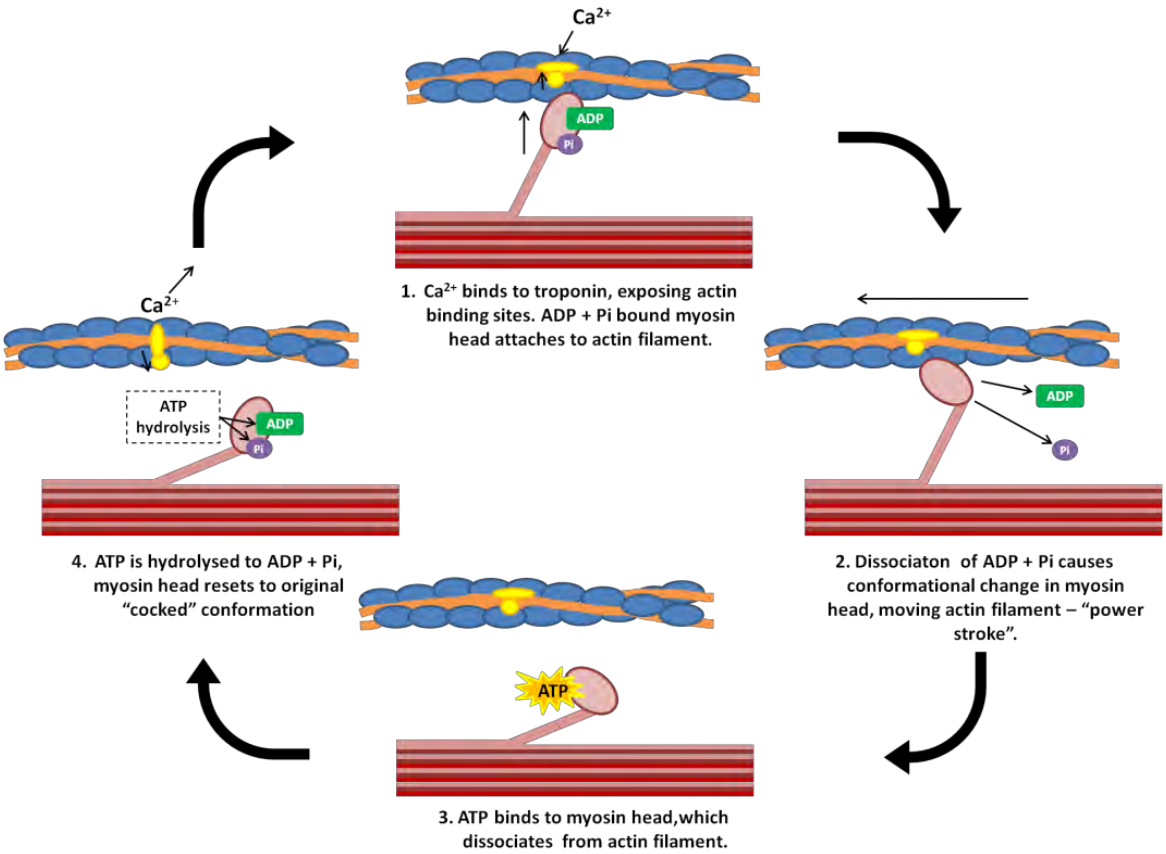

Figure 1-2 – The sliding filament model. The interaction of actin and myosin followed by ATP-dependent conformational change of the myosin "head" results in linear displacement of the actin filament relative to myosin, driving muscular contraction.

1.1.3 Skeletal muscle fibre types

Different skeletal muscle beds are responsible for varying tasks which require differing levels and intensities of activity. To accommodate for this, mammals have three different skeletal muscle fibre type variants which possess different energetic and contractile properties. These include type 1, type 2A and type 2X/B (humans/rodents respectively) fibres which are identified though differential expression of myosin heavy chain isoforms (Table 1-1) (25, 26). Type 1 fibres typically derive energy from oxidative metabolism and are termed slow-twitch fibres, while type 2X/B fast-twitch fibres primarily rely on glycolysis, a faster yet inefficient method of energy generation that does not require oxygen (27). Type 2A fibres are an intermediate of the two and as such are termed fast twitch oxidative fibres (Table 1-1).

Table 1-1 – Relative properties of skeletal muscle subtypes. Information obtained from Zierath and Hawley, 2004 (28) and Schiaffino and Reggiani, 2011 (26).

	Type 1	Type 2A	Type 2X (Humans)	Type 2B (Rodents)
Role	Prolonged, low intensity contractions	Short, high intensity contractions	Very short, very high intensity contractions	Very short, very high intensity contractions
Metabolic energy source and efficiency	Oxidative (aerobic) - high	Oxidative and glycolytic (anaerobic) - moderate	Glycolytic (anaerobic) - low	Glycolytic (anaerobic) - low
Myosin heavy chain isoform	Myh7	Myh2	Myh1	Myh4
Contraction time	Slow (90 – 140 ms)	Moderate (50 – 100 ms)	Fast (40 – 90 ms)	Very fast
Contraction force	Low	Moderate	High	Very high
Endurance	High	Moderate - high	Moderate	Low
Oxidative Capacity	High	Moderate	Low	Low
Mitochondrial Density	High	Moderate	Low	Low
Capillary Density	High	Moderate	Low	Low
Main energy storage molecules	Triglycerides	Glycogen, phosphocreatine, triglycerides	Glycogen, phosphocreatine	Glycogen, phosphocreatine

Slow-twitch fibres have an enriched blood supply, high myoglobin content and an abundance of mitochondria relative to glycolysis dependent fast-twitch fibres. As a result, slow twitch fibres are resistant to fatigue but have a slow contraction time and cannot produce as intense force, while fast twitch fibres quickly generate strong contractile force but fatigue quickly (27). The muscle fibre type compositions of individual skeletal muscle beds are heterogeneous, and reflect the metabolic and contractile demands imposed on

them by their primary function (29). Muscles responsible for high endurance, low intensity activities such as maintaining standing posture are comprised mostly of slow-twitch fibres, while muscles intended for short, explosive bouts of high intensity activity such as sprinting or heavy lifting are composed mostly of fast-twitch fibres (29). The ratio of fast to slow twitch fibres is largely genetically determined, but can also be influenced by external factors such as adaptations to exercise training (27, 30). Endurance training leads to hypertrophy and increased percentage of slow twitch fibres, whilst explosive high intensity training will result in augmentation of fast twitch fibres due to their respective roles in meeting the energy requirements for such activities (30).

1.2 Skeletal muscle development and regeneration

1.2.1 Skeletal muscle myogenesis - paraxial mesoderm differentiation

In mammalian embryos, skeletal muscle develops from the paraxial mesoderm which itself forms early in embryogenesis during the primitive streak/blastopore stage of gastrulation and also late during embryonic axis elongation in the tail bud (31). The anterior region of the nascent paraxial mesoderm then forms somites which then compartmentalise into a dorsal epithelial dermomyotome and undergo further involution to form the myotome (31). Skeletal myogenesis initially requires the commitment of premyogenic mesodermal progenitor cells to myoblasts, followed by terminal differentiation of myoblasts through to myotubes and myofibres. Differential expression of myogenic regulatory factors (MRFs), including muscle commitment and differentiation factors, tightly regulates each step of the procedure. The muscle commitment factors myogenic factor 5 (Myf5) and myoblast

determination protein 1 (MyoD) and paired box transcription factors Pax3 and Pax7 are expressed at the early myoblast stage. Initially, Pax7 is expressed throughout the dorsolateral region of nascent somites, with Pax7 positive cells adapting an ordered distribution within the medial dermomyotome. Some muscle stem/precursor cells then migrate into the myotome and contribute to muscle growth, simultaneously expressing MyoD (32, 33). Spatiotemporal regulation of this process determines muscle fibre formation rates and thus myotome size, with MyoD null zebrafish featuring fewer multinucleate fast fibres and aberrant expansion of $Pax7^{+}$ cells within the dermomyotome (33). The terminal differentiation factors myogenin (MyoG) and Mrf4 are subsequently expressed alongside MyoD, which is thought to have dual roles, as the myoblasts differentiate to myocytes (31, 34). Myocytes then exit the cell cycle and fuse together to form myotubes and eventually myofibres, which can be determined through expression of specialised cytoskeletal proteins including embryonic myosin heavy chain (Myh3),slow myosin heavy chain (Myh7), α-actins including cardiac (Actc1) and skeletal (Acta1), and desmin (31) (Figure 1-3).

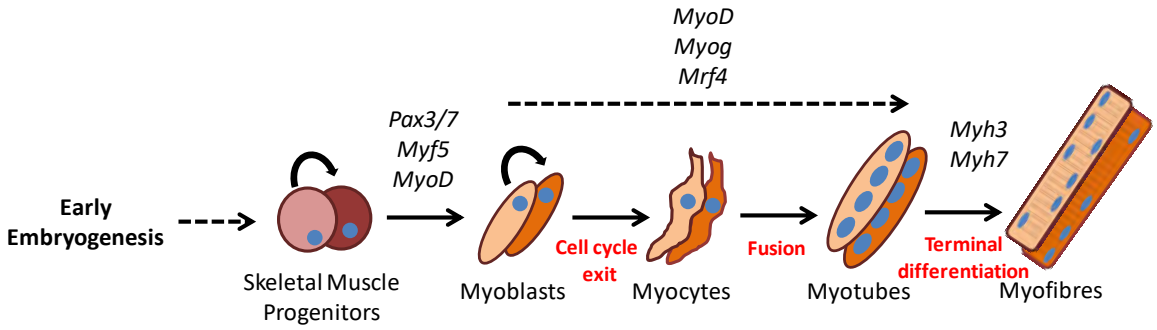

Figure 1-3 – Simplified depiction of embryonic (primary) myogenesis. MRF genes are differentially induced throughout stages of differentiation from embryonic skeletal muscle progenitor cells through to terminally differentiated myofibres. Adapted from Chal et al., 2017 (31).

1.2.2 Skeletal muscle myogenesis – delineation of embryonic and adult muscle

Embryonic myogenesis is divided into primary and secondary phases (Figure 1-4). The primary phase occurs between E10.5-12.5 in mice, and produces primary myofibres derived from $Pax3^+$ dermomyotomal progenitors which express slow MyHC and myosin light chain 1 (Myl1/MyLC1), forming early myotomes and limb muscles which act as templates for adult muscle (31). The second phase of myogenesis occurs between E14.5 and 17.5 and is characterised by a subset of $Pax3^+$ progenitors alternatively expressing Pax7, then fusing with each other or to primary myofibres giving rise to secondary, or foetal, fibres which express specific markers including β-enolase, Myl3 and Nfix (31). These secondary myofibres then begin to diverge in expression of myosin heavy chain isoforms, defining them as fast or slow twitch fibres upon transition to adult muscle (Figure 1-4) (35).

In contrast to embryonic myogenesis, postnatal growth is mostly dependent on myofibre hypertrophy through addition of myofibrils (31, 36). However, Pax7 null mice appear normal at birth but exhibit stunted postnatal development (32, 37). This is because adult skeletal muscle growth and repair is highly dependent on a self renewing population of stem cells, which are initially derived from a subset of $Pax7^+$ progenitors during embryonic myogenesis (31, 36).

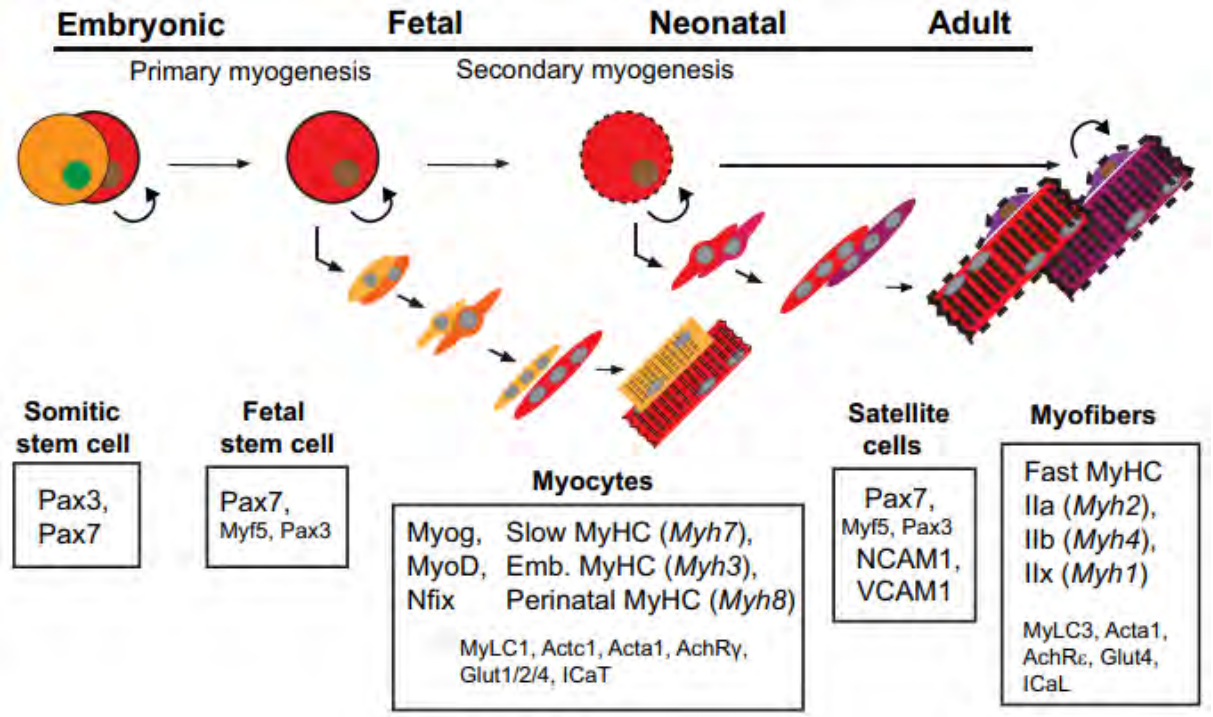

Figure 1-4 – **Primary and secondary myogenesis.** Primary myogenesis forms "template" embryonic muscle tissue from which secondary foetal myofibres are derived. AchR: Acetylcholine receptor; Glut : glucose transporter; ICaL: L-type calcium channel; ICaT: T-type calcium channel; MyLC1: Myosin light chain 1; NCAM: Neural cell adhesion molecule; Nfix: Nuclear factor 1 X-type; VCAM: Vascular cell adhesion protein. Adapted from Chal et al., 2017 (31).

1.2.3 Growth and regeneration of adult skeletal muscle

Adult skeletal muscle has a high regenerative capacity and demonstrates remarkable plasticity in response to damage and dynamic metabolic demands (38). This ability is retained through maintaining a population of adult stem cells, termed satellite cells, derived from Pax3/Pax7 expressing embryonic progenitors (39). In healthy adult muscle, satellite cells reside within a specialised niche between the basal lamina and the sarcolemma of their host myofibre where they are maintained within a quiescent state, as identified through expression of Pax7 (40). In response to growth signals, exercise, skeletal muscle damage or disease, satellite cells become activated and coexpress Pax7 with MyoD, followed by rapid proliferation and generation of sufficient myogenic precursors to fuse to and repair

damaged myofibres and/or produce new myofibres altogether (41). In a similar process to embryonic myogenesis, proliferating and differentiating satellite cells can be identified through downregulation of Pax7, nuclear localisation of MyoD, MyoG, MRF4 and Myf5, and the presence of perinuclear cytoplasmic transcripts of Myf5 (42).

Satellite cells can undergo asymmetric division, where only one daughter cell expresses the myogenic commitment factor Myf5 (43). The Myf5 expressing "satellite myogenic" daughter cell is fated to differentiate, while the non Myf5 expressing "satellite stem" daughter cell repopulates the stem cell niche, ensuring long term preservation of regenerative ability (43). Only a small percentage of satellite cells retain true "stemness", with 10-13% of quiescent satellite cells not expressing Myf5 (43, 44). Pax7 is also critical to the proliferation and survival of these cells, with Pax7 null satellite cells exhibiting 25-30% reduced proliferation and increased rates of apoptosis (45). Pax7 is also an important functional mediator of both the quiescent state and the regenerative process of satellite cells following activation. Quiescent satellite cells exhibit large, heterochromatic nuclei which is disrupted in Pax7 deficient satellite cells, implicating Pax7 as critical for maintaining quiescence (46). Loss of Pax7 also results in impaired regeneration following injury, further highlighting its importance in this process (47-50).

Other skeletal muscle progenitor cells which are genotypically distinct from satellite cells exist which are able to directly contribute to skeletal muscle growth and repair. Microvasculature located cells including mesangioblasts and pericytes are able to promote regeneration through modulation of local immune responses and secretion of trophic factors (51). This modulation of the microenvironment promotes activation of satellite cell mediated regeneration, with some subsets of pericytes also possessing the ability to directly

differentiate into myofibres themselves (51, 52). Furthermore, Twist2 positive stem cells have been recently discovered, which reside outside of the basal lamina and contribute towards the maintenance of type IIB/X myofibres during adult muscle growth and regeneration (53). Sk-34 myoendothelial cells also have myogenic potential, residing within skeletal muscle interstitial space (54). Further distinct non-satellite cell types with skeletal muscle regeneration potential include $PW1^{+}$ interstitial cells, bone marrow stem cells, CD133+ cells, muscle derived stem cells (MDSCs) and $Sca\text{-}1^{+}/ABCG2^{+}$ side population cells, all of which are able to colonise the satellite cell niche and form new myofibres upon transplantation in vivo (43, 55-57).

1.2.4 Satellite cell heterogeneity

$Pax7^{+}$ satellite cells display significant variation. Satellite cells expressing the Pax7 paralog Pax3 are associated with the diaphragm and trunk muscles, yet do not correlate with other factors including embryonic origin or metabolic fibre type (45). Satellite cells also differ greatly in expression of markers including CD34, M-cadherin, neuronal cell adhesion molecule (NCAM), c-Met, protein delta homolog 1 (DLK1) and integrin α7 (43, 58, 59). Interestingly, regeneration potential varies based on muscle bed type, with tibialis anterior (TA) derived satellite cells having diminished regenerative ability relative to extensor digitalis longus (EDL) and soleus (60).

Satellite cells may also differ according to their expressed Pax7 variant. Pax7 has four alternative transcriptional isoforms termed Pax7a, b, c and d, each of which regulate different cohorts of target genes and are differentially expressed across different tissues and stages of development (32). Recent evidence suggests that satellite cells expressing different

combinations of Pax7 isoforms have different roles and behave differently in response to skeletal muscle injury, which is dependent on both developmental stage and the nature and severity of injury (50, 61). The satellite cell pool is broadly divided into two populations; a fast responding regenerative pool and a smaller reserve population which only becomes proliferative under extensive growth or regeneration following severe injury (62). Recent studies utilising zebrafish embryos have further characterised two subsets of satellite cells determined by expression of Pax7a and/or Pax7b isoforms. Interestingly, Pax7a satellite cells preferentially contribute to the production of new myofibres for the repair of extensive single injuries to the myotome over small focal injuries, with a faster proliferative response from Pax7+ cells being noted at 4 days post fertilisation (dpf) compared with those at 7 dpf (50). Further work determined that Pax7a and Pax7b expressing cells constitute distinct lineages with differing localisations within the myotome (61). Satellite cells only expressing Pax7a primarily initiate nascent myofibre formation, while cells expressing both Pax7a and Pax7b preferentially fuse to pre-existing myofibres, contributing more to fibre growth and repair of smaller injuries (61).

1.3 Skeletal muscle and metabolism

1.3.1 Skeletal muscle metabolic pathways

Skeletal muscle is a central site of energy metabolism, accounting for 30% of resting metabolic rate rising up to 90% under conditions of peak physical activity in humans (19, 63). Contraction of skeletal muscle is dependent on free energy released by ATP hydrolysis, which also produces ADP and a Pi moiety (64). Intense and/or prolonged contractions impose major energy burdens on skeletal muscle cells, and ATP consumption can increase up to 1000-fold under acute exercise compared with consumption at rest (64). Reflecting this, skeletal muscle can alter its metabolic rate to a greater extent than any tissue in response to such widely varying energetic demands (65). Skeletal muscle also has extensive glycogen reserves, reflecting its critical role in the maintenance of systemic metabolic homeostasis and locomotion (66, 67). In response to metabolic stressors such as variable food intake, starvation and exercise, skeletal muscle facilitates glucose uptake in times of excess and glycogen breakdown when nutrients are scarce, ensuring that blood glucose levels remain within tight physiological limits (66, 67).

Alongside glycogen, energy is also stored in muscle cells in the forms of phosphocreatine and triglycerides (64). There are several routes of ATP generation available in skeletal muscle which utilise these substrates as fuel, with each varying in efficiency and speed of ATP bioavailability to suit dynamic energetic requirements. The three main systems are the phosphagen pathway, the glycolytic pathway and mitochondrial respiration (64). The phosphagen pathway is a rapid, short-term method of energy generation in which phosphocreatine is metabolised to creatine, simultaneously donating a phosphate group to

ADP to form one molecule of ATP. Upon cessation of contractions, creatine is resposphorylated to phosphocreatine by creatine kinase, which is also an indirect marker of skeletal muscle damage when detected in the blood (68). Phosphocreatine is rapidly depleted, and where contractions are sustained for longer than a few seconds cells must increasingly derive energy from the glycolytic pathway (Figure 1-5). This provides a quick and readily available source of ATP but first requires the breakdown of glycogen into glucose through glycogenolysis (64). A series of enzymatic reactions metabolises glucose to pyruvate, during which two NAD^+ molecules accept electrons and become reduced to nicotinamide adenine dinucleotide + hydrogen (NADH) and two ATP molecules per glucose molecule are produced (64). In anaerobic conditions, NAD^+ eventually becomes depleted and pyruvate is reduced to lactate by NADH being oxidised back to NAD^+ (64).

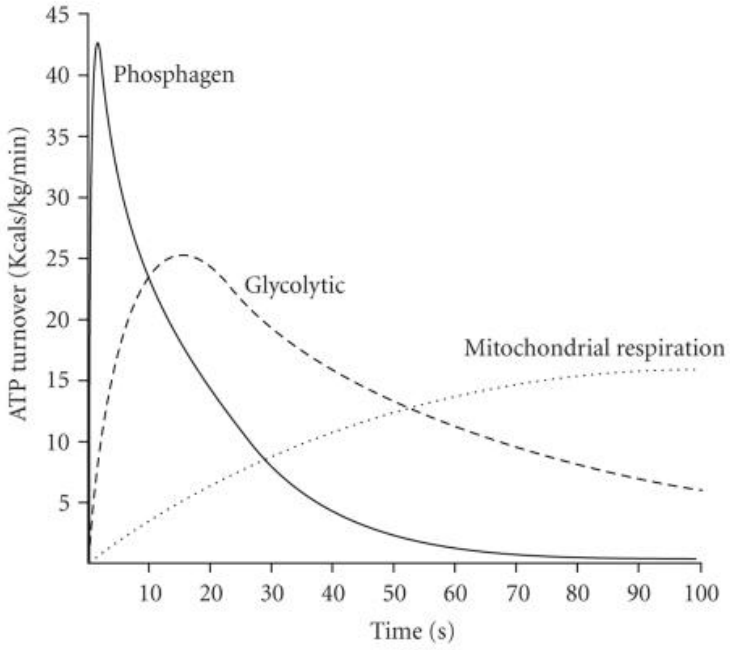

Figure 1-5 – Relative induction times of ATP generating metabolic pathways in skeletal muscle under intense activity. The phosphagen pathway provides an almost instantaneous spike of ATP to supply initial contractions before being rapidly expended. Increased glycogenolysis then promotes induction of anaerobic glycolysis, which provides ATP during aerobic "lag time". Eventually, the aerobic mitochondrial respiration rate climbs to meet the ATP burden with a concomitant decline in glycolytic activity. Figure adapted from Baker et al., 2010 (64).

The phosphagen pathway and anaerobic glycolysis are suitable for short bouts of activity that require fast access to bioavailable ATP, but they are unsustainable and not productive enough for extended periods of contraction as in endurance exercise (64). Furthermore, glycolysis is inefficient, providing only four ATP per molecule of glucose (69, 70). Prolonged contractile activity is therefore reliant on slowly induced but more efficacious oxidative respiration, which can yield between 33-34 ATP molecules per glucose (70) (Figure 1-5). In aerobic conditions, pyruvate enters mitochondria where it is converted to acetyl coenzyme A (CoA). Acetyl CoA then enters the tricarboxylic acid (TCA) cycle and is oxidised. Crucially, the TCA cycle reduces NAD^+ to NADH, providing the necessary reducing power for

oxidative phosphorylation and increased ATP production (69) (Figure 1-6). Alongside pyruvate, acetyl CoA can also be derived from the breakdown of fatty acids (71) (Figure 1-6). Triglycerides are broken down into glycerol and free fatty acids, which react with CoA producing acyl CoA. Acetyl CoA is then produced from acyl CoA through β-oxidation which enters the TCA cycle and fuels oxidative metabolism (69) (Figure 1-6). The ratio of contribution from glucose or fatty acids is tightly regulated in skeletal muscle and largely depends on activity levels and substrate availability (72). The ability of skeletal muscle to quickly upregulate one pathway against the other based on current energetic demands and substrate levels is termed metabolic flexibility, which is a critical aspect of healthy functioning skeletal muscle and whole body metabolism (72, 73).

Muscle proteins can be broken down into amino acids which can then also be converted to pyruvate, acetyl-CoA and/or particular TCA cycle intermediates (74) (Figure 1-6). However, this is typically a last resort when regular skeletal muscle energy stores are depleted, and will lead to muscle atrophy if proteins are broken down faster than they are synthesised (75).

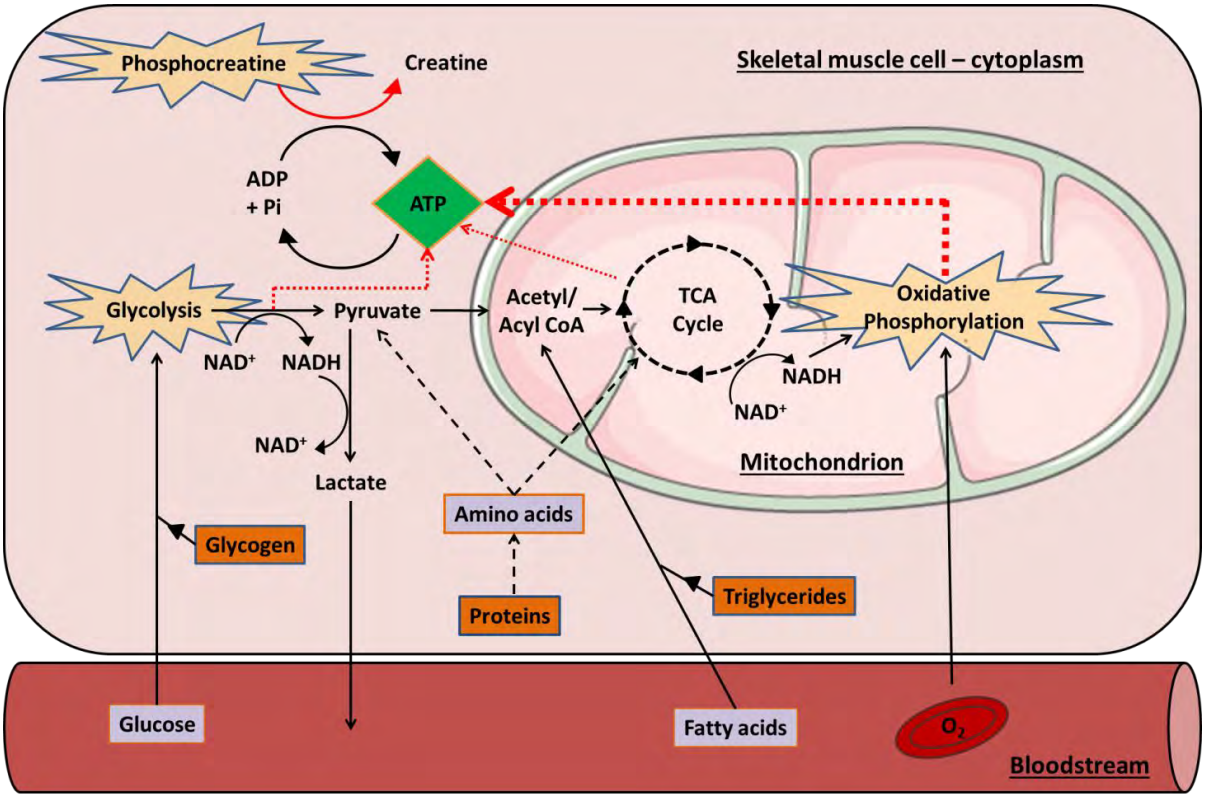

Figure 1-6 – Routes to ATP in skeletal muscle. Phosphocreatine provides rapid and efficacious ATP production but is very quickly depleted. Anaerobic glycolysis is quickly mobilised yet inefficient compared with more slowly induced oxidative phosphorylation. Acetyl (acyl)-CoA can also be produced from fatty acids via β-oxidation as well as from pyruvate generated through glycolysis. Under starvation, skeletal muscle proteins can be broken down for amino acid oxidation.

The ratio of glucose to lipid utilisation is termed the respiratory exchange ratio (RER), which is calculated by dividing O_2 intake (VO2) by CO_2 expulsion (VCO_2) (76). Oxidation of one molecule of glucose requires six molecules of O_2 and yields six molecules of CO_2 giving an RER of 1, which would indicate that glucose is the sole substrate for oxidative metabolism (76). Oxidation of a fatty acid molecule, in this example palmitic acid, consumes 23 O_2 molecules but yields only 16 CO_2 giving an RER of 0.7 indicating that fatty acids are the exclusive fuel. An RER of 0.85 suggests a 50% contribution of both, and relative proportions increase or decrease depending on direction (76). At the onset of exercise, RER initially increases as glucose comprises the predominant fuel, with relative levels of fatty acid

oxidation progressively increasing (77). Triglycerides are the largest and most energy rich fuel source available, and therefore switching to fatty acid oxidation allows for longer periods of sustained physical activity without glycogen depletion and eventual hypoglycaemia (77). High intensity exercise sees less oxidation of fatty acids relative to glucose due to lower fatty acid delivery to contracting muscle, but endurance exercise training results in a further, more efficient shift towards fatty acid oxidation over glucose (77) primarily due to increased utilisation of intramuscular triglyceride stores over non-plasma derived fatty acids (77, 78) (Figure 1-7).

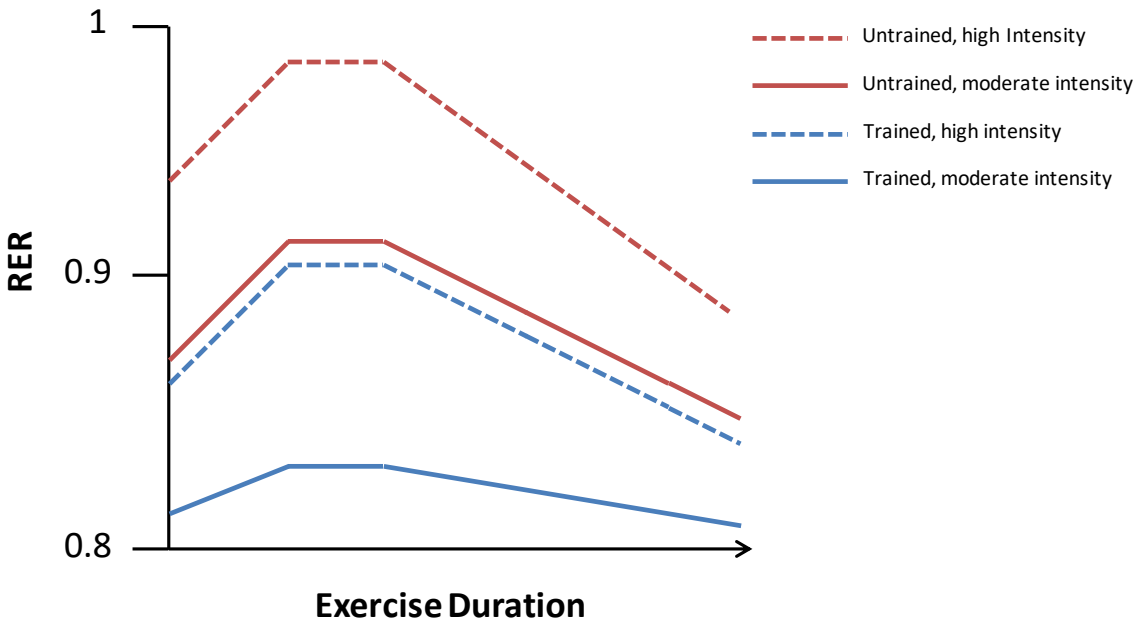

Figure 1-7 – Relative changes in RER with exercise. Exercise onset is marked by an increase in glucose oxidation followed by a gradual switch to fatty acids. High intensity exercise generally utilises a greater proportion of glucose, though endurance trained muscle is able to utilise intramuscular triglyceride stores more efficiently. Adapted from Ramos-Jimenez et al, 2008 (79).

1.3.2 Molecular adaptations of skeletal muscle to exercise

It is well known that regular exercise increases overall health and systemic fitness through improvements in basal metabolic rate, insulin sensitivity, bone density, brain health and

sleep quality as well as reducing adiposity, systemic inflammation and the risk of chronic metabolic diseases such as cardiovascular disease or type II diabetes (80). Furthermore, skeletal muscle demonstrates incredible plasticity and undergoes drastic adaptive remodelling in response to situations that perturb metabolic homeostasis, such as caloric intake, caloric restriction and increased contractility during physical exercise (65, 67). Skeletal muscle contraction is energetically demanding and results in sharp spikes of ATP consumption (64), and thus skeletal muscle must adapt in order to meet these acute energy demands and also endure sustained periods of contraction without debilitating reductions in performance and/or energy availability.

Contraction of skeletal muscle causes intracellular changes that are detected by "sensor" proteins, which in turn modulate a multitude of signalling pathways ultimately resulting in adaptation of metabolic phenotype. During contraction, an increase in cytosolic Ca^{2+} occurs upon release from the SR, which is detected by Ca^{2+}/calmodulin-dependent protein kinases (CaMK) and transduced through the p38 mitogen-activated protein kinase (MAPK)/extracellular signal-regulated kinase (ERK) pathway and the phosphoinositide 3-kinase/mammalian target of rapamycin/protein kinase B (PI3K/mTOR/AKT) pathway (81) (Figure 1-8). An increase in adenosine monophosphate (AMP) and ADP levels as ATP is rapidly hydrolysed is another important "cue" which is detected by the cellular energy status sensor AMP-activated protein kinase (AMPK) (82) (Figure 1-8). Furthermore, physical fibre deformation relative to the extracellular matrix (ECM) is detected and relayed biochemically via the focal adhesion kinase (FAK) mechanotransductor (83) (Figure 1-8). Downstream targets for these signalling pathways include histone acetyltransferases (HATs) and histone deacetylases (HDACs) which modulate chromatin access for transcription and protein

function (84), the transcriptional coactivator peroxisome proliferator-activated receptor gamma coactivator-1-alpha (PGC-1α) which mediates mitochondrial biogenesis (85) and forkhead box O (FOXO)1 and 3 which are critical modulators of metabolism and protein synthesis (86, 87). Additionally, glucose transporter type 4 (GLUT4) is translocated to the plasma membrane during exercise to enhance glucose uptake (88) and drivers of skeletal muscle hypertrophy are induced such as insulin growth factor 1 (IGF1) (89). Such pathways drive increased lipid and carbohydrate mobilisation, vascularisation, improved carbohydrate metabolism, skeletal muscle protein synthesis and augmentation of oxidative phosphorylation and mitochondrial biogenesis, ultimately resulting in skeletal muscle hypertrophy and increased energetic capacity (90).

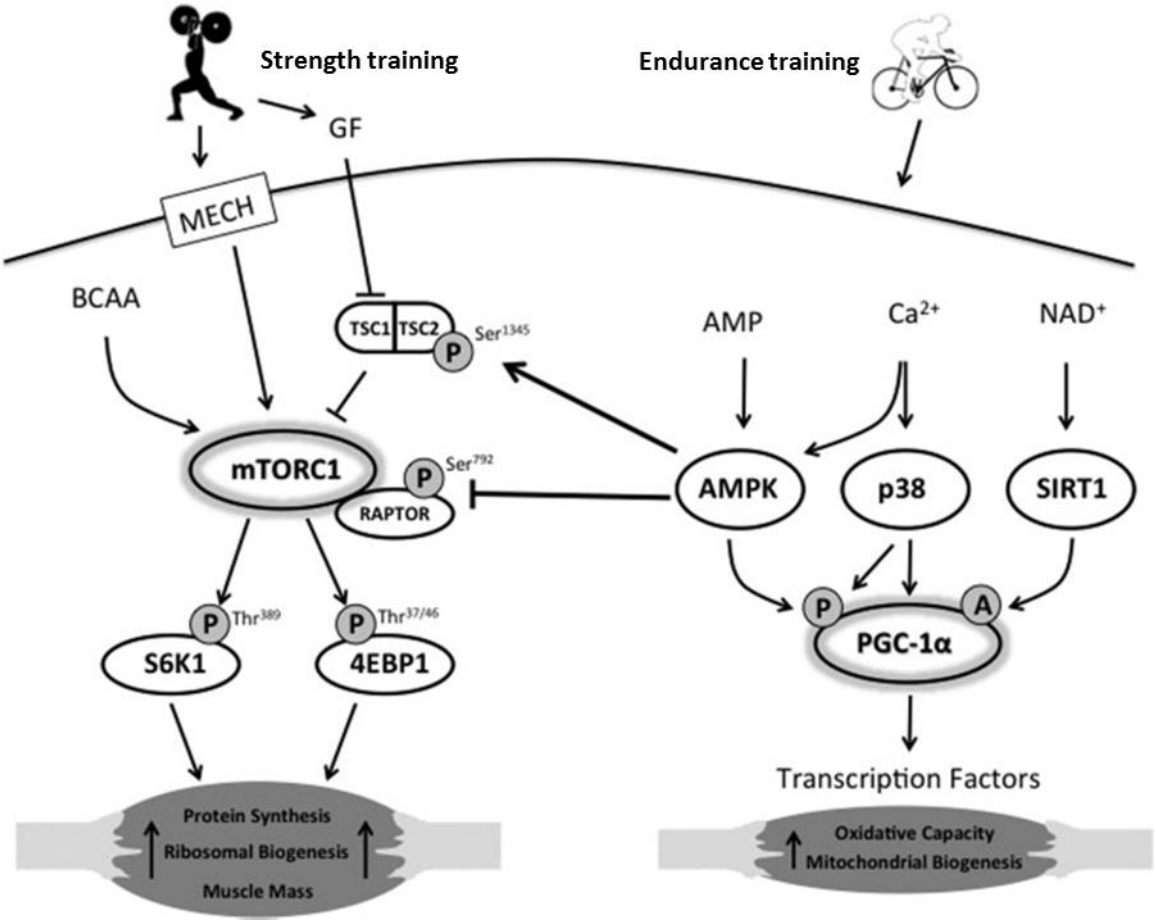

Figure 1-8 – Metabolic signalling pathways in skeletal muscle associated with different forms of exercise training. Short, intense training promotes signalling via the mTOR pathway favouring skeletal muscle hypertrophy and increased strength, while endurance training promotes signalling through PGC-1α increasing oxidative capacity. BCAA: branched chain amino acids; 4EBP1: eukaryotic translation initiation factor 4E-binding protein 1; GF: growth factors; MECH: mechanoreceptor; RAPTOR: regulatory associated protein of mTOR; S6K1: ribosomal protein S6 kinase β1; SIRT: sirtuin, TSC: tuberous sclerosis complex. Adapted from Perez-Schindler et al., 2015 (90).

The nature of metabolic adaptation in skeletal muscle is highly dependent on the type of exercise training it is subjected to (90). Over time, repeated short bouts of intense contractions favour increased muscle mass and myofibrillar protein synthesis, strength and force production, enhanced glycolytic enzyme activity and expanded glycogen and phosphocreatine stores (90). In contrast, prolonged bouts of lower intensity contractions will result in augmented oxidative capacity through increased mitochondrial biogenesis, mitochondrial protein synthesis, improved capacity for fatty acid oxidation, increased

vascularisation and reductions in skeletal muscle fibre diameter, thus favouring endurance over contractile power (90, 91).

1.4 Mitochondria and oxidative metabolism

1.4.1 Mitochondrial origins, structure and function

The mitochondrion arose from the incorporation of α-probacteria into eukaryotic precursor cells approximately two billion years ago (92). Mitochondria still retain features that allude to this ancestry such as a double membrane, multiple circular copies of a separate ~16 kilobase mitochondrial genome and the ability to fuse or divide independently of the host cell (93). Mitochondria are closely tied to many areas of eukaryotic cell function, being critical for phospholipid and haem synthesis, calcium homeostasis and activation of apoptosis (74). Their primary role is that of oxidative metabolism, and mitochondria are therefore critical to skeletal muscle function.

Mitochondria are the principal site of the TCA cycle and oxidative phosphorylation, possessing all of the molecular machinery required for these processes (93). Pyruvate, fatty acids and amino acids can all be converted to acetyl-CoA and oxidised, yielding ATP and the reductive power required for driving oxidative phosphorylation in the form of NADH and flavin adenosine dinucleotide + 2 hydrogen ($FADH_2$) (74) (Figure 1-9). Pyruvate that is generated in the cytosol is imported into mitochondria through transport across the otherwise impermeable inner mitochondrial membrane by mitochondrial pyruvate carriers 1 and 2 (MPC1/2) (94) (Figure 1-9).

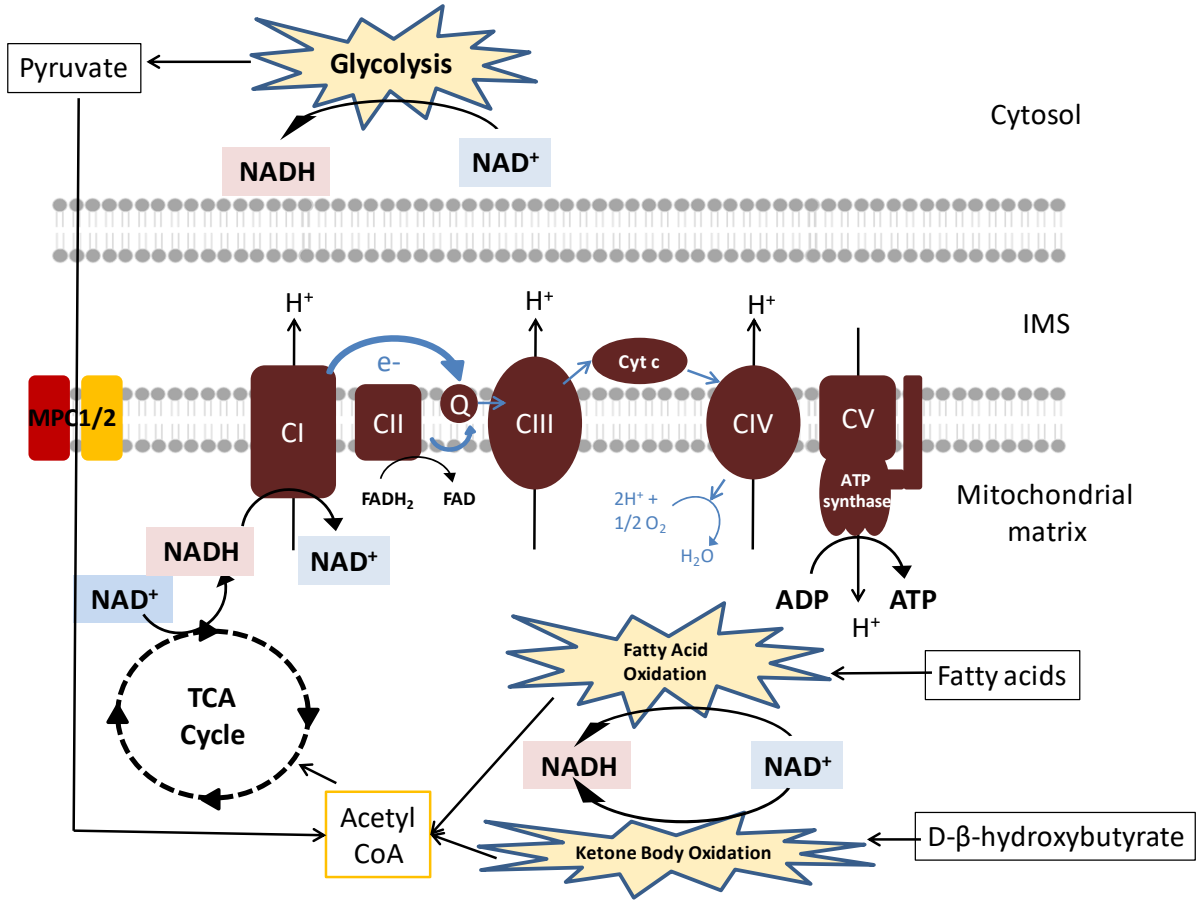

Figure 1-9 – The specific roles of NAD^+ as a redox cofactor in mitochondrial metabolism. NAD^+ is reduced to NADH in the G6P mediated step of glycolysis and also during fatty acid and ketone body oxidation within mitochondria. The resulting NADH then provides energy in the form of electron donation to the ETC, driving oxidative phosphorylation and becoming oxidised back to NAD^+.

The electron transport chain (ETC) is a sequence of large protein complexes that are embedded in the mitochondrial inner membrane (Figure 1-9). Electrons travel through these complexes via carrier molecules with increasing redox potential as the sequence progresses, releasing energy at each stage to drive thermodynamically unfavourable movement of protons from the matrix into the intra-membrane space (IMS) (74) (Figure 1-9). Firstly, complex I (NADH dehydrogenase) accepts electrons from NADH, followed by complex II (succinate dehydrogenase) accepting electrons from $FADH_2$ and complex III (cytochrome c reductase) from oxidation of reduced coenzyme Q, before oxidation of cytochrome c by

complex IV (cytochrome c oxidase) with oxygen comprising the final electron acceptor (74) (Figure 1-9). The resulting increased proton concentration in the IMS creates a potential difference across the inner membrane which ultimately drives synthesis of ATP as protons pass back through the protein channel domain of ATP synthase, causing a conformational change which energetically favours the formation of ATP from bound ADP and Pi (74, 95) (Figure 1-9).

Alternatively to pyruvate, cytosolic long chain fatty acids can be activated by acyl-CoAs to long chain fatty acyl-CoAs, converted to acylcarnitine and transported into mitochondria via the carnitine:acylcarnitine translocase (CACT) antiporter (96, 97) (Figure 1-10). Following this, acylcarnitine is subsequently reconverted to acyl-CoA then acetyl-CoA for β-oxidation (96, 97) (Figure 1-10).

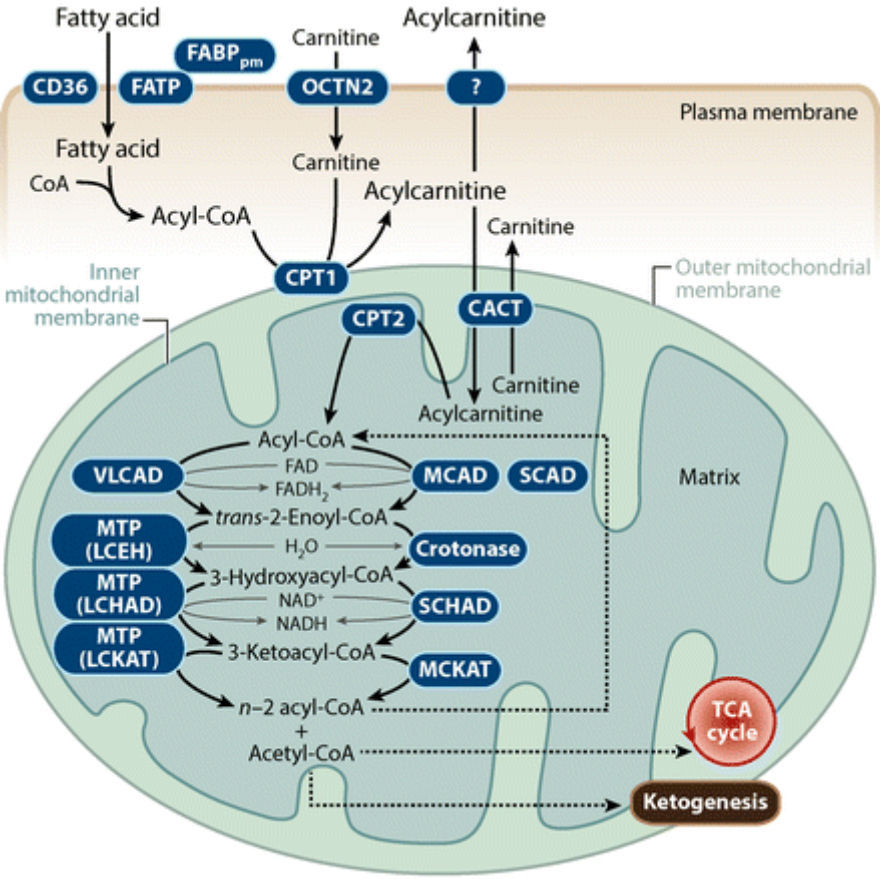

Figure 1-10 – Overview of cellular and mitochondrial fatty acid uptake and mitochondrial β-oxidation, yielding acetyl-CoA from fatty acids. NAD^+ is also reduced to NADH during the conversion of acyl-CoA to acetyl-CoA. CPT1/2, carnitine palmitoyltransferases 1 and 2; FABPpm, plasma membrane fatty acid binding protein; FATP, fatty acid transport protein; LCEH, long-chain enoyl-CoA hydratase; LCHAD, long-chain (S)-3-hydroxyacyl-CoA dehydrogenase; LCKAT, long-chain 3-ketoacyl-CoA thiolase; MCAD, medium-chain acyl-CoA dehydrogenase; MCKAT, medium-chain 3-ketoacyl-CoA thiolase; MTP, mitochondrial trifunctional protein; SCAD, short-chain acyl-CoA dehydrogenase; SCHAD, short-chain (S)-3-hydroxyacyl-CoA dehydrogenase; VLCAD, very long chain acyl-CoA dehydrogenase. Adapted from Houten et al., 2016 (96).

Glucogenic amino acids can also enter mitochondria though amino acid transporters and directly enter the TCA cycle upon degradation to pyruvate or other intermediates (98), or ketogenic amino acids can be degraded yielding acetyl CoA or converted to ketone bodies which can themselves be reconverted back to acetyl CoA (98) (Figure 1-9). The TCA cycle takes place within the mitochondrial matrix and begins with transfer of the two-carbon acetyl group from acetyl-CoA to oxaloacetate to form citrate (74) (Figure 1-11). Citrate is

then oxidised back to oxaloacetate through seven subsequent enzyme catalysed reactions, during which the two excess molecules of carbon are removed (Figure 1-11). Critically, the process liberates free energy as electrons, which is harnessed through reduction of NAD^+ to NADH and flavin adenine dinucleotide (FAD) to $FADH_2$ and utilised by the ETC to drive oxidative phosphorylation (Figure 1-11) (74). NADH is also produced from NAD^+ during the conversion of glyceraldehyde-3-phosphate to D-glycerate 1,3-bisphosphate during glycolysis and during conversion of fatty acids to acetyl-CoA (74, 96) (Figure 1-11).

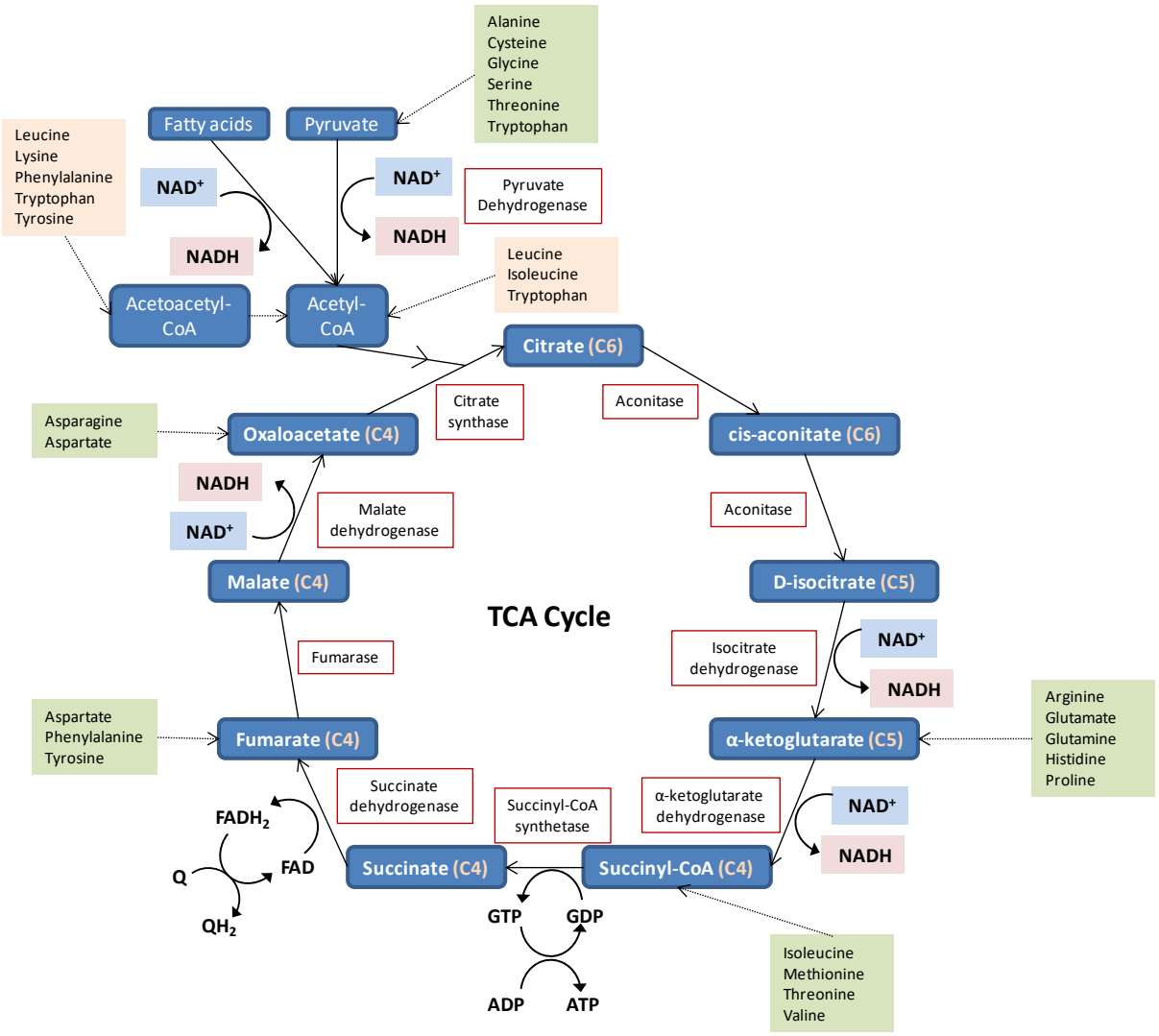

Figure 1-11 – Simplified overview of the TCA cycle illustrating the reactions in which NAD^+ is reduced to NADH, with ketogenic and glucogenic amino acids and their entry points. Intermediate metabolites are represented with blue rectangles alongside their carbon number, while enzymes are represented with red outlined rectangles. Ketogenic amino acids are shaded orange while glucogenic amino acids are shaded green.

1.4.2 Mitochondria and healthy skeletal muscle

Skeletal muscle is reliant on an efficient reticular network of mitochondria to ensure optimal ATP provision for metabolic and contractile demands, and mitochondrial health therefore correlates closely with that of skeletal muscle. The regulation of this network is highly dynamic and finely balanced between degradation and recycling of damaged and dysfunctional mitochondria (mitophagy), mitochondrial biogenesis to replace damaged

mitochondria and expand oxidative capacity where required, and subsequent mitochondrial fission/fusion events (93, 99) (Figure 1-12). As organisms age, mitochondria become increasingly damaged and inefficient through mechanisms such as oxidative stress due to increased reactive oxygen species (ROS) production, increased cellular senescence and dysregulated Ca^{2+} signalling (100). Furthermore, skeletal muscle mitochondrial biogenesis and mitophagy pathways become increasingly dysregulated with age and disuse (101, 102). The net effect is a fragmented and dysfunctional mitochondrial network which in turn leads to an energetic crisis within skeletal muscle, increasing the risk of metabolic dysfunction and disease. As aforementioned, exercise maintains skeletal muscle health by promoting mitochondrial biogenesis through activation of transcription factors such as nuclear respiratory factors (NRF) 1 and 2 via PGC-1α (103). PGC-1α also promotes mitochondrial fusion through upregulation of mitochondrial dynamin like GTPase (Opa)1 and 2, resulting in a more efficient and contiguous mitochondrial network (99).

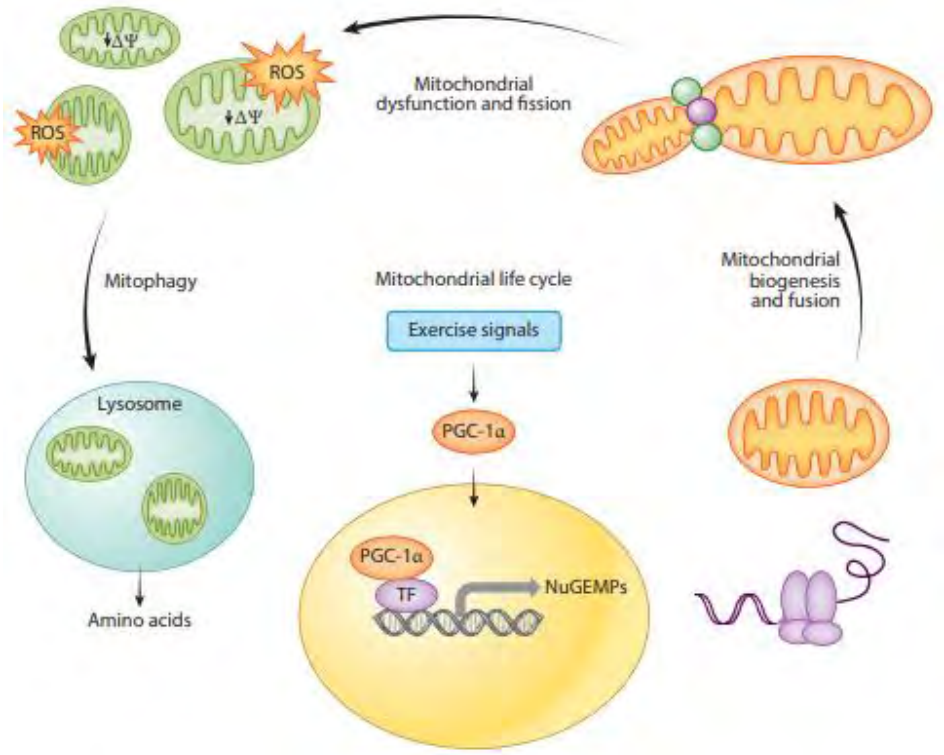

Figure 1-12 – Maintaining a healthy mitochondrial pool. Mitochondrial quality control through mitophagy must be balanced with mitochondrial biogenesis, which is induced via the transcriptional coactivator PGC1-α. TF: transcription factor; NuGEMP: nuclear genes encoding mitochondrial proteins. Adapted from Hood et al., 2019 (99).

Recently, another role of NAD^+ besides hydride transfer was discovered in which it is required for signalling pathways that mediate metabolic adaptation, including driving mitochondrial biogenesis. There is also mounting evidence for NAD^+ deficiency in aged organisms, while regular exercise has been observed to mitigate this (104, 105). NAD^+ therefore constitutes a common factor critical to metabolic health, skeletal muscle health and mitochondrial health, the nature of which appears far more complex than simply energy transfer.

1.5 Nicotinamide adenine dinucleotide

NAD^+ consists of two nucleotides joined by a phosphate group, one of which possesses an adenine nucleobase and the other a nicotinamide group (106) (Figure 1-13). NAD^+ is essential to many aspects of cellular function, with severe NAD^+ deficiency being the primary cause of Pellagra, which manifests as dermatitis, diarrhoea, dementia and eventually death (107). NAD^+ is critical to redox reactions and metabolic signalling processes, the importance of which are discussed in this section alongside the complex mechanisms by which cellular NAD^+ is generated and maintained.

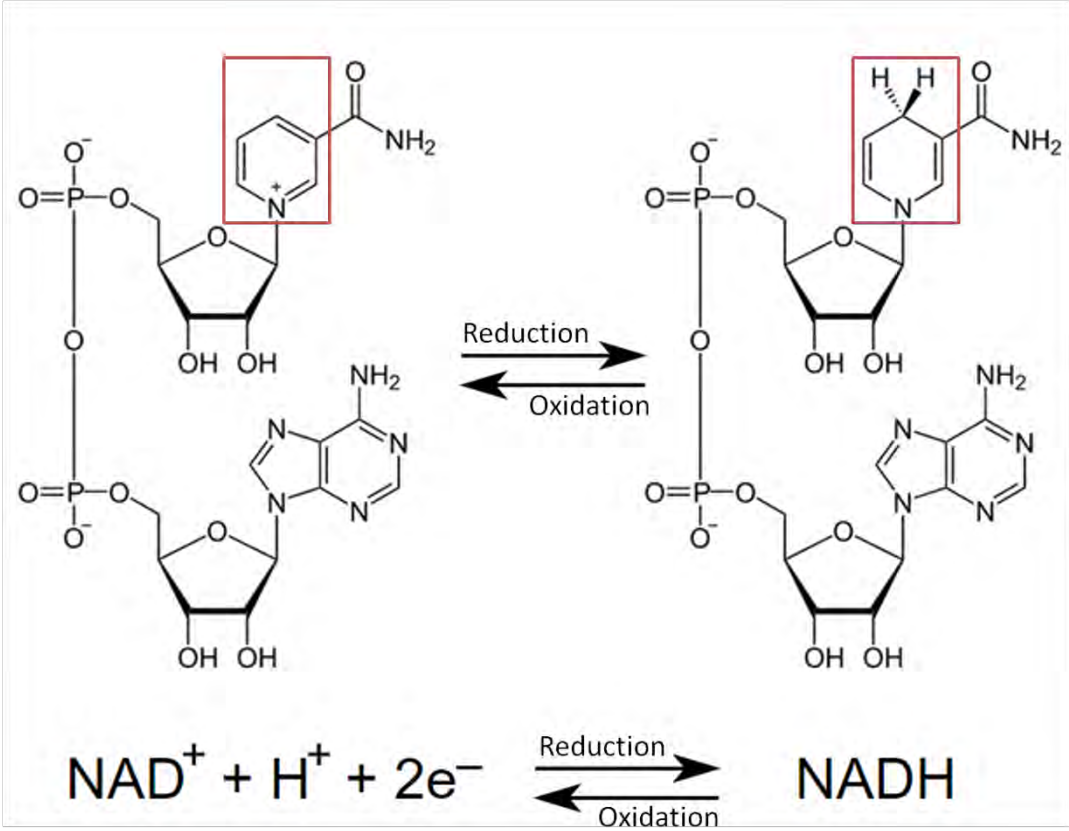

Figure 1-13 – NAD$^+$ as a redox cofactor. NAD$^+$ and NADH are critical for metabolic transhydrogenase reactions. During oxidising reactions, NAD$^+$ accepts electrons from molecules, becoming reduced to NADH. Conversely, NADH is a reducing agent and donates electrons to target molecules.

1.5.1 NAD$^+$ as a redox cofactor

The concept of the requirement of a co-factor for metabolic reactions was first unwittingly discovered by Sir Arthur Harden and William John Young, observing that boiled and filtered yeast extract enabled rapid fermentation in unboiled yeast (108). This “coenzymase” was later purified by Hans von Euler-Chelpin in 1929 (109) then described as NAD$^+$ and identified as a hydrogen transfer molecule by Otto Warburg (110, 111). NAD$^+$ is now well described in this role as the crucial hydride transfer coenzyme for oxioreductase and transhydrogenase reactions (Figure 1-13) (112).

NAD^+ exists in oxidised (NAD^+) and reduced (NADH) forms, with the reaction between the two states reversible (106) (Figure 1-13). Reductive metabolic reactions result in the removal of two hydrogen atoms and two electrons from a substrate in the form of one hydrogen cation and one hydride ion. The cation is lost while the hydride ion is accepted by NAD^+, reducing it to NADH (106).

1.5.2 $NADP^+$ and NADPH

NAD^+ and NADH also exist in phosphorylated forms ($NADP^+$ and NADPH), generated by transfer of a phosphate group from ATP in a reaction catalysed by NAD kinase (NADK) (113). $NADP^+$ and NADPH are also critical to cellular function, mediating anabolic redox reactions by providing electrons for reductive biosyntheses such as synthesis of fatty acids, proteins synthesis and DNA (113). Cells maintain a high proportion of reduced NADPH relative to $NADP^+$, achieved through various pathways such as the pentose phosphate pathway which regenerates NADPH from $NADP^+$ ultimately producing ribose-5-phosphate for nucleotide synthesis (114) and the mitochondrial nicotinamide nucleotide transhydrogenase (NNT) enzyme which utilises the proton motive force to directly transfer a hydride ion from NADH to $NADP^+$, producing NADPH (115). NADPH is a critical reducing agent for biosynthesis of fatty acids, steroids, certain amino acids and nucleotides/nucleic acids (113). It is also critical for protection against ROS, reducing antioxidants such as glutathione which removes toxic ROS by-products such as hydrogen peroxide (113). Conversely, NADPH also contributes to ROS generation for immune defence systems and signalling through activity of NADPH oxidases, and is also important in liver detoxification, providing reducing power for cytochrome P450 regeneration through cytochrome P450 reductase (113).

1.5.3 NAD^+ as a signalling cofactor

More recently, a secondary role for NAD^+ has emerged in which it plays a vital role in cell signalling. Early studies by Rechsteiner at al. discovered that NAD^+ has a half life of approximately 1 hour in mammalian cells, which is unusually short for a reversible energy transfer molecule (116), and that the stability of NAD^+ was much greater in enucleated cell types. It was further determined that most NAD^+ generated by cells is in fact continually degraded and replaced, with only a small fraction maintaining a stable redox pool (117). It is now well established that NAD^+ also acts as an essential signalling cofactor for various cellular processes, upon which cleavage of the glycoside bond occurs producing nicotinamide (NAM) and an ADP ribose (ADPr) moiety, the latter of which is transferred to acceptor molecules (118). There are three main NAD^+ dependent enzyme families; the sirtuins (SIRTs), the mono- and poly-ADP ribose transferases including the poly-ADP ribose polymerases (PARPs), and the cyclic ADP-ribose synthases (cADPR) cluster of differentiation (CD)38 and 157 (109, 118) which are discussed in section 1.7.

1.6 NAD^+ biosynthesis

NAD^+ dependent cellular signalling processes are estimated to consume 6 - 9 grams of NAD^+ per day in humans, which would result in total NAD^+ depletion within hours (109, 119). Cells therefore require efficient NAD^+ repletion mechanisms to match supply and demand. Exogenous NAD^+ is unable to cross the plasma membrane and therefore cannot replenish cellular NAD^+ levels (120). In mammalian cells, various pathways exist by which NAD^+ can be synthesised de novo or salvaged from metabolically available precursors to NAD^+, ensuring that cellular energetic demands are met and metabolic homeostasis is preserved (Figure

1-14). Mammalian cells exhibit several different routes and molecular precursors to NAD^+, which are of varying importance across different tissues (121, 122) (Figure 1-14). Broadly, NAD^+ biosynthesis pathways can be split into "non-amidated" routes from L-Tryptophan and nicotinic acid (NA), and "amidated" routes from NAM and NR (121). As NAD^+ is critical to metabolism and declines with age, these pathways constitute potential therapeutic targets.

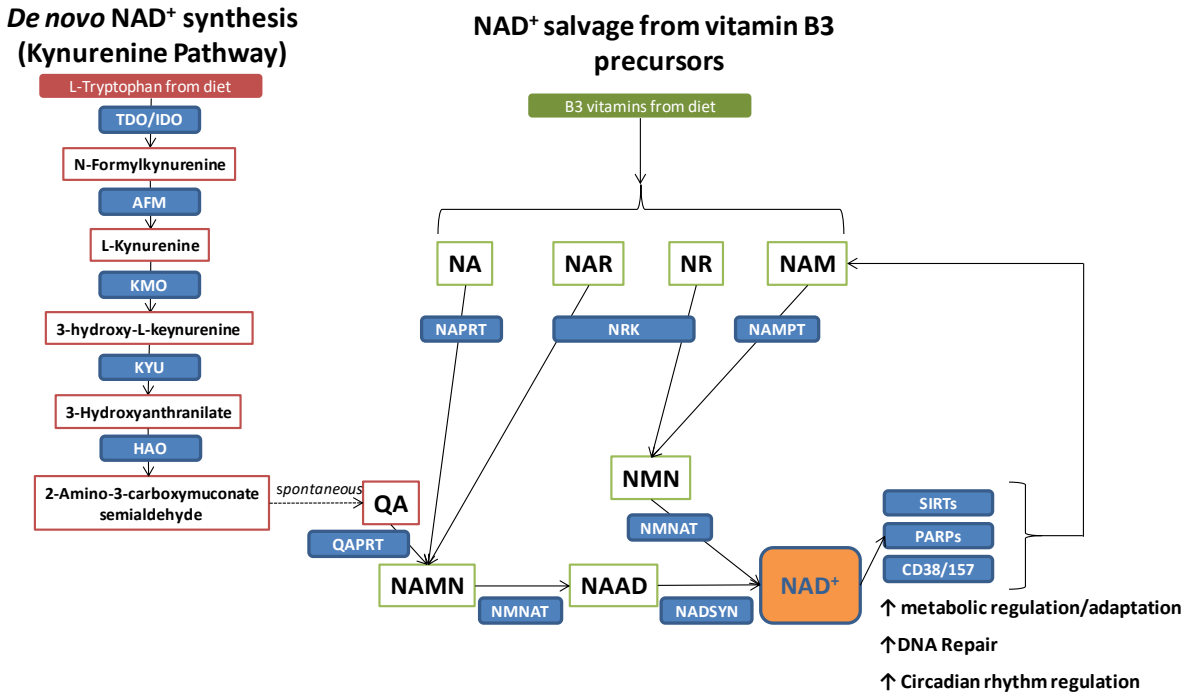

Figure 1-14 – Overview of cellular NAD^+ generating pathways. NAD^+ can be generated de novo from the amino acid L-Tryptophan via the kynurenine pathway, and also generated from the dietary vitamin B3 precursors NA, nicotinic acid riboside (NAR), NR and NAM. AFM: arylformidase; KMO: kynurenine 3-monooxygenase; KYU: kynureninase; HAO: 3-hydroxyanthranilate 3,4 dioxygenase.

1.6.1 De novo biosynthesis of NAD^+

Cells can synthesise NAD^+ de novo from the essential amino acid L-tryptophan in a process termed the kynurenine pathway. Initially, tryptophan is converted to N-formylkynurenine in a reaction catalysed by the rate limiting enzymes indoleamine 2,3-dioxygenase (IDO) or tryptophan 2,3-dioxygenase (TDO) (Figure 1-14). N-formylkynurenine is converted to amino-

3-carboxymuconate semialdehyde (ACMS) in a series of four subsequent reactions, which then undergoes oxidation or spontaneous cyclisation to quinolinic acid (QA). The enzyme QA phosphoribosyltransferase (QAPRT) then converts QA to nicotinic acid mononucleotide (NAMN), which is adenylated to form nicotinic acid adenine dinucleotide (NAAD) by the enzyme nicotinamide mononucleotide adenylyltransferase (NMNAT), before NAAD is finally converted to NAD^+ in an ATP and glutamine dependent amidation reaction catalysed by NAD synthetase (NADSYN) (123, 124) (Figure 1-14).

1.6.2 NAD^+ salvage from vitamin B3 precursors

De novo NAD^+ biosynthesis via the kynurenine pathway occurs in many tissues and is particularly active within the liver (125). However, it is not sufficient to maintain NAD^+ homeostasis alone (123) and QAPRT has been shown to be inessential to the normal development of mice (126), suggesting that most NAD^+ is resynthesised or "salvaged" from chemically similar precursors. These precursor molecules are collectively known as vitamin B3 or niacin and are obtained from the diet (127). These metabolites include NA, NAM and NR, with different pathways responsible for salvaging NAD^+ from each of them. Furthermore, vitamin B3 precursors are much more efficacious in generating NAD^+ with 60 mg of tryptophan required to generate the same amount from just 1 mg of niacin (128) (Figure 1-15). The applicability of these compounds as supplementations to boost cellular NAD^+ is currently of great interest.

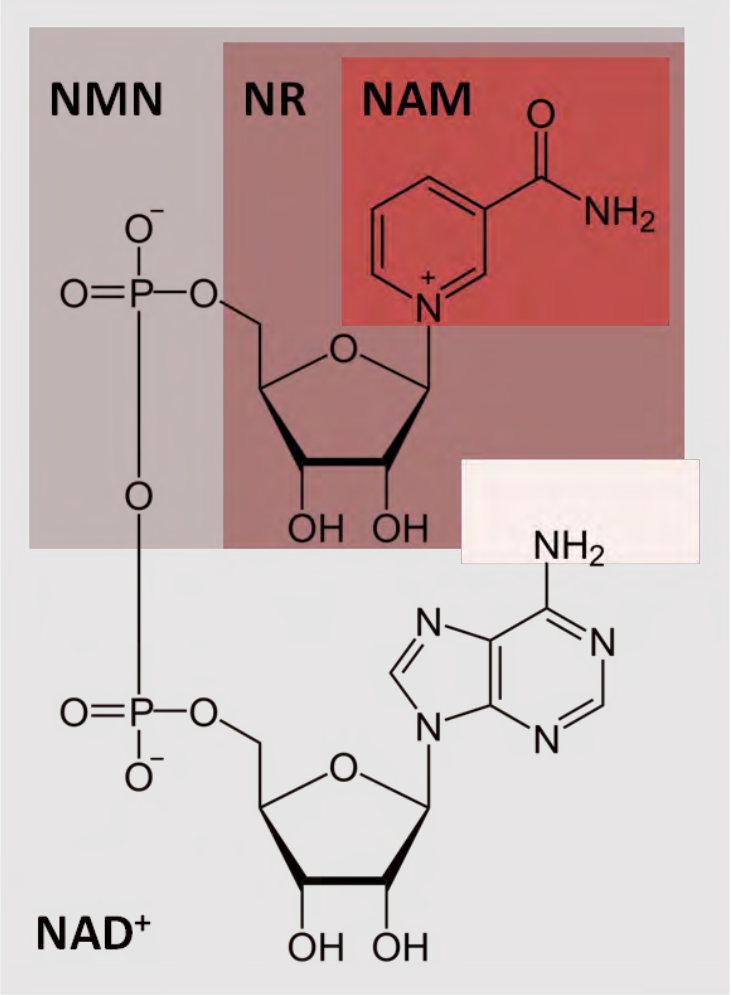

Figure 1-15 – Molecular structure of NAD$^+$ and intermediate precursors. NAD$^+$ NAM, NR and nicotinamide mononucleotide (NMN) all possess a nicotinamide moiety.

1.6.3 NAD$^+$ salvage from nicotinic acid

The conversion of NA to NAD$^+$ is referred to as the classical Preiss-Handler pathway in light of the original discoverers (129). Similarly to QA conversion in de novo NAD$^+$ biosynthesis, NA is phosphoribosylated via NA phosphoribosyltransferase (NAPRT) to NAMN utilising 5-phospho-α-D-ribose-1-diphosphate, which then proceeds down the same pathway as de novo derived NAMN, producing NAD$^+$ (130) (Figure 1-16). The final ATP-dependent conversion of NAAD to NAD$^+$ by NADSYN is a rate limiting step both for salvage from NA and de novo synthesis, and NADSYN expression varies across mammalian tissues (131). High

NADSYN activity levels are detected in liver, small intestine, testis and kidney but very low levels are present in the heart and skeletal muscle (131).

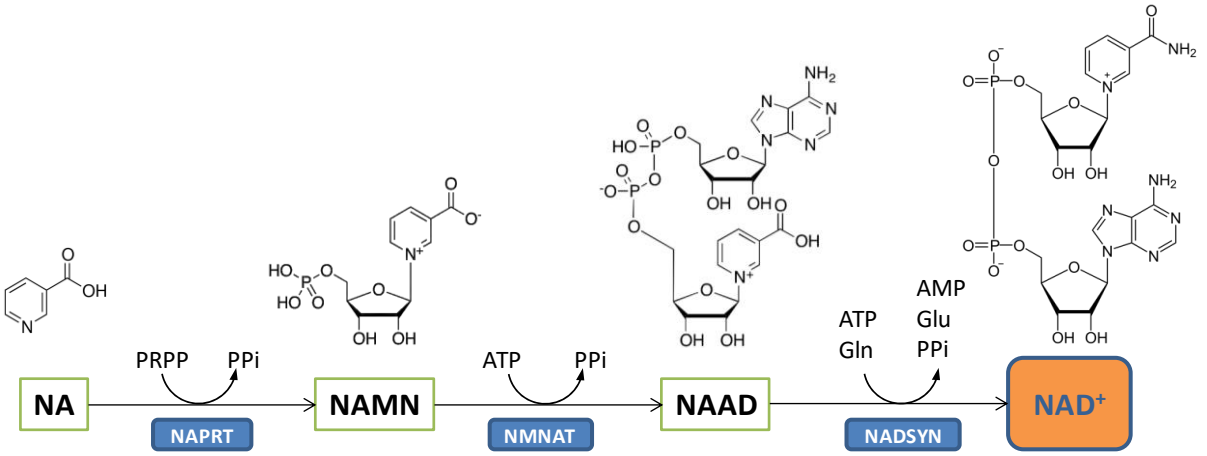

Figure 1-16 – NAD$^+$ salvage from NA. NA is converted to NAMN in a reaction catalysed by NAPRT, which is subsequently converted to NAAD via NMNAT. NAAD must then be converted to NAD$^+$ via NADSYN in an ATP dependent reaction. Gln = glutamine, Glu = glutamate, PRPP = 5'-phosphoribosyl-1-pyrophosphate, PPi = pyrophosphate.

NA supplementation is known to raise intracellular NAD$^+$ levels through this pathway (132) and is historically the most documented vitamin B3 precursor from a therapeutic perspective. NA has long been used as an effective treatment for dyslipidaemia (133) and managing the progression of atherosclerosis (134). The NA derivative acipimox acts through inhibition of the triglyceride lipase enzyme, which reduces plasma triglycerides and low density lipoprotein (LDL) while simultaneously boosting circulating high density lipoprotein (HDL) cholesterol levels (135). NA treatment was also found to enhance mitochondrial respiration in human skeletal muscle despite low NADSYN activity, but a subsequent increase in skeletal muscle lipid content and reduced insulin sensitivity was also observed (136). These side effects, coupled with a painful vasodilatory skin "flushing" effect due to the activation of GPR109A receptors in the skin (134, 137) limit the clinical applicability of NA as an NAD$^+$ boosting compound.

1.6.4 NAD^+ salvage from nicotinamide

NAD^+ can also be salvaged from NAM. Firstly, NAM is converted to NMN by nicotinamide phosphoribosyltransferase (NAMPT) in a 5'-phosphoribosyl-1-pyrophosphate (PRPP) and ATP dependent reaction, and following this NMN is converted to NAD^+ by NMNAT (138) (Figure 1-17). Alongside dietary sources, NAM is also produced when NAD^+ is consumed by NAD^+ dependent enzymes, and thus salvage via NAMPT constitutes a direct NAD^+ recycling pathway (139). Furthermore, NAMPT is downregulated upon NAD^+ reaching 90% of physiological levels (132, 140, 141) while NAM is a negative regulator of SIRT activity (142-145), thus constituting a self-regulating negative feedback mechanism.

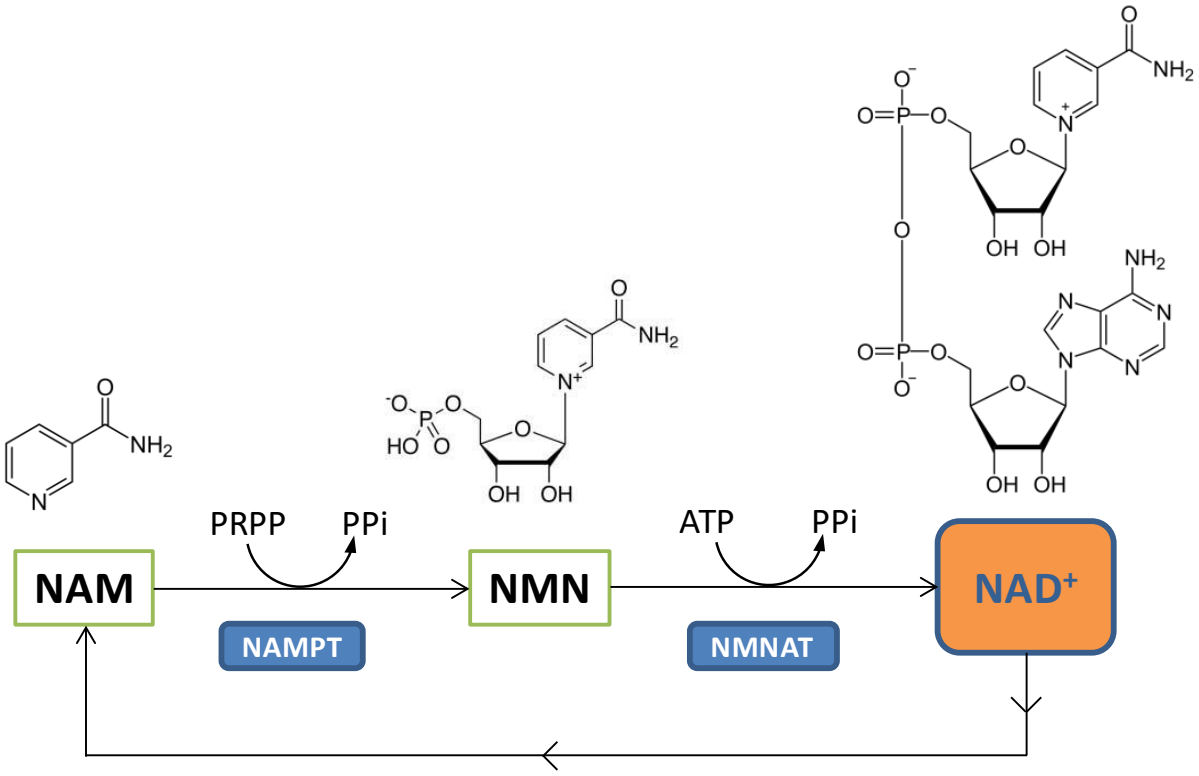

Figure 1-17 – NAD$^+$ salvage from NAM. NAM is phosphoribosylated forming NMN, a reaction which is catalysed by NAMPT. NMN is then converted to NAD$^+$ by NMNAT. NAM is produced upon enzymatic breakdown of NAD$^+$, and therefore this pathway constitutes a direct NAD$^+$ recycling mechanism.

NAMPT is highly conserved and is described in many different roles. NAMPT exists in monomeric and homodimeric forms both intracellularly and extracellularly (eNAMPT), and was initially called pre-B cell colony enhancing factor (PBEF) after its early description as a cytokine (146). It was also thought to be an insulin mimetic and termed visfatin, though this has been questioned (147). NAMPT dimerisation is critical to its type II phosphoribosyltransfrase activity (148, 149), and within cells is primarily located within the cytosol and nucleus. Monomeric eNAMPT is thought to have pro-inflammatory effects independent of NAD$^+$ salvage, and has been identified as a potential therapeutic target for inflammation driven disease states such as type II diabetes (150).

NAMPT expression is ubiquitous, and the recycling of NAM to NAD^+ via NAMPT is thought to be the primary NAD^+ biosynthesis pathway in cells, although a recent study has suggested that NAMPT may not be as critical to the maintenance of mitochondrial NAD^+ levels relative to the rest of the cell in liver (151). Nonetheless, mammalian NAMPT KO models are embryonic lethal (152) and the specific small molecule NAMPT inhibitor FK866 severely decreases cellular NAD^+ levels over time (153), impairing oxidative metabolism and NAD^+ dependent signalling pathways (138) as well as the NAD^+ dependent glucose-3-phosphate dehydrogenase (G3PD) glycolysis step (154) leading to cell death.

Despite the importance of the NAMPT pathway to NAD^+ homeostasis, NAM is thought to be less suitable for boosting NAD^+ dependent signalling due to its inhibitory effects on SIRT activity alongside NAD^+ levels having an inhibitory effect on NAMPT activity (132, 142). It has also been reported that NAMPT is down-regulated with age (104), although a recent study reported improved glucose homeostasis in aged HFD fed mice alongside increased hepatic acetylation of SIRT1 targets upon administration of NAM, despite no increases in NAD^+ or $NADP^+$ (155). Short term NAM supplementation has been successfully used to increase NAD^+ levels in cases of severe redox stress, demonstrating protective effects against oxidative stress induced apoptosis (156) and in mouse models of cerebral ischaemia (157). In these conditions, severely depleted NAD^+ levels led to excitotoxicity, which was ameliorated by repletion of NAD^+ with NAM treatment also having a down-regulatory effect on SIRTs and PARPs, preventing NAD^+ overconsumption (157).

1.6.5 NAD^+ salvage from nicotinamide riboside

Recently, an alternative route to NAD^+ has been discovered from the NAD^+ intermediate NR (14). NR is phosphorylated to NMN by the cytosolic NRK enzymes in an ATP dependent reaction, after which NMN is converted to NAD^+ by NMNAT1, NMNAT2 and NMNAT3 (14, 138, 158) (Figure 1-18). NR was long known as an NAD^+ precursor in certain strains of bacteria that do not possess the enzymes for carrying out de novo NAD^+ biosynthesis or salvage from NA (159) but it was not until 2004 that NR was discovered as a viable NAD^+ precursor in humans, along with the mammalian NRK enzymes of which two isoforms exist (NRK1 and NRK2) (14). The same study found that NR was present in cow's milk, implying that NR is a dietary source of NAD^+ (14, 160). Serious interest in the NRK enzymes and NR as a potential therapeutic arose with the observation that exogenous NR treatment could extend lifespan of yeast by enhancing Sir2 signalling (161). Exogenously administered NR is able to rescue depleted NAD^+ levels in cells which NAM salvage is inhibited (15, 16), demonstrating the viability of NAD^+ salvage from NR. NR is also produced retrospectively from NMN by CD73 enzymes (162, 163), though endogenous circulatory NR levels are relatively low (164) and the contribution of this phenomenon to overall NAD^+ salvage remains unclear.

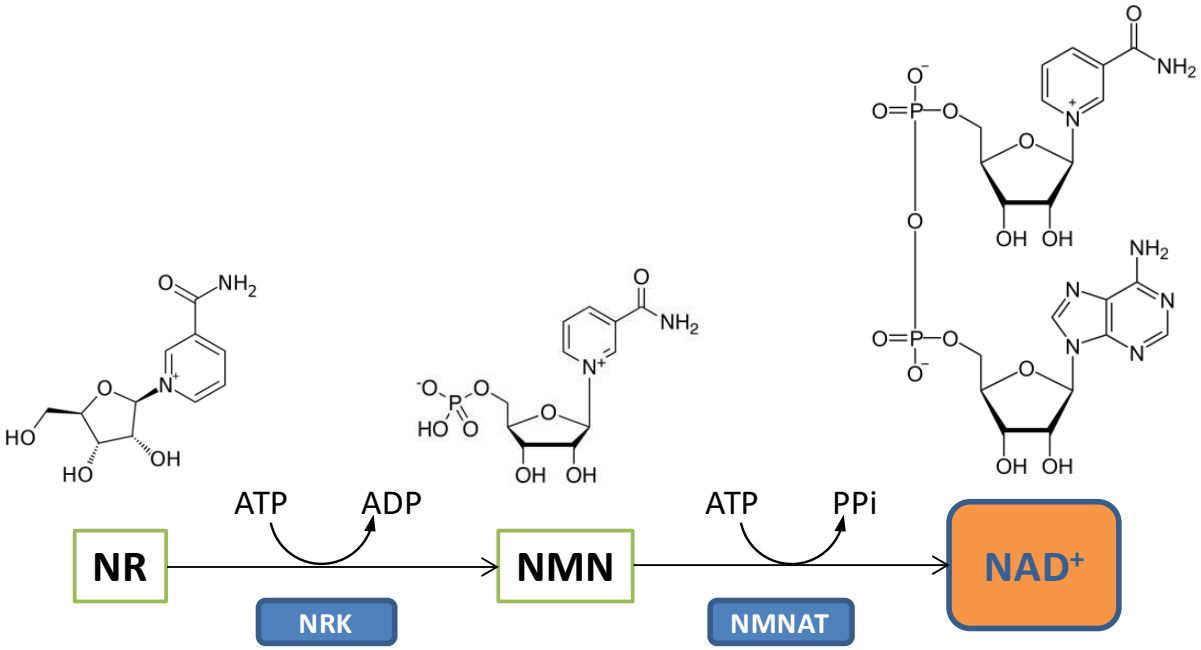

Figure 1-18 – NAD$^+$ salvage from NR. Phosphorylation of NR is catalysed by NRK forming NMN, which is then converted to NAD$^+$ via NMNAT.

Exogenous NR has demonstrated a high capacity for boosting intracellular NAD$^+$ levels in many tissues and has shown to be more effective at boosting cellular NAD$^+$ levels than both NAM and NA (15, 164). In mice, chronic oral NR administration improved oxidative metabolism through increased NAD$^+$ levels in skeletal muscle, brown adipose tissue and liver, resulting in higher SIRT activation and subsequent deacetylation of PGC-1α, FOXO1 and superoxide dismutase (SOD)2 in these tissues. This effect also protected against high fat diet (HFD) induced pathological weight gain, insulin resistance and substrate inflexibility (165). Similar results with improved metabolic flexibility (166) have been reported alongside improvements in various disease models such as type II diabetes (167) and non-alcoholic fatty liver disease (NAFLD) (168).

Functional improvements in mitochondrial myopathy through upregulation of mitochondrial biogenesis and the mitochondrial unfolded protein response (UPR) have been reported (169), with NR also partially rescuing a phenotype of mitochondrial dysfunction

defective in the NAD^+-SIRT1-PGC-1α axis through promotion of mitophagy (170). Other reports include prolonged rodent lifespan (171) and reduced cognitive decline in rodent models of Alzheimer's disease (172). The positive effects of NR are thought to be largely due to the increased activity of SIRTs, as evidenced with fatty liver reversal and induction of mitochondrial UPR being diminished in SIRT1 knockout (KO) mice (173), with a similar ameliorated effect in a SIRT3 KO model of noise induced hearing loss (174).

In humans, NR is orally bioavailable and well tolerated (164, 175), and has demonstrated NAD^+ boosting effects and enhancement of the NAD^+ metabolome in circulating peripheral blood monocytes (PBMCs) and plasma (164, 175). Potential positive effects concerning cardiovascular health such as reduced blood pressure and arterial stiffness have been noted (175), as well as a reduction in circulating inflammatory cytokines (176). However, a further study noted that 12 weeks of NR supplementation reduced hepatic fat content by 2% relative to 0.2% in the placebo group but did not improve insulin sensitivity or glucose metabolism in obese men (177). The effects of NR on humans still remain inconclusive, necessitating further research into the NRK pathways and NR as an NAD boosting supplement.

Recently, a reduced form of nicotinamide riboside (1-[(2R,3R,4S,5R)-3,4-Dihydroxy-5-(hydroxymethyl)tetrahydrofuran-2-yl]-4H-pyridine-3-carboxamide (NRH)) was discovered to be orally bioavailable and more stable in plasma than NR (178). NRH processing is dependent on adenosine kinases (AKs) and independent of the NRKs (178). NRH was reported to alleviate cisplatin induced kidney injury (178), though the full potential of NRH in boosting NAD^+ levels has yet to be determined.

1.6.6 NAD^+ salvage from exogenous NMN

NAD^+ salvage from the amidated precursors of NAM and NR both share a common intermediate molecule, NMN (Figure 1-14), which is also a potential NAD^+ boosting compound. NMN is not classed as a vitamin B3 compound due to its phosphate group and uncertainties surrounding its cellular uptake, but similar NAD^+ boosting and rescuing effects have been observed to that of NR supplementation (15, 16). Similar metabolic improvements to those reported with NR have been attained with exogenous NMN administration in aged, obese and NAD^+ deficient NAMPT KO mice, including improved glucose and lipid dynamics (179-182), mitochondrial function (183-185), retinal function (186) and cognitive function (187, 188).

The first orally administered NMN clinical trial recently concluded in young, healthy males in which it appeared safe and well tolerated (189), but further research is required into the capacity for NMN to raise NAD^+ levels under ageing and metabolic stress in humans. With high tolerance levels and efficacy, current knowledge indicates that NMN and NR are the two most viable candidate compounds for improving NAD^+ levels with age, metabolic stress and NAD^+ deficiency linked disease states.

1.6.7 Cellular uptake of exogenous NMN and NR

Cellular nutrient uptake mechanisms have been found to play an important role in the overall cellular bioavailability of NAD^+ derived from exogenous NR and NMN. It is thought that NAM and NR enter the cell directly through the plasma membrane (190, 191) with NR possibly also entering through equillibrative nucleoside transporters (ENT) (16, 123, 192) (Figure 1-19). This is not possible for NMN due to its phosphate group (13), and two main

models are proposed for exogenous NMN uptake. The first proposes that NMN is dephosphorylated to NR before cellular entry by ectonucleotidases such as CD73 (13) (Figure 1-19). Stable isotope labelling studies have supported this theory (16) and therefore, NR could provide more efficacious augmentation of cellular NAD^+ owing to the requirement of one fewer enzymatic step. However, it has also been proposed that NMN is directly transported into the cell (180). The Na+/K+ Cl^- transporter Slc12a8 was recently reported as a direct transporter of NMN (193), though the findings of the study were challenged on technical grounds (194) (Figure 1-19). It has also been determined that the NRK enzymes are required for NMN to have intracellular NAD^+ boosting effects within hepatocytes and skeletal muscle (15, 16), therefore supporting the model of extracellular NMN conversion to NR prior to cellular entry (Figure 1-19). The importance of the NRK enzymes therefore extends beyond that of NAD^+ boosting from NR itself. The mechanisms by which extraneous NMN is converted to NR are thought to be directly related to variations in cellular permeability of NR and NMN (15, 16).

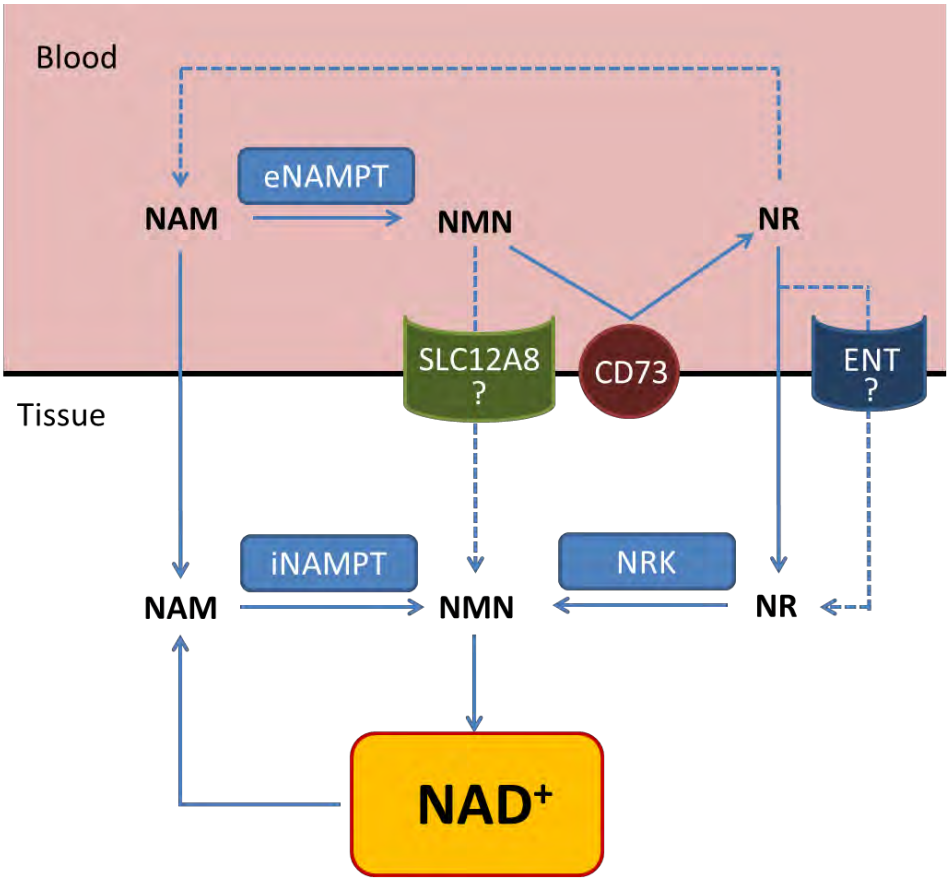

Figure 1-19 – Current model of exogenous NAM, NR and NMN processing and cellular entry. NAM and NR are able to cross the plasma membrane directly, though NR uptake is also thought to be facilitated by ENT transporters. The plasma membrane is impermeable to NMN due to its phosphate group, and so must be dephosphorylated to NR before entry, though there is evidence for a direct NMN transporter (193).

1.6.8 Subcellular compartmentalisation of NAD^+, NAD^+ salvage enzymes and NAD^+ dependent signalling enzymes

NAD^+ is not uniformly distributed within cells, with organelles possessing distinctly regulated NAD^+/NADH pools that reflect their redox and signalling requirements. Different organelles exclusively express specific isoforms of NAD^+ salvage and signalling enzymes, reflecting their primary functions (Figure 1-20). It is generally accepted that three distinct subcellular pools of NAD^+ exist between the cytosol, nucleus and mitochondria. NAD^+ is able to freely cross the nuclear membrane through pores, thus the cytosolic and nuclear pools are similar

(Figure 1-20). Most studies propose mitochondrial NAD^+ concentrations of greater than 250 µM (111, 195) with nuclear NAD^+ at approximately 70 µM (196) and cytoplasmic NAD^+ being lower still, though exact cytosolic measurements are difficult (197) (Figure 1-20). Cellular distribution of NAD^+ also varies dramatically across cell types, for example with 70% of total NAD being mitochondrial in cardiomyocytes compared with 50% in neurons (198), reflecting differences in oxidative capacity and cellular function. In terms of nuclear segregation, a link between NAD^+ compartmentalisation and nuclear transcription in developing adipocytes has been described, regulating glucose metabolism and differentiation through nuclear NAD^+ bioavailability (199).

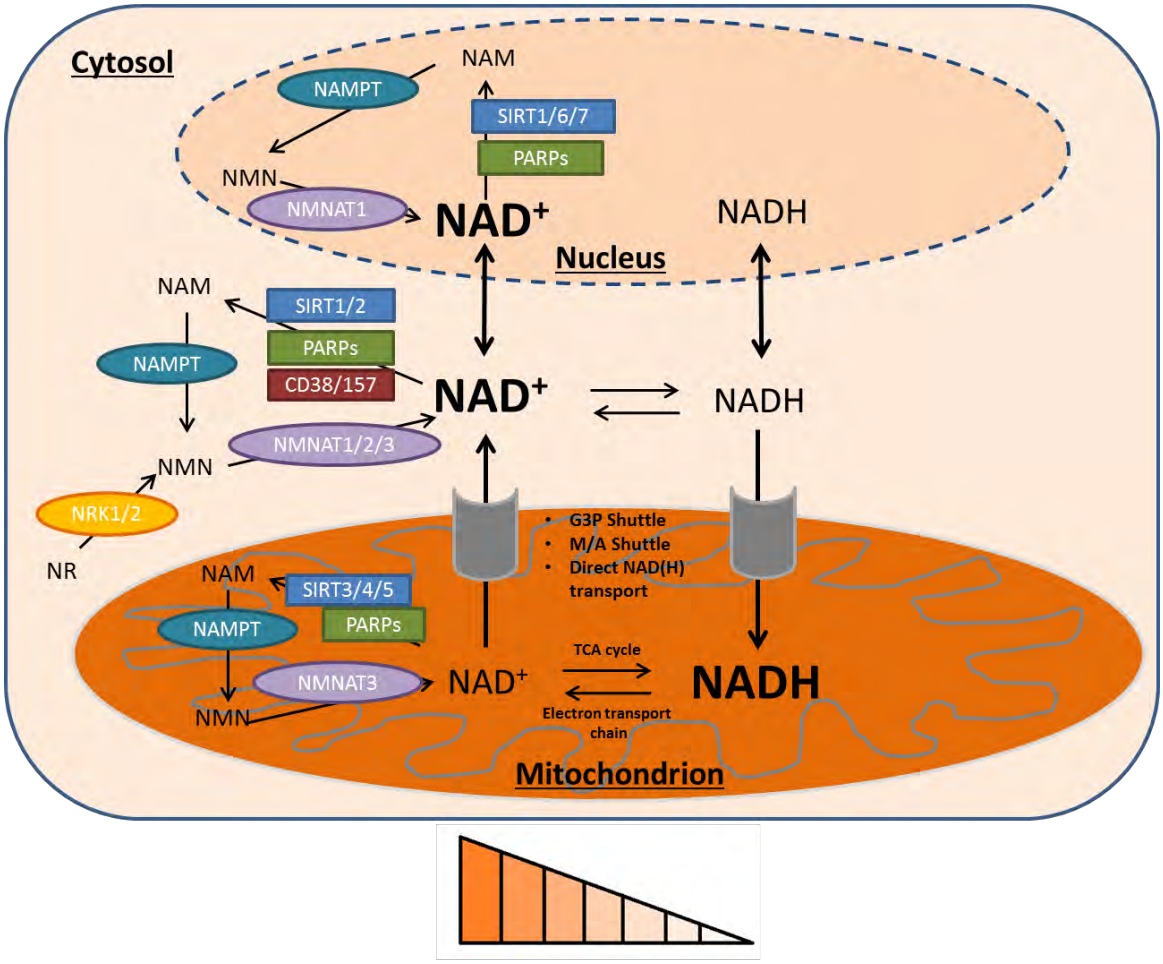

Figure 1-20 – Segregation of NAD^+ pools, with localised NAD^+ salvage and co-dependent signalling enzymes within cells. NAD^+ and NADH can freely cross the nuclear membrane via nuclear pores. A high concentration of NAD^+ and a strongly reductive redox environment is maintained within mitochondria via the G3P shuttle, the malate/aspartate shuttle and potentially direct NAD(H) transport. The highly reductive redox environment within mitochondria favours electron donation to ETC proteins, driving oxidative phosphorylation.

NAD^+ is unable to cross the mitochondrial membrane, with evidence suggesting that the mitochondrial pool is almost entirely sequestered from the rest of the cell to preserve oxidative phosphorylation during metabolic stress. Sufficient mitochondrial NAD^+ levels appear to be critical to cell survival (111), though severe depletion of cytosolic NAD^+ does not result in immediate impairment of oxidative phosphorylation, with mitochondrial NAD^+ levels shown to be maintained for 24 hours and functionally for up to 3 days (200).

Additionally, fluctuations in mitochondrial NAD^+ do not correlate with cytosolic and nuclear flux, which appear more closely related (201). Mitochondria also show resistance to whole-cell NAD^+ perturbations, where a hepatocyte NAMPT KO mouse line demonstrated a 50% reduction in cellular NAD but only a 20% reduction in mitochondria (151).

The TCA cycle depends on pyruvate and electrons from NADH generated in the cytosol from glycolysis. In skeletal muscle, NAD^+ levels within mitochondria are an order of magnitude higher than cytoplasmic NAD^+ at approximately 3.15 mM/kg and 0.15 mM/kg respectively (202), though it is not certain how this balance is maintained. The critical NAD^+ salvage enzymes NAMPT and NMNAT3 are present within mitochondria (111) suggesting a degree of intra-mitochondrial NAD^+ generation. However, this is not thought to be critical to mitochondrial NAD^+ levels given that NMNAT3 KO mouse models exhibit no mitochondrial NAD perturbations in liver, heart and skeletal muscle (191) and NAMPT KO mice demonstrate only a 20% reduction in mitochondrial NAD^+ compared to 50% in the cytosol (151). However, recent evidence suggests that NAD^+ is in fact directly imported into mammalian mitochondria through an as yet undetermined NAD^+ transporter (120) (Figure 1-20), though the observed segregation between mitochondrial and cytosolic NAD^+ concentrations would suggest that this is tightly regulated. Furthermore, deregulated NAD^+ influx produced deleterious mitochondrial effects in HEK293 cells when direct NAD^+ transfer was facilitated through transgenic expression of an Arabidopsis thaliana NAD^+ transporter (203).

Mitochondria also retain a highly reductive environment with NAD^+:NADH ratios at around 7-8 compared with between 60-700 in the more oxidative cytoplasm (112, 204). This is achieved through electron import via glyceraldehyde-3-phosphate (G3P) and malate-

aspartate shuttles simultaneously translocating reducing equivalents into the cytosol (205), meaning that cytosolic NAD^+ levels can still present a viable measure of mitochondrial health and redox status (112).

The compartmentalisation and dynamics of NAD^+ within cells across multiple organelles remains unclear, particularly within organelles besides mitochondria and nuclei. Specific cellular and subcellular disparities in NAD^+ levels between organelles may also characterise metabolic disease states and drive ageing metabolic phenotypes, highlighting the importance of this knowledge (206). Various technologies have been developed to elucidate this further, such as a synthetic NAD^+ consuming PARP1 construct which can be targeted to specific organelles using tagged cell localisation signals (207). This allows for inference of NAD^+ dynamics through relative poly-ADP-ribosylation levels and NAD^+ turnover (207, 208). Furthermore, organelle targetable fluorescent protein biosensors are under development, which bind NAD(P) altering their fluorescence signature (201, 209, 210). This technology is currently being refined for both basic research and direct medial use (209).

1.7 NAD^+ dependent signalling pathways

The three main classes of NAD^+ dependent enzymes are SIRTs, ADP-ribose polymerases and the cyclic ADP-ribose synthases CD38 and CD157 (118). Despite their shared reliance on NAD^+, these enzymes have highly disparate functions (Figure 1-21), and this section will outline their relative contributions to NAD^+ bioavailability and metabolic health.

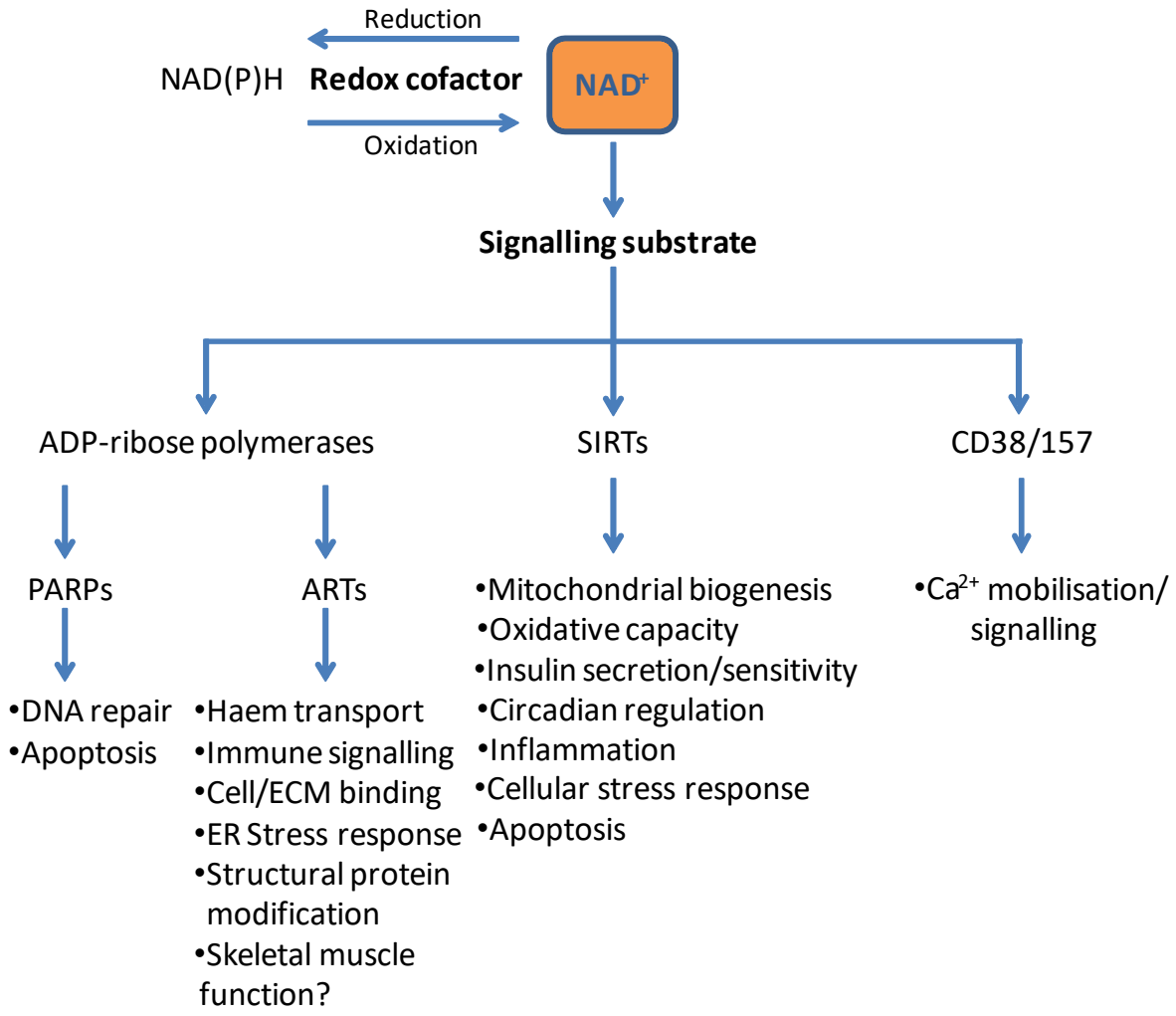

Figure 1-21 – NAD$^+$ as both a redox cofactor and signalling substrate. NAD$^+$ is also critical for regulating key cellular processes as a consumed substrate for NAD$^+$ dependent signalling enzymes. Adapted from Elhassan et al., 2017 (211).

1.7.1 Sirtuins

The sirtuins are a family of seven NAD$^+$ class III histone deacetylase enzymes, of which seven sirtuin homologs (SIRT1-7) exist in mammals with varying roles, targets and subcellular locations. The family is named for its homology to the NAD$^+$ dependent yeast gene silencing protein Sir2 (212). Overexpression of Sir2 orthologs was initially reported to increase lifespan in Saccharomyces cerevisiae, Caenorhabditis elegans and Drosophila melanogaster through mechanisms linked with caloric restriction (213-215) though these observations were

recently attributed to non-standardised genetic backgrounds (216). SIRT expression and activity has been implicated in mammalian longevity (217, 218) though any direct mechanisms remain undetermined. Nonetheless, recent years have seen a wealth of research into mammalian SIRTs, which have been identified as important metabolic "sensors" for the cell as the activity of SIRTs is dependent on NAD^+ availability, and therefore intrinsically linked to cellular energy status (219, 220).

SIRT-mediated signalling pathways can induce systemic metabolic adaptations through modulating diverse cellular functions including mitochondrial biogenesis, metabolic substrate switching, gluconeogenesis and insulin sensitivity (221) , cellular stress responses (222), deoxyribose nucleic acid (DNA) repair (223), cell cycle control(224, 225), inflammation (226), circadian rhythm (227) and autophagy (228). Most SIRTs function by removing acetyl groups from target proteins including metabolic transcription factors, modulating their activity. This is achieved through cleavage of NAD^+, where the free acetyl group is accepted by ADPr becoming O-acetyl-ADP-ribose (OAADPr) (229) (Figure 1-22). SIRT2 is primarily localised to the cytoplasm and is thought to modulate inactive cytoplasmic transcription factors, while SIRT1, 6 and 7 are localised to nuclei where they regulate active nuclear transcription factors and chromatin remodelling proteins such as histones (230). SIRT3, 4 and 5 are localised to mitochondria where they "sense" redox state and induce appropriate responses to maintain metabolic homeostasis (230).

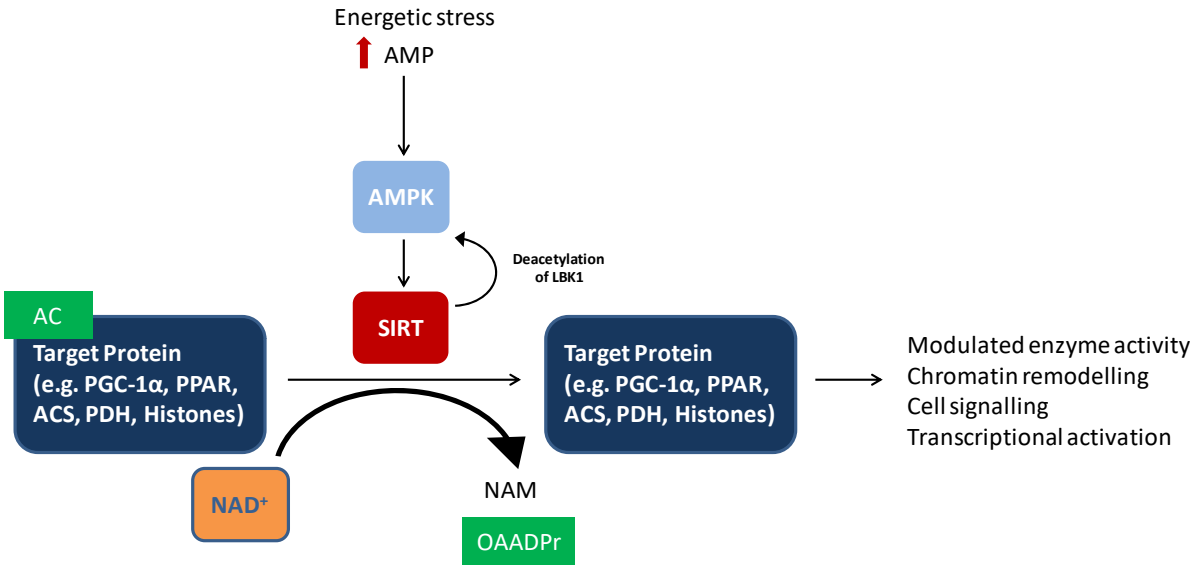

Figure 1-22 – Simplified mechanism of SIRT action. AMPK activates SIRTs which catalyse the removal of acetyl groups from target proteins in an NAD^+ dependent reaction, modulating target protein activity and eliciting cellular changes such as increased mitochondrial biogenesis.

SIRT1 and 3 present with the most metabolically relevant roles, and have wide ranging impacts on systemic metabolism. SIRT1 is also regulator of gluconeogenic gene expression in the liver, promoting liver gluconeogenesis in fasting conditions (221) but also suppressing aberrant gluconeogenesis in conditions of type 2 diabetes upon the SIRT1 activator metformin (231, 232). SIRT1 also improves insulin sensitivity in pancreatic beta cells (233) and can shift transcriptional programming towards mitochondrial fatty acid oxidation through PGC-1α and peroxisome proliferator-activated receptors (PPAR) (234) protecting against systemic obesity (Figure 1-22). SIRT1 overexpressing high fat diet (HFD) fed mice also showed improvements in glucose tolerance through tighter regulation of liver gluconeogenesis (235) with a similar study reporting beneficial effects from SIRT3 overexpression in NAFLD (236). In skeletal muscle, SIRT1 increases oxidative capacity and mitochondrial biogenesis through activation of PGC-1α and increases insulin sensitisation and enhanced glucose/fatty acid metabolism through PPARs (237) , alongside protection

against skeletal muscle atrophy through inhibition of FOXO proteins (238) (Figure 1-22). SIRT3 is the most active mitochondrial sirtuin, and positively modulates mitochondrial activity through deacetylation of ETC complexes I and II and acetyl-CoA synthetase (ACS) (239). Like SIRT1, SIRT3 also influences metabolic substrate preference but through modulation of pyruvate dehydrogenase (PDH) acetylation status rather than transcription factors in response to substrate availability (240) (Figure 1-22). Additionally, SIRT3 protects mitochondrial integrity and the mitochondrial genome through interactions with 8-oxoguanine-DNA glycosylase 1 (OGG1) which repairs oxidative DNA damage (241), and can also induce antioxidant genes through interaction with FOXO3a (242).

SIRT activity is NAD^+ dependent and thus induced under conditions of metabolic stress that are accompanied with a decrease of ATP and increase in bioavailable NAD^+, with both SIRT1 and SIRT3 activity regulated by AMPK activation and exercise (220, 229, 243-245). SIRT1 can also reciprocally activate AMPK through deacetylation and activation of the AMPK activating kinase liver kinase B1 (LKB1) (246, 247) (Figure 1-22). SIRTs are thus responsible for much of the beneficial metabolic adaptations that accompany caloric restriction and exercise in skeletal muscle (248) and whole body metabolism (220, 249). Due to these roles, dysregulation of SIRT signalling are likely a contributing factor and potential therapeutic target in many metabolism related disease states including type II diabetes (250), vascular disease (251), NAFLD (252) and mitochondrial disease (253). It is therefore clear that SIRT signalling is critical to the preservation of metabolic health, which is itself dependant on cellular NAD^+ bioavailability.

1.7.2 ADP-ribose polymerases

Poly ADP-ribose polymerases are enzymes which catalyse the transfer of ADP-ribose moieties to target proteins (118). The ADP-ribose moieties are derived from NAD^+, therefore constituting a cellular source of NAD^+ consumption (254). There are two major classes, poly-ADP ribose polymerases (PARPs) and ADP ribosyltransferases (ARTs) (254).

1.7.2.1 **PARPs**

PARPs are NAD^+ dependent enzymes of which there are 17 different isoforms in mammals, with the most widely studied being PARP1 and PARP2 (118). PARP1 and PARP2 transfer poly ADP-ribose moieties derived from the breakdown of NAD^+ to target proteins, thus modulating their function and activity (255). Their primary function is to activate DNA repair mechanisms, though they also have roles in chromatin modulation and gene transcription, cell proliferation and apoptosis (255). Although PARPs have few direct regulatory roles in metabolism, they are indirectly important in a metabolic context as major depletors of bioavailable NAD^+ through consumption (256). Persistent PARP activation depletes bioavailable NAD^+ by up to 80% whilst significantly increasing NAM levels, which itself inhibits SIRT activity (257, 258). Similarly, SIRT1 activation results in PARP downregulation (259), implying that SIRTs and PARPs compete for the same intracellular NAD^+ pool (257, 259). SIRT activity suppresses PARP activity in conditions of NAD^+ excess (258), but SIRT1 has a higher Michaelis constant value (Km) for NAD^+ than PARP1, therefore the ability of SIRTs to counterbalance PARP activity decreases as bioavailable NAD^+ depletes (118). Furthermore, PARP2 has also been shown to directly suppress SIRT1 activity through interaction with the

SIRT1 promoter (257, 260), although absence of both PARP1 and PARP2 does not affect SIRT2 or SIRT3 (257).

PARP activity increases with age as DNA damage accumulates, resulting in decreased NAD^+ bioavailability and downregulated SIRT activity, which is further exacerbated by PARPs having a higher affinity for NAD^+ (118, 261-263). Multiple studies assessing PARP inhibition have reported protective metabolic effects in skeletal muscle and other tissues through preventing excessive PARP NAD^+ consumption and thus inducing SIRT activity (257, 262-265). However, the wider applicability of this as a chronic metabolic intervention is questionable due to the risk of exacerbating genomic instability through impaired PARP mediated DNA damage repair mechanisms (261, 266).

1.7.2.2 **ARTs**

ARTs differ to PARPs in that they exclusively transfer single ADP-ribose moieties to target proteins rather than ADP-ribose polymers. Most ART family enzymes (ART1, 2, 3 and 4) are bound to the external surface of the plasma membrane via a glycosyl-phosphatidyl-inositol (GPI) anchor, though ART5 is an extracellular secreted enzyme (267). The main function of ARTs is to catalyse the mono ADP-ribosylation of arginine side chains on extracellular protein substrates such as the immune modulator P2X7 and the haem binding protein haemopexin (268, 269), though several intracellular proteins contain Arg-ADPr residues and are thought to be ART substrates, including BiP, GAPDH and Tubulin (267, 270-272). Many skeletal muscle and heart proteins are mono-ADP ribosylated, and mice deficient in ART1 showed muscular weakness suggesting that ART activity is of particular importance to skeletal muscle (268). There is evidence to suggest that ARTs are important for skeletal muscle cell membrane/ECM interactions and by extension skeletal muscle growth and repair, with ART-

mediated ADP-ribosylation of integrin tails temporally modulating their affinity for laminin (273-277).

1.7.3 Cyclic ADP ribose synthases

The Cyclic ADP ribose synthases CD38 and CD157/BST-1 are membrane-bound ectoenzymes that also function as receptors in immune cells, governing multiple cell functions such as cell adhesion, immune signalling and metabolic disease (278). They also produce cADPR from NAD^+, which acts as a second messenger that influences Ca^{2+} signalling and release alongside the inositol trisphoshate (IP3) pathway (279). As with PARPs, these enzymes consume bioavailable NAD^+ at a considerable rate, with production of one cADPR molecule requiring hydrolysis of ~100 NAD^+ molecules (280). CD38 has a major impact on cellular NAD^+ levels in mammals (281), and CD38 inhibition has been shown to increase NAD^+ levels and improve glucose and lipid homeostasis in obese mice (282). Additionally, CD38 KO mouse models have demonstrated increased NAD^+ levels and protection against obesity and metabolic dysfunction improvements in metabolic health (283), as well as improving age related metabolic decline through upregulation of SIRT3 (284). However, NAD^+ mimetic CD38 inhibitors may also inhibit SIRT1 (285) and disrupt calcium signalling processes (285), suggesting that as with PARP inhibition, they may not constitute appropriate targets for metabolic interventions.

1.8 NAD^+, ageing and disease

1.8.1 Ageing, NAD^+ bioavailability and metabolic health

Biological ageing is defined as progressive physiological changes leading to senescence and/or a decline of biological function and capacity for metabolic adaptation to stress (286, 287). Generally, ageing cells exhibit increased DNA damage, diminished mitochondrial function, increased levels of ROS and lower ATP turnover (287, 288). It is becoming increasingly well established that perturbed NAD^+ homeostasis is a causative factor in many metabolic disease states such as type II diabetes (180, 289). Critically, the risk of many of the discussed disease states that are attributable to insufficient NAD^+ levels increases with age (290). It is now widely appreciated that biological ageing is accompanied with a decline in bioavailable cellular NAD^+ levels, resulting in subsequent redox dysfunction and downregulation of NAD^+ dependent metabolic signalling mediated by the sirtuins (291). This link in mammals was first established in pancreatic β-cell specific SIRT1 overexpressing mice, where young mice demonstrated improved glucose-stimulated insulin secretion which diminished with age. Critically, the phenotype could be rescued through raising intracellular NAD^+ levels, implicating NAD^+ bioavailability as the cause (182). A decline in NAD^+ with age has been observed in nematode worms (292) and many rodent studies in most tissues (13). Though human data is relatively scarce, a similar decline has been observed in human skin (263) and liver (168). There are many proposed mechanisms for this decline, such as the aforementioned hyperactivation of PARPs (118). Alongside PARPs, CD38 expression is shown to increase with age (284), with CD38 knockout mice resisting age associated declines in

metabolic function and mitochondrial respiration (293), implicating CD38 as another major contributor to the decline in bioavailable NAD^+.

1.8.2 Sarcopenia and healthspan

In the context of skeletal muscle, ageing manifests as a progressive loss of strength and muscle mass (4), insulin resistance and a reduced capacity for metabolic function and adaptation which is exacerbated by disuse, malnutrition and stress (5). Severe loss of skeletal muscle mass and function is termed sarcopenia, a multi-faceted disease state attributed to combinations of disuse, malnutrition, muscular anabolic/catabolic imbalance, inflammatory disease states and hormonal changes with age (6). A hallmark of sarcopenia is the loss of skeletal muscle fibre number, though fibre atrophy is often present particularly within type II fibres (294). Though the clinical definitions of sarcopenia are poorly defined, it strongly correlates with an accelerated decline in healthspan, increased risk of mortality and predisposition to metabolic disease including type 2 diabetes, obesity and cardiovascular disease (295, 296) (Figure 1-23).

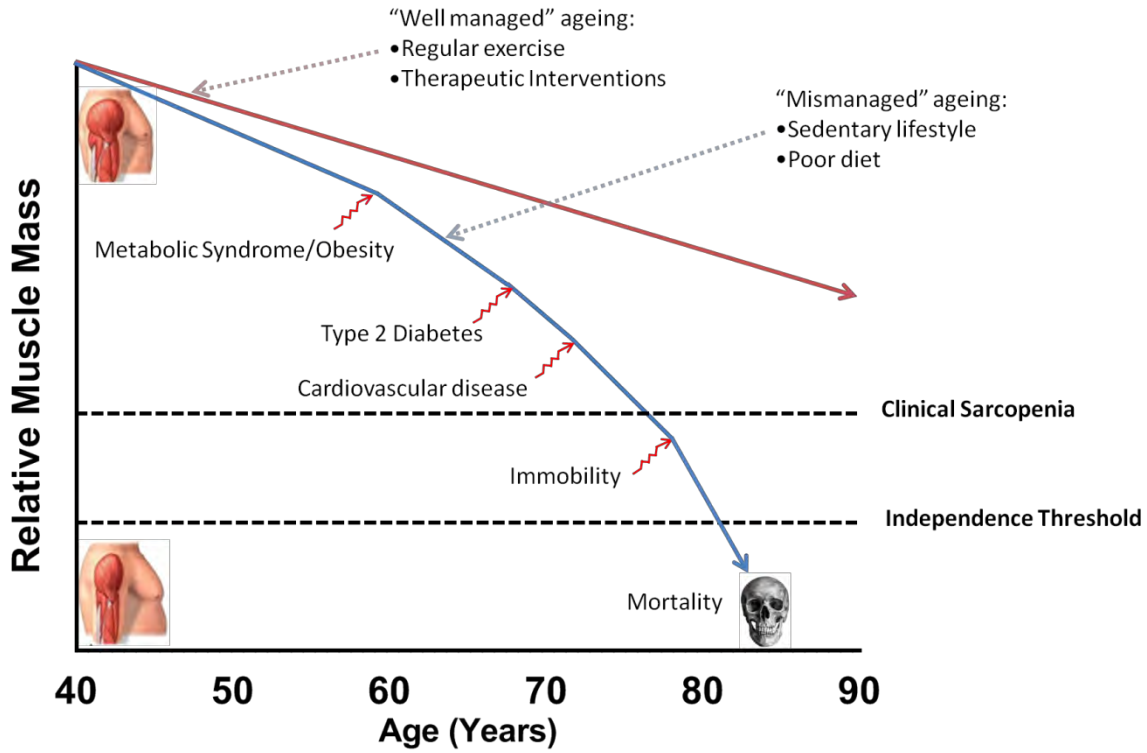

Figure 1-23 – The relationship between skeletal muscle mass, ageing and metabolic health. Poorly managed skeletal muscle health leads to increased metabolic decline with age, while regular exercise, a balanced diet and/or NAD^+ boosting therapeutic strategies could increase healthspan with age.

The molecular causes of age related skeletal muscle loss remain poorly defined, though cited factors include blunted responses to anabolic signals and downregulated hypertrophic pathways (297), increased proteasomal activity (298), a reduced capacity for regeneration due to increased satellite cell senescence (299-301), impaired amino acid intake (302) and sensing (303), increased inflammation (304), increased lipid infiltration (305) and mitochondrial dysfunction caused by impaired mitochondrial biogenesis and mitophagy (99, 101, 306). As previously discussed, lower NAD^+ bioavailability leads to decreased SIRT activity and thus impaired mitochondrial biogenesis and metabolic adaptation. Evidence suggests that this is also the case within skeletal muscle and could also contribute to the aetiology of muscular dysfunction and subsequent metabolic disease, with

models of severe skeletal muscle NAD^+ depletion reporting severe yet reversible muscle weakness and metabolic dysfunction (11). Increasing SIRT activity via caloric restriction led to attenuated age related loss of muscle mass in rats through upregulation of PGC-1α (307) and reduced muscle oxidative stress/oxidation status (308, 309). Rodent studies suggest a decline in NAD^+ with age ranging from 15-85% (11, 180, 184, 284, 292). However, as skeletal muscle NAD^+ levels and subsequent NAD^+ dependent signalling pathways are also regulated through exercise (104, 245, 310, 311), it is unclear whether depleted cellular NAD^+ is a primary cause or a secondary effect of age related sarcopenia, which itself leads to reduced physical activity (Figure 1-24). As NAD^+ precursor availability has been found to influence cellular NAD^+ levels, such nutrient based interventions may be a viable therapeutic intervention against progression of sarcopenia alongside physical activity, particularly in cases where muscle weakness and immobility limit access to exercise. Because of this, much research has been focused on understanding the relationships between NAD^+ biosynthetic pathways and their viability for supplementation in order to boost cellular NAD^+ levels. In the context of today's ageing and increasingly sedentary society (312, 313), further understanding of biochemical pathways associated with skeletal muscle preservation and restoration is required to address the issue of healthspan correlating poorly with lifespan.

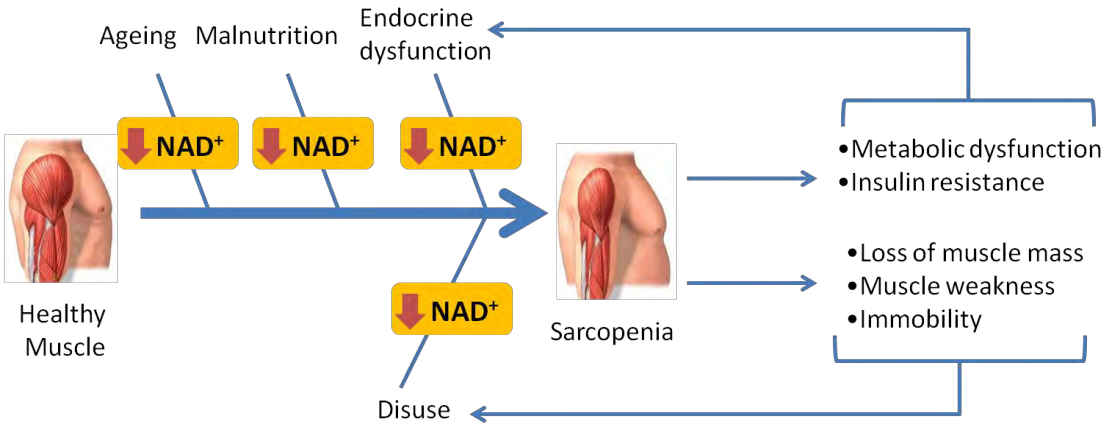

Figure 1-24 – Sarcopenia is a self-exacerbating disease. Sarcopenic risk factors decrease skeletal muscle NAD^+, leading to further metabolic dysfunction and increased disuse.

1.9 Skeletal muscle NAD^+ dynamics

With the acknowledgement of the importance of NAD^+ homeostasis in skeletal muscle and overall metabolic health, research interest in skeletal muscle NAD^+ salvage pathways and optimal supplementation strategies has seen a marked increase. The key skeletal muscle salvage pathways have been identified, though the interplay and contextual importance of the routes to NAD^+ available to skeletal muscle remains unclear.

1.9.1 Skeletal Muscle NAD^+ Salvage Pathways

Initial metabolic profiling on skeletal muscle determined that the NMNAT1 enzyme is highly active relative to NADSYN, indicating that skeletal muscle is reliant on salvage through amidated routes (NAM and NR) over de novo synthesis or the Press-Handler pathway (121). The most highly expressed NAD^+ salvage enzymes in skeletal muscle are NAMPT, NRK2 and NMNAT1 (15) (Figure 1-25), and infusions of labelled L-tryptophan and NA determined that a negligible proportion of skeletal muscle NAD^+ is synthesised from these precursors (314) confirming the sole importance of the amidated salvage pathways.

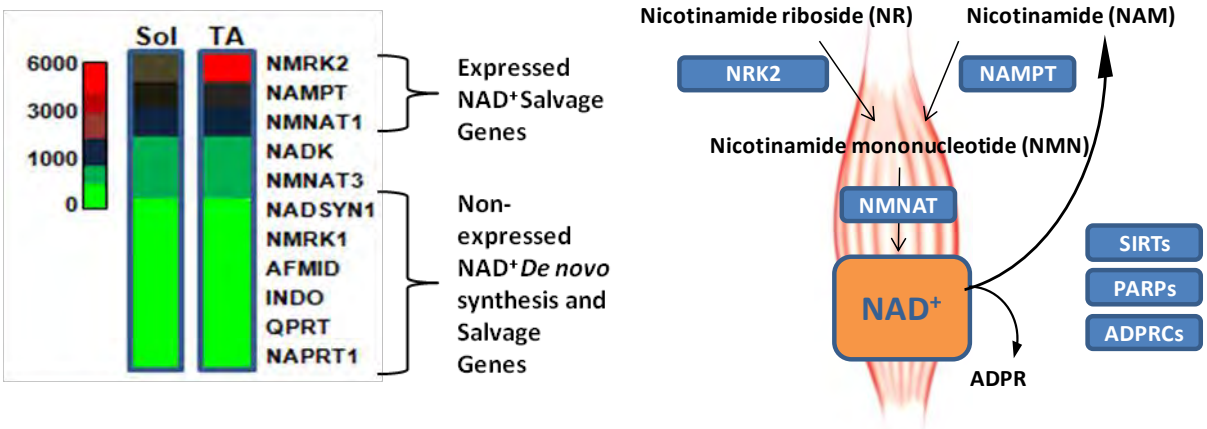

Figure 1-25 – Skeletal Muscle NAD$^+$ salvage mechanisms. Expression of de novo and Priess-Handler pathway enzymes are negligible, while NR and NAM processing enzymes are highly expressed. NRK2 is strongly expressed relative to NRK1, which is almost negligible. Adapted from Fletcher et al., 2017 (15).

Recycling of NAM back to NAD via NAMPT appears to be the most important pathway in skeletal muscle for maintaining NAD$^+$ homeostasis, with NAMPT inhibition via FK866 alone resulting in a significant decrease in cellular NAD$^+$ levels (15). A skeletal muscle specific NAMPT KO mouse model exhibited an 85% decrease in skeletal muscle NAD$^+$ content, compromising bioenergetics and leading to a 60% decline in ATP (11). This in turn led to a significant decline in skeletal muscle function including loss of mass, endurance, strength, improper glucose metabolism, increased inflammation and accelerated progressive degeneration with age (11). Critically, this phenotype could be rescued with oral NR administration (11). Skeletal muscle specific overexpression of NAMPT increased NAD$^+$ levels by 50% without perturbing the NAD$^+$/NADH ratio, but did not improve mitochondrial biogenesis or function and mice aged between 3-9 months were not protected from HFD induced obesity (315). Conversely, a more recent study with a NAMPT specific overexpression mouse model reported an increase in exercise performance and mitochondrial capacity following voluntary exercise training (316) suggesting that augmented NAD$^+$ salvage could improve adaptations to training. NAMPT expression is also

known to decrease with age correlating closely with exercise capacity (104), a trend which can be reversed with exercise training in both rodents (105) and humans (104). The link between NAMPT, SIRT1 and exercise is clear (317) having also been linked to increased mitochondrial volume and potentially increased endurance (318, 319) with NAMPT overexpressing mice retained a greater capacity for exercise with age (11). Current knowledge suggests that augmenting skeletal muscle NAD^+ levels in absence of physiological NAD^+ deficit provides only subtle functional benefits at most (315), but could significantly prolong healthy skeletal muscle function under conditions of NAD^+ deficiency such as in ageing and pathophysiological disease states. In contrast to NAMPT, NRK loss of function models do not exhibit a severe phenotype, with no significant perturbations to the NAD^+ metabolome (15, 16). NRK1 KO, NRK2 KO and double NRK1/NRK2 KO mice appear functionally normal in terms of skeletal muscle NAD^+ metabolome, structure and development, gene expression, mitochondrial function and bioenergetics (15). A recent study also noted no change in skeletal muscle NAD^+ levels but a concurrent decrease in Nmrk1 expression in aged NRK2 KO mice, alongside a maladaptive skeletal muscle response to endurance exercise with of enhanced slow myosin gene expression but a concurrently increased IL-15 myokine expression, which activates mTOR signalling and may be required to preserve muscle mass in the absence of NRK2 (320). Taken together, this suggests a specific role for NRK2 in maintaining the skeletal muscle NAD^+ pool with age.

1.9.2 Skeletal muscle NAD^+ supplementation strategies

Despite the perceived redundancy of the NR/NRK salvage pathway in general NAD^+ homeostasis within skeletal muscle, the metabolic value of the NRK enzymes may derive

from their seemingly essential role for exogenous NMN and NR processing. As previously discussed in section 1.6.7, neither NR nor NMN are able to influence skeletal muscle cellular NAD^+ levels in the absence of functional NRK activity (15). Two NRK isoforms exist, though there appears to be a functional redundancy between them in this regard (15). Furthermore, despite the importance of NAMPT to skeletal muscle homeostasis, NAM is an ineffective skeletal muscle NAD^+ boosting precursor relative to NR and NMN (15) , which is likely due to the rate limiting effect of high NAD^+ levels on NAMPT (132, 140, 141). The functional benefits from increased NAD^+ signalling may also be less pronounced with NAM supplementation due to the inhibitory effects of excess NAM on SIRTs (142-145). Conversely, orally administered NR has demonstrated significant NAD^+ boosting effects in aged satellite cells, improving mitochondrial function and preventing senescence which had positive effects on skeletal muscle and enhanced murine lifespan (171). Additionally, skeletal muscle NRK2 expression has not been shown to decline with age unlike NAMPT (104), together implicating the NR/NRK pathway as a more suitable candidate for boosting skeletal muscle NAD^+ levels.

NAD^+ repletion through exogenous NR and NMN supplementation has demonstrated improvements in skeletal muscle function and skeletal muscle mitochondrial function in models of ageing (181, 184), injury (171), muscular dystrophy (321) and mitochondrial disease (253). Furthermore, NR (11, 15) and NMN (15) are able to rescue NAD^+ levels in models of dysfunctional NAD^+ recycling via NAMPT, suggesting clearly delineated roles for NAM recycling and the NRK pathway. Interestingly, exogenous NR was able to rescue skeletal muscle fibre size and ATP production in NAMPT KO mice despite having little impact on the total and mitochondrial NAD^+ pool (11), suggesting that while NR salvage via NRK2

may be dispensable for general skeletal muscle homeostasis, NRK2 is able to produce an independent, efficiently used subfraction of total NAD^+ if NAM recycling is impaired.

1.10 Nicotinamide riboside kinases

The current skeletal muscle NAD^+ salvage model suggests that the NR/NRK pathway is inessential for general maintenance of NAD^+ homeostasis, which is broadly covered through NAM recycling via NAMPT. However, NRKs are is required for extraneous NR and NMN processing (15, 16), and may therefore constitute an auxiliary NAD^+ salvage pathway which is more effective at raising skeletal muscle NAD^+ levels with age and under conditions of metabolic stress. Interestingly, NRK1 is able to fully compensate for the loss of NRK2 in this regard within skeletal muscle, despite almost negligible expression levels (15). However, evidence suggests that NRK2 has skeletal muscle specific roles that stretch beyond that of simply an alternative route to NAD^+. This section will review current knowledge of the NRKs, focusing on the potential importance of NRK2 in skeletal muscle.

1.10.1 Discovery and kinetic properties of the NRKs

The NRK enzymes catalyse the phosphorylation of NR to NMN, and this initial reaction is thought to be rate limiting for the production of NAD^+ from NR (16). The two mammalian NRK isoforms, NRK1 and NRK2, are 57% homologous and are the sole enzymes responsible for phosphorylation of NR to NMN (14, 158). The existence of mammalian NRKs was predicted and subsequently confirmed as a result of observations that NR supplementation could extend yeast lifespan by increasing NAD^+ bioavailability, and thus increased Sir2 activity (14). Both isoforms have a high affinity for NR in the low micromolar range, with

NRK1 having a slightly higher affinity than NRK2 (Table 1-2). NRK1 can utilise both ATP and guanosine triphosphate (GTP) as a phosphate donor while NRK2 is ATP specific (158). Nicotinic acid riboside (NAR) is also a viable substrate for NRK1 and NRK2 and thus constitutes an additional NAD^+ precursor, which is then converted to NAMN and eventually NAD^+ by the same enzymes as with the Preiss-Handler pathway (158). The NRKs are closely related to human uridine/cytidine kinase 2 (UCK2) (158), retaining KM values for both uridine and cytidine in the millimolar range (322). Interestingly, while affinity for cytidine between NRK1 and 2 is comparable, NRK2 has a 10-fold higher affinity for uridine than NRK1 (322).

Table 1-2 – NRK1 and NRK2 enzyme kinetics and substrate specificities. The NRKs have a high affinity for NR and NAR, though NRK2 is unable to utilise GTP as a phosphate donor. Data obtained from Tempel et al., 2007 (158).

Substrate	KM (mM)	Kcat (/S)	Kcat/KM (/S/M)
NRK1:			
NR + ATP	0.088	0.6	6800
NR + GTP	0.068	0.34	5000
NAR + ATP	0.051	0.21	4100
NRK2:			
NR + ATP	0.19	0.75	3900
NR + GTP	30	1.7	57
NAR + ATP	0.063	0.34	5400

To date, many studies into utilising exogenous NR substrate for boosting cellular NAD^+ have been performed while relatively few have sought to establish endogenous roles of the NRK enzymes (323). The critical NAD^+ salvage pathways and dynamics within skeletal muscle have recently been narrowed down (15), with some insight into the roles of NRKs with regards to the NAD^+ metabolome through loss of function models (15, 16). Unlike

NAMPT KO models, global deletion of either or both NRK isoforms simultaneously does not produce a significant phenotype in mice in terms of health, development or the NAD^+ metabolome (15), suggesting that NRK enzymes are inessential for general NAD^+ homeostasis in mammals. However, recent research suggests a role for NRK1 in liver in protection against diet induced pathology (323), suggesting that the NRK pathway could constitute an important auxiliary pathway to NAD^+ under times of metabolic stress.

NRK1 and NRK2 have very different expression patterns throughout mammalian tissues, hinting at divergent tissue specific roles. NRK1 is expressed ubiquitously, while NRK2 is specific to cardiac and skeletal muscle, though still detectable at very low levels in brown adipose tissue and liver (Figure 1-26) (15, 165). The reasons for the muscle specificity of NRK2 remain unclear, though recent evidence suggests that besides simply constituting an additional route to NAD^+, NRK2 may also function as an inducible response to metabolic stress.

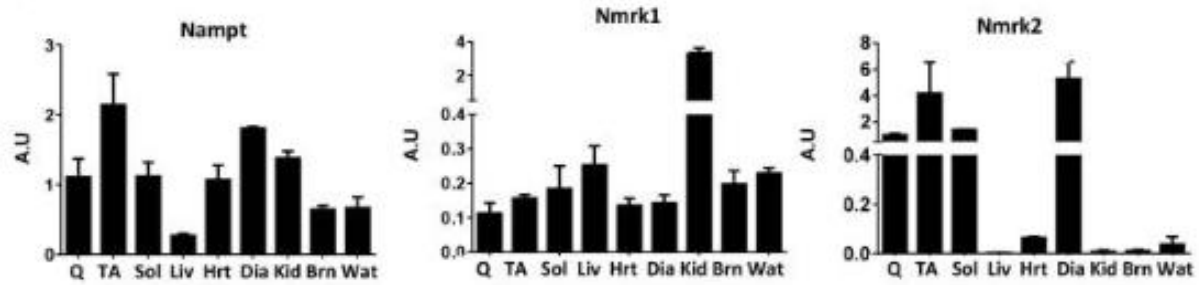

Figure 1-26 – Relative mRNA expression levels of Nampt, Nmrk1 and Nmrk2 across mouse tissues. NAMPT and NRK1 are ubiquitous, while NRK2 is specific to skeletal muscle and cardiac muscle at a lower level. Q: quadriceps; TA: tibialis anterior; Sol: soleus; Liv: liver; Hrt: heart; Dia: diaphragm; Kid: kidney; Brn: brown adipose tissue; Wat: white adipose tissue. Adapted from Fletcher et al., 2017 (15).

1.10.2 NRK2 is induced in response to energetic stress

As well as being a potentially exploitable pathway for exogenous NAD^+ boosting, recent data suggest another role of the NRK pathway in adaptation to redox and metabolic stress under various pathophysiological states. NRK2 was initially discovered to be significantly upregulated in a mouse model of severe myopathy and redox stress (324), with no concurrent upregulation of NRK1 (324, 325). Loss of function of hexose-6-phosphate dehydrogenase (H6PDH) mice, an endoplasmic reticulum (ER) localised enzyme necessary for local NADPH production, exhibit decreased muscular NAD^+ manifesting as mitochondrial dysfunction, depletion of type IIa fibres and intrafibrillar vacuoles (324, 325), with NRK2 being upregulated >60-fold at messenger ribose nucleic acid (mRNA) level. The model was recently revisited to establish functional roles for this induction, and while NR supplementation partially restored NAD^+ homeostasis, no improvements in metabolic or mitochondrial phenotype were observed (325). Double H6PDH/NRK2 KO mice presented significant further NAD^+ depletion but no significant increases in phenotypic severity (325),

implying that while upregulated NRK salvage appears to bolster the NAD^+ pool under severe energetic stress, it is not sufficient to ameliorate the severe phenotype to any extent (325).

NRK2 was also significantly upregulated in injured muscle at 24 hours post injury in a mouse model of lower limb trauma (326), as well as in models of lethal cardiomyopathy where NR supplementation improved lifespan by 50% (327), supporting the hypothesis that NRK2 is upregulated to support NAD^+ biosynthesis under extreme energetic stress. More work in models of dilated cardiomyopathy and cardiac hypertrophy observed a downregulation of NAMPT alongside an upregulation of NRK, and again NR supplementation led to phenotypic improvements (328). It was further established that in cardiac cells, the upregulation of NRK2 occurs in response to signalling via AMPK and PPARα in times of energetic stress (328). This NAD^+ dependent induction has also been observed in skeletal muscle, where inhibition of NAMPT and subsequent depletion of NAD^+ resulted in significant NRK2 upregulation (15). Interestingly, NRK2 was also upregulated in injured dorsal root ganglion neurons where baseline expression levels are typically negligible (329) indicating that this potential role of NRK2 may not be limited to skeletal and cardiac muscle.

A critical observation across these studies is that NRK2 upregulation alone does not raise NAD^+ levels sufficiently to improve physiopathological phenotypes, which could be explained by low (~7 nM) (314) or undetectable endogenous circulating NR levels (164, 314). However, improvements are often noted with exogenous NR supplementation, and a significant albeit phenotypically irrelevant additive depletion of NAD^+ was observed when NRK2 was knocked out alongside H6PDH (325), thus the physiological relevance of this upregulation still remains unclear.

1.10.3 Skeletal muscle NAD^+ salvage, circadian rhythm and NRK2

Intracellular NAD^+ concentrations oscillate in a 24 hour rhythm in many tissues, contributing towards temporal metabolic regulation (330). NAMPT expression is regulated by the mammalian master circadian rhythm regulating transcription factor complex circadian locomotor output cycles kaput:brain and muscle ARNT-like 1 (CLOCK:BMAL1) (331), which is in turn regulated by the activity of the NAD^+ dependent signalling mediator SIRT1 through differential modulation of histone acetylation status (227, 332). This relationship has been well characterised in white adipose tissue (WAT), liver and embryonic fibroblasts, with NAMPT loss of function models exhibiting dysregulated circadian gene expression profiles and abnormal intracellular NAD^+ concentration profiles (332, 333). Such disruption of circadian clock components impairs the coordination of critical cellular processes such as chromatin remodelling, gene expression, protein activity and protein turnover (334, 335). From a metabolic perspective, the resultant improper oscillation of metabolite levels is known to impact metabolic homeostasis and has been implicated in disease states such as obesity, diabetes and cardiovascular disease (335).

Though the NAMPT-SIRT1-CLOCK:BMAL1 interdependency is well characterised, less is known about the circadian regulation of the NRK enzymes. Differential circadian expression of NRK1 has been documented in mouse liver which was disrupted in CLOCK deficient mice (336), but little is known of this in skeletal muscle. Skeletal muscle has its own independent molecular clock system (337) by which processes such as structural remodelling, metabolic status and mitochondrial dynamics are regulated (337). Many of these processes are regulated by transcription factors that are directly influenced by NAD^+ dependent signalling such as PGC-1α (338) and PPAR-γ (339), suggesting that circadian

oscillations in NAD^+ are of great importance to skeletal muscle metabolism. RNA microarray data indicates an oscillating circadian expression profile for NRK2 in mouse skeletal muscle which is not as distinctively observed in NAMPT, implying that the relative contributions of individual salvage routes to NAD^+ bioavailability may be temporally variable (340) (Figure 1-27). NRK2 could therefore constitute an important temporal regulator of skeletal muscle metabolic status.

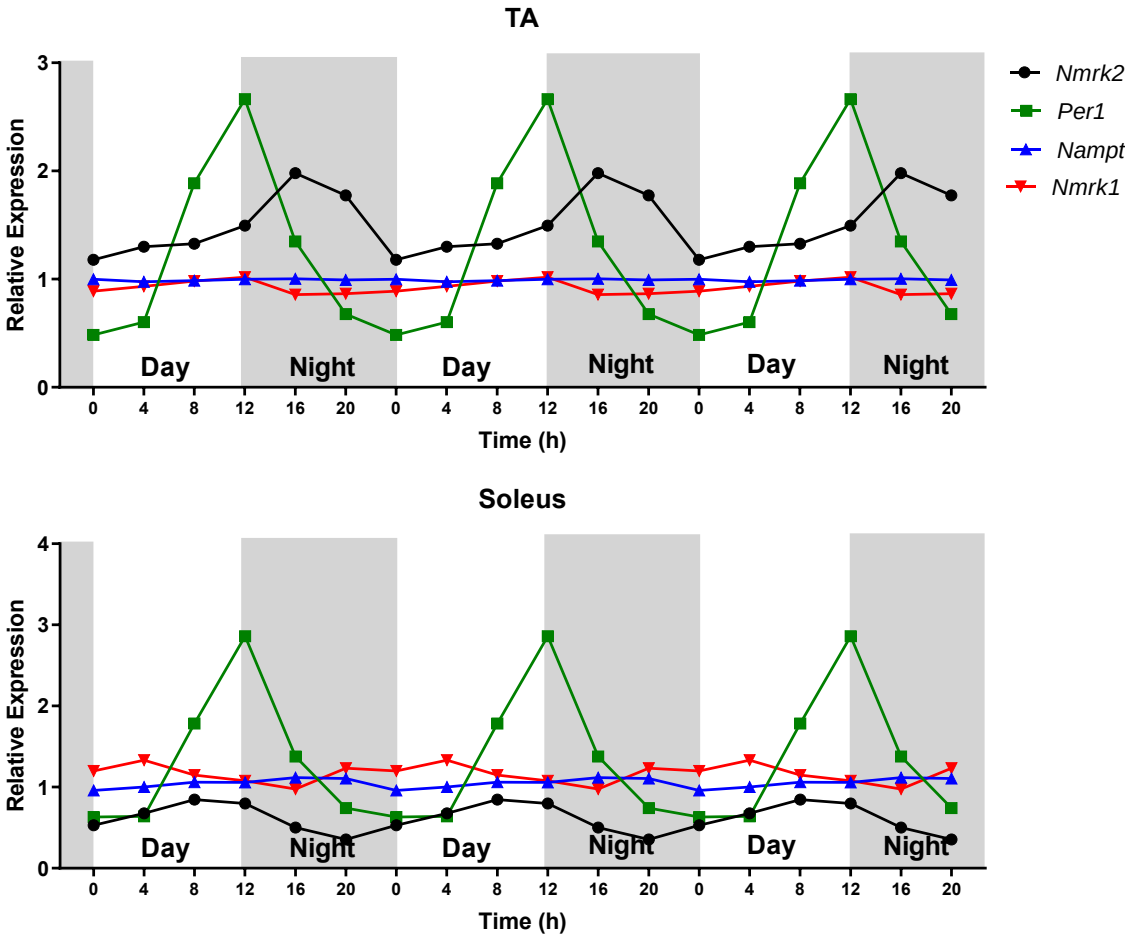

Figure 1-27 – Circadian mRNA Expression profiles of Nmrk2, Nampt, and Nmrk1 alongside the core clock gene Per1 in TA, a predominantly glycolytic skeletal muscle bed, and soleus, a predominantly oxidative muscle. Expression levels of NRK2 oscillate at greater amplitude than Nampt and Nrk1 in both TA and soleus. Data obtained from Dyar et al., 2013 (340).

1.10.4 NRK2 and myogenesis, differentiation and cell adhesion

NRK2 may also play critical roles in musculoskeletal development and differentiation. Prior to its classification as a nicotinamide riboside kinase, a protein homologous to NRK2 was initially identified in the mouse C2C12 myoblast cell line, termed skeletal muscle-specific integrin β1 binding protein (MIBP) (341). The same study identified differential expression patterns where MIBP was strongly expressed at myogenic fusion before being downregulated during differentiation (341), with constitutive overexpression of MIBP preventing fusion and terminal differentiation. Further work established a specific interaction between MIBP and the α7β1 integrin subtype (342), which is a critical modulator of cytoskeletal actin and basement membrane laminin interactions in skeletal muscle (343). Furthermore, a direct effect of MIBP on expression of the focal adhesion protein paxillin and a significant disruption to integrin/laminin binding in MIBP overexpressing C2C12s was identified (342).

Upon the discovery of human NRK2 and its affinity for NR, it was also determined that MIBP is actually a truncated 186 amino acid splice variant of NRK2 which is devoid of enzymatic activity (14). additional studies on the catalytically active zebrafish NRK2 homolog NRK2b reported that specific knockdown of NRK2b affected embryonic somite formation and disrupted myotomic and myotendinous junction (MTJ) actin deposition (344), which was again traced to aberrant integrin/laminin interactions (specifically integrin α6/α7) and paxillin recruitment within the basement membrane. Crucially, further work determined that the phenotype could be rescued through the addition of NAD^+ to the embryonic medium indicating that the NAD^+ salvage activity of NRK2 is important for skeletal muscle cell adhesion (345).

Despite these observations, NRK2 KO mice develop normally and do not exhibit overt muscular abnormality (15). This developmental phenotype could therefore be present in zebrafish due to a lack of alternative NAD^+ salvage routes whilst the NRK salvage route is largely redundant in mice. However, it is intriguing that overexpression of catalytically inactive MIBP in a murine cell line produces a similar effect to the loss of function zebrafish model, suggesting that a delicate balance of temporal NRK2 expression levels during myogenesis could be important Furthermore, MIBP interacts with integrin α7β1 in C2C12s (342). It is therefore possible that MIBP overexpressing cells demonstrated impaired myotube fusion and differentiation due to a stoichiometric imbalance between inactive MIBP and active NRK2, leading to competitive inhibition of NRK2 associating with integrin/laminin complexes thus impairing localised NAD^+ production. Additionally, a recent human study determined that oral NR supplementation induces upregulation of actin filament processing, cell motility and cell adhesion genes in skeletal muscle, suggesting an NR/NRK specific role in these processes (176). These potential roles of NRK2 remain unclear, necessitating further research (17).

1.11 Project rationale

This introduction has served to outline current knowledge of the multi-faceted roles of and routes to NAD^+ as a redox cofactor and signalling molecule, highlighting the importance of NAD^+ in many essential cellular processes. While research into the complex interplay between mechanisms by which NAD^+ is biosynthesised is extensive, the roles of the more recently discovered NRK mediated NR salvage pathways are still not known, particularly within skeletal muscle given its importance to overall metabolic health. Understanding the

links between ageing, decreased NAD^+ bioavailability, metabolic dysregulation and reduced health span is of utmost importance in the increasingly aged, sedentary and obese population of the modern world (312, 313). Robust understanding of how NAD^+ is synthesised and metabolised, alongside the tissue specific consequences of alterations to NAD^+ dependent signalling, is essential to establishing therapeutic strategies for treating NAD^+ linked pathophysiological states and prolonging healthspan with age.

The exact role of NRK2 mediated NAD^+ biosynthesis in skeletal muscle metabolic homeostasis still remains elusive. Recent work has utilised NRK loss of function models to gain better understanding of its role in NAD^+ salvage from exogenous amidated precursors (15, 16). Little is also known about the specific roles of NRK2 itself, such as the physiological relevance of its upregulation under energetic stress, its circadian expression patterns and its hypothesised roles in myogenesis, differentiation and cell adhesion (17, 344, 345). Relatively few in vivo NRK gain of function studies have been carried out, which could offer further insights into such additional proposed roles and the metabolic and physiological relevance of the pathway in skeletal muscle under specific metabolic conditions. The main aims of the project were therefore to ascertain the effects of NRK augmentation on skeletal muscle NAD^+ dynamics and metabolism in response to altered nutrition, exercise, ageing and availability of NR precursor, as well as to characterise other potential roles of NRK2 in skeletal muscle.

1.12 Hypothesis and objectives

It is hypothesised that NRK2 mediated NAD^+ salvage constitutes a critical pathway for the adaptation of skeletal muscle to metabolic stress. Lifetime augmentation of this pathway

may ameliorate age related NAD^+ decline and improve healthspan under ageing and altered nutrition.

The specific objectives of this project are:

- To validate and characterise a skeletal muscle specific NRK2 overexpressing mouse strain under basal metabolic conditions and exercise (Chapter 3).
- To establish the metabolic and physiological outcomes of lifetime skeletal muscle NRK/NR salvage pathway augmentation in aged mice, with or without chronic oral NR supplementation (Chapter 4).
- To interrogate potential alternative roles of NRK2 in skeletal muscle structure and function (Chapter 5).

CHAPTER 2 – MATERIALS AND METHODS

Unless otherwise stated, all reagents described were obtained from Sigma-Aldrich (Poole, Dorset, UK).

Specific modifications and additional methods are found within corresponding chapters.

2.1 Animal care

Mice were housed in standard IVC cages (Green Line IVC Sealsafe PLUS, Techniplast, USA), with standardised sawdust, paper bedding and a red tinted house for shelter, in sex and litter matched groups of 2-4. Mice were fed ad libitum with standard rodent chow (EURodent Diet 14%, Labdiet, St Louis, Missouri, USA) and kept on a 12:12 light/dark cycle (06:00 lights on, 18:00 lights off).

2.2 Mouse models

The mouse model primarily used for this study utilised the Cre-Lox recombination system, by which somatic gene recombination was introduced. The system encompasses two key components; LoxP sites, which are 34 base pair (bp) long DNA sequences consisting of two 13 bp palindromic sequences flanking an 8 bp long spacer region, and Cre recombinase, an enzyme which recognises and splices these LoxP sites (346). A gene or region of interest that is flanked with LoxP sites will be deleted, inverted or translocated, depending on the position and/or orientation of the LoxP sites (347, 348).

2.2.1 NRK2.Tg mice

The nicotinamide riboside kinase 2 gene is abbreviated to Nmrk2 while the protein product is termed NRK2. Skeletal muscle specific NRK2 overexpressing mice are hereafter referred to as NRK2.Tg mice.

NRK2.Tg mice possess an inactive (conditional) form of the transgenic Nmrk2 allele, which is spliced into the ROSA26 locus on chromosome 6 of the mouse genome (Figure 2-1). This inactivity is maintained by a LoxP flanked STOP codon downstream of the constitutively active CAG promoter, inhibiting transcription of the Nmrk2 transgene and thereby resulting in a phenotypically wild type (WT) mouse (Figure 2-1). The LoxP sites are orientated in the same direction, and therefore in the presence of Cre recombinase the STOP codon is deleted, resulting in constitutively active transcription of the Nmrk2 transgene and constitutive translation of NRK2 protein (Figure 2-1). Hemizygous NRK2.Tg mice were developed by Taconic Biosciences (Rensselaer, New York, USA) on a C57BL6/NTac background.

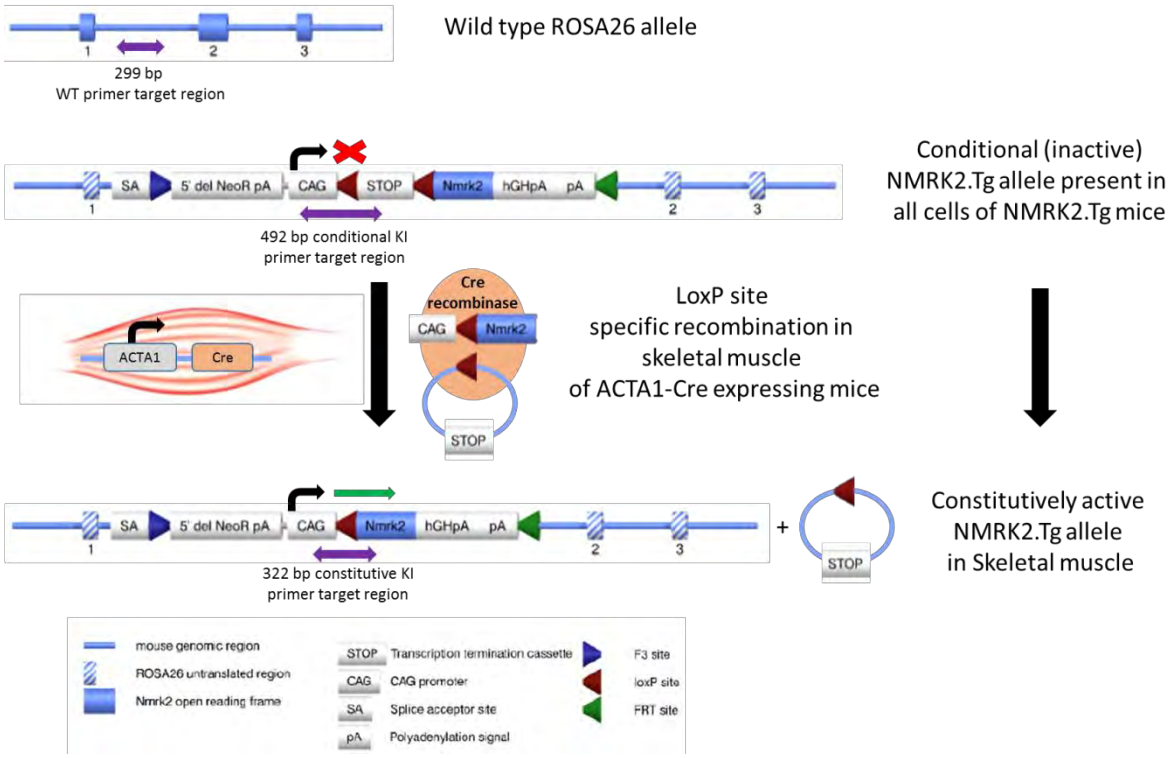

Figure 2-1 – The molecular basis of Cre/LoxP recombination in the skeletal muscle specific NRK2 overexpressing mouse model and genotyping polymerase chain reaction (PCR) loci. In the presence of Cre recombinase, the LoxP flanked stop codon is removed, allowing for constitutive overexpression of the NRK2 transgene through the CAG promoter. The ROSA26 reaction will only proceed if the transgenic construct is absent, while the transgenic nmrk2 cassette detection reaction will only produce a band if the cassette is present.

2.2.2 ACTA1-Cre mice

Cre recombinase is a 38 kDa tyrosine recombinase enzyme derived from the P1 bacteriophage (349). It mediates site specific recombination events akin to the mechanism of type I topisomerases, and has a high affinity for LoxP sites (350). The transgenic NRK2.Tg strain must be crossed with a transgenic Cre recombinase expressing strain to produce an NRK2 overexpressing mouse. In this case, NRK2.Tg mice were crossbred with a transgenic mouse strain possessing a form of Cre recombinase gene that is under the control of the skeletal muscle actin (Acta1) promoter. Therefore Cre recombinase is only transcribed in

tissues where the Acta1 gene is active, resulting in muscle specific overexpression of NRK2 (Figure 2-2).

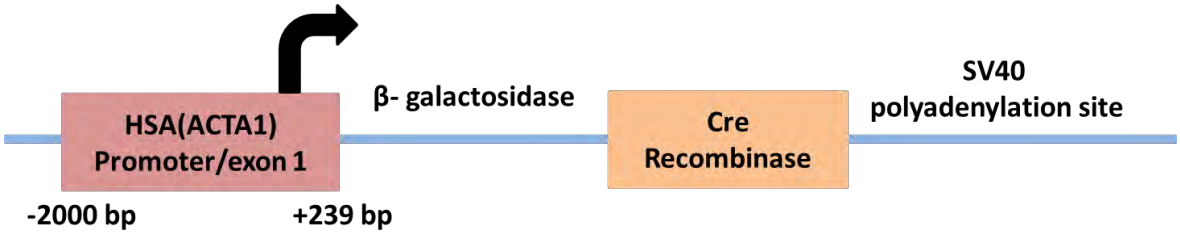

Figure 2-2 – The transgenic Cre recombinase construct. The Cre recombinase gene is under the control of the Acta1 promoter which is only active within striated muscle, ensuring muscle specific expression.

Hemizygous FVB.Cg-Tg(Acta1-cre)79Jme/J mice were obtained from Jackson Laboratory (Bar Harbor, Maine, USA) on a C57BL6/J background (JAX stock #006139). To create the transgene, the promoter and first exon of the HSA gene from -2000 to +239 relative to the transcription start site was isolated from the pHSA2000CAT plasmid (351). A second host pGS5 plasmid contained the rabbit β-globin intron, Cre recombinase transgene, SV40 polyadenylation signal and a SalI-HindIII-SalI linker region inserted in the SalI restriction site of pGS5. The 2339 bp HindIII restriction fragment of the pHSA2000CAT plasmid was cloned into the HindIII site of the pGS5 plasmid. Following this, the PGS5 construct was then injected into zygote pronuclei of C57BL/6JxSJL F1 mice, and embryos replanted into pseudopregnant CD1 foster mice (352). Using a β-galactosidase reporter assay, it was determined that the mouse exhibits uniform and robust Cre recombinase expression in skeletal muscle throughout the lifetime of the animal, including in skeletal muscle cells of embryonic somites and also sporadically within cardiomyocytes, without any expression in non-striated muscle (352). The strain was originally referred to as HSA-Cre79, but is hereafter referred to as ACTA1-Cre (352).

2.2.3 NRK2.Tg/ACTA1-Cre target animal breeding strategy

All animals used for experiments were derived from the F1 NRK2.Tg/ACTA1-Cre crossed background and were either Nmrk2.Tg+/- (functionally wild type control animals hereafter referred to as WT) or Nmrk2.Tg+/-/Acta1-Cre+/-. These target animals were achieved through an in house breeding strategy outlined in Figure 2-3. Mice inherited alleles at predicted Mendelian frequencies and were born at the expected 50:50 male:female ratio.

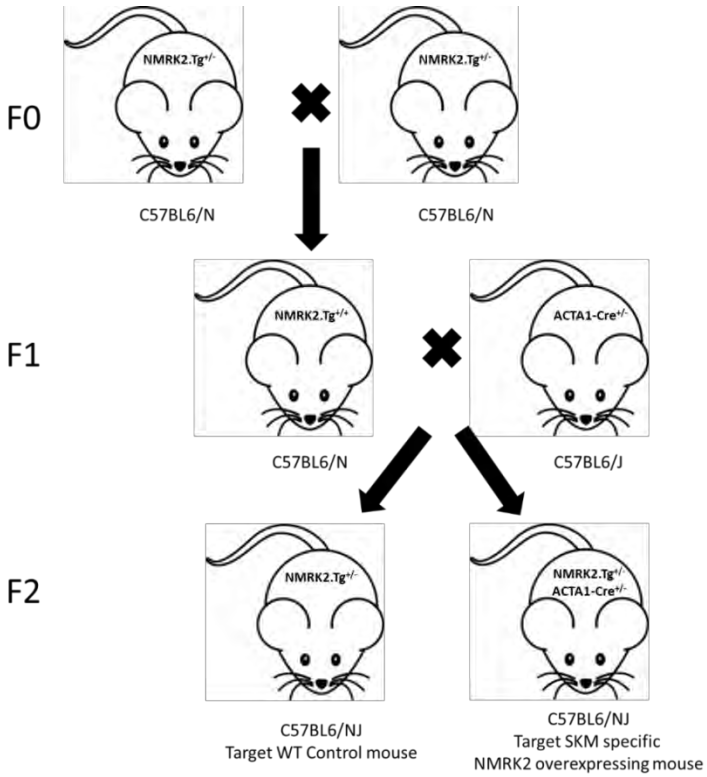

Figure 2-3 – Breeding strategy for NRK2.Tg/ACTA1-Cre target animals. Hemizygote NMRK2.Tg mice were crossed to produce a heterozygote NMRK2.Tg mouse, which was then crossed with a hemizygous ACTA1-Cre mouse to generate hemizygous floxed or NRK2 overexpressing animals.

2.2.4 Mouse genotyping – DNA extraction

Mice were genotyped before experimentation to verify the presence of the conditional Nmrk2.Tg allele and identify if the mouse was positive or negative for the Acta1-Cre

construct. DNA was extracted from ear clips in the first instance or tail clips for verification after tissue collection. Approximately 5 mg tissue was placed into 200 µl tail lysis buffer (100 mM Tris HCl (pH 8.5), 5 mM ethylenediaminetetraacetic acid (EDTA), 300 mM NaCl) with 5 µl proteinase K (Promega, Wisconsin, USA) to digest proteins and release DNA. Samples were incubated at 55 ^{o}C in a dry heat block to optimise proteinase K activity overnight before incubation at 95 ^{o}C for 1 hour to denature the proteinase K enzyme prior to polymerase chain reaction (PCR).

2.2.5 Mouse genotyping - PCR

PCR is a well described technique by which DNA can be amplified exponentially from a small original template. DNA Samples are heated to 95^{o}C to denature to single strands and the temperature then lowered to approximately 60 ^{o}C to allow primers complimentary and unique to the sense (reverse) and antisense (forward) strands of a gene of interest to anneal to the original DNA template. The reaction temperature is then increased to 72 ^{o}C where oligonucleotides are extended, starting at the sites of primer binding, by Taq DNA polymerase activity in the presence of Mg2+ as an enzymatic cofactor and free deoxynucleotide triphosphate (dNTP) “building blocks”. These heating, annealing and extension steps are cycled multiple times, generating an exponential increase in template copies as cycles progress until sufficient product is produced for detection.

PCR Reactions were set up for each sample using 10 µl 2x BioMix Red (Bioline, London, UK), 7 µl nuclease free water (Promega, Wisconsin, USA), 0.5 µl of each relevant forward and reverse primer (10 pmol/µl final concentration) and 1 µl DNA template, giving an overall reaction volume of 20 µl. All primer sequences were obtained from Taconic

Biosciences (USA) and synthesised by Alta Bioscience (Birmingham, UK). Primer sequences and expected product sizes are detailed in Table 2-1. PCR reactions were performed in a thermal cycler (Applied Biosystems GeneAmp® PCR System 2700, ThermoFisher Scientific, Massachusetts, USA), for which the parameters are described in Table 2-2. NMRK2.Tg WT (intact ROSA26 locus) and conditional NMRK2.Tg allele PCR reactions were performed in duplex in the same reaction tubes as no cross reactions were observed.

Table 2-1 – NRK2.Tg/ACTA1-Cre genotyping PCR primer sequences.

Primer	**Sequence (5'>3')**	**Product Size (base pairs)**
ROSA26 WT forward	CTCTTCCCTCGTGATCTGCAACTCC	299
ROSA26 WT reverse	CATGTCTTTAATCTACCTCGATGG	
NMRK2.Tg conditional allele forward	TGGCAGGCTTGAGATCTGG	492
NMRK2.Tg conditional allele reverse	CCCAAGGCACACAAAAAACC	
Cre Forward	GCTGCCACGACCAAGTGACAGCAA	402
Cre Reverse	GTTATTCGGATCATCAGCTACACC	

Table 2-2 – NRK2.Tg/ACTA1-Cre genotyping PCR reaction conditions.

PCR Cycle Step	Temperature (°C)	Time (sec)	
Initial Denaturisation	95	300	
Denaturisation	95	30	x 38 cycles (ROSA26, conditional and constitutive reactions) x 35 cycles (Cre recombinase reaction)
Annealing	60 (ROSA26, conditional and constitutive reactions) 57 (Cre recombinase reaction)	30	
Extension	72	60	
Final Extension	72	600	
Final Hold	4	∞	

2.2.6 DNA gel electrophoresis

Amplified DNA fragments are separated according to size through propulsion through an agarose gel via electrophoresis. Agarose gel is porous, allowing DNA fragments to travel through it when an electric current is applied across the gel. DNA has an overall negative charge and will move towards the positive electrode. Smaller fragments are able to travel further over the same voltage and time, allowing for separation of different sized fragments into “bands” quantified through comparison with a DNA “ladder” of known fragment sizes.

18 µl of PCR product was ran on a 2% agarose/Tris-Borate EDTA (TBE) gel with 1:10,000 GelRed (Biotum, USA) at 100 V for 45 minutes alongside 5 µl 100 base pair DNA ladder (New England Biolabs, Massachusetts, USA). Gel bands were visualised using a Syngene G-Box and GeneSnap software (Syngene International Ltd, India). Mouse genotype

was determined by the presence or absence of bands at expected sizes as indicated in Table 2-1 and represented in Figure 2-4.

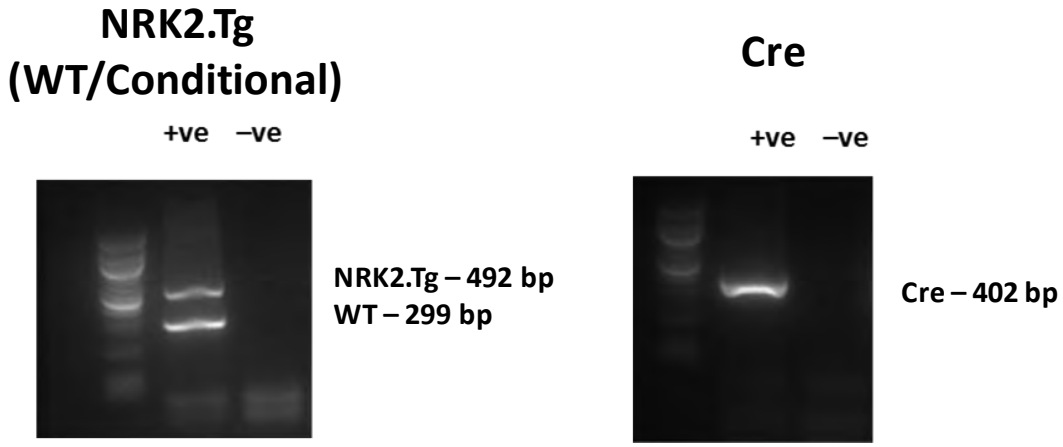

Figure 2-4 – Example images of Wild type (WT), NRK2.Tg and Cre recombinase bands.

2.3 Mouse tissue collection

Routinely, mice were sacrificed via cervical dislocation and death confirmed by cessation of heartbeat. Tissues were immediately harvested, placed into a 2 mL cryotube, immediately snap-frozen in liquid nitrogen and stored at -80 ^{o}C. Where skeletal muscle beds and organs were weighed, one hindlimb was dissected quickly and tissues were instantly snap frozen followed by the heart and liver to minimise biological degradation of samples for metabolomics and ribonucleic acid (RNA) analysis. Muscles on the other hindlimb were dissected afterwards and weighed before being snap frozen.

2.3.1 Tissue preparation – pulverising and weighing

Tissue samples were stored in cryotubes (Starsedt, Germany) at –80 ^{o}C until use. For maximum experimental accuracy and minimum biological degradation, the tissue preparation method was designed to provide the most accurate tissue weight

measurements without thawing. When required, samples were withdrawn and placed onto dry ice. A polystyrene box was filled with liquid nitrogen and all equipment (pestle and mortar, sample tubes, spatula, tweezers, micro spoon and metal funnel) was placed in the box until temperature equilibration. Frozen tissue was pulverised into a fine powder using a pestle and mortar before being poured back into the cold cryotube. Equipment was cleaned with 70% ethanol between samples to avoid cross-contamination.

To weigh tissue samples, sample tubes were pre-cooled in liquid nitrogen on a plastic rack. The cold tube was placed on a calibrated microbalance (Accuris Instruments Analytical Series W3100-210, Dublin, Ireland) and tared. The required amount of tissue was weighed and the sample quickly returned to liquid nitrogen.

2.4 Constitutive allele detection

2.4.1 DNA extraction and PCR

Where higher purity DNA templates were required as for detection of the constitutive Nmrk2.Tg allele in skeletal muscle, total genomic DNA was extracted from ~20 mg tissue using a QIAGEN DNeasy Blood and Tissue Kit (QIAGEN, Germany). DNA was eluted in 30 µl buffer AE (10 mM Trizma-chloride (Tris-Cl), 0.5 mM EDTA pH 9.0). Concentration and purity was determined using a Nanodrop© ND-1000 (Labtech International, Cambridge, UK). 1 µl nuclease free water (NFW) was first measured as a blank, after which 1 µl DNA sample was measured for concentration and purity. Samples returning a 260/280 nm ratio between 1.8 and 2.0 were sufficiently pure. Extracted DNA samples were stored at -20 ^{o}C prior to PCR. PCR was performed according to Table 2-2 using primers detailed in Table 2-3.

Table 2-3 – NRK2.Tg/ACTA1-Cre constitutive allele validation PCR primer sequences.

Primer	Sequence (5'>3')	Product Size (base pairs)
NMRK2.Tg constitutive allele Forward	TGGCAGGCTTGAGATCTGG	322
NMRK2.Tg constitutive allele Reverse	TCCCACTGTTTAAAGCCGTC	

2.5 RNA analysis

Extraction and quantification of RNA is a method by which gene expression levels is determined, because transcription of messenger RNA (mRNA) is the first step towards production of a functional protein product. mRNA is single stranded and inherently unstable, thus extracted RNA must be reverse transcribed to complimentary DNA (cDNA) before amplification and analysis.

2.5.1 RNA extraction

Approximately 20 mg frozen tissue was placed into 800 µl TRI-Reagent™ RNA isolation reagent in a 2 ml microfuge tube along with a 5 mm steel bead (QIAGEN, Germany). Samples were placed into a cassette cooled to 4 ^{o}C and tissue was homogenised using a TissueLyser II (QIAGEN, Germany) by shaking at 30 cycles per second for 2 minutes. After homogenisation, 160 µl chloroform was added and the mixture vortexed for 10 seconds before being incubated at room temperature (RT) for 5 minutes. The mixture was centrifuged at 12000 x g for 10 minutes at 4 ^{o}C and the aqueous RNA-containing phase was transferred to a new tube. Isopropanol (400 µl) was added to the isolated aqueous phase and incubated at -20 ^{o}C for 30 minutes to allow for RNA precipitation before centrifugation at 12000 x g for 10

minutes at 4 ^{o}C to pellet RNA precipitate. The supernatant was removed and the RNA pellet washed with 800 µl 75% ethanol, vortexed and centrifuged at 12000 x g for 5 minutes at 4 ^{o}C. Ethanol was removed and the pellet air dried at room temperature for 10 minutes before resuspension in 30 µl NFW. RNA concentration and purity was determined through spectrophotometry using a Nanodrop© ND-1000 (Labtech International, Cambridge, UK). NFW (1 µl) Samples returning a 260/280 nm ratio of between 1.8 and 2 were sufficiently pure. Extracted RNA samples were stored at -80 ^{o}C prior to reverse transcription.

2.5.2 Reverse transcription

RNA template was diluted to a concentration of 100 ng/µl, of which 10 µl was used per sample for a total of 1 µg RNA. A High Capacity Reverse Transcription Kit (ThermoFisher Scientific, Massachusetts, USA) was then used to reverse transcribe the RNA to cDNA. A reverse transcription master mix was made with reagent quantities as listed in *Table 2-4*, of which 10 µl was added to the 10 µl RNA samples. Samples were placed in a thermal cycler (Applied Biosystems GeneAmp® PCR System 2700, USA) to the specifications detailed in Table 2-5.

Table 2-4 – Reverse transcription reaction composition.

Reagent	Volume per sample (µl)
Nuclease free Water	3.2
Reverse Transcription Buffer	2
Random Primers	2
MultiScribe© Reverse Transcriptase	1
RNase Inhibitor	1
Deoxynucleotide (dNTP) mix	0.8

Table 2-5 – Reverse transcription PCR reaction conditions.

Temperature (°C)	Time (min)
25	10
37	120
85	5
4	∞

2.5.3 Quantitative realtime PCR (qPCR)

Quantitative realtime PCR (qPCR) is a method by which gene expression can be analysed. qPCR differs to normal PCR in that the amount of amplified DNA is quantified with every cycle as the PCR protocol progresses. Several methods of qPCR are available, all involving real time quantification of a signal proportional to amplified DNA levels. When performed on cDNA transcribed from mRNA and compared with a reference gene which is expressed

stably across all samples, highly sensitive quantification of targeted gene expression levels can be obtained.

2.5.4 qPCR – TaqMan probes

TaqMan™ probes (ThermoFisher Scientific, USA) are oligonucleotides with 5'-3' regions that are complimentary to the gene of interest. A unique donor fluorophore and an acceptor fluorophore, or quencher, are conjugated to the 5' and 3' ends of the oligonucleotide respectively. When intact, photons emitted by excitation of the donor fluorophore are absorbed by the proximally located quencher due to the concept of fluorescence resonance energy transfer (FRET). Upon probe hybridisation and extension, the probe is cleaved by Taq polymerase 5' exonuclease activity, releasing the donor fluorophore into solution eliminating the quenching effect and allowing for detection of the fluorescent signal. A specific fluorescence signal directly proportional to the amount of DNA amplified is generated and used for quantification (Figure 2-5A).

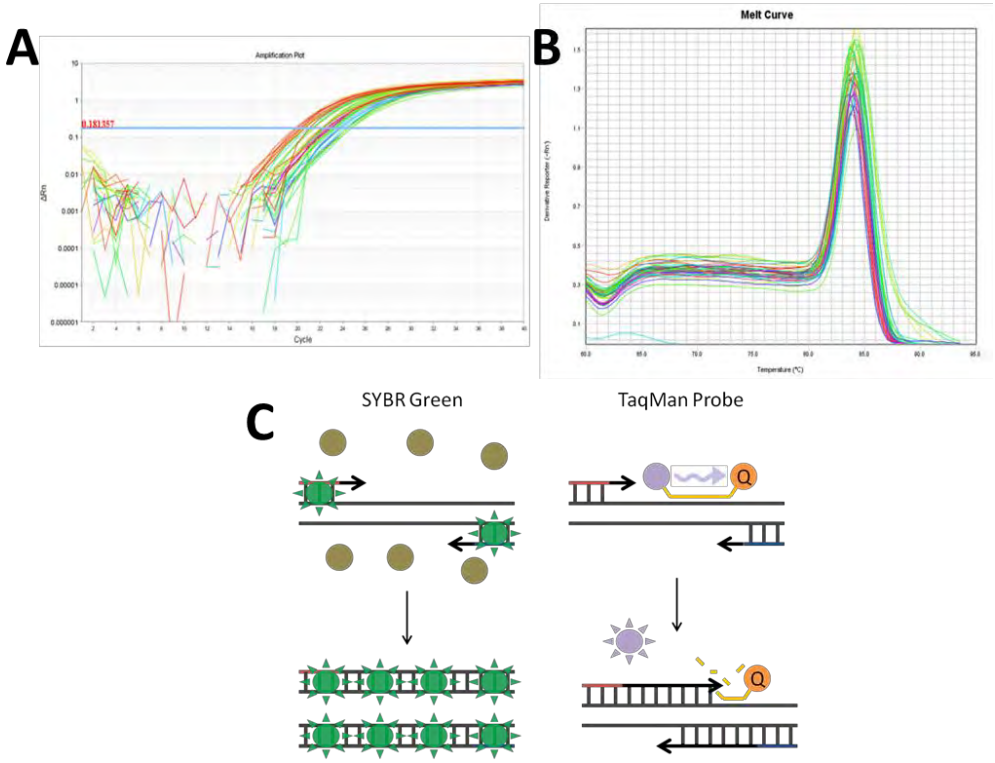

Figure 2-5 – Quantitative PCR output curves and molecular mechanisms. A. Example of a qPCR amplification plot. Fluorescence signal rises with each cycle which is represented on a logarithmic scale. The threshold value is set at the point of exponential replication for all samples. B. Example image of a SYBR green melt curve. A single peak is present, indicating a viable primer pair. C. Diagrammatic representation of SYBR green vs. TaqMan quantification methods. SYBR green dye intercalates with dsDNA and fluoresces, with fluorescent signal being proportional to dsDNA abundance. In contrast, TaqMan probes release a fluorophore into the reaction mixture upon destruction of the probe by DNA polymerase.

Assay on Demand 6-carboxy-fluorsciein (FAM)/6-carboxylate-tetramethyl-rhodamine (TAMRA) probes (ThermoFisher Scientific, Massachusetts, USA) were used in a reaction volume of 10 µl using 5 µl 2x TaqMan Universal PCR Mix (ThermoFisher Scientific, Massachusetts, USA), 3.5 µl NFW, 0.5 µl probe and 1µl cDNA template. Reactions were performed in duplex. Cycle threshold (cT) values were normalised to a ribosomal RNA subunit 18s or glucuronidase beta (GUSB) VIC/TAMRA endogenous control (ThermoFisher Scientific, Massachusetts, USA). For initial mouse characterisation, 18s was used as a reference gene because the cT values were tight between samples. However, this was not the case for the aged cohort, in which there was significant variation. GUSB was instead used

as there was no significant variation between samples. qPCR was performed using an ABI7900HT system (ThermoFisher Scientific, Massachusetts, USA) at 95 ^{o}C for 10 min then 40 cycles of 95 ^{o}C for 15 s and 60 ^{o}C for 1 min. Data was collected as cT values from which ΔcT values were calculated relative to the reference gene and normalised to arbitrary units.

2.5.5 qPCR – SYBR Green

Due to difficulties with the NRK2 TaqMan probe, an alternative method of qPCR was utilised for analysis of NRK2 expression levels in SYBR Green (ThermoFisher Scientific, Massachusetts, USA). SYBR Green qPCR mastermix contains a dye which is inert while in solution but fluorescent when intercalated with double stranded DNA (dsDNA). As the amount of dsDNA in the sample increases, more dye is incorporated resulting in a stronger fluorescent signal. With every cycle, total fluorescence is measured which is proportionate to the amount of dsDNA in the sample allowing for real time quantification of PCR product (Figure 2-5C). Unlike commercially optimised TaqMan probes which contain primers and probe all in one for a given gene of interest, the SYBR green qPCR method requires addition of forward and reverse primers.

A major obstacle in SYBR Green accuracy is specificity of primers to the gene of interest. Some primer sets may amplify nonspecific areas of the transcriptome alongside the intended region, resulting in the formation of two different dsDNA products and confounding results due to nonspecific signal amplification. An extra step is included on the SYBR Green qPCR reaction to detect this, where a DNA heat dissociation curve is performed after amplification is complete. When heated, dsDNA denatures into single stranded DNA (ssDNA). The specific temperature at which this occurs is dependent on base composition

and fragment size. By incrementally increasing temperature and observing fluorescence levels throughout, the point at which a dsDNA product of given size and composition denatures can be identified through a sudden drop in fluorescence (Figure 2-5B). If this occurs more than once, a nonspecific duplex product is also being amplified and the reaction must be redesigned. The optimised singleplex primer set is detailed in Table 2-6.

Table 2-6 – Optimised Nmrk2 SYBR green forward and reverse primer sequences.

Primer	**Sequence (5'>3')**	**Product Size**
NRK2 1.1 Forward	AAACTCATCATAGGCATTGGAGG	~620 bp
NRK2 4.1 Reverse	CGGGGACTTCATGCCATCTAA	

Reactions were performed to 10 µl volume and in duplex. Each reaction contained 5 µl 2x SYBRGreen™ mastermix, 0.5 µl forward and 0.5 µl reverse primer (10 pmol/µl final concentration), 3 µl NFW and 1µl cDNA template. The same PCR thermocycler settings were used as in section 2.2.4. Denaturisation, annealing and extension steps were cycled 33 times, followed by a dissociation curve protocol upon completion of the run.

2.6 Protein analysis

Protein was extracted from tissue samples and analysed using Western blotting to assess sample protein expression levels. Western blotting is a well-established technique where whole protein lysates are separated on basis of size using gel electrophoresis, followed by immunodetection of proteins of interest. Cell or tissue samples are lysed and homogenised in a strongly reducing buffer, which denatures protein secondary and tertiary structures

through disruption of disulphide bonds, and sodium dodecyl sulphate (SDS) which bestows a uniform negative charge across denatured proteins to ensure that their electrophoretic migration rate is influenced by molecular mass only. Separated proteins are transferred to a membrane which is incubated with a primary antibody specific to the protein of interest, followed by a secondary horseradish peroxidase (HRP) conjugated antibody specific to the primary. Addition of electrochemiluminescence (ECL) substrate results in a localised chemiluminescent signal proportional to the size and intensity of the protein band which is captured using x-ray film. Though Western blotting is a qualitative method, semi-quantitative analysis can be performed on band size and intensity.

2.6.1 Polyacrylamide gel preparation

Acrylamide gels (12%) were made in house using Bio-Rad gel casting equipment to a thickness of 1.5 mm. Table 2-7 specifies reagents used per gel.

Table 2-7 – 12% polyacrylamide gel composition.

Reagent	Stacking Gel	Resolving Gel
30% Protogel™ Acrylamide solution (Geneflow, Lichfield, UK) (ml)	0.6	4
4x Protogel™ Stacking or Resolving Buffer (Geneflow, Lichfield, UK) (ml)	1.25	2.5
Double distilled water (ddH_2O) (ml)	2.6	3
Tetramethylethylenediamine (TEMED) (µl)	15	10
1.5% Ammonium Persulfate (APS) (ml)	0.2	0.5

Stacking and resolving gel mixes were made by mixing all reagents with APS added last to initiate acrylamide polymerisation. Resolving gels were prepared first and poured into the casts followed by a layer of 70% ethanol to ensure a level top edge before incubation for 30 minutes at RT until fully polymerised. Stacking gel was then added to the top of the set resolving gel and a 10 well comb inserted before incubation for 30 minutes at RT. Gels were stored hydrated with running buffer (0.1 M Tris pH 7.4, 0.1 M glycine, 0.1% w/v SDS) at 4 ^{o}C until use.

2.6.2 Protein extraction and quantification

Tissue was manually homogenised in a 1.5 ml microfuge tube and 250 µl ice cold radioimmunoprecipitation assay (RIPA) extraction buffer (50 mM Tris HCl [pH 8], 150 mM NaCl, 1 % w/v Nonidet P-40 (NP40), 0.5% w/v sodium deoxycholate, 1 mM EDTA and 0.1% w/v SDS) supplemented with 1 protease and phosphatase inhibitor Tablet (ThermoFisher Scientific, Massachusetts, USA) per 10 ml RIPA buffer. Homogenised samples were freeze-thawed twice on dry ice to ensure thorough lysis, then vortexed for 5 seconds and centrifuged at 13,000 x g at 4°C for 10 minutes to pellet debris.

Protein concentration of the extracted lysate was determined via DC™ Protein Assay (Bio-Rad, California, USA) using bovine serum albumin (BSA) standards in RIPA buffer ranging from 0-12.5 mg/ml. Samples and standards were measured in duplicate on a clear flat bottomed 96 well plate with 5 µl standard or sample combined with 25µl of BioRad protein assay reagent A (supplemented with 20µl of reagent 5 per 1ml of reagent S) followed by 200 µl reagent B. The plate was incubated for 15 minutes at RT then absorbance measured at 750 nm using a Victor3 1420 Multilabel Counter (Perkin Elmer, Massachusetts, USA). Sample lysate protein concentrations were then determined by extrapolation from a standard curve plotted from standard measurements.

2.6.3 Lysate preparation and immunoblotting

Protein samples were made to a concentration of 30 µg/µl. Laemmli buffer (5 µl, 200 mM Tris-HCl [pH 6.8], 50% glycerol, 12.5% β-mercaptoethanol, 10% SDS, 0.02% bromophenol blue) was added and made up to 20 µl with dH_2O, then heated to 98 ^{o}C for 3 minutes before cooling at 4 ^{o}C for 10 minutes. Polyacrylamide gels were placed into the gel running apparatus (Bio-Rad, California, USA) which was filled with running buffer (0.1 M Tris pH 7.4, 0.1 M glycine, 0.1% w/v SDS). Protein lysates were loaded into wells (15 µl), alongside 7 µl protein ladder (New England Biolabs, Massachusetts, USA). Gels were electrophoresed at 120 V for 90 minutes or until dye front termination. Separated proteins were then transferred to a nitrocellulose membrane using an iBlot (Invitrogen, California, USA) and ponceau stain was used to visualise the protein bands and check quality of transfer. Phosphate-buffered saline (PBS) with 0.5% w/v Tween 20 (PBS-T) was used for all subsequent membrane washes. The membrane was blocked to prevent nonspecific antibody

binding with 5% w/v BSA in PBS-T, then washed and primary antibody added to relevant membrane sections in PBS-T and incubated at 4 ^{o}C on a gentle shaker overnight. Membranes were washed once every 15 minutes four times and species appropriate secondary HRP - conjugated antibodies (Dako Laboratories, Denmark) were added at 1 in 10,000 in PBS-T and incubated for 2 hours on a gentle shaker at RT. Membranes were washed once every 15 minutes four times and then exposed to ECL substrate (GE Amersham, Buckinghamshire, UK) for 5 minutes at RT. Blue x-ray film was exposed to the membranes using a developing cassette in a dark room for the required exposure time and developed (Xograph compact X4, Xograph Healthcare, UK).

2.7 NAD$^+$/NADH quantification

NAD$^+$/NADH concentrations were determined using a commercially available colorimetric NAD$^+$/NADH quantification kit (BioVision, California, USA). The assay uses a cycling enzyme that catalyses the conversion of NAD$^+$ to NADH before quantifying NADH levels. When NADH developer reagent is added, sample colour intensity is directly proportional to total NADH present (Figure 2-6). Total NAD$^+$/NADH levels are determined by the addition of the cycling enzyme to unmodified samples, while NADH levels are determined by heating the samples to 60 ^{o}C for 30 minutes before cycling, which destroys all NAD$^+$ but leaves NADH intact. NAD$^+$ levels were determined by subtracting the NADH value from the total NAD$^+$/NADH value.

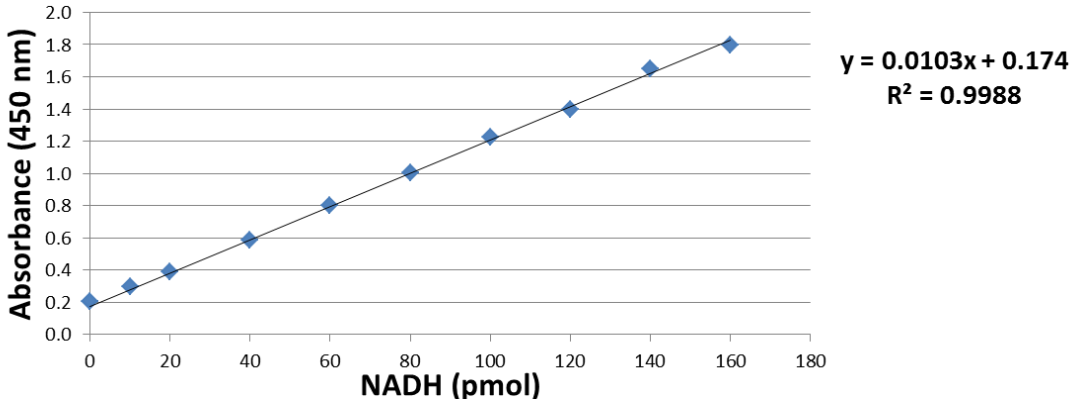

Figure 2-6 **– Example standard NADH curve for analysis of results generated using the NAD$^+$/NADH Quantitation Kit (Biovision, California, USA).**

All steps were performed on wet ice unless otherwise stated. Approximately 10 mg (TA, quadriceps) or 5 mg (soleus) tissue was homogenised in 400 µl NAD$^+$/NADH extraction buffer by shaking on a TissueLyser II (QIAGEN, Germany) at 30 cycles per second for 2 minutes. Homogenised samples were freeze thawed twice on dry ice lysis before a 10 second vortex and centrifugation at 14, 000 x g for 5 minutes at 4 ^{o}C. Supernatant (200 µl) was transferred into two separate sample tubes. The NADH sample was incubated at 60 ^{o}C in a dry heat block for 30 minutes to decompose NAD$^+$. For TA and quadriceps, total NAD samples were diluted 1 in 10 and NADH samples 1 in 4 with extraction buffer, while soleus samples were diluted 1 in 5 and 1 in 2 respectively. 50 µl diluted total NAD and NADH for was loaded onto a flat bottomed clear 96 well plate in duplicate, along with NADH standards of known concentration between 0-160 pmol in duplicate from which the standard curve was calculated (Figure 2-6). The NAD$^+$ cycling enzyme was reconstituted and 2 µl enzyme and 98 µl cycling buffer was loaded per sample. The plate was incubated at room temperature for 10 minutes to allow for full NAD$^+$ cycling to NADH before addition of 10 µl NADH developer per well. The plate was incubated at RT for 30 minutes – 2 hours for to developer to take effect. The plate was read every 30 minutes and the best incubation time

was selected for analysis on the basis of standard curve linearity without signal saturation.

Absorbance measurements at 450 nm were obtained using a Wallac Victor3 1420 Multilabel plate reader (Perkin Elmer, Massachusetts, USA). The calculated NAD^+ and NADH values were normalised to sample protein concentration to control for variation in tissue volume between samples, determined with the DC™ Protein Assay described in section 2.6.2 on the unheated total NAD^+/NADH samples.

2.8 High resolution respirometry

Respirometry is a method for quantifying mitochondrial function. The most common methods involve measuring oxygen flux in cells or tissue samples, where oxidative capacity can be determined as a function of oxygen consumption over time. Respirometry was performed using an OROBOROS Oxygraph-2k (O2k) system (OROBOROS Instruments, Innsbruck, Austria). The O2k utilises a highly sensitive polarographic O_2 flux measurement system to determine the oxidative capacity of milligram sized samples of tissue, cell suspensions or isolated mitochondria. A higher rate of oxygen flux implies a greater rate of oxidative phosphorylation, as more oxygen is required at any given time as the final electron acceptor. Alternative respiratory states are induced by incubating samples with combinations of respiratory substrates and mitochondrial complex inhibitors, allowing for thorough interrogation of the molecular machinery critical to oxidative phosphorylation (353). The HRR protocol on permeabilised muscle fibres was derived and adapted from Doerrier et al., 2018 (354).

2.8.1 Tissue preparation

Mice were culled via cervical dislocation and TA and soleus muscles immediately extracted and placed into ice cold biopsy preservation medium (BIOPS – 2.77 mM calcium-potassium-egtazic acid [CaK_2EGTA], 7.23 mM potassium-egtazic acid [K_2EGTA], 5.77 mM Na2ATP, 6.56 mM magnesium chloride hexahydrate [$MgCl_2.6H_2O$], 20 mM taurine, 15 mM NA2-phosphocreatine, 20 mM imidazole, 0.5 mM dithiothreitol [DTT], 50 mM 2-[N – morpholino]ethanesulfonic acid (MES); adjusted to pH 7.1 with 5 M potassium hydroxide[KOH]). Muscle fibres were gently teased apart and permeabilised through incubation in 50 µg/ml saponin/BIOPS for 30 minutes at 4 ^{o}C. Saponin selectively permiablilises cell membranes via the removal of cholesterol, depleting endogenous metabolites and allowing entry of experimentally controlled exogenous concentrations. Crucially, mitochondrial membranes remain intact, preserving their functional integrity (355). Permeabilised muscle samples were then washed in mitochondrial respiration buffer (MiR05 - 0.5 mM EGTA, 3 mM $MgCl_2.6H_2O$, 60 mM lactobionic acid, 20 mM taurine, 10 mM KH_2PO_4, 20 mM 4-(2-hydroxyethyl)-1-piperazineethanesulfonic acid (HEPES), 110 mM D-sucrose, 1 g/l fatty acid free BSA, adjusted to pH 7.1 using 5 M KOH) for 10 minutes at 4 ^{o}C. Mitochondrial function ex vivo was then determined using a two-chamber Oxygraph O2k (OROBOROS Instruments, Innsbruck, Austria) corrected for tissue wet weight. Individual tissue samples weighing between 2-4 mg were placed into each chamber in 2 ml MiR06 (MiR05 + 280 units/ml catalase).

2.8.2 O2k protocol

Chambers were initially oxygenated to 380-400 nmol/ml through injection of 3 µl 200 µM H_2O_2, after which baseline respiratory measurements were obtained by measuring oxygen flux in absence of exogenous substrates. Oxygen concentration levels were kept between 250-400 nM/ml to avoid hypoxia and chambers were reoxygenated via the addition of 2 µl 200 µM H_2O_2 as required. Malate (0.05 mM) and 0.2 mM octanoyl-carnitine (TOCRIS Bioscience, Bristol, UK) was added first to induce β-oxidation through acylcarnitine excess, at which point the O_2 flux derived from proton leak, proton slip, cation cycling and electron leak was determined prior to ATP synthase activity (FAO LEAK) (Figure 2-7). ADP was then titrated to saturation through initial addition of 3mM and further increments of 1mM until maximal oxidative phosphorylation (OXPHOS) capacity was achieved, reflected by no further increase in oxidative flux (FAO OXPHOS). Malate (2 mM) and 10 mM glutamate were then added to reflect complex I specific respiration (CI OXPHOS) (Figure 2-7). Malate and glutamate activate dehydrogenases which reduce NAD^+ to NADH, feeding electrons into complex I via NADH-ubiquinone oxidorecuctase (356). Outer mitochondrial membrane integrity was then checked through addition of 10 µM cytochrome c, as isolation procedures can result in damage and compromised function. Cytochome c is released upon damage to the outer mitochondrial membrane, the concentration of which is a limiting factor in mitochondrial respiration. If the addition of exogenous cytochrome c increased oxygen flux rate by >15%, mitochondrial outer membrane integrity was regarded as compromised and the data was rejected (BEFORE CYT C). Succinate (10 mM) was then added to stimulate electron flow from complex II through action of the $FADH_2$ linked succinate dehydrogenase subunit, at which point total OXPHOS capacity from complex I and II was determined (CI+II

OXPHOS) (Figure 2-7). Carbonyl cyanide-4-(trifluoromethoxy)phenylhydrazone (FCCP) was then titrated in 0.5 µM increments until maximum O_2 flux, which uncouples mitochondria by dissipating the proton gradient across the inner mitochondrial membrane (353) and removes any influence exerted on the ETC by ATP synthase, phosphate transporters or adenine nucleoside translocase (353). The electron transfer state (ETS) is represented by maximal O_2 flux, describing maximum OXPHOS capacity (Figure 2-7). The complex I inhibitor rotenone was then added (5 µM) to establish the contribution of electron flow from complex II only (CII ETS), followed by addition of 2.5 µM antimycin A, a complex III (cytochrome bc1) inhibitor which completely arrests the ETC allowing for quantification of residual, non-mitochondrial respiration (ROX) (Figure 2-7). Respiratory substrate stocks were suspended in dH_2O while uncouplers and inhibitors were suspended in absolute ethanol.

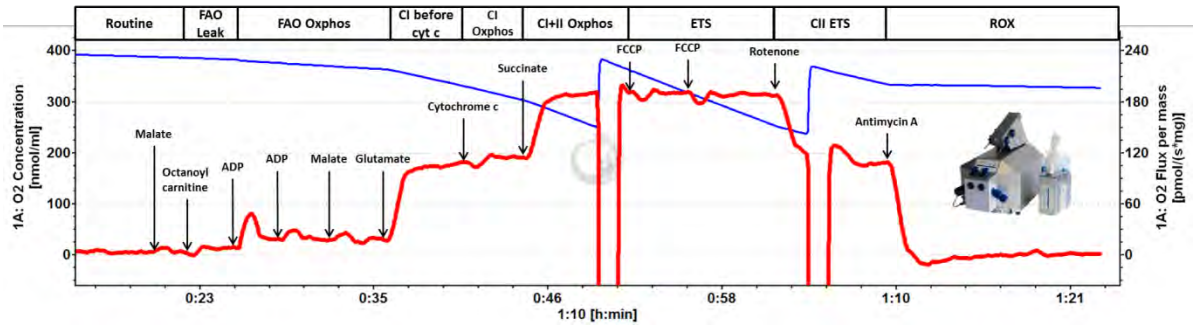

Figure 2-7 – Example trace of a high resolution respirometry experiment. The blue line indicates absolute O_2 concentration while the red line represents O_2 flux. Metabolic substrates and inhibitors are added to the sample chamber to induce successive respiratory states as indicated above the graph and within the text.

2.9 Metabolomics

Metabolomics is the high throughput quantification of metabolites. Metabolomic techniques can be targeted where ions are quantified from known metabolites of interest allowing for specific and accurate quantification when coupled with internal standards.

2.9.1 Targeted metabolomics - gas chromatography mass spectrometry (GCMS)

Gas chromatography mass spectrometry (GCMS) was utilised for targeted analysis of TCA cycle metabolite concentrations. GCMS utilises gas chromatography coupled with mass spectrometry to separate and detect polar, thermostable metabolites. Samples are injected, vaporised and transferred to a chromatography column by a carrier gas. Different molecules interact differently with the column, separating sample components. After separation, the mass spectrometer (MS) ionises samples and then quantifies mass-to-charge (m/z) ratio of ions. Firstly, samples undergo electron ionisation (EI), achieved by heated filaments emitting electrons which collide with gas phase molecules as they elute. This occurs in a vacuum and is deemed "hard" ionisation, meaning molecules are highly fragmented (357). Individual metabolites have different fragmentation patterns, and each fragment has different retention times dependent on molecular weight (defined as the time it takes for a given molecule to cross a magnetic field, or time-of-flight) (358). A qualifier ion, selected from the mass spectrum of a given target compound, is used to identify metabolites and they are quantified relative to other metabolite abundance on this basis. Thus, metabolite concentrations can be quantified relative to each other or an internal standard, and information can be obtained on individual aspects of molecular structure (358).

2.9.1.1 GCMS - sample extraction

500 µl HPLC grade methanol chilled to -20 ^{o}C and 200 µl 2.5 µg/ml glutaric acid in ddH_2O was added to 30 mg frozen tissue in a 2 ml microfuge tube with a 5 mm steel bead (QIAGEN, Germany). Samples were placed into a cassette cooled to -20 ^{o}C and tissue was

homogenised using a TissueLyser II (QIAGEN, Germany) by shaking at a frequency of 30 cycles per second for 2 minutes. Lysed samples were span at 14,000 x g at 4 ^{o}C for 5 minutes and the supernatant transferred to a 13 x 100 mm glass tube (ThermoFisher Scientific, Massachusetts, USA). Protein contaminants were precipitated by adding 1.4 ml 2:1 acetone:isopropanol solution chilled to -20 ^{o}C, vortexing vigorously for 10 seconds and agitating at 750 rpm on an orbital shaker (Fisherbrand multi-tube vortexer, ThermoFisher Scientific, Massachusetts, USA) for 10 minutes. Samples were then centrifuged at 3220 x g for 5 minutes to pellet protein. Supernatant was transferred to a fresh glass tube and 1 ml high performance liquid chromatography (HPLC) grade water with 500 µl chloroform chilled to -20 °C was added before agitating the samples as before. Samples were then centrifuged at 4000 rpm for 5 minutes and the top aqueous polar fraction transferred into 2 ml microfuge tubes. Of the final extract, 10% was placed into a fresh microfuge tube and fully dried for 2 hours at 45 ^{o}C and 5 torr of vacuum pressure using a Savant SPD1010 SpeedVac Concentrator (Thermo Fisher Scientific, Massachusetts, USA) and stored at -80 ^{o}C until chemical derivatisation.

2.9.1.2 **GCMS - Derivatisation**

Prior to GCMS analysis, samples must be chemically derivatised to reduce molecular polarity and hydrogen bond formation and increase volatility and thermostability of metabolites. This is achieved through the addition of a silyl group to molecules as a substitution for active hydrogen, allowing metabolites to withstand the GCMS protocol without degradation.

Dried GCMS samples were incubated at 95 ^{o}C for 10 minutes to ensure removal of all moisture before solubilisation in 40 µl 2% methoxyamine HCl in pyridine. Samples were vortexed for 1 minute, shaken vigorously for 5 minutes then incubated at 60 ^{o}C for one hour.

60 µl derivatisation agent was then added (N-tertbutyldimethylsilyl-N-methyltrifluoroacetamide (MTBSTFA) with 1% w/v tertbutyldimethyl-chlorosilane (TBDMSCI)) and the sealed samples incubated for 1 hour at 60 ^{o}C. Samples were centrifuged at 13,000 rpm for 5 minutes and the clear supernatant transferred to a chromatography vial with glass insert (Thermo Fisher Scientific) immediately prior to GCMS analysis.

2.9.1.3 **GCMS - sample analysis**

Samples were analysed using an Agilent 7890B Series GC/MSD gas chromatograph with a medium polar range polydimethylsiloxane GC column (DB35-MS), coupled with a mass spectrometer (Agilent Technologies, Santa Clara, USA). The GC-MS was tuned to a full width at half maximum (FWHM) peak width of 0.6 atomic mass units (amu) in a mass range of 50-650 m/z using perfluorotributylamine (PFTBA) tuning solution. Helium was used as a carrier gas and set to a flow rate of 1 ml/min^{-1}. Sample (1 µl) was then injected into the GCMS in splitless mode. Inlet liner temperature was set to 270 ^{o}C and oven temperature was set to 100 ^{o}C for 1 minute then ramped to 280 ^{o}C at a rate of +5 ^{o}C/min^{-1}. The temperature was then further ramped to 320 ^{o}C at a rate of +10 ^{o}C/min^{-1} and held at 320 ^{o}C for 5 minutes. Compound detection was performed in full scan mode in the 50-650 m/z range with 2-4 scans/sec^{-1}, a source temperature of 250 ^{o}C and a transfer line temperature of 280 ^{o}C. A solvent delay time of 6.5 minutes was included to ensure all solvent had eluted from the column before the heating element engaged. The injector needle was cleaned with methanol and hexane between samples to prevent cross contamination. Raw data was converted to common data format (CDF) and further data processing was performed using Metabolitedetector software.

2.9.2 Untargeted metabolomics - liquid chromatography mass spectrometry (LCMS)

Untargeted metabolomics involves registration of all ions within a specific mass range with the aim of uncovering differences in novel metabolites for further analysis. These ions can be identified through comparisons with retention times of known standards and/or compared against metabolite mass databases. Untargeted metabolomics was performed via liquid chromatography mass spectrometry (LCMS). LCMS differs to GCMS in that it utilises a liquid solvent rather than an inert gas as the mobile phase, allowing for identification and quantification of a broader range of compounds (359).

2.9.2.1 LCMS – sample preparation

Ice cold LCMS extraction buffer (1ml, 50:30:20 methanol:acetronitrile:water, all HPLC grade) was added to approximately 10 mg frozen tissue per sample with a cold 5 mm metal bead. Samples were placed into a cassette cooled to -20 ^{o}C and tissue was homogenised using a TissueLyser II (QIAGEN, Germany) by shaking at a frequency of 30 cycles per second for 2 minutes. Lysates were span at 14,000 x g at 0 ^{o}C for 15 minutes to pellet solid debris, then the supernatant transferred to glass chromatography vials (ThermoFisher Scientific, Massachusetts, USA). Extracted samples were stored at -80 ^{o}C until analysis.

2.9.2.2 LCMS – sample analysis

Pre-prepared LCMS samples were collaboratively analysed by Dr David Watson (University of Edinburgh, UK). Samples were prepared and injected in a randomised order to avoid sampling bias. Untargeted metabolomics analysis was performed using an Accela HPLC system interfaced to an Exactive Orbitrap mass spectrometer (ThermoFisher Scientific,

Massachusetts, USA). ZIC-pHILIC (150 x 4.6 mm, 5 µm) HPLC columns (HiChrom, Reading, UK) were used for liquid chromatographic separations. The ZIC-pHILIC mobile phase consisted of 20 mM ammonium carbonate in HPLC-grade water (solution A) and acetonitrile (solution B). The solvent gradient was 80% acetonitrile at 0 minutes, 20% at 30 minutes, 8% between 31-36 minutes and 80% between 37-45 min at a flow rate of 0.3 mL/min. Auxilliary gas flow rates and the nitrogen sheath were maintained at 17 and 50 AU. The electrospray ionisation (ESI) interface was set to positive/negative dual polarity mode with a spray voltage of 4.5 kV in positive mode and 4 kV in negative mode, with the ion transfer capillary temperature at 275 ^{o}C. Full scan data were obtained within 75-1200 amu in m/z ratio for both ionisation modes. Data collection and processing was performed using Xcalibur 2.1.0 software (ThermoFisher Scientific, Massachusetts, USA), and data extraction and statistical analysis was performed using MZMatch software (SourceForge, La Jolla, USA). Metabolites were identified, filtered and compared using a macro-enabled Microsoft Excel Ideom file, and identified metabolites were evaluated manually through peak quality evaluation and matching with retention times of known standard mixtures ran to the same protocol. Furthermore, library searches were carried out against metabolite mass data within the Human Metabolome Data Base (HMDB) and the Kyoto Encyclopedia of Genes and Genomes (KEGG). All metabolites were determined within 3 ppm of their exact masses.

2.10 Indirect calorimetry

A large proportion of this project initially involved installing, calibrating, optimising and developing standard operating procedures for a recently acquired indirect calorimetry system for mice, both for effective assessment of basal metabolism via home cage analysis

and for assessment of responses to metabolic stress in real time through integration with a single lane treadmill. Indirect calorimetry involves the quantification of O_2 utilised and the amount of CO_2 emitted by an organism, from which heat production and energy expenditure is calculated. This gives a wealth of information on energy expenditure and overall metabolic status. Traditionally, heat production was directly analysed as a measure of energy expenditure, but this can be inferred much more precisely and noninvasively from indirect measurement of metabolic gas exchange, which also allows for assessment of substrate preferences and metabolic flexibility.

The method assumes that all oxygen consumed by an organism goes towards oxidation of carbohydrates and lipids in the production of ATP (though amino acids are also oxidised, the relative contribution in this case is assumed to be negligible), and all CO_2 emitted is produced as a result of such metabolic reactions and processes (360). For mice, room air is used a reference for comparison with respiratory air sampled from sealed metabolic cages in which the subject animals reside individually (Figure 2-8). From this, the relative change in O_2 and CO_2 composition as a result of respiration ($\Delta O_2/\Delta CO_2$) is calculated. From these values, the VO_2 and VCO_2, defined as the volume of O_2 consumed and CO_2 produced over a given time period, can be further calculated using the sample air flow rate. Heat production can be calculated as a measure of energy expenditure using VO_2 and VCO_2 values. These values can be further normalised to body weight (BW) or lean body mass (LBM). Additionally, substrate utilisation can be determined as the RER, which is calculated as VCO_2/VO_2 (76).

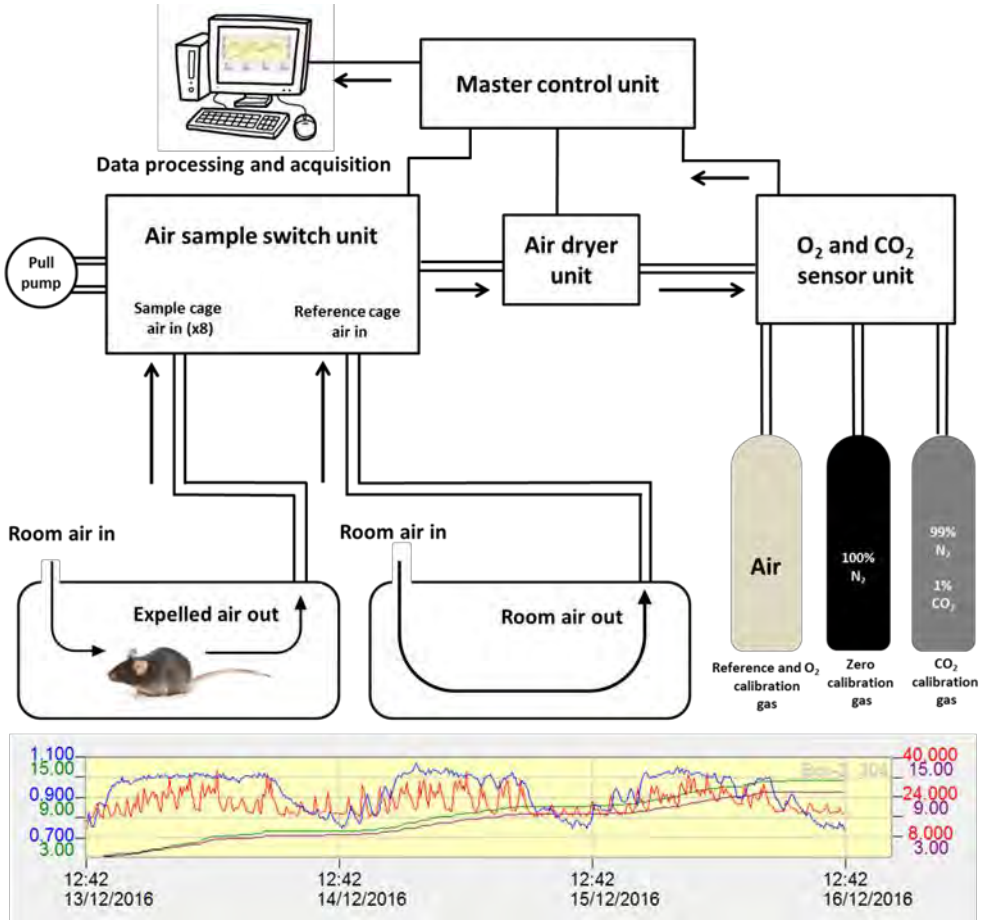

Figure 2-8 – Schematic diagram of the TSE Systems PhenoMaster and example output graph. The TSE PhenoMaster works on the "pull" principle whereby air is drawn through reference and mouse cages by a negative pressure pump and analysed for O_2 and CO_2 composition at a set flow rate. Air from occupied mouse cages is sequentially compared against room air drawn through the empty reference cage. The red line represents energy expenditure, the blue line represents RER and the green and purple lines represent cumulative food and water intake respectively.

Indirect calorimetry was performed using a TSE PhenoMaster 8 cage system (TSE Systems, Bad Homburg, Germany), which assesses eight mice simultaneously (Figure 2-8, Figure 2-9). Cage configuration is depicted in Figure 2-9. Mice are placed individually in airtight cages and air is pulled through the cage at a set flow rate, which is then analysed for O_2 and CO_2 concentration relative to reference room air (Siemens OXYMAT/ULTRAMAT 6) (Figure 2-9). The system collects data from each box sequentially over nine minutes, after which the sequence restarts. During the first minute, room air composition is measured

which serves as a blank measurement followed by sequential sampling of exhaust air from cages 1-8 for one minute each, allowing for the best balance between measurement accuracy and resolution. All indirect calorimetry experiments took place over five days on a 12:12 6:00/18:00 light/dark cycle in a light, noise and temperature controlled room. The most accurate box flow rate was ascertained as 0.4 l/min, with these parameters being determined by ΔO_2 and ΔCO_2 values remaining between 0.2-1% for greatest measurement accuracy.

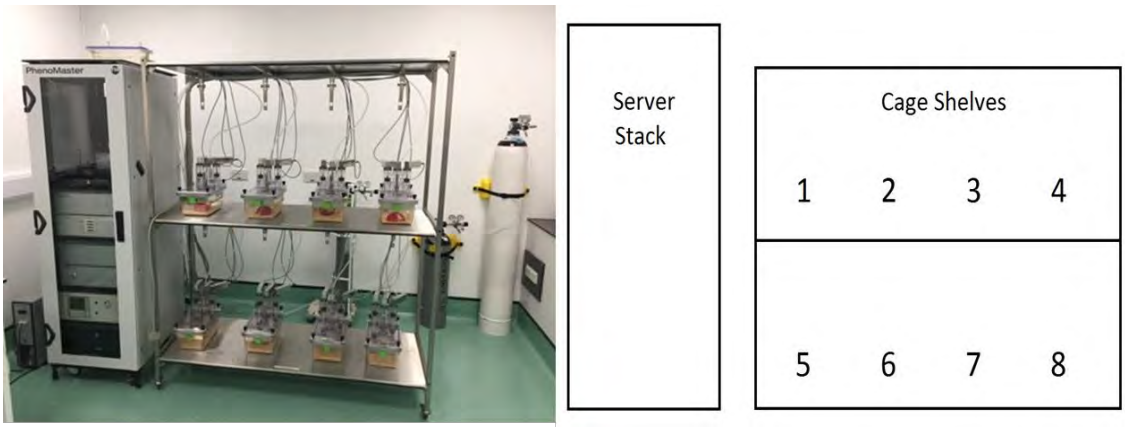

Figure 2-9 – Photograph of TSE PhenoMaster and schematic diagram of home cage layout. Room temperature, lighting intensity and on/off timings and operator disturbance were strictly controlled for all experiments. Mice were assigned experimental cages at random to avoid positioning bias.

2.10.1 Mouse acclimatisation and experimental procedure

An important aspect of home cage calorimetry is that mice are properly acclimatised to the environment and unstressed, for both welfare and data validity reasons. Consistency of environment is also important, thus the same lighting conditions, amount of bedding materials and red, round shelter style was used for every animal.

On Day 1, Mice were weighed and placed onto the TSE PhenoMaster in their home cages with their littermates at 12:00 to allow for acclimatisation to the new environment

and food/water hoppers, which provide food and water ad libitum. The sample flow rate was set to 0.38 l/min, the box air flow rate set to 1 l/min and ventilation port opened to 10 mm to accommodate for more than one mouse per cage. On day 2 at 12:00, mice were removed from the home cages, weighed and their overall condition checked. Mice were then placed into new cages in isolation with three handfuls of new bedding swapped for soiled bedding to aid with acclimatisation to isolation. The box flow rate was reduced to 0.4 l/min and ventilation port reduced to 2 mm before the mice were placed back onto the TSE PhenoMaster in isolation for the 24 hour isolation acclimatisation phase. On the morning of day 3, mice were visually checked for signs of stress at 09:00 and food/drink consumption was recorded. If mice were not eating and/or drinking (determined as less than 1 g of food or 1 ml of water) they were removed from the experiment. For the data collection phase, mice were then left undisturbed until 13:00 on day 5, where they were removed. Food/drink consumption data was checked again and mice were weighed. If the mice had not eaten or drank and/or had lost more than 20% body weight since day 1, the data was excluded from the experiment.

2.11 Intraperitoneal glucose tolerance tests (IPGTTs)

An intraperitoneal glucose tolerance test (IPGTT) involves establishing fasting blood glucose levels then intraperitoneally injecting a concentrated glucose solution into a mouse, after which blood glucose levels are monitored at set time intervals. The rate at which an organism can clear excess glucose from the blood is determined by many variables including insulin production and insulin sensitivity of peripheral energy storage tissues (muscle, liver and fat) (361). Alongside fasting glucose levels, these measurements therefore give valuable

insight into whole body metabolic status (361). Mice were fasted for 6 hours prior to the experiment to avoid postprandial variations in blood glucose levels. Stress can be a major determinant of resting blood glucose, and the protocol was designed to reduce stress and maintain consistency as much as possible. Food was withdrawn at 08:00 with the experiment always starting at 14:00 to avoid circadian bias. Mice were weighed, marked and treated with EMLA^{TM} 5% analgesic cream (Aspen Pharmacare, Durban, South Africa) on the tail to minimise pain and stress. Mice were then restrained using a red tinted restraining tube and an incision was made in the left tail vein using a scalpel from which the baseline blood glucose measurement was taken using a glucometer (AccuChek Aviva, Roche, Basel, Switzerland). Mice were then injected intraperitoneally with 2 g/kg L-glucose. Blood glucose measurements were then taken at 15, 30, 60 and 120 minutes post glucose administration. Mice were returned to their home cages between measurements and blood was always withdrawn from the same incision point in the tail to minimise further stress.

2.12 Graphical and statistical analysis

Graphical and statistical analysis was performed using GraphPad Prism V8. Student's unpaired t tests were used when comparing unrelated groups to controls with paired t tests being used for comparison of response to NR in the same animal. For comparisons of multiple variables, Ordinary two-way analysis of variance (ANOVA) with Sidak's multiple comparisons test was used to assess statistical significance between relevant groups. Statistically significant relationships are represented for group mean variance of genotype, age, NR supplementation and any interdependency of these variables alongside direct post hoc comparison of individual groups. Western blot densitometry, PCR band intensity and

skeletal muscle fibre type cross sectional area analyses were performed using ImageJ V1.48V. Indirect calorimetry parameters were calculated using TSE PhenoMaster Software V5.0 and analysed as a trace of absolute (not normalised to body weight) hourly averages over time, mean comparisons of absolute day and night hour values and as linear regression models with each parameter plotted against body weight and subjected to analysis of covariance (ANCOVA) as outlined in Fernandez-Verdejo et al., 2019 (362). For gene expression, qPCR data was plotted as arbitrary units with statistical analysis performed on mean ΔCt values.

CHAPTER 3 – METABOLIC CHARATERISATION OF NRK MEDIATED NAD^+ SALVAGE IN SKELETAL MUSCLE

3.1 Introduction

The functional roles of the NRK salvage pathway within skeletal muscle are poorly understood. Studies utilising cellular models of skeletal muscle NRK augmentation have suggested roles of NRK2 in skeletal muscle development and adhesion (341) as well as being the rate limiting enzyme for NAD^+ salvage from NR (16). Further studies investigating global NRK1 and/or NRK2 KO mouse models have inferred that the NRKs may be inessential for regular skeletal muscle metabolic homeostasis (15). However, NRK2 upregulation has been identified in a model of severe myopathy (325). The same study reported a decrease in skeletal muscle NAD^+ levels with simultaneous knockout of NRK2 in this model, implying that the upregulation of NRK2 is of functional relevance (325). NRK2 is also upregulated in conditions of impaired skeletal muscle NAD^+ homeostasis (15). It has also been suggested that NRK2 expression levels follow a circadian oscillatory pattern within skeletal muscle, and the functional relevance of such observations remains unclear.

The consequences of NRK2 upregulation in skeletal muscle have not been investigated in vivo outside of pathological settings, in which it is difficult to identify specific functional effects directly attributed to NRK2 upregulation alongside complex and severe pathological phenotypes. The validation and characterisation of a skeletal muscle NRK2 overexpressing mouse model will therefore allow for direct observation of any functional consequences caused by constitutive NRK2 overexpression both basally and in the context of experimentally controlled metabolic stressors, offering insight into the role of the NRK2 protein and the wider metabolic relevance of the NRK salvage pathway in skeletal muscle.

3.1.1 Validation of novel skeletal muscle specific NRK2.Tg mouse model

The NRK2.Tg mouse is a novel strain which utilises complex molecular genetic mechanisms to achieve tissue specific overexpression of a transgene. Various aspects of tissue specific Cre/loxP systems are prone to error and thus the model must be thoroughly validated. Such problems may include failures in the Cre recombinase mediated genetic recombination of the transgene, inhibited or error-prone mRNA transcription and protein translation, translation of a misfolded and/or non-functioning transgenic protein product, saturation and pathological aggregation of unfolded protein within the ER and ribosomal machinery, and aberrant activation of the transgene within untargeted tissues (363). All of these potential issues must be discounted prior to phenotypic experimentation, which was the initial focus of this chapter.

3.1.2 Characterisation of young NRK2.Tg metabolic phenotype

The metabolic consequences of skeletal muscle specific NRK2 overexpression are unknown. Skeletal muscle is critical to the maintenance of whole body metabolic homeostasis as a major site of energy metabolism and as a storage organ for metabolic substrates including glycogen, triglycerides and proteins (64). NAD^+ has widespread roles both in oxidative metabolism as a redox cofactor and as a critical signalling molecule for metabolic adaptation (112), and therefore the augmentation of NAD^+ salvage pathways within skeletal muscle can have metabolic consequences ranging from altered NAD^+ consumption/salvage dynamics, altered redox ratios affecting oxidative metabolism and altered responses to metabolic stressors such as exercise (315, 318). It was therefore critical to establish any such effects

both for the elucidation of any functional roles of the NRK pathway within young, healthy mice and to serve as a baseline for comparison against responses to further metabolic stressors that were introduced later in the project, such as altered nutrition and ageing.

This chapter aimed to first conclusively validate the NRK2.Tg mouse model before establishing any metabolic consequences of skeletal muscle NRK2 overexpression in young NRK2.Tg mice, both at basal levels and in response to energetic stress. To achieve this, NRK2.Tg mice were monitored for developmental differences throughout adolescence and assessed for potential differences in expression of other NAD^+ salvage and signalling enzymes, NAD^+ dynamics both at basal levels and when supplemented with NR precursor, 24 hour whole body metabolic status, real-time and biochemical metabolic responses to acute exercise and mitochondrial oxidative capacity.

3.2 Materials and methods

3.2.1 Animal care

Animals were housed in conditions detailed in section 2.1. To monitor body weight gain during adolescence, WT and NRK2.Tg mice were weighed every 7 days from 4 to 11 weeks of age at 10:00 am.

3.2.2 Intraperitoneal NR administration

Mice were injected with 400 mg/kg nicotinamide riboside chloride (Chromadex, California, USA) in PBS and immediately returned to their home cages. Mice were culled via cervical dislocation after one hour post injection and tissues collected according to section 2.3. IP

injection and tissue collections were performed between 10:00-12:00 to minimise circadian variability.

3.2.3 Tissue collection

Mice were culled and tissues collected according to section 2.3.

3.2.4 Genomic DNA extraction, PCR and electrophoresis

DNA from mouse earclips was extracted according to the protocol outlined in section 2.2.4, while DNA from mouse TA and soleus was extracted using a QIAGEN DNeasy Blood and Tissue Kit (QIAGEN, Germany) and assessed for purity using a Nanodrop© ND-1000 (Labtech International, Cambridge, UK) as detailed in section 2.4.1. PCR was performed according to section 2.2.5 and analysed via gel electrophoresis as detailed in section 2.2.6.

3.2.5 RNA extraction, reverse transcription and qPCR

RNA was extracted from mouse quadriceps samples as detailed in section 2.5.1 and reverse transcription was performed according to the protocol detailed in section 2.5.2. For qPCR analysis, all genes besides Nmrk2 were assayed using TaqMan probes following the protocol detailed in section 2.5.4. Nmrk2 was optimised and assayed using the SYBRGreen™ gene expression assay method to the protocol detailed in section 2.5.5. Table 3-1 contains the list of TaqMan™ probes used in this chapter. For qPCR data presented in section 3.3.1, 18s was used as a reference gene, while qPCR data presented in section 3.3.2 was normalised to Gusb.

Table 3-1 – TaqMan™ probes used in chapter 3.

Gene	Accession Number
18S (reference gene)	4333760T (Cat no.)
Gusb (reference gene)	Mm01197698_m1
Nadk	Mm00446804_m1
Nadsyn1	Mm00513448_m1
Nampt	Mm00451938_m1
Nmnat1	Mm01257929_m1
Nmrk1	Mm00521051_m1
Parp1	Mm01321084_m1
Sirt1	Mm01168521_m1
Sirt3	Mm00452131_m1

3.2.6 Protein Extraction, lysate preparation and Immunoblotting

Protein was extracted and quantified from ~30mg TA, quadriceps and cardiac tissue according to section 2.6.2. Protein lysates were prepared from 30 µg/µl protein per sample according to section and separated via SDS-PAGE electrophoresis according to section 2.6.3 on 12% polyacrylamide gels made as outlined in section 2.6.1. Separated proteins were then transferred to nitrocellulose membranes using an iBlot Dry Blotting System (ThermoFisher Scientific, Massachusetts, USA) before blocking and probing with primary (Table 3-2) and secondary antibody followed by film exposure and image processing as detailed in section 2.6.3.

Table 3-2 – Table of primary antibodies used for immunoblotting in chapter 3.

Antibody Species/ Specificity	Source	Product Code	Immunoblotting Dilution
Rabbit α NRK2	BioGenes (Germany)	N/A	1:1000
Mouse α-Tubulin (B-7)	Santa Cruz Biotechnologies (USA)	SC-5286	1:1000

3.2.7 NAD+/NADH quantification

Frozen TA, soleus and quadriceps tissue were pulverised using a pestle and mortar. 5 mg soleus and 10 mg TA and quadriceps was weighed according to section 2.3.1 then homogenised in 400 µl NAD/NADH Extraction buffer in a 1.5 ml microfuge tube using a tissue plunger. NAD^+ and NADH levels were quantified using the NAD^+/NADH quantitation kit (Biovision, California, USA) as detailed in section 2.7.

3.2.8 Home cage metabolic quantification

Acclimatisation and indirect calorimetry was performed on 12 week old female WT and NRK2.Tg mice over 48 hours according to the protocol detailed in section 2.10.1.

3.2.9 Mouse acute exercise

As well as home cage indirect calorimetric analysis, the TSE PhenoMaster features a TSE CaloTreadmill, upon which the acute exercise runs in this study were performed (TSE Systems, Bad Homburg, Germany). The TSE CaloTreadmill is an airtight single lane treadmill which replaces the first home cage, from which exhaust air is fed through to an O_2 and CO_2 analyser integral to the TSE PhenoMaster (Siemens OXYMAT/ULTRAMAT 6). Using room air for comparison as a zero value, the system is able to measure gas exchange as a mouse runs, allowing for quantification of metabolic response to exercise (Figure 3-1).

Male WT and NRK2.Tg mice aged between 3-7 months of age were acclimatised to treadmill running according to section 3.2.9.1 and subjected to the acute exercise protocol detailed in section 3.2.9.2.

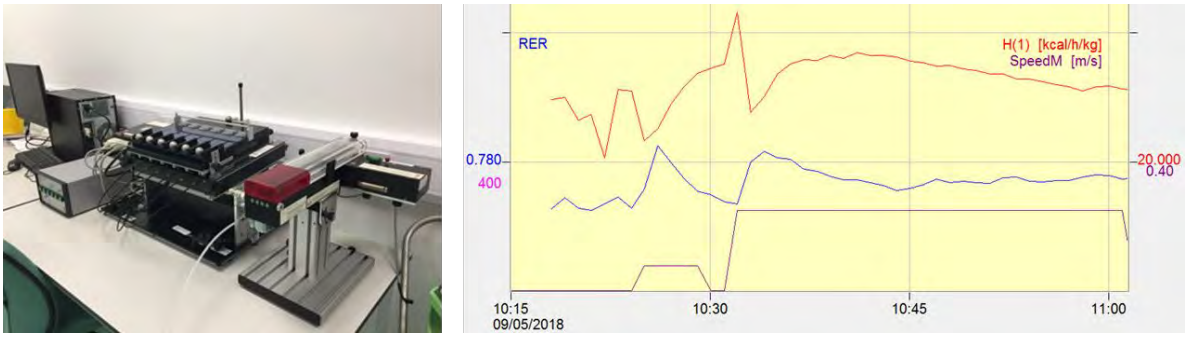

Figure 3-1 – Photograph of TSE Systems six lane training treadmill, CaloTreadmill and an example of a mouse metabolic trace in response to an acute exercise protocol. The red line indicates energy expenditure, the blue line represents RER and the purple line represents treadmill speed.

3.2.9.1 **Acclimatisation**

The acclimatisation process was designed to introduce mice to the concept of treadmill running but not induce a trained phenotype. Mice were acclimatised to treadmill running by a three day acclimatisation protocol on a six lane mouse treadmill (TSE Systems, Bad Homburg, Germany). On day 1, mice were placed onto the unmoving belt for 10 minutes to allow for familiarisation with the surroundings. Then mice were ran at 5 m/min for 10 minutes at a +10^{o} incline to introduce them gently to the moving belt. On day 2, mice were placed on the unmoving belt for 10 minutes then ran at 5 m/min at a +10^{o} incline for 5 minutes, followed by a 2 minute rest then 10 m/min for 10 minutes at a +10^{o} incline. On day 3, mice were placed on the unmoving belt for 10 minutes then ran at 5 m/min at a +10^{o} incline for 5 minutes, followed by a 2 minute rest then 15 m/min at +10^{o} incline for 15 minutes. Throughout acclimatisation, mice were freely allowed to seek refuge from the belt but were encouraged back on through use of an air puff if unwilling. This was repeated for a maximum of 3 times per mouse, and if mice were still unwilling after this they were removed from the experiment.

3.2.9.2 **Acute exercise protocol**

Acute exercise runs were carried out using a TSE CaloTreadmill in conjunction with a TSE PhenoMaster (TSE Systems, Bad Homburg, Germany). A +10^{o} incline was selected to ensure that the mice had to work sufficiently to induce metabolic responses associated with moderate to intense exercise (364). The belt speed of 15 m/min and duration of 30 minutes was selected through both reference to literature, which suggests that the maximum sustained speed for a C57/BL6 mouse ranges between 14-17 m/min (365), and also through trial and error and optimisation to establish speed tolerances of the NMRK2.Tg/ACTA1-Cre mice, where around 75% of mice assessed were able and willing to complete 30 minutes of exercise at this intensity without prior training. The sample flow rate was set to 0.38 l/min and box flow rate set to 0.5 l/min, ensuring that ΔO_2 and ΔCO_2 values remained between 0.2-1% for greatest measurement accuracy. At the beginning of the protocol, room air was sampled for 2 minutes and used as a zero measurement value and exhaust gas from the CaloTreadmill was sampled every minute thereafter. Mice were allowed to acclimatise to the belt and chamber for 10 minutes before a 5 m/min, +10^{o} incline warm-up run for 5 minutes. Mice were then rested for 2 minutes before running at 15 m/min at a +10^{o} incline for 30 minutes. Unwilling mice were encouraged to run through use of a slider, but if this was required more than 3 times the mouse was removed from the experiment. Mice were immediately culled via Schedule 1 cervical dislocation and tissues collected upon completion of the exercise protocol.

3.2.10 GCMS

GCMS was performed on WT and NRK2.Tg quadriceps to quantify anaplerotic amino acids and central carbon metabolites of the TCA cycle according to section 2.9.1. Samples were extracted according to section 2.9.1.1 followed by derivatisation (section 2.9.1.2) and analysis (section 2.9.1.3).

3.2.11 High resolution respirometry

To quantify mitochondrial respiratory capacity, WT and NRK2.Tg mouse TA and soleus was assessed via high resolution respirometry according to section 2.8. Tissue preparation was performed according to section 2.8.1 followed by experimentation and analysis according to section 2.8.2.

3.2.12 Intraperitoneal glucose tolerance tests

IPGTTs were performed on 3 month old female WT and NRK2.Tg mice according to the protocol detailed in section 2.11.

3.3 Results

3.3.1 NRK2 is robustly overexpressed in NRK2.Tg skeletal muscle

Initially, reliable identification methods of intended target animal genotypes had to be established as well as thorough validation of the mouse model on genomic, transcriptomic and proteomic levels. Furthermore, tissue specific overexpression of an exogenous transgene via Cre/LoxP recombination is reliant on complex molecular genetic systems which can be prone to error, such as aberrant expression of the transgene outside of target tissues or failures in genetic recombination (363). Such possibilities had to be discounted before experimentation could begin.

PCR was performed on NRK2.Tg floxed control (hereby referred to as WT) mouse tissue and NRK2.Tg/ACTA1-Cre (hereby referred to as NRK2.Tg) tissue to determine the presence of a conditional transgenic NRK2.Tg allele and an intact ROSA26 locus in tissue other than skeletal muscle confirming target animal hemizygosity (Figure 3-2A). Possession of the ACTA1/Cre allele was also determined via PCR through the presence or absence of a band (Figure 3-2B), which served as an identifier of target NRK2 overexpressing animals against floxed controls going forward. Recombination of the conditional allele into the constitutively active conformation was also confirmed within skeletal muscle in TA and soleus as well as absence of this band within the floxed control mice (Figure 3-2C).

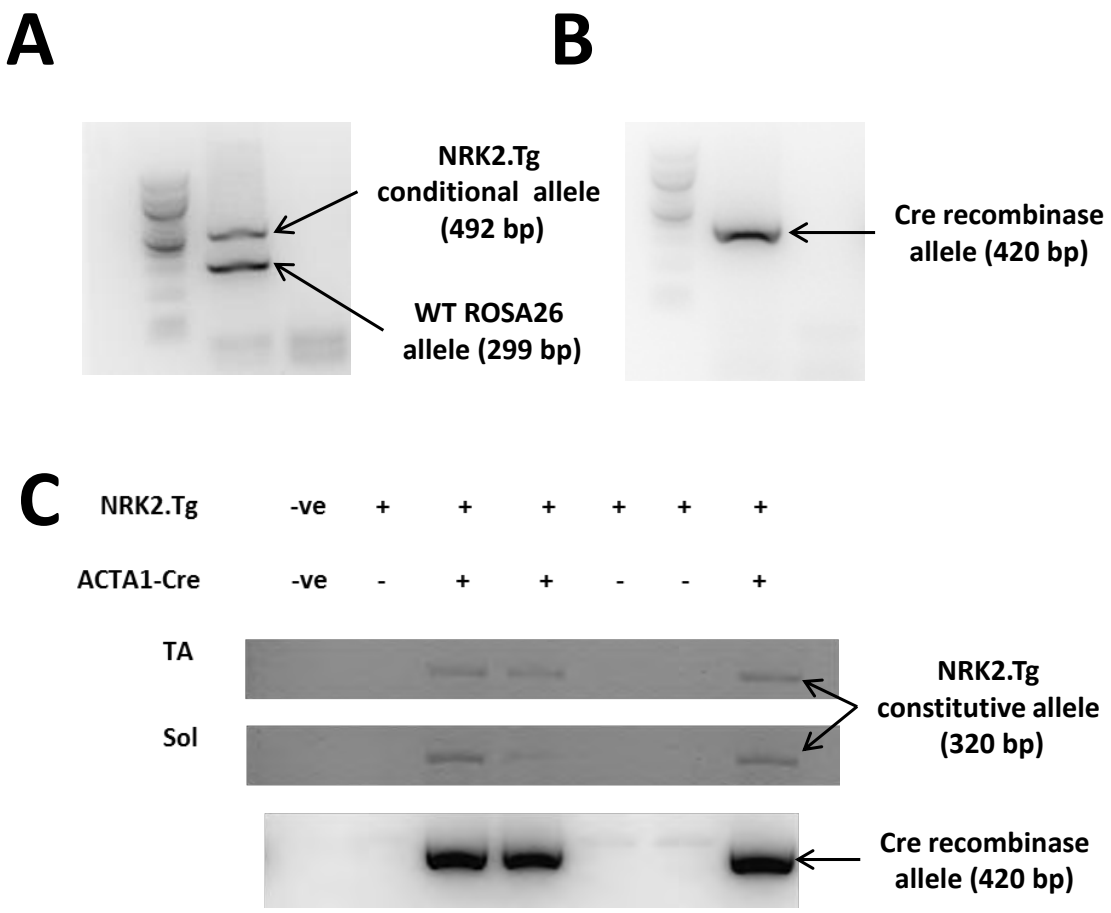

Figure 3-2 – NRK2.Tg genotyping and verification of NRK2.Tg transgene recombination in skeletal muscle of mice positive for Cre recombinase. A. PCR Amplification of the conditional NRK2.Tg and WT ROSA26 locus in mouse ear tissue indicating target animal hemizygosity. B. PCR amplification of the Cre recombinase allele in mouse ear tissue. C. PCR amplification of the constitutive NRK2.Tg allele in skeletal muscle (TA and soleus) in floxed (WT) vs. NRK2.Tg mice. n=3.

After qualitative detection of the recombined constitutive NRK2.Tg allele within Cre recombinase positive mice, the next priority was to determine proper functioning of the constitutive allele through quantification of transgenic transcriptional activity and NRK2 protein levels in WT and NRK2.Tg mice. Quantitative PCR confirmed significant overexpression of Nmrk2 mRNA within NRK2.Tg skeletal muscle (TA and soleus) and heart with approximately five-fold upregulation in these tissues relative to WT controls (Figure 3-3A,B). Endogenous Nmrk2 mRNA levels were higher in TA than soleus in WT mice, agreeing

with previous observations that NRK2 expression levels are greater within the predominantly type II TA muscle than the type I soleus (15). This was also reflected in NRK2.Tg mice albeit approximately five-fold higher (Figure 3-3A, B). NRK2 expression levels in NRK2.Tg liver and kidney were comparable to WT levels, indicating that overexpression of NRK2 was specific to muscle as intended (Figure 3-3B). Assessment of protein levels in NRK2.Tg quadriceps identified significant upregulation of NRK2 relative to WT levels by approximately three-fold (Figure 3-3C,E) and floxed control mice had comparable NRK2 protein levels to that of genotypically WT mice, indicating no aberrant expression of transgenic NRK2 in floxed mouse muscle (Figure 3-3D,E).

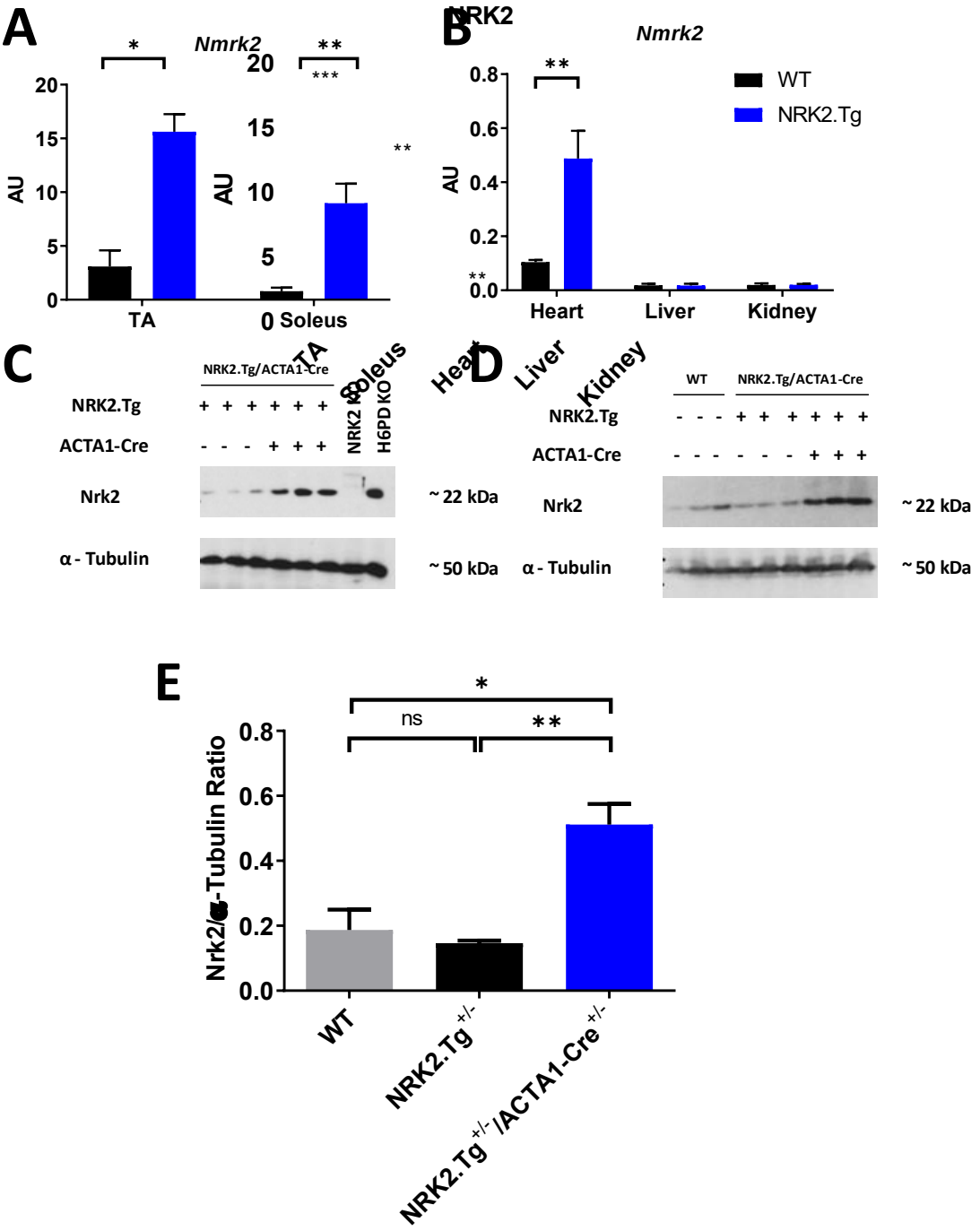

Figure 3-3 – NRK2 is significantly and specifically overexpressed in NRK2.Tg muscle. A+B. Quantification of NMRK2 mRNA transcript levels using qPCR in TA, soleus, heart, liver and kidney. C. Immunoblot of NRK2 protein levels in floxed and Cre recombinase expressing mouse quadriceps with positive (H6PD KO) and negative (NRK2 KO) controls D. Immunoblot of NRK2 protein levels in genotypically WT, floxed and Cre recombinase expressing mouse quadriceps. E. Semi-quantitative densitometry analysis of WT, floxed and Cre recombinase positive immunoblot band intensity. Mice were 3 months of age. Data presented as mean ± standard error of the mean (SEM). Statistical significance was determined by student's unpaired t test (* $p < 0.05$, ** $p < 0.01$, *** $p < 0.001$). n = 3.

Elevated NRK2 protein levels were also identified in NRK2.Tg cardiac muscle at approximately five fold upregulation relative to WT, though absolute NRK2 levels were significantly lower than within transgenic skeletal muscle (Figure 3-4).

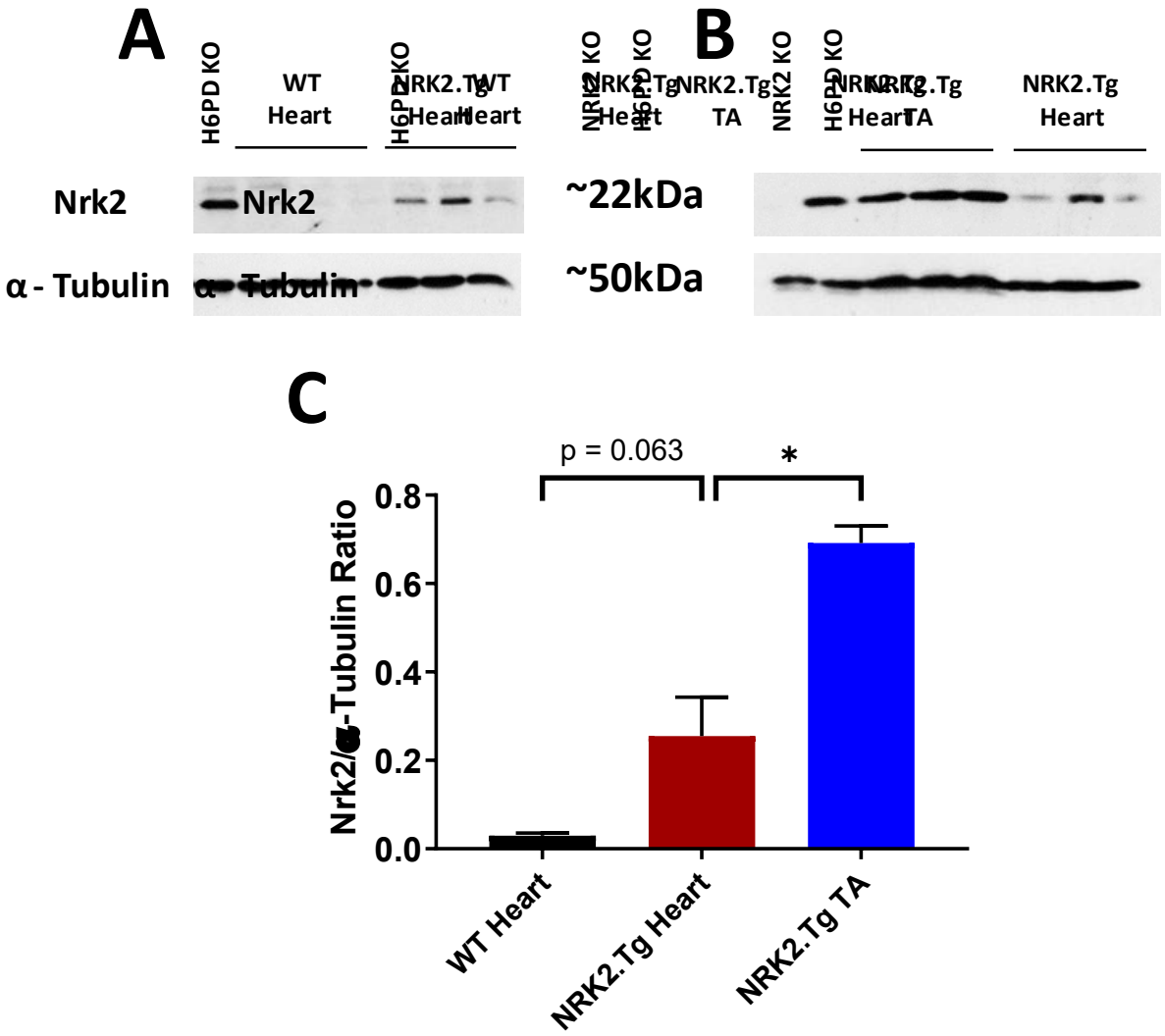

Figure 3-4 – NRK2 is significantly overexpressed in NRK2.Tg cardiac muscle. A. Immunoblot of floxed vs. NRK2.Tg NRK2 protein levels in cardiac tissue. B. Immunoblot of NRK2.Tg TA vs. cardiac tissue NRK2 protein levels. C. Semi-quantitative densitometry analysis of NRK2 immunoblot band intensity in floxed cardiac tissue vs. NRK2.Tg cardiac tissue vs. NRK2.Tg TA. Data presented as mean ± SEM. Statistical significance was determined by student's unpaired t test (* $p < 0.05$, ** $p < 0.01$, *** $p < 0.001$). n = 3.

3.3.2 NRK2.Tg mice develop normally with no induction of the unfolded protein response in skeletal muscle

To assess the impact of skeletal muscle NRK2 overexpression on development, NRK2.Tg mice were monitored weekly throughout adolescence from 4 to 11 weeks old, displaying no overt behavioural changes and comparable rates of development in terms of weekly increases in body weight (Figure 3-5).

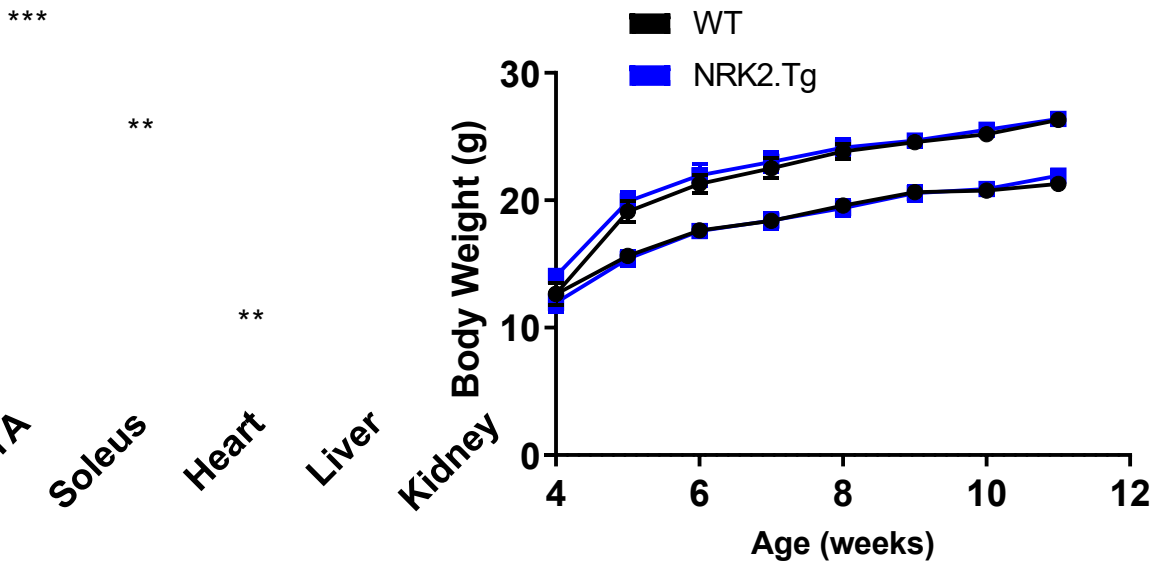

Figure 3-5 – Male and Female NRK2.Tg mice develop normally through adolescence. Body weight measurements of male and female WT and NRK2.Tg mice from 4-11 weeks of age. Statistical significance was determined by student's unpaired t test between WT and NRK2.Tg per weekly timepoint (* $p < 0.05$, ** $p < 0.01$, *** $p < 0.001$). Data presented as mean ± SEM. n = 5-7.

Constitutive overexpression of transgenic proteins can induce ER stress responses and activate the UPR in the cells of host organisms, potentially resulting in misfolded and non-functional transgenic protein products and/or off-target phenotypic effects caused by pathological protein aggregation within the ER (366). Expression levels of the ER chaperones pro-apoptotic transcription factor, DNA-damage-inducible transcript 3 (Ddit3) and heat

shock protein α5 (Hspa5), which are upregulated in response to ER stress (367), were quantified and determined to be comparable between WT and NRK2.Tg mouse muscle indicating that the UPR is not activated in NRK2.Tg muscle (Figure 3-6A,B).

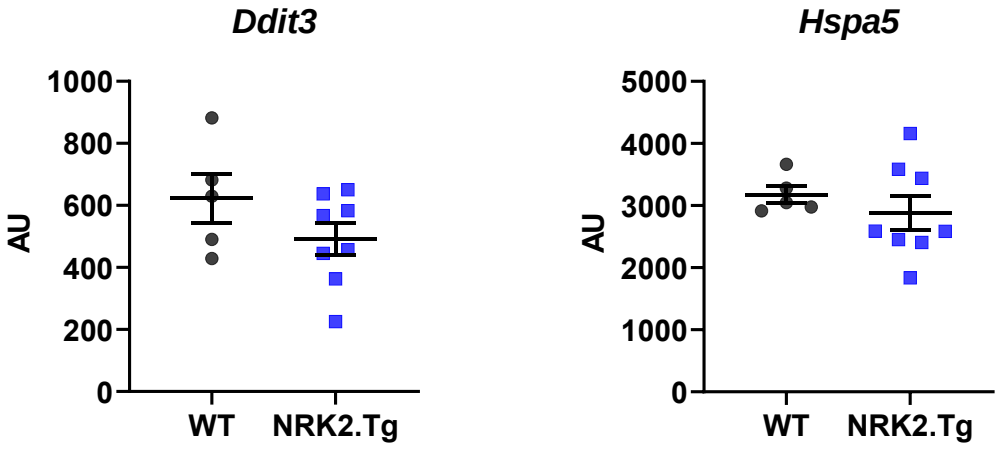

Figure 3-6 – The unfolded protein response is not induced in NRK2.Tg Skeletal Muscle. Quantification of mRNA transcript levels of Ddit3 and Hspa5 from 11 week old WT and NRK2.Tg mouse quadriceps. Data presented as mean ± SEM with individual data points representing one biological replicate. Statistical significance was determined by student's unpaired t test (* $p < 0.05$, ** $p < 0.01$, *** $p < 0.001$). n = 5-8.

3.3.3 NRK2 overexpression does not affect expression levels of NAD+ salvage and signalling enzymes

Altering NAD^+ biosynthesis dynamics within cells has been shown to influence relative expression levels of other NAD^+ salvage pathway components (15) and NAD^+ dependent signalling enzymes such as the sirtuins (368). Expression levels of key NAD^+ salvage and NAD^+ dependent enzymes were therefore examined to establish any potential effects of constitutive NRK2 overexpression within skeletal muscle. Expression levels of the rate limiting de novo NAD^+ biosynthesis enzymes Ido1 and Qprt and the key shared de novo/Priess Handler rate limiting enzyme Nadsyn1 (131) were all unchanged along with the

NADP generating enzyme Nadk (Figure 3-7). Expression levels of Nampt, the key mediator of NAD^+ salvage from NAM in skeletal muscle (11), was also unchanged as well as Nmnat1, the most highly expressed enzyme isoform in skeletal muscle catalysing the conversion of NMN to NAD^+ (15) and the alternative Nmrk2 isoform Nmrk1 (Figure 3-7). Expression levels of key NAD^+ dependent signalling enzymes Sirt1, Sirt3 and Parp1 were also not significantly altered (Figure 3-7). These results indicate that skeletal muscle NRK2 overexpression does not influence NAD^+ biosynthetic and NAD^+ dependent enzymes at the transcript level in young, metabolically unchallenged mice.

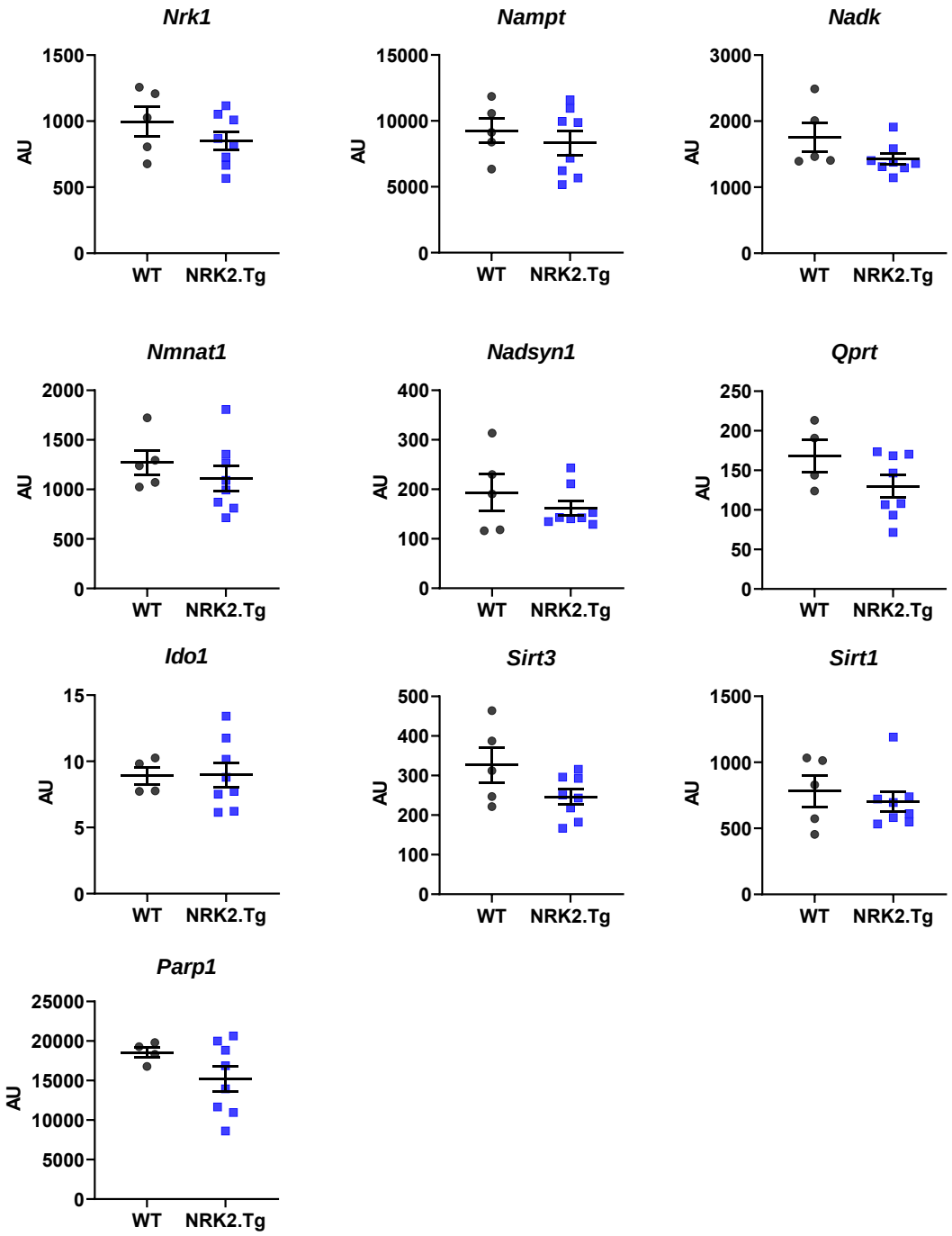

Figure 3-7 – Expression levels of NAD$^+$ biosynthesis and NAD$^+$ dependent signalling enzymes are unaffected by NRK2 overexpression in young skeletal muscle. Quantification of mRNA transcript levels of NAD$^+$ processing and dependent enzymes WT and NRK2.Tg quadriceps in 3 month old mice. Data presented as mean ± SEM with individual data points representing one biological replicate. Statistical significance was determined from ΔCt values by student's unpaired t test (* $p < 0.05$, ** $p < 0.01$, *** $p < 0.001$). n = 5-8.

3.3.4 NAD^+ boosting through NR supplementation is more efficacious in NRK2.Tg skeletal muscle

Given the primary role of NRK2 as an NAD^+ salvage enzyme, the effects of NRK2 overexpression on the whole cell skeletal muscle NAD^+ metabolome were next investigated, both at basal levels and with an excess of NR substrate. The NRKs are rate limiting enzymes for the production of NAD^+ from NR (16), and therefore perturbations to in vivo NAD^+ metabolism were hypothesised upon NRK2 overexpression. Basal NAD^+ and NADH levels were not significantly altered between WT and NRK2.Tg muscle across quadriceps (mixed fibre type), TA (predominantly type II fibres) and soleus (predominantly type I fibres) (369) (Figure 3-8), indicating that endogenous substrate availability could be a limiting factor and NRK2 overexpression alone may not impact on the NAD^+ metabolome.

An upward trend in NAD^+ and NADH concentration was observed in all muscle beds one hour post NR supplementation, with NR supplementation producing a significant elevation in quadriceps NAD^+, TA NADH and tNAD, and soleus NAD^+, NADH and tNAD (Figure 3-8). No discernible effect on NAD^+/NADH ratio was noted in any muscle bed (Figure 3-8). NR supplemented NRK2.Tg skeletal muscle NAD^+ levels were significantly elevated relative to basal measurements alongside a marked additive increase in TA and soleus NAD^+ levels relative to WT NR supplemented muscle (Figure 3-8). Interaction analysis determined a significant increase in the boosting efficacy of NR in NRK2.Tg mice for TA NAD^+ and total NAD levels, with a strong comparable trend in soleus NAD^+ ($p = 0.089$) and total NAD ($p = 0.061$) (Figure 3-8). However, this trend was not observed in quadriceps (Figure 3-8). NAD^+/NADH

ratios were marginally elevated in NRK2.Tg quadriceps and TA relative to WT irrespective of NR supplementation, though this was not statistically significant (Figure 3-8).

Together, these results support previous assertions of NRK enzymes being rate limiting for the production of NAD^+ from NR (16) and also imply that intraperitoneally injected NR is bioavailable to skeletal muscle at one hour post administration. The availability of NR substrate also appears critical, with these data suggesting that endogenous NR levels are not sufficient to provide an NAD^+ boosting effect with increased NRK2 enzyme concentration. These results also serve as additional model validation, with the significant increase in NR efficacy in boosting NAD^+ within NRK2 overexpressing skeletal muscle indicating that the transgenic NRK2 protein product is functional.

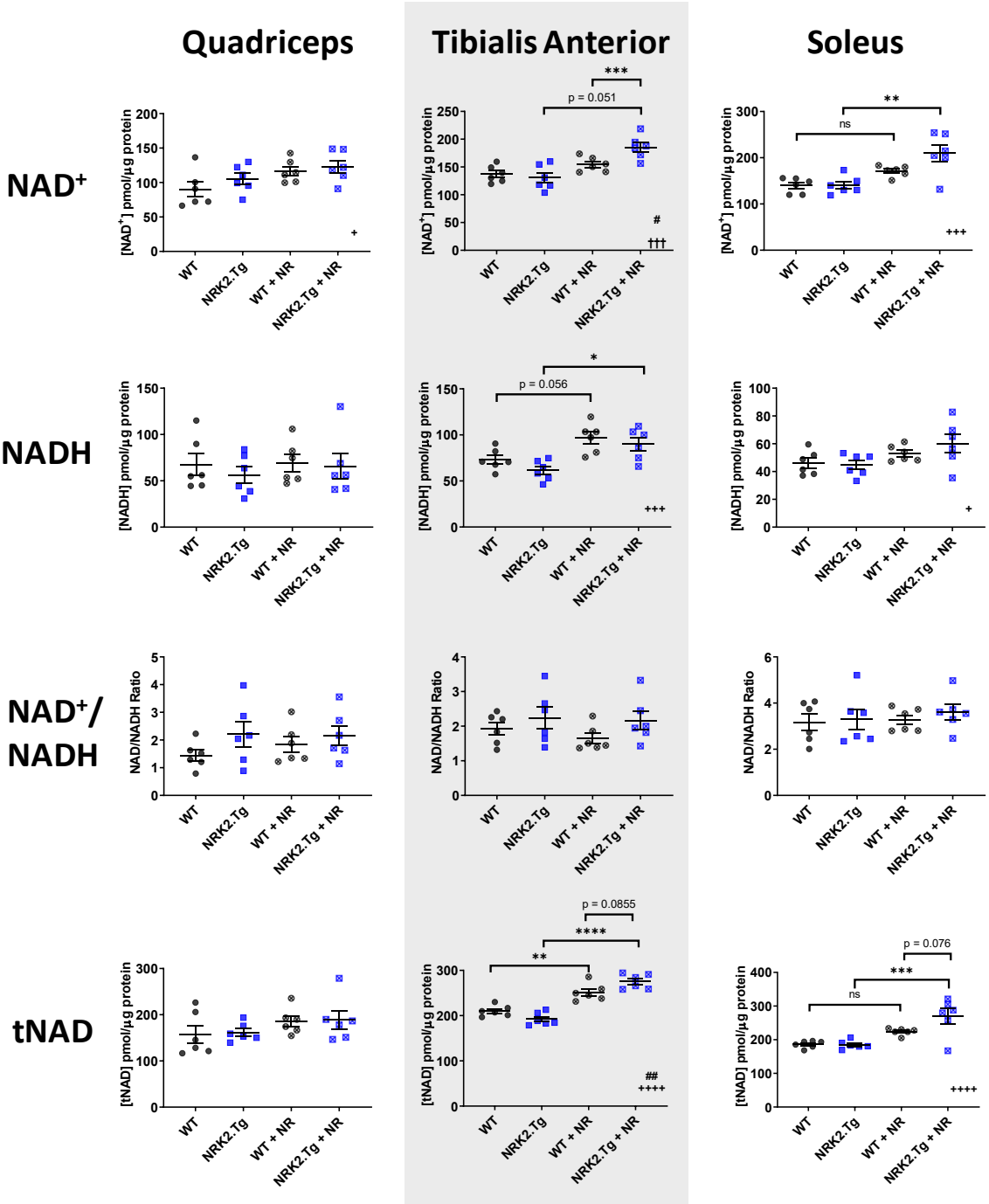

Figure 3-8 – NAD$^+$ levels are significantly elevated in response to NR supplementation in NRK2 overexpressing TA and soleus. Quantification of NAD$^+$, NADH, NAD$^+$/NADH ratio and total NAD levels in WT and NRK2.Tg mouse skeletal muscle, with or without intraperitoneal NR supplementation and 1 hour incubation followed by immediate cull. Mice were 11 weeks of age. Data presented as mean ± SEM with individual data points representing one biological replicate. Statistical significance was determined by ordinary two way ANOVA with Sidak's multiple comparison tests (* $p < 0.05$, ** $p < 0.01$, *** $p < 0.001$, **** $p < 0.0001$). n = 6. # = statistically significant interaction between genotype and NR supplementation; + = statistically significant variation upon NR administration; † = statistically significant variation between WT and NRK2.Tg mice.

3.3.5 Skeletal muscle NRK2 overexpression does not affect the metabolic response to acute exercise

Intense acute exercise imposes severe metabolic stress and ATP deficit on skeletal muscle (64) eliciting a metabolic response in order to maintain energetic homeostasis, for which NAD^+ is critical (310). Skeletal muscle NRK2 is upregulated in response to impaired NAD^+ homeostasis (15) and metabolic stress (325). Furthermore, NRK2 has also been implicated as a key mediator in skeletal muscle development (341, 342, 344), and therefore any potential developmental or structural differences in NRK augmented muscle could impact on exercise ability. It was hypothesised that chronic NRK augmentation within skeletal muscle may alter the metabolic response to exercise. Untrained WT and NRK2.Tg mice were subjected to 30 minutes of controlled intense treadmill exercise with real-time metabolic response assessed via indirect calorimetry. Absolute energy expenditure, RER and VO_2 traces were not significantly different between WT and NRK2.Tg mice at any single timepoint throughout the protocol with area under the curve (AUC) values also being comparable (Figure 3-9). Linear regression and ANCOVA analysis comparing AUC values with body mass indicated a positive correlation for energy expenditure and VO_2 but no significant differences in slope angle, elevation or Y intercept between WT and NRK2.Tg mice for all three parameters, implying no significant metabolic differences when controlled for differences in body mass (Figure 3-9).

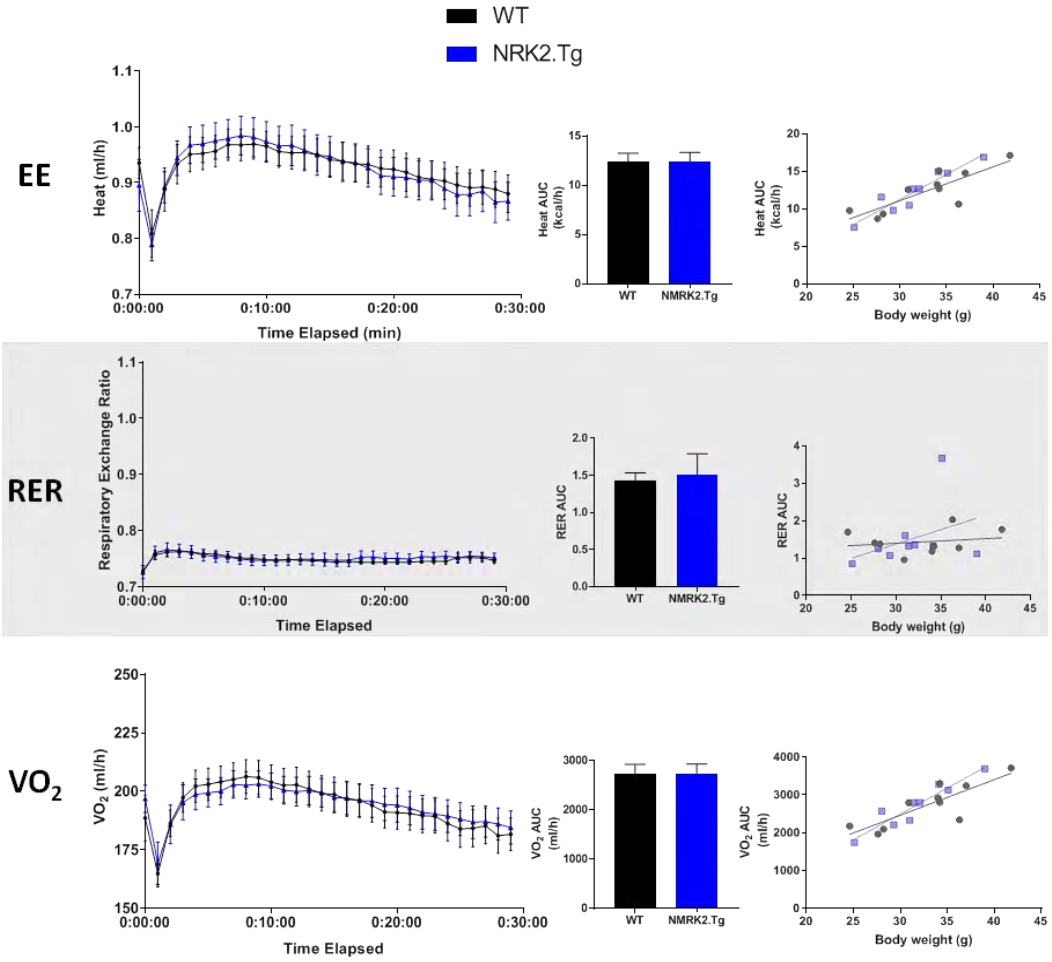

Figure 3-9 – Metabolic response to acute exercise is comparable between WT and NRK2.Tg mice. Energy expenditure (EE), respiratory exchange ratio (RER) and VO_2 of WT and NRK2.Tg mice subjected to 30 minutes of acute treadmill exercise presented as a 30 minute trace, area under the curve (AUC) and linear regression against body mass. Data presented as mean ± SEM. Statistical significance of corresponding trace timepoints and AUC were determined by student's unpaired t test (* $p < 0.05$, ** $p < 0.01$, *** $p < 0.001$). n = 9-10.

Skeletal muscle NAD^+ and NADH levels were quantified in skeletal muscle immediately extracted and snap frozen after cessation of acute exercise. No significant changes in skeletal muscle NAD^+ concentrations were observed between sedentary and exercised animals with or without overexpression of NRK2 (Figure 3-10). Exercised NRK2.Tg mice had slightly elevated NADH levels relative to exercised WT mice and elevated total NAD levels as a result, though these observations were not statistically significant.

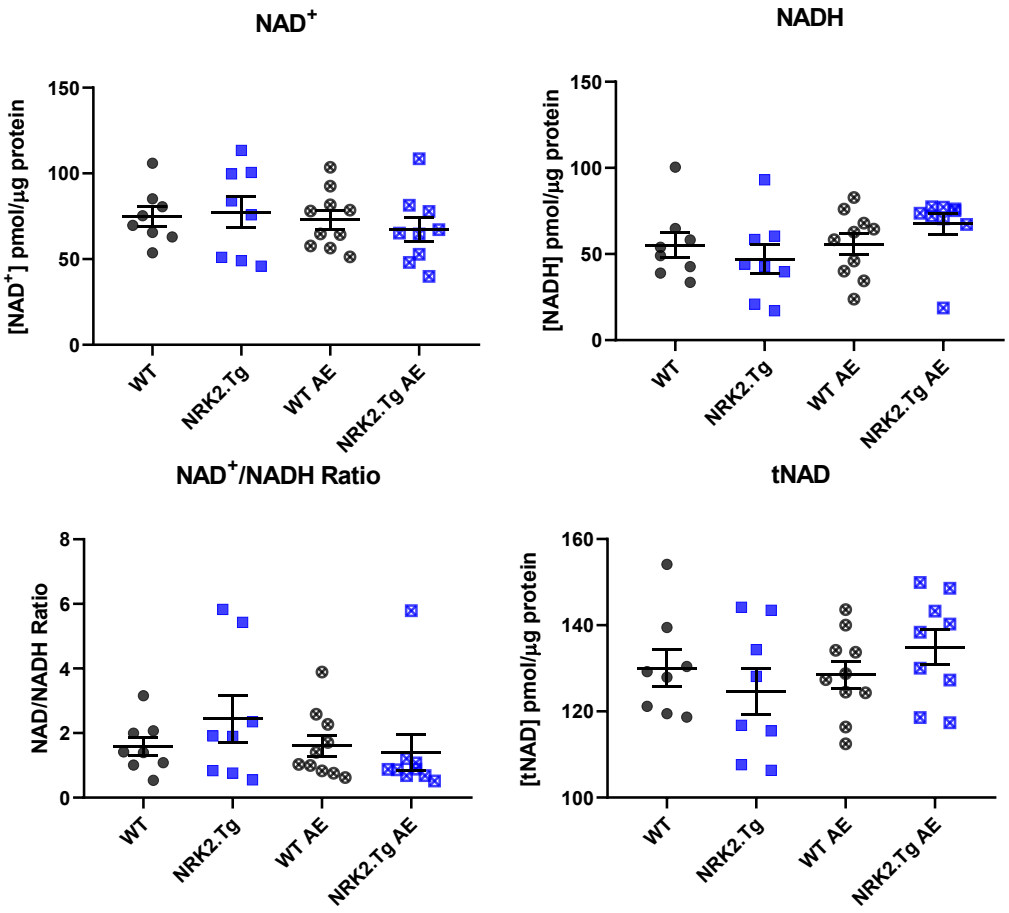

Figure 3-10 – NAD$^+$ levels are unaffected and comparable between WT and NRK2.Tg TA muscles immediately after acute exercise. Quantification of NAD$^+$, NADH, NAD$^+$/NADH ratio and total NAD levels in male WT and NRK2.Tg mouse TA which were sedentary or culled immediately after cessation of acute exercise (AE). Data presented as mean ± SEM with individual data points representing one biological replicate. Statistical significance was determined by ordinary two way ANOVA with Sidak's multiple comparison tests (* $p < 0.05$, ** $p < 0.01$, *** $p < 0.001$, **** $p < 0.0001$). n = 8-10. # = statistically significant interaction between genotype and acute exercise; + = statistically significant variation upon acute exercise; † = statistically significant variation between WT and NRK2.Tg mice.

3.3.6 NRK2 overexpression does not affect skeletal muscle central carbon metabolism or mitochondrial oxidative capacity

Given the importance of NAD$^+$ to oxidative metabolism, skeletal muscle central carbon metabolism in the context of NRK augmentation was next assessed. Impairment of NAMPT

driven NAD^+ biosynthesis results in NAD^+ deficit and subsequent energetic stress, manifesting as perturbations to TCA cycle metabolite flux (370). Although augmentation of the NRK pathway was not expected to perturb oxidative metabolism, NAD^+ availability remains a major factor and quantification of NAD^+ and NADH+ levels from a single timepoint cannot provide information on NAD^+ flux rates and utilisation. It was therefore deemed important to establish both basal TCA metabolite and amino acid levels alongside changes in response to exercise within NRK2 overexpressing mouse muscle to establish any potential changes within molecular oxidative metabolism.

Several anaplerotic amino acids were significantly depleted in response to acute exercise. Serine, glycine and alanine are glucogenic amino acids that are able to enter the TCA cycle through conversion to pyruvate under energetic stress (94, 371), with serine and alanine being significantly depleted after acute exercise in both WT and NRK2.Tg mice (Figure 3-11). Asparagine can be converted to aspartate and subsequently enter the TCA cycle as oxaloacetate, and asparagine was significantly reduced in exercised mice with a subsequent increase in aspartate (Figure 3-11). A similar relationship was observed between glutamine and glutamate levels, where glutamine is converted to glutamate which is then further converted to the TCA cycle intermediate 2-oxoglutarate (371) (Figure 3-11). Furthermore, the TCA cycle intermediates citrate, fumarate and malate were significantly increased in exercised vs. sedentary mice (Figure 3-11). These observations are indicative of energetic stress and subsequent upregulation of anaplerotic pathways to feed the TCA cycle to meet increased energetic demand, implying that the exercise protocol was effective at inducing energetic deficit and metabolic stress. However, no significant differences were

observed in such responses between WT and NRK2.Tg mice, indicating that NRK2 overexpression does not alter the oxidative response to exercise within skeletal muscle.

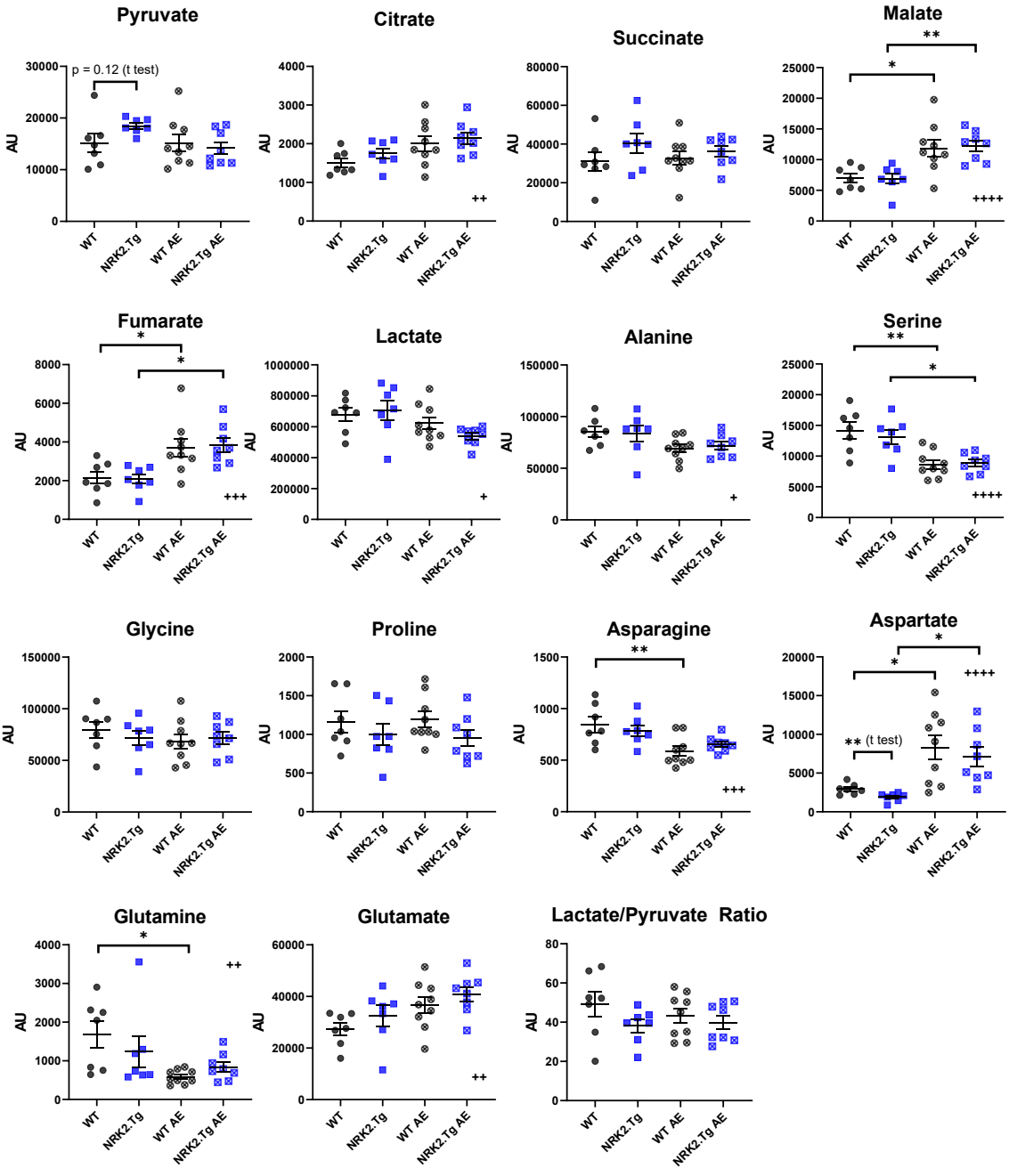

Figure 3-11 – Skeletal muscle TCA cycle intermediates and amino acid content were not significantly altered between WT and NRK2.Tg mice that were subjected to acute exercise, though aspartate levels were significantly decreased in sedentary NRK2.Tg muscle. GCMS quantification of metabolically relevant TCA cycle intermediates and amino acids in male WT and NRK2.Tg mouse quadriceps which were sedentary or culled immediately after cessation of acute exercise (AE). Statistical significance was determined by ordinary two way ANOVA with Sidak's multiple comparison tests (* $p < 0.05$, ** $p < 0.01$, *** $p < 0.001$, **** $p < 0.0001$). n = 8-10. # = statistically significant interaction between genotype and acute exercise; + = statistically significant variation upon acute exercise; † = statistically significant variation between WT and NRK2.Tg mice.

Despite few differences in central carbon metabolism between exercised WT and NRK2.Tg mice, basal pyruvate levels appeared elevated within NRK2.Tg skeletal muscle though this was not statistically significant and lactate/pyruvate ratios were not significantly perturbed (Figure 3-11). Additionally, basal aspartate levels were significantly decreased relative to WT muscle, suggesting some potential perturbations to basal oxidative metabolism in NRK2.Tg muscle. Skeletal muscle mitochondrial fatty acid oxidative capacity was therefore assessed both in predominantly type II (TA) and type I (soleus) muscle beds. As expected (369), the more oxidative soleus muscle presented with significantly higher oxidative flux rates for every respiratory state but fatty acid leak state and residual oxygen consumption, but no significant differences between WT and NRK2.Tg muscle were observed in either TA or soleus suggesting that NRK augmentation alone does not affect skeletal muscle oxidative respiratory capacity (Figure 3-12).

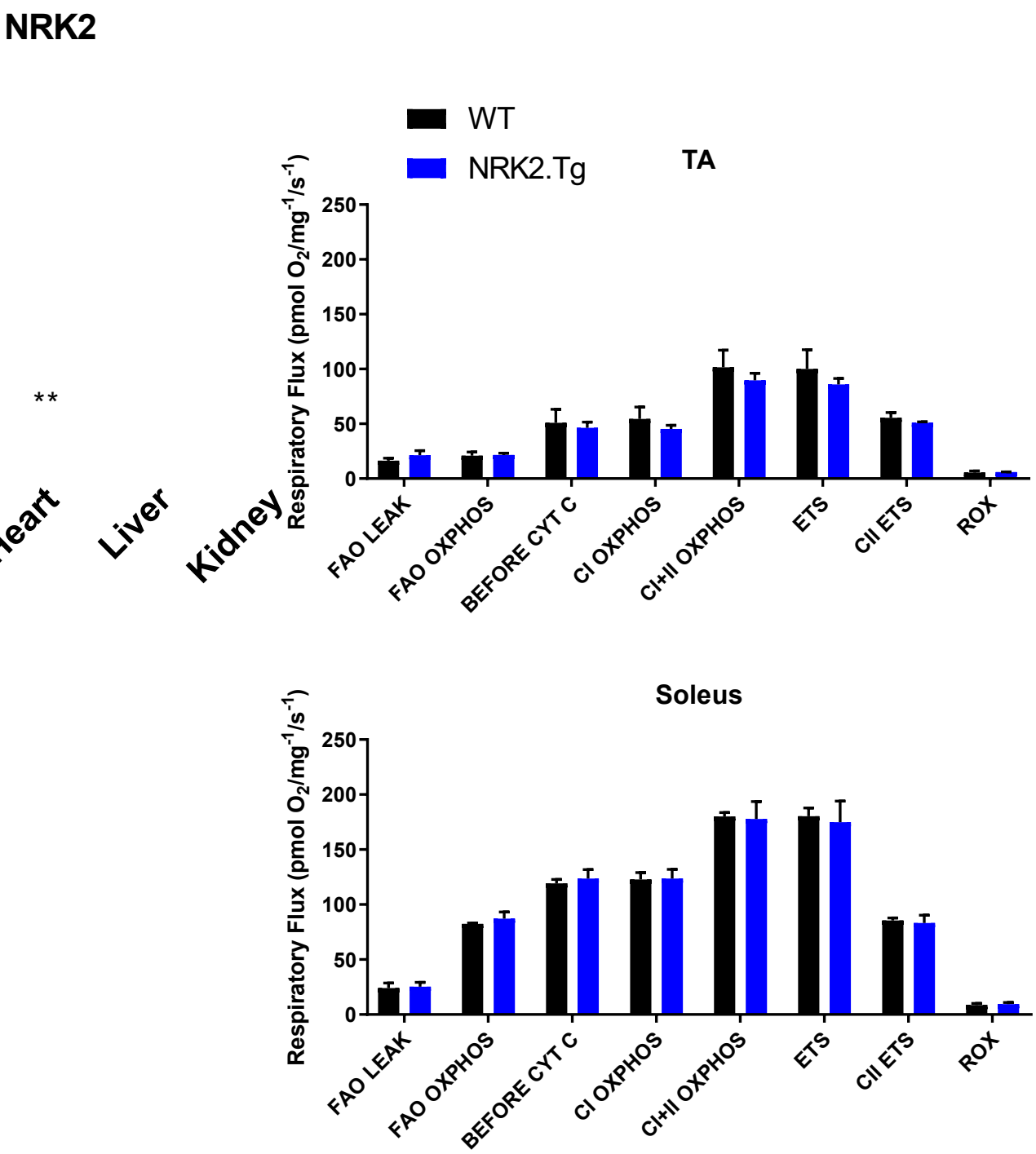

Figure 3-12 – Mitochondrial respiratory capacity is comparable between WT and NRK2.Tg mouse TA and soleus. FAO capacity of TA and soleus from female 3 month old WT and NRK2.Tg mice. Data presented as mean ± SEM. Statistical significance between groups was determined by student's unpaired t test at each respiratory state (* $p < 0.05$, ** $p < 0.01$, *** $p < 0.001$). n = 3.

3.3.7 Skeletal muscle NAD^+ levels are significantly elevated in NRK2.Tg skeletal muscle during the active phase

NAD^+ salvage enzymes are differentially expressed throughout the day under the control of circadian regulatory genes such as the CLOCK:BMAL1 complex, modulating NAD^+ levels and consequent metabolic processes throughout the day (227, 330). Publically available gene expression data (NCBI GEO Profiles) also implies that NRK2 is differentially regulated in skeletal muscle over 24, with the functional relevance of this dynamic regulation remaining unclear. This experiment aimed to clarify this through observation of functional consequences with constitutive NRK2 overexpression in vivo compared to normal circadian regulation in WT mice. Interestingly, NRK2.Tg NAD^+ levels were significantly elevated at zeitgeber (ZT) 16 (22:00) in both TA and soleus and additionally at ZT20 (02:00) in TA (Figure 3-13). In contrast, NADH levels were almost significantly decreased at ZT12 and ZT20, resulting in significant elevation of the NAD^+/NADH ratio at ZT12 (18:00) and ZT16, though this effect was not observed within soleus where the NAD^+/NADH ratio was instead significantly elevated at ZT 0 (06:00) (Figure 3-13). These observations suggest that NRK2 expression levels could play a key role in NAD^+ homeostasis, significantly augmenting the skeletal muscle NAD^+ pool if there is an excess of NRK2 enzyme during active hours.

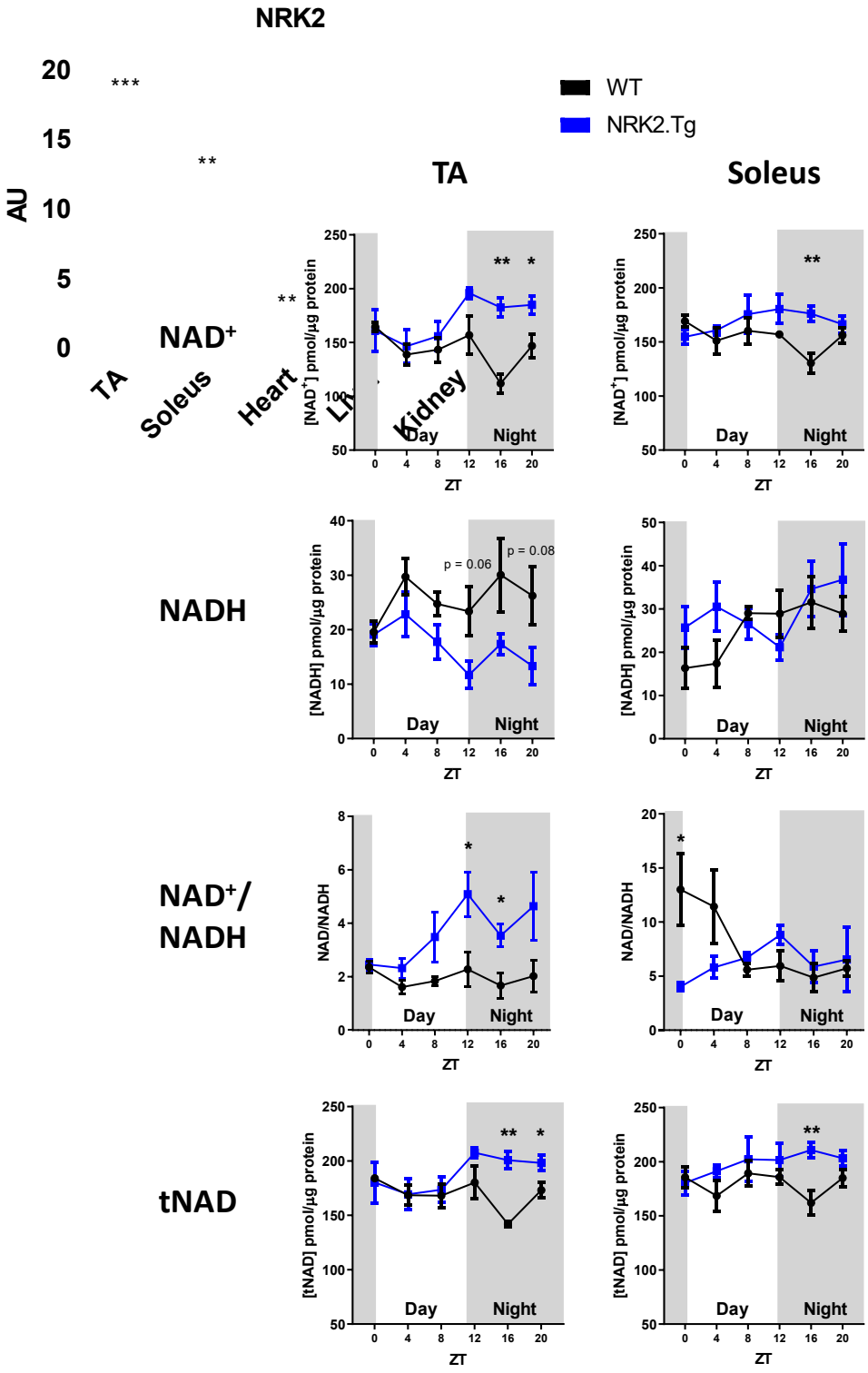

Figure 3-13 – NRK2.Tg mice present with significantly elevated NAD^+ levels during active hours in TA and soleus. Quantification of NAD^+, NADH, NAD^+/NADH ratio and total NAD levels in TA and soleus collected from 3 month old male WT and NRK2.Tg mice at 4 hour intervals over a 24 hour period. Data presented as mean ± SEM. Statistical significance was determined by student's unpaired t test between WT (* $p < 0.05$, ** $p < 0.01$, *** $p < 0.001$). n = 4 per timepoint.

These observations of circadian NAD^+ elevation were then compared against NRK2 protein expression levels. In both TA and soleus, WT NAD^+ levels were lowest at ZT16 (Figure 3-13), though quantification of TA NRK2 protein levels throughout 24 hours via immunoblotting indicated that strongest upregulation of NRK2 protein occurs during ZT8 and ZT12 with very little detection of NRK2 at other timepoints (Figure 3-14). NRK2.Tg NAD^+ levels trended upwards relative to WT levels at these times, though this was not statistically significant. In contrast, NRK2 protein was strongly detected at every timepoint in NRK2.Tg TA as would be expected from the presence of the constitutively active NRK2.Tg transgene (Figure 3-14).

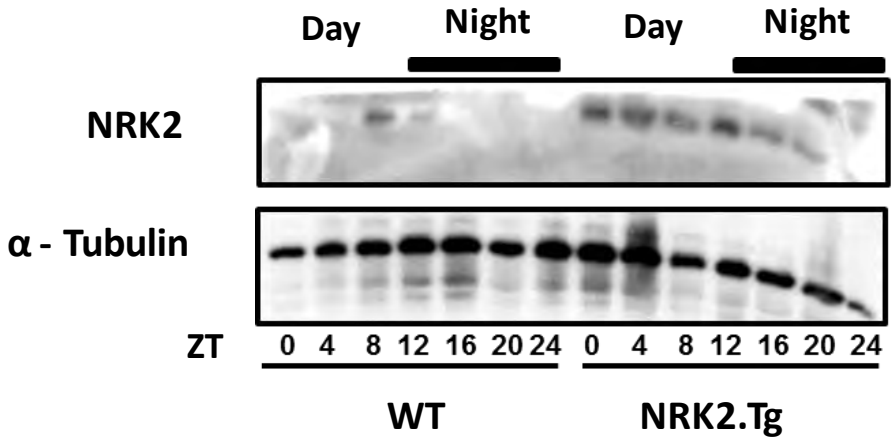

Figure 3-14 – Circadian variation in Nmrk2 protein levels in WT and NRK2.Tg TA. Representative immunoblot indicating variable circadian expression levels of NRK2 in WT skeletal muscle and constitutive circadian expression in NRK2.Tg muscle. n = 1.

3.3.8 Skeletal muscle NRK2 overexpression does not affect whole body metabolic phenotype or glucose tolerance

Having observed that NRK2 overexpression may augment NAD^+ levels during night hours, it was then important to ascertain any functional metabolic consequences caused by constitutive NRK2 overexpression. 48 hour home cage monitoring indicated that the mice consumed approximately 24 calories over 48 hours with an increased rate of consumption

during dark (active) hours accompanied by increased energy expenditure and VO_2 as would be expected during periods of activity. Furthermore, RER values peaked during these times indicating a switch to carbohydrate metabolism, with fatty acid oxidation proportionally more favoured during inactive hours (Figure 3-15). However, no significant differences in these parameters were observed in skeletal muscle NRK2 overexpressing mice. Over the 48 hours both during light and dark phases. When subjected to linear regression and ANCOVA, no significant differences in slopes, elevations or Y intercepts were observed in any parameter when plotted against body weight indicating that no there are no significant metabolic differences when adjusted for body weight. Taken together, these results indicate that skeletal muscle NRK2 overexpression does not alter whole body metabolic phenotype despite apparent elevation in skeletal muscle NAD^+ levels during active hours.

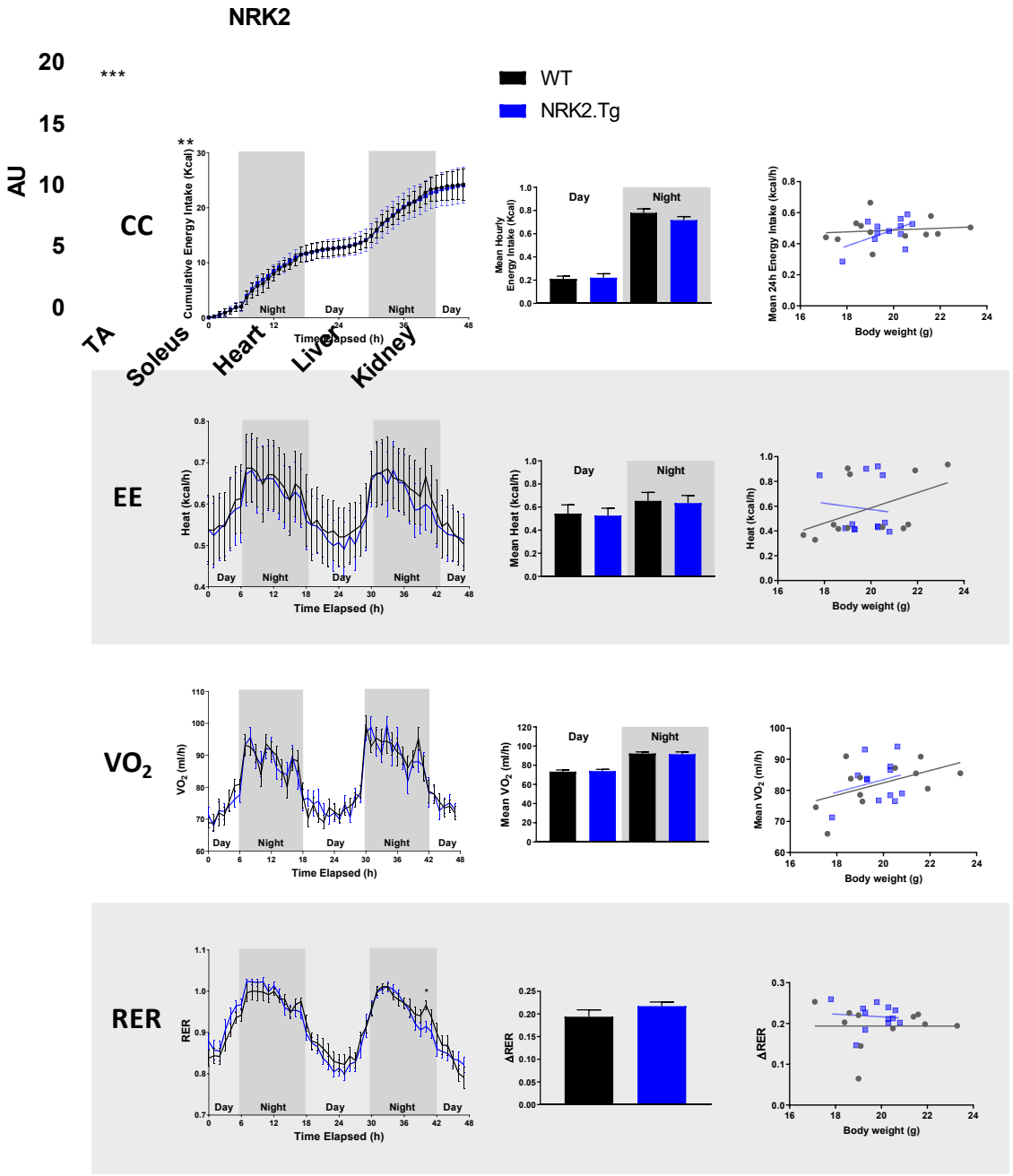

Figure 3-15 – Whole body basal metabolic phenotype is comparable between WT and NRK2.Tg mice over 48 hours. Indirect calorimetric analysis of 3 month old female WT and NRK2.Tg mice quantifying caloric consumption (CC), energy expenditure (EE) and VO_2 presented as a trace of hourly averages, average day/night values and linear regression relative to body weight. RER is presented as a trace of hourly averages and ΔRER, a representation of metabolic flexibility which is calculated by subtracting the average of the 5 highest values during the night phase from the average of the 5 lowest values during the day phase. Data presented as mean ± SEM. Statistical significance of corresponding trace timepoints and average day/night values were determined by student's unpaired t test (* $p < 0.05$, ** $p < 0.01$, *** $p < 0.001$). n = 12.

Given the importance of skeletal muscle in whole body glucose homeostasis as a major insulin responder and carbohydrate reserve organ (66) and the importance of NAD^+ in glucose tolerance and insulin response levels (165, 180), IPGTT were performed to assess any potential changes in speed and efficacy of the excess blood glucose clearing response with NRK augmentation. Blood glucose clearance rates were closely comparable between WT and NRK2.Tg mice (Figure 3-16), NRK2 indicating that augmentation of the NRK pathway within skeletal muscle does not affect whole body glucose metabolism in young mice.

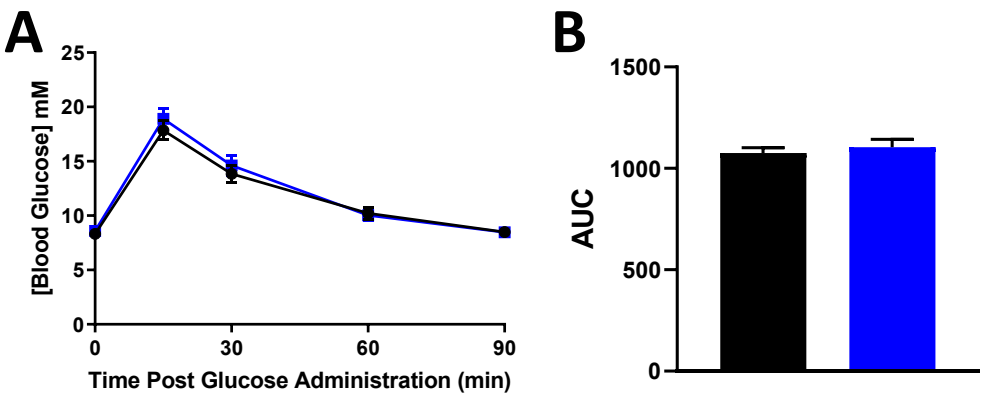

Figure 3-16 – Glucose tolerance is comparable between WT and NRK2.Tg mice. Baseline blood glucose measurements followed by 15, 30, 60 and 90 minutes post glucose administration in 3 month old female WT and NRK2.Tg mice (A) alongside AUC analysis (B). Data presented as mean ± SEM. Statistical significance of corresponding trace timepoints and AUC were determined by student's unpaired t test (* $p < 0.05$, ** $p < 0.01$, *** $p < 0.001$). n = 6-8.

3.4 Discussion

The results of this chapter validated and comprehensively established the basal metabolic phenotype of NRK2.Tg mice that will form the basis of onward experimental work for two main reasons. Firstly, to now better evaluate the functional consequences of constitutive in vivo overexpression of NRK2 within skeletal muscle, and inform how NRK2 upregulation under metabolic stress can influence metabolism. Secondly, the results provide a comparative baseline for upcoming experiments involving ageing and altered nutrition. The NRK2.Tg mouse model was thoroughly validated at the genomic, transcriptomic, protein and functional level, demonstrating no induction of the UPR, no detection of aberrant transgene expression within the skeletal muscle of floxed control mice or any expression of transgenic NRK2 outside of muscle tissue in either floxed or skeletal muscle specific NRK2 overexpressing mice.

Although cardiac muscle was not a primary target tissue for NRK2 overexpression, higher expression levels were detectable at RNA and protein level at approximately the same fold change relative to WT expression as in skeletal muscle, though absolute expression levels were far less. ACTA1 is expressed in the heart, albeit at a lower magnitude in comparison to skeletal muscle as the cardiac actin (ACTC) isoform constitutes the vast majority (372). This low level of expression however appears enough to induce some transcription of Cre recombinase in some cardiac fibres, resulting in NRK2 overexpression.

NRK2 overexpression did not significantly affect development, with mice developing through adolescence into adulthood with no discernible differences in body weight or behaviour. This indicates that though NRK2 has been shown to have roles within myogenesis

(344) and myotube fusion and differentiation (341), constitutive skeletal muscle overexpression of NRK2 does not severely impact on embryonic myogenesis or normal development through adolescence. During embryogenesis, skeletal muscle tissue mainly expresses ACTC rather than skeletal muscle actin which gradually switches to skeletal muscle actin (ACTA1) as gestation progresses (372). Furthermore, a recent study quantifying gene expression throughout activation and differentiation stages of an in vitro human embryonic muscle stem cell model suggests that ACTA1 mRNA levels remain very low during cycling $Pax7^{+}$, quiescent $Pax7^{+}$ and activated $Pax7^{+}/MyoG^{+}$ stages, with a marked increase upon downregulation of Pax7 and subsequent differentiation into striated muscle (373). Initial quantification of the ACTA1-Cre mouse model corroborated this, with Cre transcription detected within embryonic somites at 9.5 days post coitum (dpc) within elongated and differentiated muscle cells in a rostrocaudal orientation, progressing to strong expression in dorsal-ventral running fibres within segmental blocks of the myotome (352). These data suggest that NRK2 overexpression is minimal within embryonic myogenic precursors during embryonic development and that in this model, the NRK2.Tg allele may not be active in embryonic skeletal muscle during critical developmental stages with the majority of development occurring under normal expression levels of NRK2. While it is thought that endogenous Nmrk2 expression is primarily confined to mature, striated muscle (374), further investigations into temporal expression patterns of endogenous Nmrk2 during embryogenesis would be beneficial, though a different model of NRK2 overexpression would be required to further investigate the effects of NRK2 overexpression on embryonic myogenesis.

Overexpression of NRK2 did not significantly affect basal skeletal muscle NAD^+ and NADH levels at 10:00. This agrees with previous observations that while the NRKs are rate limiting in the overall production of NAD^+ from NR (16), substrate bioavailability is also a key factor. It is likely that endogenous NR levels are insufficient to saturate available NRK enzyme at physiological expression levels with the conversion of NR to NMN operating far below the Vmax of NRK2, thus increasing enzyme concentrations does not increase cellular NAD^+ levels. This may also explain why mRNA expression levels of other key skeletal muscle NAD^+ salvage enzymes and NAD^+ dependent signalling enzymes were unaffected, which also agrees with the observed redundancy of the NRK salvage pathway relative to NAM recycling via NAMPT in the preservation of skeletal muscle NAD^+ homeostasis under resting metabolic conditions (15, 16). The observation of significantly elevated NAD^+ levels in NRK2.Tg skeletal muscle relative to WT muscle in conditions of NR substrate excess reaffirmed the idea that NRK mediated phosphorylation of NR to NMN is the rate limiting step the conversion of NR through to NAD^+, and also determined that transgenic NRK2 exhibits functional kinase activity within NRK2.Tg skeletal muscle. NR is unstable in blood (375, 376) and plasma (16) , undergoing hydrolysis to NAM and ADPr with a half-life of approximately three minutes (314). However, the observed additive effect with NR supplementation in NRK2 overexpressing skeletal muscle confirms that at least some NR must reach skeletal muscle intact when injected intraperitoneally up to at least one hour post administration, a phenomenon that has until now only been confirmed in labelled NR administered through intravenous injection (314).

NAD^+ and NADH are critical in contracting muscle through its role as a redox cofactor driving oxidative metabolism (310). Furthermore, NAD^+ consumption is significantly

increased through increased SIRT activity, driving metabolic adaptation to meet cellular energy requirements (317). Despite this imposed reliance of contracting skeletal muscle on NAD^+ salvage from NAM and NR (15), NRK2 overexpression did not significantly affect the real time metabolic response to exercise and no differences in skeletal muscle NAD^+ levels or post-exercise TCA cycle metabolite concentrations were observed in muscle collected immediately after cessation of exercise.

NAD^+, NADH and total NAD concentrations were not significantly different between sedentary and exercised skeletal muscle immediately after exercise in either genotype, nor were any significant perturbations to the NAD^+/NADH ratio. Animal studies have suggested increases in skeletal muscle NAD^+ and the NAD/NADH ratio following exercise (105, 248) though other studies have conversely suggested increases in NADH and a reduction in NAD^+ (377) as well as no immediate changes in NAD^+ during contraction (378) or immediately following exercise (220), the latter of which these data corroborate. The picture is also complicated in contracting human muscle (310), though exercise intensity is thought to significantly impact on NAD^+/NADH dynamics, with one study reporting reduced NADH levels but no impact on NAD^+/NADH ratio under lower intensity and elevated NAD^+ and NAD^+/NADH ratio under intense exercise (379). The animal licensing regulations under which the exercise data presented in this chapter was generated did not allow for determination of VO2max and thus no means of accurate determination of exercise intensity, constituting a study limitation. Furthermore, no differences in skeletal muscle lactate levels were observed between sedentary and exercised muscle, though this could be explained through rapid clearance from skeletal muscle into the blood (380). Despite this, differences in TCA

metabolites were apparent indicating that the exercise protocol was efficacious enough to elicit an oxidative metabolic response.

It is again likely that the NAD^+ metabolome was unchanged between WT and NRK2.Tg animals due to insufficient endogenous levels of endogenous NR precursor, resulting in no effect of enzyme overexpression on the NAD^+ metabolome. However, the NAD^+/NADH and central carbon metabolite quantification methods available for this thesis only provided a snapshot of absolute concentrations and could offer no information on synthesis and flux rates, which may have varied between WT and NRK2.Tg animals, though it is clear that NAD^+ was maintained at sufficient levels throughout the exercise protocol in both genotypes with both WT and NRK2.Tg animals being equally capable of completing the designated exercise protocol. Furthermore, it could be assumed that the skeletal muscle NAD^+ salvage pathways could sufficiently maintain metabolic homeostasis under the imposed energetic stress of the acute exercise protocol due to the mice being young and healthy, and therefore further augmentation of NAD^+ salvage would not improve metabolic phenotypes past the physiological optimum (315).

The observed trend of elevated basal pyruvate and significantly lower aspartate levels in NRK2.Tg skeletal muscle indicated a potential dysregulation of oxidative metabolism, prompting examination of maximal fatty acid oxidation (FAO) capacity of NRK2.Tg TA and soleus relative to WT muscle. No significant differences in O_2 flux were observed under any respiratory state indicating that such differences are not relevant to maximal mitochondrial function, and it could be further concluded from this experiment that augmentation of the NRK pathway does not significantly alter mitochondrial capacity or increase mitochondrial volume in slow and fast twitch muscle types in young mice.

The transient yet significant elevation in TA and soleus NAD^+ concentrations during night time hours was an unanticipated observation given the consensus that endogenous NR concentrations are insufficient to influence changes to the NAD^+ metabolome regardless of NRK2 levels (164, 314). Most interestingly, differences in skeletal muscle NAD^+ levels coincided with times at which a disparity was observed between normal circadian fluctuations of NRK2 expression in WT muscle and constitutive overexpression in NRK2.Tg tissue. Mice are nocturnal and more physically active during night hours, which could explain the observed increase in NAD^+ and decrease in NADH (310), a trend which was apparent in NRK2.Tg TA relative to WT muscle but not soleus, although data in section 3.3.5 suggested no changes in NAD^+ as a result of physical activity. However, other mouse studies have reported no immediate changes in skeletal muscle NAD^+ after exercise but a significant rise 3 hours afterwards (220). It could be assumed that the mice had been active and feeding for at least 3-4 hours prior to collection at ZT16, and it is therefore possible that constitutive overexpression of NRK2 could potentiate contraction induced rises in skeletal muscle NAD^+ over sustained bouts of activity through augmentation of NRK mediated NAD^+ salvage from NR.

Mice also consume food at a greater rate during night hours, therefore ingesting more niacin which could raise endogenous NR levels to effective levels for NAD^+ boosting with more NRK2 enzyme, though NR levels in the regular animal chow are undetermined. NR is present in other foodstuffs such as milk (160) with NR dependent bacteria able to thrive in the gut (381), and NR is known to be orally bioavailable (164), although a more recent study has suggested that orally ingested NR may not reach skeletal muscle tissue intact (314). More studies into prolonged exercise bouts, trained phenotypes and/or NR supplementation

methods are required to elucidate functional mechanisms behind this transient NAD^+ boosting effect in NRK2.Tg skeletal muscle.

Despite the observed nocturnal skeletal muscle NAD^+ boosting effects, no significant differences were observed in metabolic phenotype, with mice consuming comparable levels of calories, expending similar amounts of energy and effectively switching between carbohydrates and lipids as main fuel sources during times of heightened activity and rest as is expected in healthy animals (67). Furthermore, glucose tolerance levels were unaffected in NRK2.Tg mice. Skeletal muscle is of central importance to systemic metabolism as a key site of energy storage and energy expenditure with high adaptability to conditions of metabolic stress (18), processes which are reliant on sufficient cellular NAD^+ levels (11, 220, 382). The metabolic flexibility of skeletal muscle is also directly driven by NAD^+ dependent activity of SIRTs (237). However, increasing NAD^+ bioavailability past physiological requirements is unlikely to improve metabolic phenotypes that are already optimal in young, healthy and metabolically unstressed mice (315). Furthermore, increasing skeletal muscle NAD^+ levels alone in young and healthy animals does not promote a shift towards a more oxidative metabolic phenotype (315), which could explain why no improvements in mitochondrial oxidative capacity were observed despite possible transient NAD^+ boosting in NRK2.Tg skeletal muscle. To further determine the roles of the NRK2 pathway in skeletal muscle, the next step was therefore to establish any beneficial metabolic consequences resulting from skeletal muscle NRK pathway augmentation in context of metabolic stressors such as altered nutrition and ageing.

CHAPTER 4 – METABOLIC RESPONSE TO AGEING IN MICE WITH MUSCLE-SPECIFIC OVEREXPRESSION OF NRK2

4.1 Introduction

4.1.1 NRK2 Augmentation in young mice

The previous chapter confirmed significant and specific NRK2 overexpression in skeletal muscle of NRK2.Tg mice, in which NAD^+ levels are more efficaciously boosted in response to IP administered NR. Circadian variations in endogenous NRK2 expression levels were also confirmed, with significant transient increases in skeletal muscle NAD^+ in NRK2.Tg skeletal muscle which could be attributed to constitutive NRK2 overexpression. However, no significant functional metabolic differences were observed between WT and NRK2.Tg mice both basally and in response to exercise, agreeing with previous observations that increasing skeletal muscle NAD^+ levels past optimum physiological levels does not confer additional metabolic benefits (315). However, metabolic stressors are accompanied by a drastic compensatory increase in cellular NAD^+ consumption, placing significant demands on NAD^+ salvage systems for maintaining NAD^+ homeostasis (289, 310). Under chronic conditions of metabolic dysfunction such as with ageing, this results in a cellular NAD^+ deficit as NAD^+ repleting pathways are downregulated and/or unable to keep pace with increased cellular requirements (105, 315), leading to metabolic decline and pathophysiological disease states (289).

4.1.2 NAD^+ and metabolic decline with age

A sedentary lifestyle results in metabolic decline with age in the form of insulin resistance, obesity, impaired mitochondrial biogenesis and function, impaired metabolic flexibility and increased inflammation (67, 383, 384). This predisposes individuals to disease states such as

type II diabetes, NAFLD, cardiovascular disease and sarcopenic obesity (385, 386). Many ageing rodent models also report a significant decline in cellular NAD^+ levels within liver (168, 284, 292, 387), adipose tissue (180, 284) and skeletal muscle (11, 171, 180, 184, 284, 292, 387). This loss of bioavailable NAD^+ is cited as both a cause and a symptom of age related metabolic decline, and is driven by a multitude of factors including NAMPT expression and activity levels declining significantly in aged skeletal muscle (105, 315) and upregulation of NAD^+ consuming enzymes such as PARPs and CD38, ultimately leading to suppressed SIRT activity and impaired oxidative metabolism (261, 284, 292). This phenotype is thought to be self-sustaining in that lower SIRT activity decreases mitochondrial biogenesis and turnover (388, 389), leading to increased ROS generation from defective mitochondria and more DNA damage (390), and thus ever increasing PARP NAD^+ consumption (261, 389, 391, 392). In absence of nutritional and/or exercise interventions, severe metabolic impairment and clinical sarcopenia arises resulting in an ever declining metabolic phenotype (296). Given the importance of skeletal muscle as a site of energy metabolism and substrate storage, dysfunctional skeletal muscle significantly impairs whole body metabolic homeostasis and overall healthspan.

4.1.3 NRK salvage as an inducible path to NAD^+ under metabolic stress

Though NRK2 is dispensable for maintaining general skeletal muscle NAD^+ homeostasis (15, 16), it is upregulated in response to severe redox stress (325). Furthermore, a negative effect on skeletal muscle NAD^+ levels was observed upon knocking out NRK2 (325). Such observations may implicate NRK2 as an inducible auxiliary route to NAD^+ in skeletal muscle under metabolic stress. Many studies have already reported functional metabolic

improvements and protective effects with NR (11, 165, 167, 168, 173) and NMN (180, 181, 184) supplementation in models of ageing and/or obesity. It is therefore possible that chronic augmentation of the NRK pathway through constitutive NRK2 overexpression and/or chronic NR supplementation could prevent sarcopenia and metabolic decline associated with insufficient NAD^+ levels in skeletal muscle, improving whole body metabolism as a result (19). It is also important to note that endogenous NRK2 expression within skeletal muscle is dynamic over 24 hours and associated with circadian regulation, as determined in the previous chapter. A lifetime of chronic NRK2 overexpression may therefore present significant metabolic consequences in aged mice.

To further investigate the functional relevance of the skeletal muscle NRK salvage pathway in vivo, the next objective was to establish any adaptive metabolic consequences of constitutive NRK2 overexpression in response to metabolic stress imparted through the ageing process. Furthermore, the metabolic effects of chronic oral NR administration in aged animals was investigated, both in light of NR as a potential therapeutic option for combating age and NAD^+ associated pathophysiology and to further establish the metabolic relevance of NRK2 through a model of constitutive NRK pathway augmentation under conditions of substrate excess. It was hypothesised that under conditions of inactivity, obesity and ageing, skeletal muscle NRK pathway augmentation via NRK2 overexpression and/or NR precursor supplementation could counterbalance the cellular NAD^+ deficit resulting from downregulation of NAD^+ salvage mechanisms and upregulation of NAD^+ consumption pathways, improving the oxidative metabolic phenotype under chronic metabolic stress (Figure 4-1).

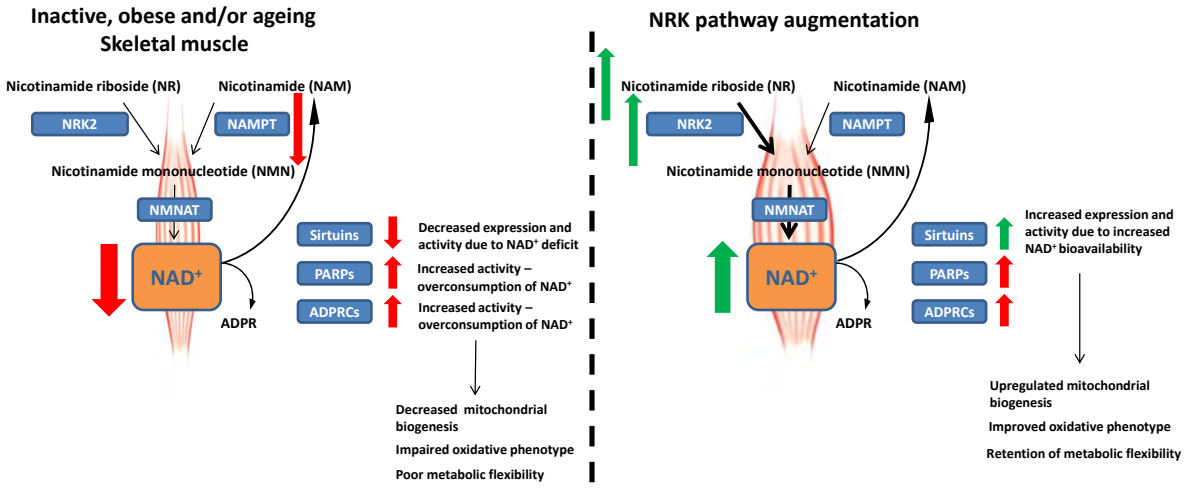

Figure 4-1 – Hypothesised in vivo metabolic consequences of NRK2 overexpression and/or NR supplementation in aged skeletal muscle. In ageing muscle, NAMPT is downregulated whilst PARP and cyclic ADP-ribose synthase activity increases (261, 284, 292). As a result, NAD^+ consumption outweighs NAD^+ repletion, creating an NAD^+ deficit that contributes towards metabolic decline through downregulated SIRT activity. Augmentation of the NRK salvage pathway through constitutive NRK2 overexpression and NR precursor supplementation could boost cellular NAD^+ levels in skeletal muscle, thereby improving aged and obese metabolic phenotypes.

Specifically, this chapter aimed to:

- Characterise the molecular and physiological consequences of lifetime constitutive skeletal muscle NRK2 overexpression in aged mice.
- Assess the applicability of orally administered NR in augmenting the skeletal muscle NAD^+ metabolome and overall metabolic health with age.
- Establish the relationship between NRK2 levels and NR substrate levels given the observed affects on the NAD^+ metabolome in aged skeletal muscle.

4.2 Materials and methods

4.2.1 Animal care

Age related deteriorations in skeletal muscle signalling, structure and function manifest at around 18 months of age in C57BL/6 mice (393-396), and ageing past 18 months significantly increases the risk of potentially confounding comorbidities which are often undetectable until post mortem analysis. It was therefore decided that in vivo metabolic profiling would be carried out on 18-20 month old mouse cohorts, with tissue analysis performed on 21-23 month old mice upon completion of in vivo experimentation. Mice were bred and aged in-house, with ageing mice kept in conditions as detailed in section 2.1. Mice were monitored daily for signs of illness and weighed weekly after 52 weeks of age to ensure welfare standards and to assess the impact of oral NR supplementation on animal health and behaviour. Mice with overt comorbidities were excluded from experiments.

4.2.2 Oral NR supplementation

To investigate the effects of skeletal muscle NRK2 overexpression in aged mice under conditions of nutrient excess, regular drinking water was replaced with 5 g/L nicotinamide riboside chloride. This concentration was selected based on previous studies into the supplemental efficacy of orally administered NR which utilised approximately 400 mg/kg/day NR, taking into account observed average daily mouse water consumption and average body weight of 18 month old WT and NRK2.Tg mice (164, 165, 167), with the aged mice in this study consuming approximately 325 mg/kg/day. 5 g nicotinamide riboside chloride (Chromadex, California, USA) was dissolved in 1 l tap water and filter sterilised through a 0.2

µm pore diameter filter. The addition of NR to tap water was not found to significantly alter pH levels, which was determined as approximately 6.5 for both the regular tap water and with 5 g/L NR. This was deemed acceptable based on evidence that NR retained ~95% stability after 1 week when dissolved in drinking water (11) and was most stable in water around neutral pH levels (160).NR water bottles were protected from light with the water replaced every third day to further minimise degradation.

4.2.3 Indirect calorimetry

Indirect calorimetry experiments were performed on 18 month old female WT and NRK2.Tg mice according to the acclimatisation and experimentation protocols detailed in section 2.10.1. Indirect calorimetry was repeated to the same specifications after 4 weeks of NR supplementation in the NR supplemented cohort.

4.2.4 IPGTTs

IPGTTs were performed on 18 month old mice one week after indirect calorimetry as detailed in section 2.11. For welfare reasons, 40% glucose was used instead of 20% glucose allowing for administration of half the regular volume of glucose solution. Mice of the NR supplementation cohort were then placed onto NR water 72 hours post IPGTT to ensure full recovery prior to supplementation. IPGTTs were then repeated to the same specifications a week after the second metabolic assessment via indirect calorimetry (5 weeks post onset of NR supplementation).

4.2.5 High resolution respirometry

After cervical dislocation and tissue collection, TA and soleus from 22-24 week old WT and NRK2.Tg mice with or without 16 weeks of NR supplementation was assessed via high resolution respirometry according to section 2.8. Mice were culled and tissue collected between 10:00 and 12:00. Tissue preparation was performed according to section 2.8.1 followed by high resolution respirometry according to section 2.8.2.

4.2.6 NAD^+ quantification

Snap frozen quadriceps from aged WT and NRK2.Tg animals with or without oral NR supplementation was pulverised and 10 mg tissue weighed according to section 2.3.1. Tissue samples were then homogenised in 400 µl NAD^+/NADH Extraction buffer and NAD^+ and NADH levels were quantified using the NAD^+/NADH quantitation kit (Biovision, California, USA) as detailed in section 2.7.

4.2.7 RNA extraction, reverse transcription and qPCR

RNA was extracted from mouse quadriceps samples as detailed in section 2.5.1 and reverse transcription was performed according to section 2.5.2. For qPCR analysis, all genes besides Nmrk2 were assayed using TaqMan probes following the protocol detailed in section 2.5.4. Nmrk2 was optimised and assayed using the SYBRGreen gene expression assay method to the protocol detailed in section 2.5.5. GUSB was used as the endogenous control gene for all qPCR performed within this chapter for reasons outlined in section 2.5.4.

4.2.8 Targeted Metabolomics

Female WT and NRK2.Tg 22-24 month old quadriceps samples were extracted derivatised and analysed via GCMS to quantify key anaplerotic amino acids and TCA cycle intermediates according to section 2.9.1.

4.2.9 Untargeted Metabolomics

Female WT and NRK2.Tg 22-24 month old quadriceps samples were prepared for LCMS analysis according to section 2.9.2.

4.3 Results

4.3.1 The in vivo effects of chronic skeletal muscle NRK augmentation on ageing metabolic phenotype

A decline in bioavailable NAD^+ is thought to be a key contributor to the functional decline of skeletal muscle with age, which in turn leads to overall metabolic decline and predisposition to metabolic disease (11, 171, 180, 184, 284, 292, 387). Based on the role of NRK2 as an NAD^+ salvage enzyme that is upregulated under conditions of metabolic stress (325), it was hypothesised that augmentation of the skeletal muscle NRK pathway could ameliorate this age related decline in NAD^+ and ameliorate the associated decline in skeletal muscle metabolic health. WT and NRK2.Tg mice were therefore aged to 18-23 months before metabolic phenotyping experiments were performed.

4.3.2 Aged NRK2 overexpressing skeletal muscle presents with upregulated Nmrk1, Nampt and SIRTs

Previous studies have reported significant changes in NAD^+ salvage enzyme expression levels with age as well as NAD^+ dependent signalling enzymes within skeletal muscle (105). To further investigate these reports and establish any effects of chronic NRK2 overexpression on NAD^+ signalling and salvage dynamics in aged skeletal muscle, expression levels of key NAD^+ salvage and NAD^+ dependent enzymes were assessed in aged WT and NRK2.Tg mice and also compared directly with expression levels in young skeletal muscle. Interestingly, expression levels of NRK2 were lower in aged WT mice relative to young WT mice with a similar statistically significant trend observed in NRK2.Tg mice, though Nmrk2 remained

significantly overexpressed relative to WT in both young and aged mice (Figure 4-2). Nmrk1 levels were unexpectedly upregulated in aged mice relative to young, particularly so within NRK2.Tg mice (Figure 4-2). Furthermore, Nampt and Nmnat1 were significantly upregulated in aged NRK2.Tg mice relative to young NRK2.Tg mice which was not observed in WT mice, suggesting that chronic NRK2 overexpression may also augment expression levels of other key skeletal muscle NAD^+ salvage enzymes with age (Figure 4-2). Expression levels of Sirt1 and Sirt3 trended upwards in aged NRK2.Tg mice relative to young mice. This was not observed in either SIRT isoform within WT mice, suggesting that NRK2 overexpression could marginally increase SIRT expression levels with age. Parp1 expression levels were also unexpectedly lower in aged relative to young WT muscle, which was not observed in NRK2.Tg muscle. These changes suggest that NRK2 overexpression could affect NAD^+ salvage and signalling dynamics in aged skeletal muscle.

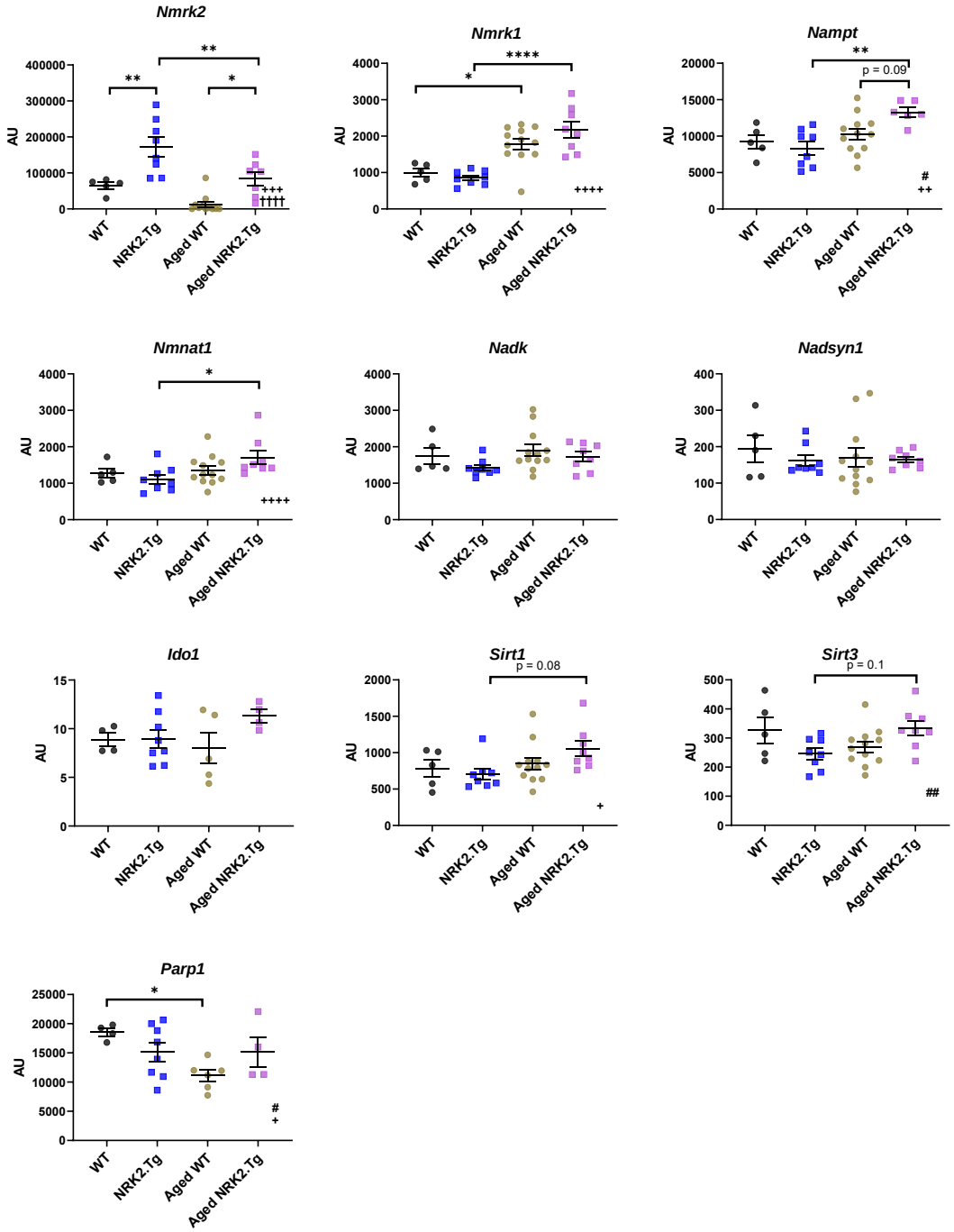

Figure 4-2 – Expression levels of key skeletal muscle NAD$^+$ salvage enzymes, NADK and SIRTs in female young and aged WT vs. NRK2.Tg quadriceps. Quantification of mRNA transcript levels of NAD$^+$ processing and dependent enzymes WT and NRK2.Tg quadriceps in 3 month and 20-22 month old female mice. Data presented as mean ± SEM with individual data points representing one biological replicate. Statistical significance was determined by ordinary two way ANOVA (* $p < 0.05$, ** $p < 0.01$, *** $p < 0.001$). n = 5-8. # = statistically significant interaction between genotype and age; + = statistically significant variation between young and aged mice; † = statistically significant variation between WT and NRK2.Tg mice.

4.3.3 NRK2 overexpression does not significantly alter aged skeletal muscle bioenergetics

Observations in section 3.3.3 and previous studies (15, 16) implicate NRK2 as the rate limiting enzyme for the production of NAD^+ from NR, with previous studies suggesting that skeletal NAD^+ declines with age, contributing towards a diminished metabolic phenotype (11, 171, 180, 184, 284, 292, 387). It was therefore critical to establish the effects of age and NRK pathway augmentation on the skeletal muscle NAD^+ metabolome. NAD^+, NADH and total NAD levels were quantified in young and aged WT and NRK2.Tg quadriceps. Remarkably, skeletal muscle NAD^+ levels were unchanged with age, with NADH, total NAD concentrations and NAD^+:NADH ratios all comparable (Figure 4-3). These data indicate that skeletal muscle NAD^+ levels do not decline with age in this model, and chronic NRK augmentation within skeletal muscle does not affect absolute NAD^+ concentrations within aged skeletal muscle.

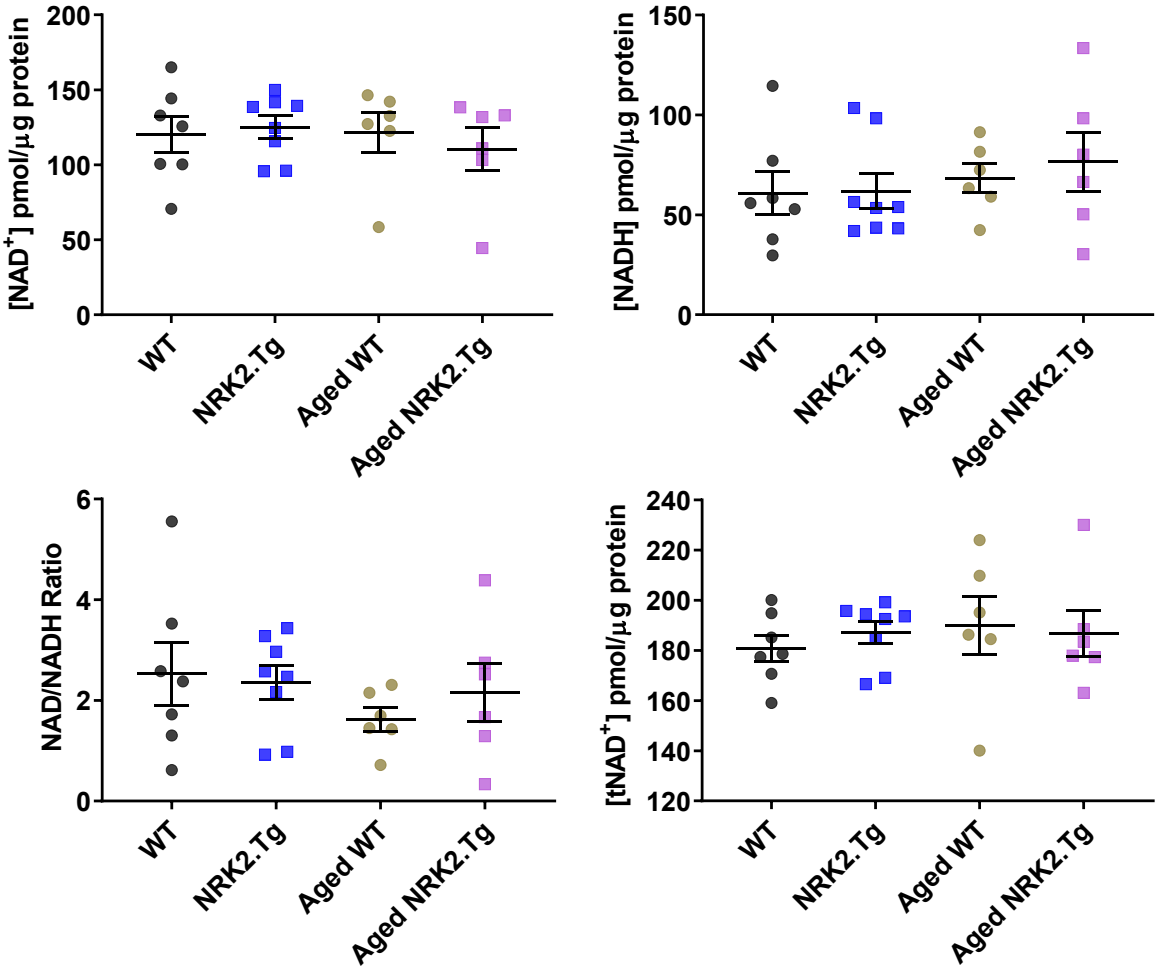

Figure 4-3 – Skeletal muscle NAD$^+$ dynamics are not significantly altered between young or aged WT and NRK2Tg mice. Quantification of NAD$^+$, NADH, NAD$^+$/NADH ratio and total NAD levels in quadriceps collected from 3 month old WT and NRK2.Tg mice and 20-24 month old mice. Data presented as mean ± SEM with individual data points representing one biological replicate. Statistical significance was determined by ordinary two way ANOVA with Tukey's multiple comparison tests (* $p < 0.05$, ** $p < 0.01$, *** $p < 0.001$, **** $p < 0.0001$). n = 6-8. # = statistically significant interaction between genotype and age; + = statistically significant variation between young and aged mice; † = statistically significant variation between WT and NRK2.Tg mice.

To further validate these unexpected observations and estimate cellular energetic status, quadriceps tissue from young and aged WT and NRK2.Tg mice was analysed via untargeted LCMS. Again, no significant differences between young and aged skeletal muscle NAD$^+$ levels were observed (Figure 4-4). Furthermore, ATP levels were not significantly

changed with age, indicating sufficient energy production at rest in all animals (Figure 4-4). Concentrations of NAM and the clearance metabolite N-methylnicotinamide (MeNAM) were not significantly altered between all groups.

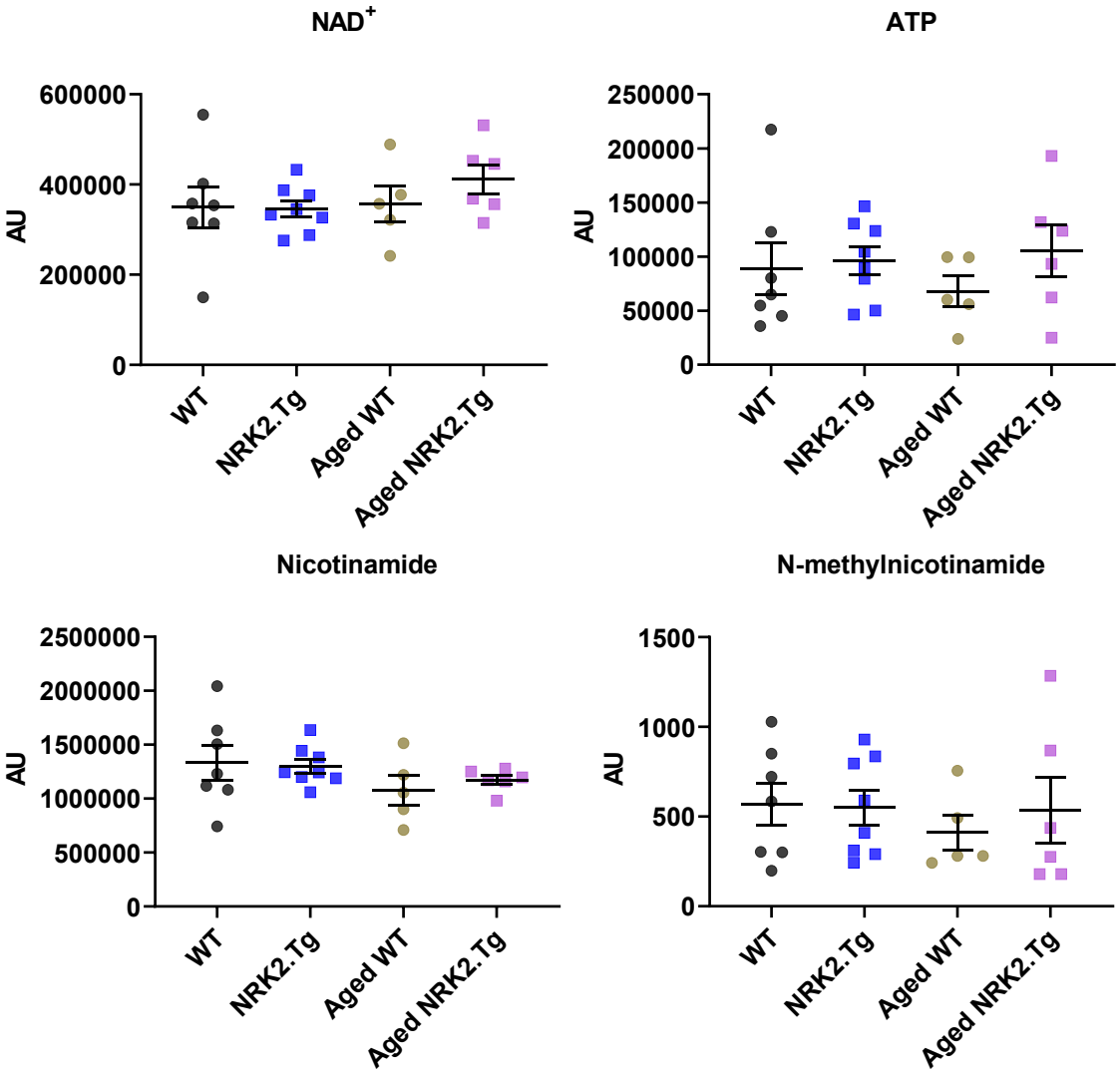

Figure 4-4 – Skeletal muscle NAD$^+$, ATP, NAM and MeNAM levels are comparable between young and aged WT and NRK2.Tg mice. LCMS Quantification of NAD$^+$, ATP, NAM and MeNAM levels in quadriceps collected from female 3 month old and 22-24 month old WT and NRK2.Tg mice. Data presented as mean ± SEM with individual data points representing one biological replicate. Statistical significance was determined by ordinary two way ANOVA with Sidak's multiple comparison tests (* $p < 0.05$, ** $p < 0.01$, *** $p < 0.001$, **** $p < 0.0001$). n=5-7. # = statistically significant interaction between genotype and age; + = statistically significant variation between young and aged mice; † = statistically significant variation between WT and NRK2.Tg mice.

Based on observations of increased NAD^+ levels in male NRK2.Tg mice during night hours in section 3.3.7, a similar experiment was then performed to validate these observations in female mice and to establish if the boosting effect persists with age. Skeletal muscle from young and aged WT and NRK2.Tg mice was harvested at 22:00 during the dark active phase followed by quantification of the NAD metabolome. Unprecedentedly, the significant nightly NAD^+ boosting effect seen in young male TA and soleus was not present within young female quadriceps. This suggests potential sex specific or muscle bed specific variations in circadian regulation of NAD^+ levels with regards to skeletal muscle NRK augmentation. Furthermore, no significant differences in total NAD^+, NADH, and NAD/NADH ratio were observed across all groups (Figure 4-5). However, total NAD levels were significantly lower in aged mice (Figure 4-5), a phenomenon which was not observed in skeletal muscle collected at 10:00 (Figure 4-3), but no significant differences were observed between WT and NRK2.Tg skeletal muscle. These data suggest a dysregulation of the NAD metabolome in aged mice during active hours whereby total levels of NAD are diminished but cellular redox status is unaffected, and constitutive overexpression of the NRK2 enzyme is not sufficient to ameliorate this effect.

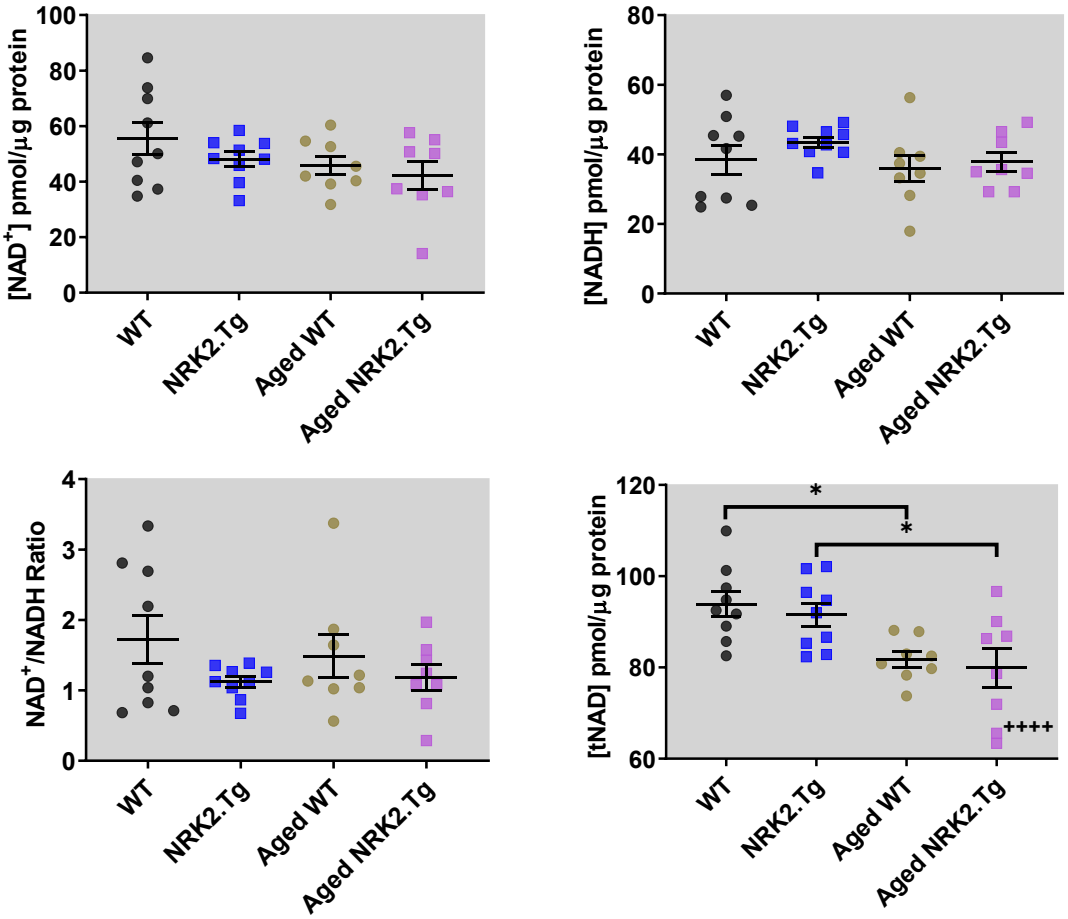

Figure 4-5 – Aged skeletal muscle total NAD levels are significantly depleted during active hours, with NRK2 overexpression having no significant effects on the skeletal muscle NAD metabolome in young or aged female mice. Quantification of NAD^+, NADH, NAD^+/NADH ratio and total NAD levels in quadriceps collected from female 3 month old and 18-20 month old WT and NRK2.Tg mice at 22:00. Data presented as mean ± SEM with individual data points representing one biological replicate. Statistical significance was determined by ordinary two way ANOVA with Tukey's multiple comparison tests (* $p < 0.05$, ** $p < 0.01$, *** $p < 0.001$, **** $p < 0.0001$). n = 8-9. # = statistically significant interaction between genotype and age; + = statistically significant variation between young and aged mice; † = statistically significant variation between WT and NRK2.Tg mice.

Female young and aged skeletal muscle metabolic profiles were also compared using GCMS to assess changes in central carbon metabolism with age in WT and NRK2.Tg mice. Skeletal muscle alanine, proline and asparagine concentrations were significantly decreased with age, with a more significant decrease in proline and asparagine observed in WT mice

relative to NRK2.Tg mice (Figure 4-6). Several TCA cycle intermediate concentrations trended downwards with age in WT skeletal muscle, including succinate and malate, though again these downward ageing trends were not present within NRK2 overexpressing skeletal muscle (Figure 4-6). These data suggest some preservation of free amino acid levels in NRK2 overexpressing skeletal muscle with age and some amelioration of altered TCA cycle dynamics in NRK2.Tg skeletal muscle. Notably, the upward trend in pyruvate and significantly reduced aspartate levels observed in young male NRK2.Tg mice in section 3.3.5 were not present in the young female cohort used for this experiment.

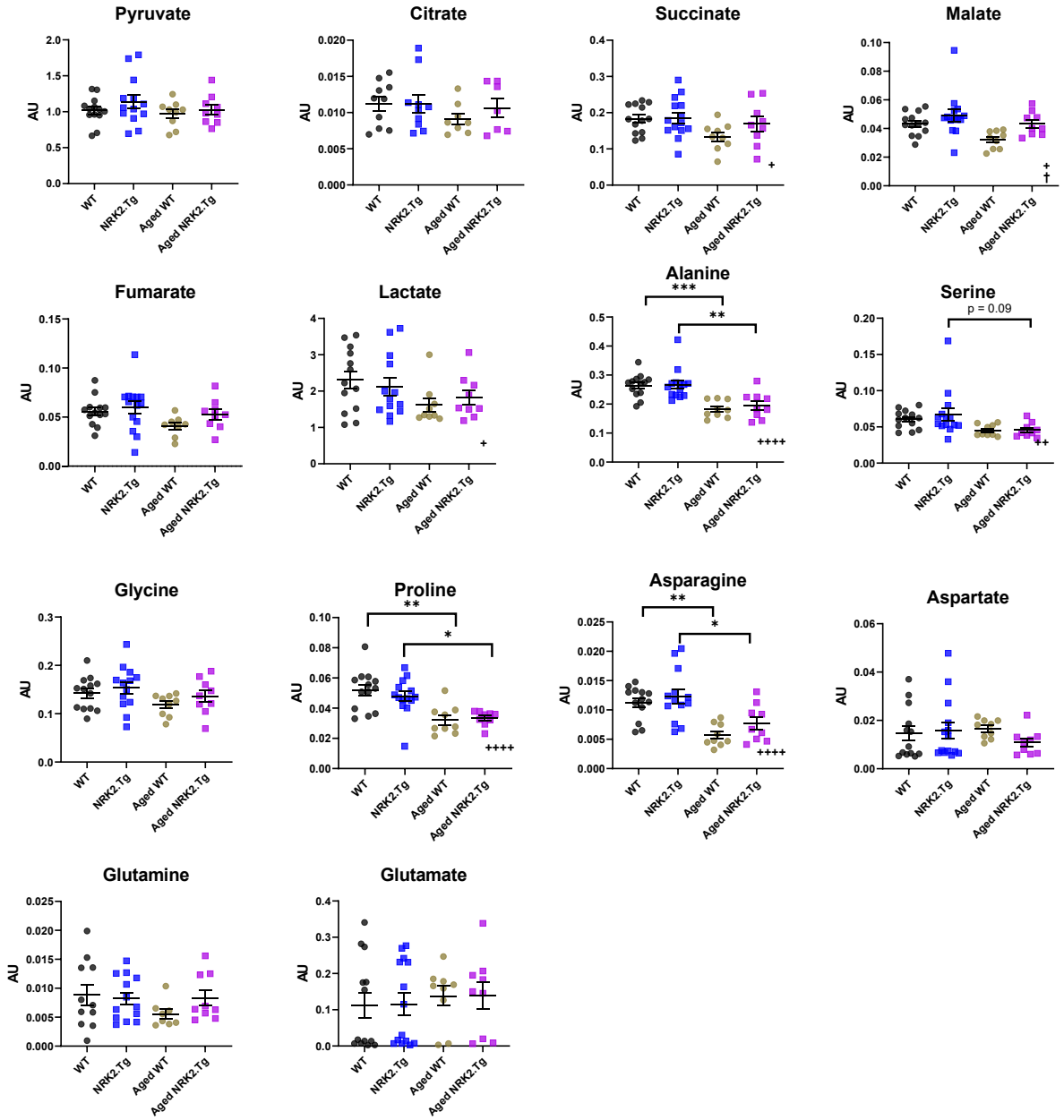

Figure 4-6 – Skeletal muscle alanine, proline and asparagine concentrations were significantly lower in aged mice independent of genotype. GCMS quantification of metabolically relevant TCA cycle intermediates and amino acids in young (3 month old) and aged (22-24 month old) female WT and NRK2.Tg mouse quadriceps. Statistical significance was determined by ordinary two way ANOVA with Sidak's multiple comparison tests (* $p < 0.05$, ** $p < 0.01$, *** $p < 0.001$, **** $p < 0.0001$). n = 8-10. # = statistically significant interaction between genotype and age; + = statistically significant variation between young and aged mice; † = statistically significant variation between WT and NRK2.Tg mice.

4.3.4 The effects of NRK2 overexpression on aged skeletal muscle mitochondrial oxidative capacity

Mitochondrial function declines with age due to decreased mitochondrial biogenesis and mitophagy, resulting in impaired oxidative metabolism, metabolic flexibility and reduced cellular capacity for managing metabolic stress (100-102). NAD^+ dependent signalling pathways promote upregulation of these processes, and therefore NAD^+ bioavailability is a critical factor in maintaining a healthy mitochondrial pool with age. Direct assessment of maximal oxidative capacity was therefore performed to assess the impact of constitutive NRK2 overexpression on skeletal muscle mitochondrial health with age. No significant differences in respiratory flux were observed between aged WT and NRK2.Tg TA or soleus muscle, indicating that NRK2 overexpression does not significantly alter skeletal muscle mitochondrial respiratory capacity with age (Figure 4-7). However, an upward trend in complex I, I+II and electron transfer state oxygen flux in NRK2.Tg TA relative to WT was present (Figure 4-7), suggesting a potentially slight augmentation of oxidative capacity within type II fibre dominant muscle with increased NRK2 levels.

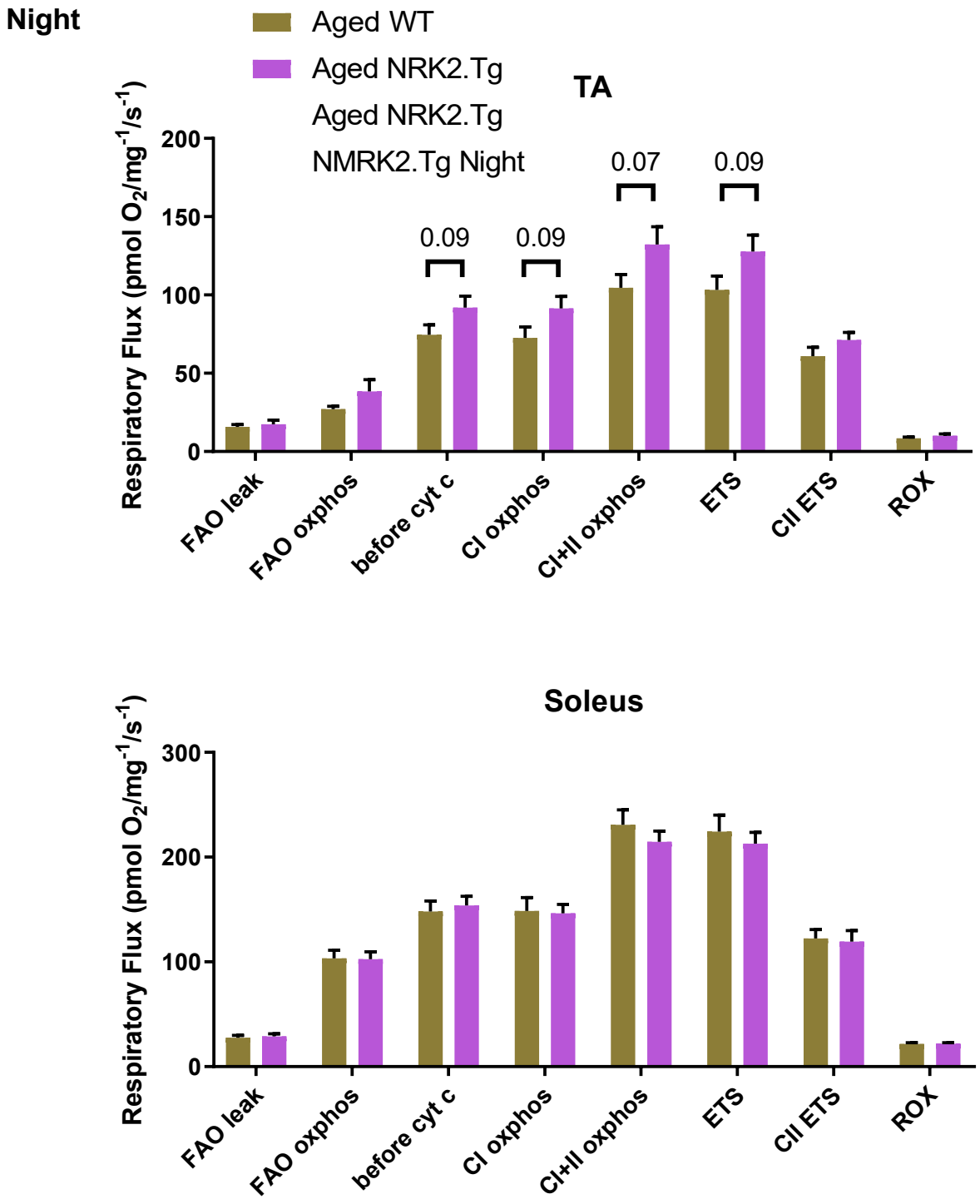

Figure 4-7 – Skeletal muscle mitochondrial respiratory capacity is not significantly altered between aged WT and NRK2.Tg mice, though oxidative capacity in NRK2.Tg TA is elevated. FAO capacity of TA and soleus from 20-22 month old WT and NRK2.Tg mice. Data presented as mean ± SEM. Statistical significance was determined by student's unpaired t test at each respiratory state (* $p < 0.05$, ** $p < 0.01$, *** $p < 0.001$). n = 7.

4.3.5 The effects of skeletal muscle NRK2 overexpression on aged metabolic phenotype

Given the importance of skeletal muscle to overall metabolic status (19) and NAD^+ bioavailability being a central factor in skeletal muscle metabolic health (11, 171, 180, 184, 284, 292, 387), aged WT and NRK2.Tg mice were also subjected to 48h metabolic tracing via home cage indirect calorimetry in order to assess any systemic metabolic connotations of skeletal muscle NRK2 overexpression.

In terms of body weight, aged mice were significantly heavier than young mice with a greater spread of individual values (Figure 4-8). No significant differences in body weight were observed between WT and NRK2.Tg mice in the aged cohort, suggesting that chronic skeletal muscle NRK2 overexpression does not affect weight gain associated with ageing and a sedentary lifestyle (Figure 4-8).

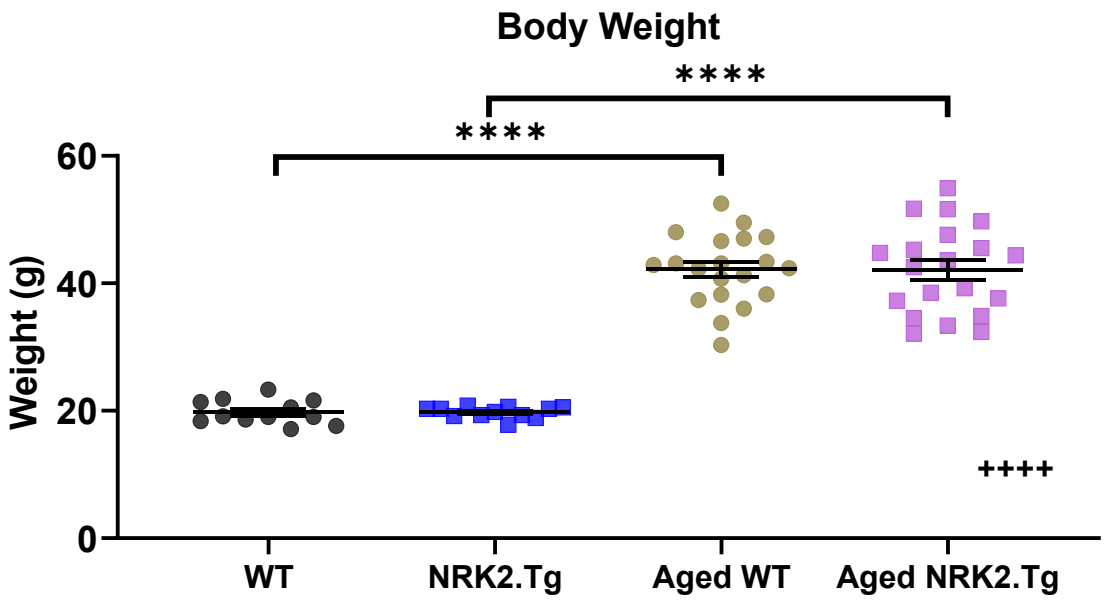

Figure 4-8 – Aged mice are significantly heavier than young mice, with no significant difference between genotypes. Body weights of female 3 month and 18 month old (aged) WT and NRK2.Tg mice. Data presented as mean ± SEM with individual data points representing one biological replicate. Statistical significance was determined by student's unpaired t test (* $p < 0.05$, ** $p < 0.01$, *** $p < 0.001$). n = 12-20. # = statistically significant interaction between genotype and age; + = statistically significant variation between young and aged mice; † = statistically significant variation between WT and NRK2.Tg mice.

Upon metabolic assessment via home cage calorimetry, the differences between young and aged mice were immediately apparent with aged mice having significantly lower ΔRER values relative to young mice as determined in section 3.3.8 (young = 0.194 ± 0.051, aged = 0.14 ± 0.036, p = 0.0029 for WT; young = 0.2172 ± 0.032, aged = 0.1527 ± 0.04, p = <0.0001 for NRK2.Tg), with a clearly blunted switch to carbohydrate metabolism during active hours in aged mice (Figure 4-9). These observations indicate proportionally reduced carbohydrate metabolism and an age related impairment of metabolic substrate switching. Absolute VO_2 hourly averages over 24 hours were also significantly higher in aged mice relative to young mice throughout the day (young = 82.01 ml/h ± 2.09, aged = 115.3 ml/h ± 1.79, p = <0.0001 for WT; young = 82.96 ml/h ± 1.99, aged = 115.8 ml/h ± 1.61, p = <0.0001 for NRK2.Tg) despite a significant yet relatively modest increase in caloric intake per hour

(young = 0.487 Kcal/h ± 0.02, aged = 0.566 Kcal/h ± 0.029, p = 0.055 for WT; young = 0.478 Kcal/h ± 0.025, aged = 0.583 Kcal/h ± 0.026, p = 0.011 for NRK2.Tg) with comparable feeding patterns (Figure 4-9). Furthermore, hourly averages for energy expenditure were comparable between young and aged mice (young = 0.574 Kcal/h ± 0.06, aged = 0.571 Kcal/h ± 0.01, p = 0.096 for WT; young = 0.56 Kcal/h ± 0.06, aged Kcal/h = 0.057 ± 0.007, p = 0.83 for NRK2.Tg) despite aged mice being significantly heavier (Figure 4-8). Though clear differences in metabolic phenotype between young and aged animals were present, no significant differences in caloric intake, energy expenditure or VO_2 were observed between aged WT and NRK2.Tg mice were observed indicating that chronic lifetime NRK2 overexpression does not affect aged whole body metabolic phenotype (Figure 4-9). RER traces and ΔRER values were also comparable between aged WT and NRK2.Tg mice, though interestingly the slope elevation of ΔRER plotted against body weight for NRK2.Tg mice was significantly higher than WT mice, implying that NRK2.Tg mice were more metabolically flexible when normalised to individual body weights (Figure 4-9).

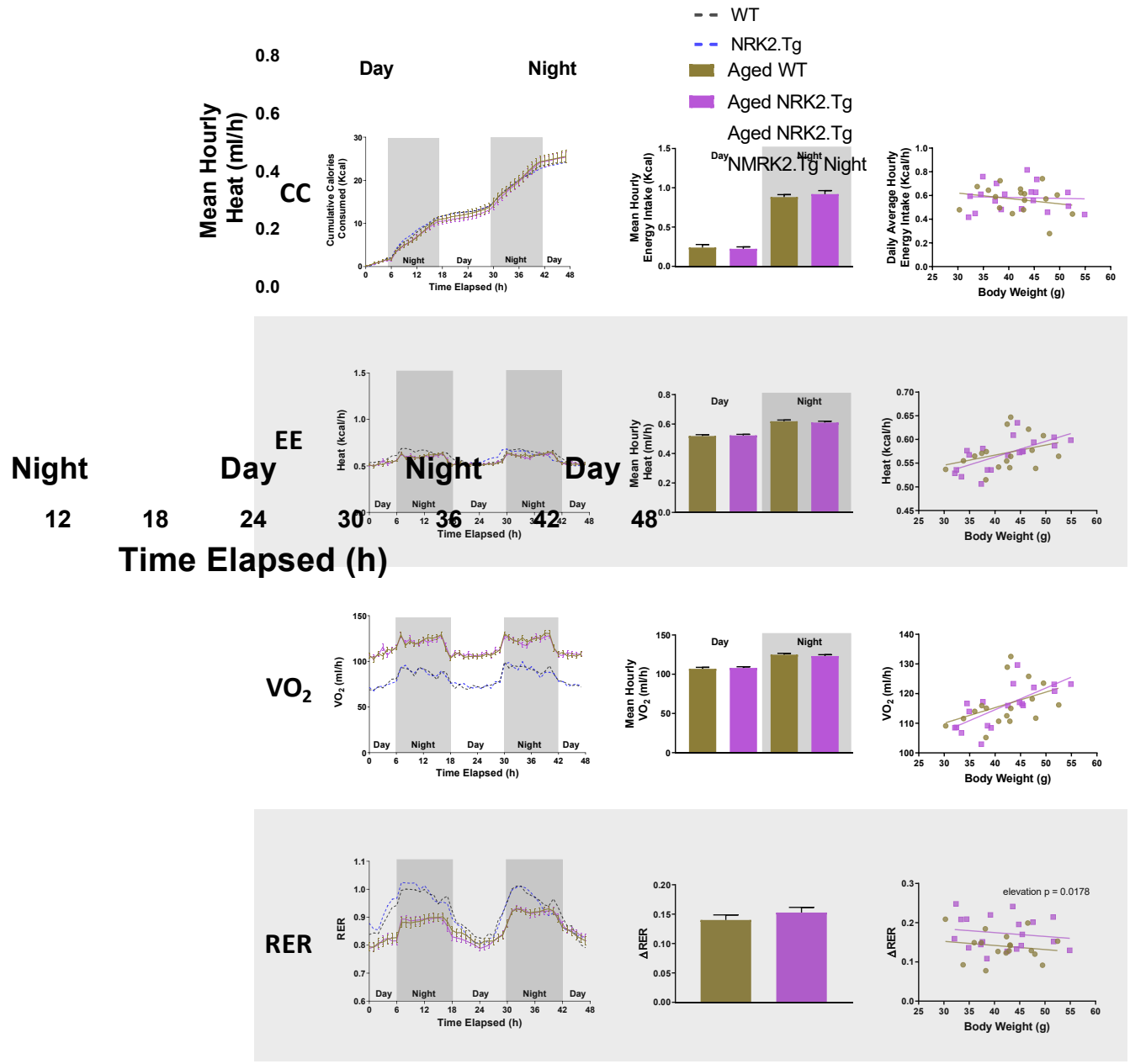

Figure 4-9 – Whole body basal metabolic phenotype is comparable between aged WT and NRK2.Tg mice over 48 hours. Indirect calorimetric analysis of 18-20 month old female WT and NRK2.Tg mice quantifying caloric consumption (CC), energy expenditure (EE) and VO_2 presented as a trace of hourly averages, average day/night values and linear regression relative to body weight. RER is presented as a trace of hourly averages and ΔRER, a representation of metabolic flexibility which is calculated by subtracting the average of the 5 highest values during the night phase from the average of the 5 lowest values during the day phase. Data presented as mean ± SEM. Statistical significance of corresponding trace timepoints and average day/night values were determined by student's unpaired t test. Linear regression plots were analysed via ANCOVA. (* $p < 0.05$, ** $p < 0.01$, *** $p < 0.001$). n = 20.

IPGTTs were also performed on aged WT and NRK2.Tg mice to establish any effects of NRK augmentation in skeletal muscle on glucose tolerance in aged animals. Aged mice presented with impaired glucose tolerance relative to young mice, though no genotype specific differences were apparent indicating that skeletal muscle NRK augmentation has no effect on glucose tolerance with age (Figure 4-10).

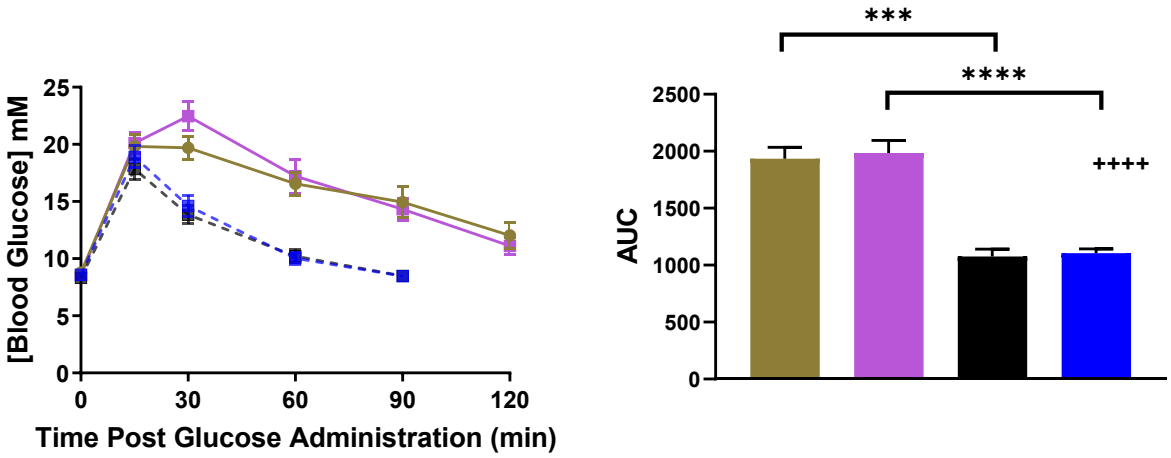

Figure 4-10 – Aged WT and NRK2.Tg mice have comparable glucose tolerance. Baseline blood glucose measurements followed by 15, 30, 60 and 90 minutes post glucose administration in 18-20 month old female WT and NRK2.Tg mice alongside glucose tolerance levels in 3 month old WT and NRK2.Tg mice. Data presented as blood glucose concentration with time and AUC values (mean ± SEM). Statistical significance was determined by two way ANOVA (* $p < 0.05$, ** $p < 0.01$, *** $p < 0.001$). n = 6-8. # = statistically significant interaction between genotype and age; + = statistically significant variation between young and aged mice; † = statistically significant variation between WT and NRK2.Tg mice.

4.3.6 Oral NR supplementation is well tolerated and does not affect aged metabolic phenotype with or without skeletal muscle NRK augmentation

The availability of NR substrate is thought to be a rate limiting factor in the ultimate production of NAD^+ (16). In section 3.3.4, NRK2 enzyme expression level was also established in section as a rate limiting factor for NAD^+ production, with NRK2.Tg skeletal muscle producing a more efficacious NAD^+ boosting response in conditions of NR precursor excess. In order to further investigate the metabolic roles of the NRK2 pathway with age and the interplay between enzyme and substrate bioavailability, aged WT and NRK2 mice were chronically administered an excess of NR precursor orally within drinking water for four weeks, in place of regular drinking water. The NR water was well tolerated and did not result in body weight discrepancies or adverse health consequences (Figure 4-11).

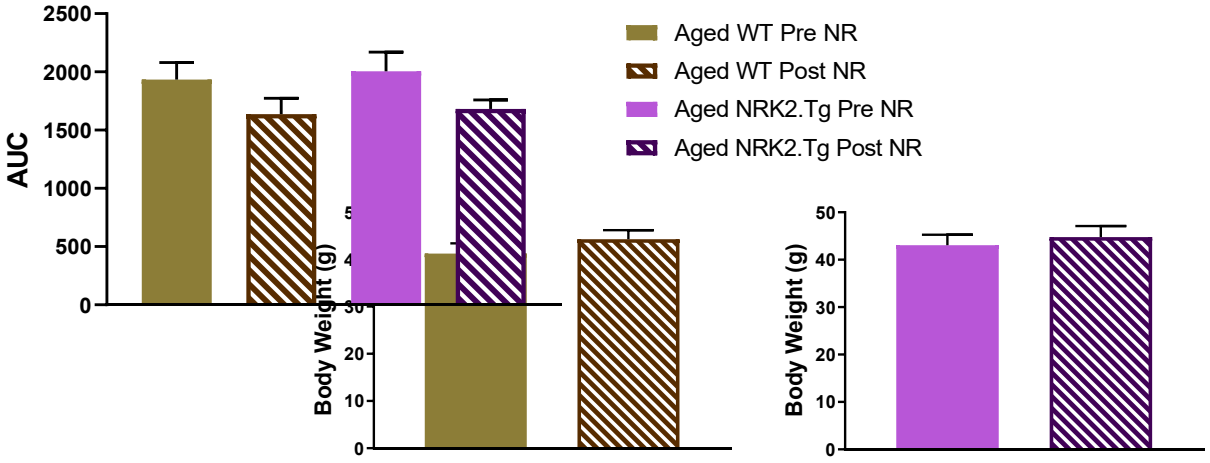

Figure 4-11 – Orally administered NR is well tolerated in aged WT and NRK2.Tg mice. Body weight comparison of aged WT and NRK2.Tg mice before and after 4 weeks of drinking water replacement with 5 g/l NR. n = 12.

4.3.7 Oral NR supplementation does not affect skeletal muscle bioenergetics with or without NRK augmentation

As NRK2 catalyses phosphorylation of NR to NMN which is rate limiting for the production of NAD^+ (16), the effects of exogenous oral NR supplementation on the skeletal muscle NAD metabolome were assessed in aged WT and NRK2.Tg mice. Chronic oral NR supplementation did not significantly alter skeletal muscle NAD^+, NADH or total NAD^+ concentrations or NAD^+/NADH ratios in either WT or NRK2.Tg mice (Figure 4-12). Given that a direct NAD^+ boosting effect was observed in skeletal muscle upon IP NR administration in section 3.3.4 which was augmented in the presence of increased NRK2 enzyme, these observations suggest that orally administered NR may not be directly bioavailable to skeletal muscle.

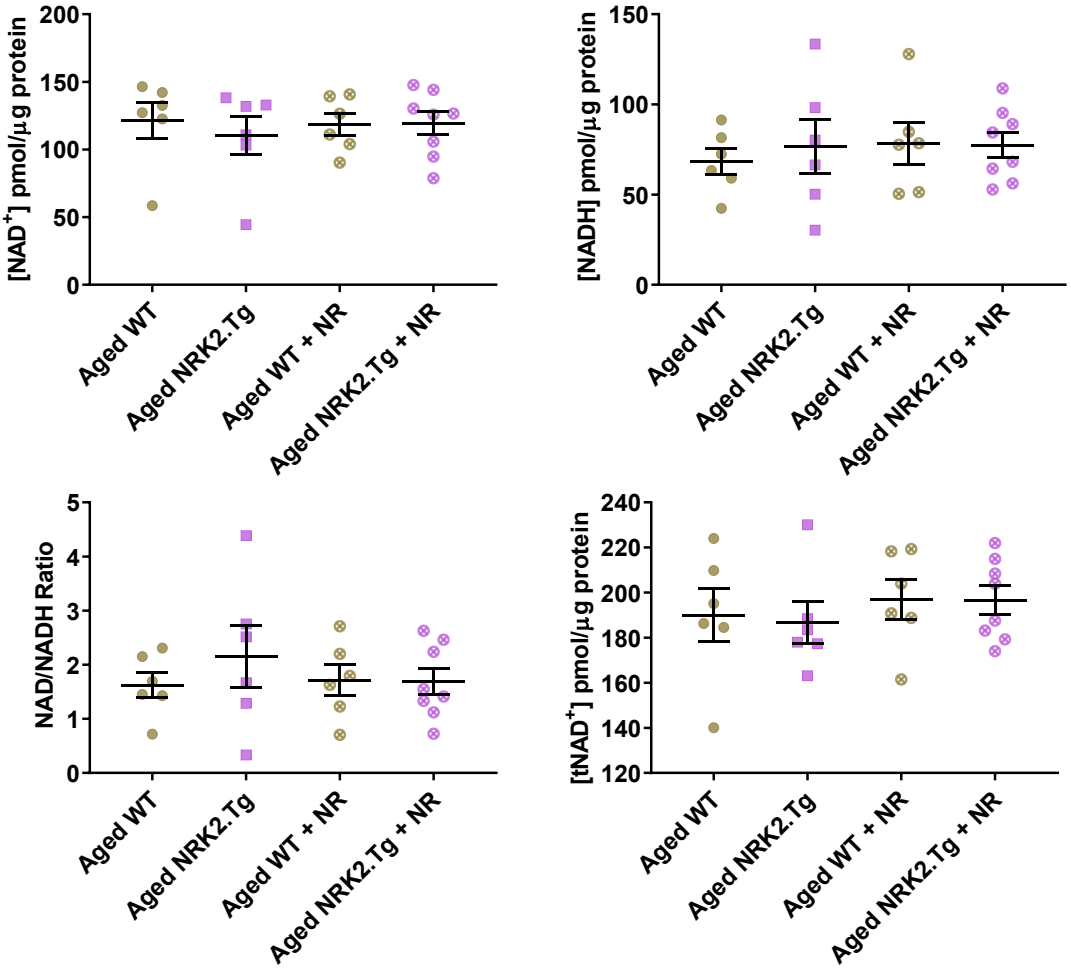

Figure 4-12 – Skeletal muscle NAD^+ dynamics are not significantly altered between aged WT and NRK2Tg mice with or without oral NR supplementation. Quantification of NAD^+, NADH, NAD^+/NADH ratio and total NAD levels in quadriceps collected from 20-24 month old mice with or without 9 weeks of oral NR supplementation. Data presented as mean ± SEM with individual data points representing one biological replicate. Statistical significance was determined by ordinary two way ANOVA with Sidak's multiple comparison tests (* $p < 0.05$, ** $p < 0.01$, *** $p < 0.001$, **** $p < 0.0001$). n = 7-8. # = statistically significant interaction between genotype and NR supplementation; + = statistically significant variation with NR supplementation; † = statistically significant variation between WT and NRK2.Tg mice.

These observations were again supported with LCMS analysis, which also determined that skeletal muscle ATP and NAM levels were not significantly affected by oral NR supplementation (Figure 4-13). However, MeNAM levels were raised in NR supplemented skeletal muscle for both WT and NRK2.Tg mice (Figure 4-13). Excess NAM is converted to

MeNAM by the nicotinamide N-methyltransferase (NNMT) enzyme and constitutes a methylated clearance metabolite (397). These data therefore indicate that orally administered NR affects the skeletal muscle NAD metabolome despite no direct observations of elevated NAD^+ levels, though this is independent of NRK2 expression levels.

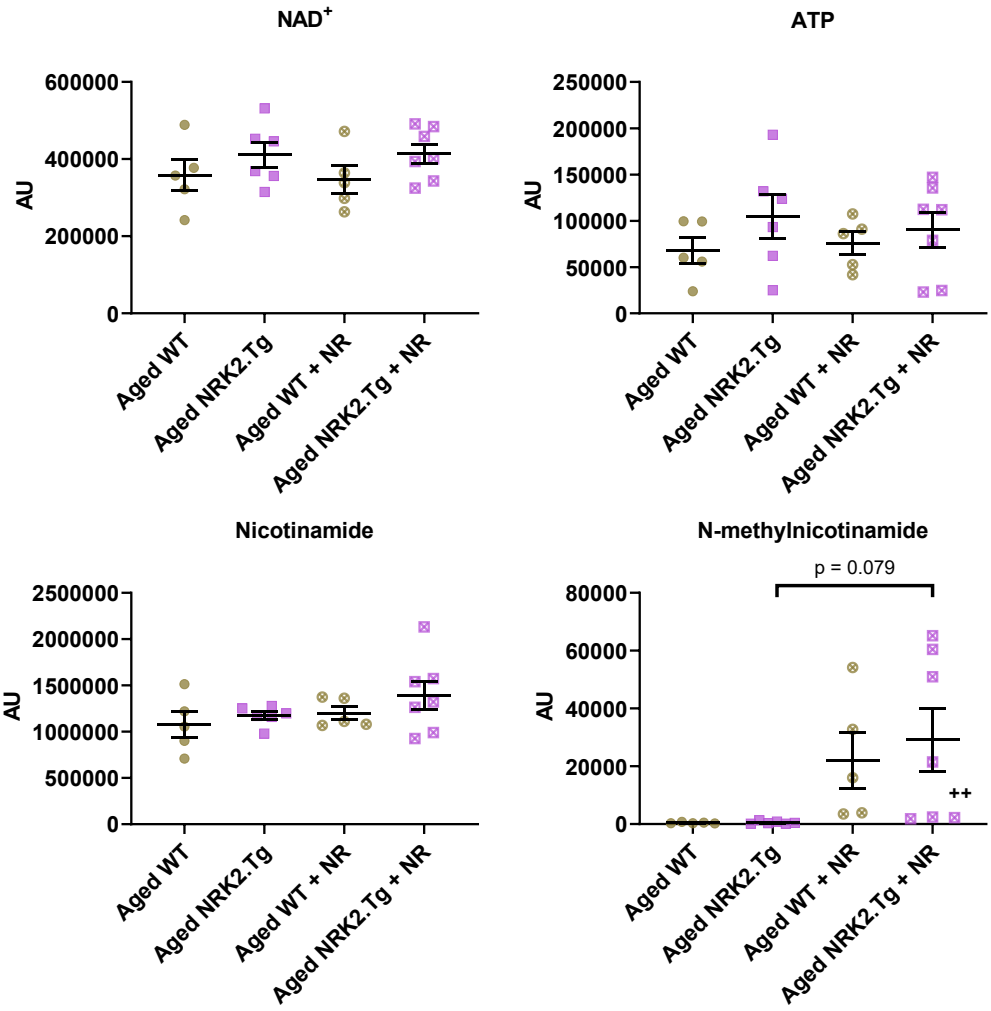

Figure 4-13 – Skeletal muscle NAD$^+$, ATP, and NAM levels are unaffected by oral NR supplementation in aged WT and NRK2.Tg mice, though MeNAM levels are elevated. LCMS Quantification of NAD$^+$, ATP, NAM and MeNAM levels in quadriceps collected from female 3 month old and 22-24 month old WT and NRK2.Tg mice with or without NR supplementation. Data presented as mean ± SEM with individual data points representing one biological replicate. Statistical significance was determined by ordinary two way ANOVA with Sidak's multiple comparison tests (* $p < 0.05$, ** $p < 0.01$, *** $p < 0.001$, **** $p < 0.0001$). n = 5-8. # = statistically significant interaction between genotype and NR supplementation; + = statistically significant variation with NR supplementation; † = statistically significant variation between WT and NRK2.Tg mice.

Any potential effects of NRK augmentation and/or NR supplementation on skeletal muscle TCA cycle metabolite levels and anaplerotic amino acids were next investigated using GCMS. No significant changes were observed in any examined metabolites between aged WT and NRK2.Tg mice. Interestingly, NR supplementation increased skeletal muscle lactate

levels within NRK2.Tg skeletal muscle which could imply an increased rate of glycolysis (398), though this was not a statistically significant observation and a concurrent depletion of pyruvate was not present. NR supplementation had no observable effects on any other metabolite in either genotype (Figure 4-14). Though no significant effects were observed, strong trends were apparent between aged WT and NRK2.Tg mice around specific metabolites irrespective of oral NR supplementation. Aged NRK2.Tg skeletal muscle presented with increased asparagine levels and subsequently decreased aspartate (Figure 4-14), as was also observed in young NRK2.Tg quadriceps in section 3.3.6. Glutamine levels were also elevated in NRK2.Tg skeletal muscle though glutamate levels were not significantly changed, with malate significantly increased and fumarate trending towards an increase (Figure 4-14). These data suggest subtle perturbations to TCA cycle metabolism and amino acid metabolism in aged NRK2.Tg skeletal muscle.

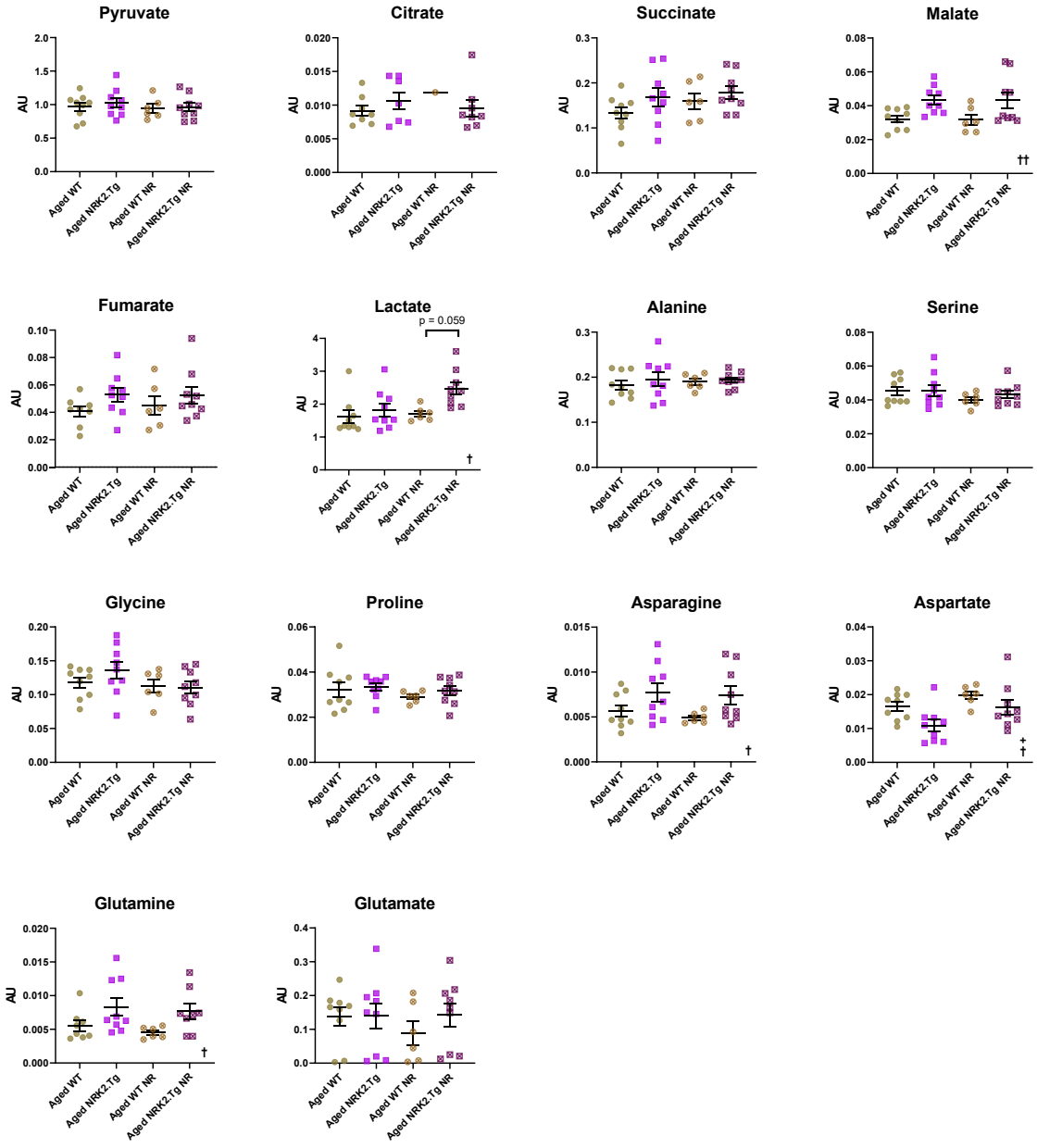

Figure 4-14 – Oral NR supplementation significantly increases skeletal muscle lactate levels in NRK2.Tg mice. GCMS quantification of metabolically relevant TCA cycle intermediates and amino acids in female WT and NRK2.Tg 22-24 month old mouse quadriceps with or without oral NR supplementation. Statistical significance was determined by ordinary two way ANOVA with Sidak's multiple comparison tests (* $p < 0.05$, ** $p < 0.01$, *** $p < 0.001$, **** $p < 0.0001$). n = 8-10. # = statistically significant interaction between genotype and age; + = statistically significant variation between young and old mice; † = statistically significant variation between WT and NRK2.Tg mice.

4.3.8 Oral NR supplementation does not significantly affect aged skeletal muscle mitochondrial oxidative capacity with or without skeletal muscle NRK augmentation

Any potential effects of oral NR supplementation on mitochondrial oxidative capacity were next assessed on WT and NRK2.Tg TA and soleus via high resolution respirometry. No significant differences in respiratory flux were observed in aged WT (Figure 4-15) or NRK2.Tg (Figure 4-16) TA or soleus muscle after NR supplementation, suggesting that orally administered NR does not affect aged skeletal muscle oxidative capacity regardless of NRK2 expression levels.

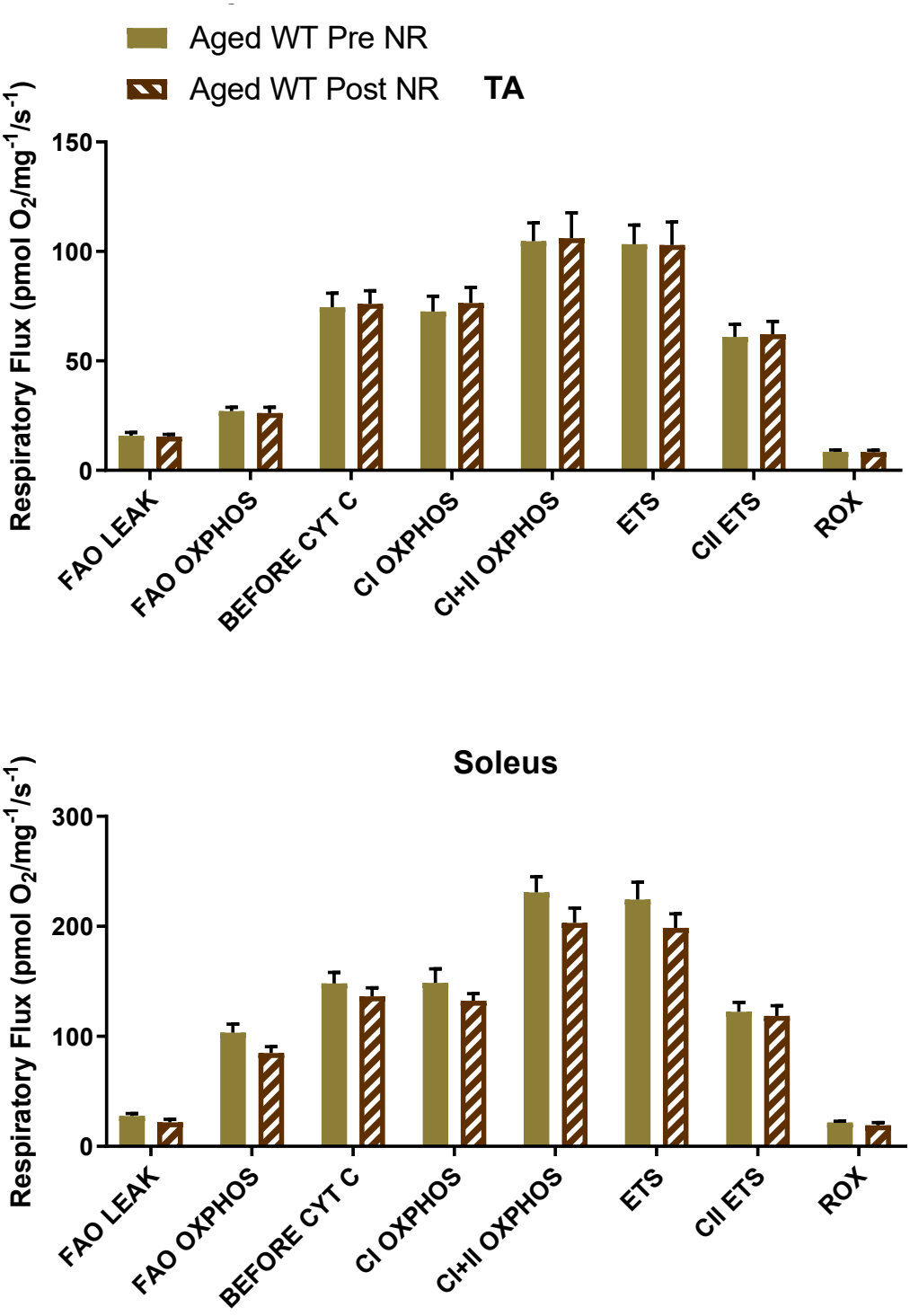

Figure 4-15 – Aged skeletal muscle mitochondrial respiratory capacity is not significantly altered with oral NR supplementation in WT mice. FAO capacity of TA and soleus from 20-22 month old WT mice with and without 9 weeks of oral NR supplementation. Data presented as mean ± SEM. Statistical significance was determined by student's unpaired t test at each respiratory state (* $p < 0.05$, ** $p < 0.01$, *** $p < 0.001$). n = 7.

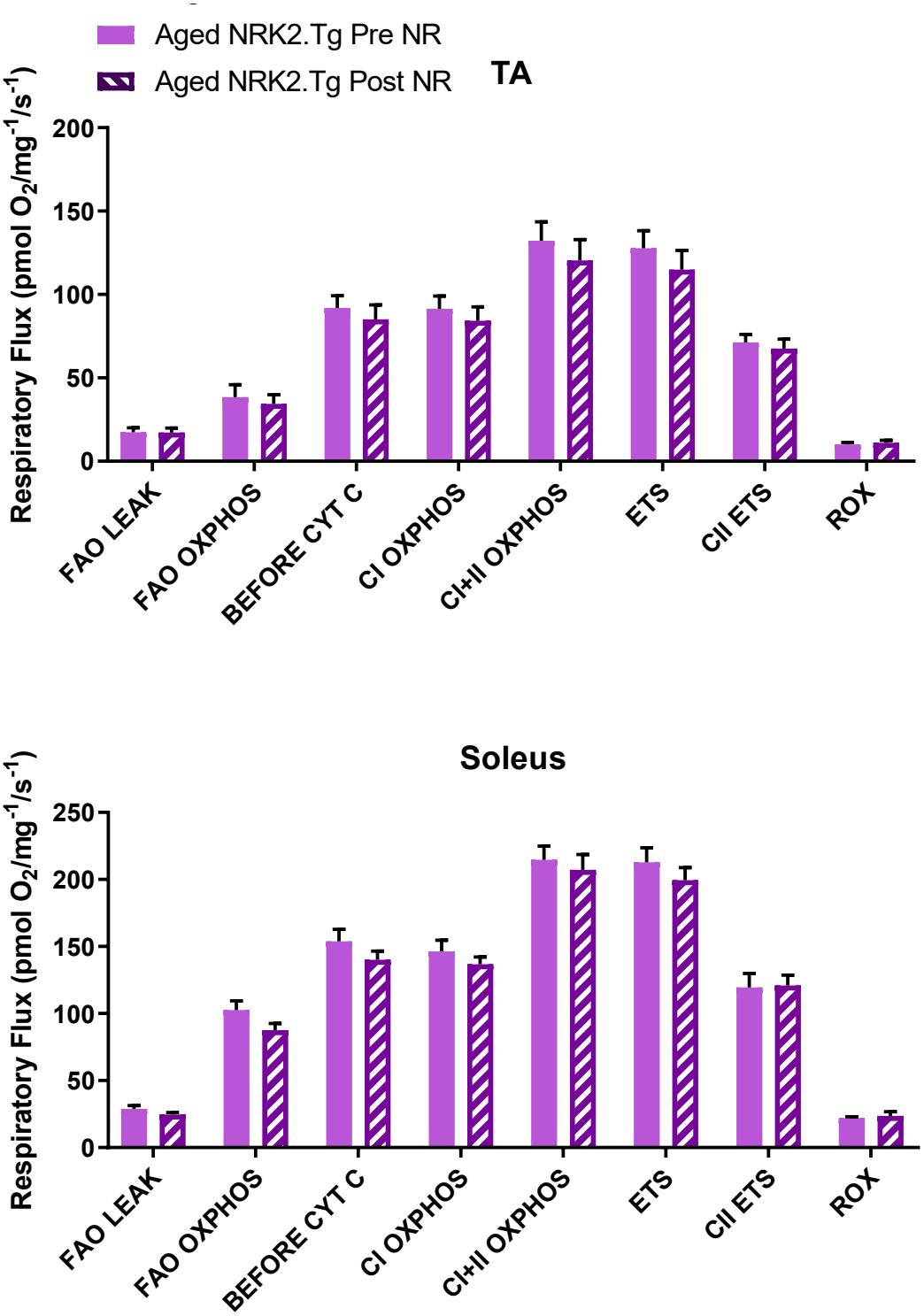

Figure 4-16 – Aged skeletal muscle mitochondrial respiratory capacity is not significantly altered with oral NR supplementation in NRK2.Tg mice. FAO capacity of TA and soleus from 20-22 month old NRK2.Tg mice with and without 9 weeks of oral NR supplementation. Data presented as mean ± SEM. Statistical significance was determined by student's unpaired t test at each respiratory state (* $p < 0.05$, ** $p < 0.01$, *** $p < 0.001$). n = 7-9.

4.3.9 Oral NR supplementation does not significantly affect aged whole body metabolic phenotype with or without skeletal muscle NRK augmentation

In order to determine the effects of oral NR supplementation on aged metabolic phenotype, whole body metabolic parameters of aged WT and NRK2.Tg mice were assessed immediately prior to NR supplementation and again after four weeks of NR water through 48h home cage indirect calorimetry. Energy expenditure, VO_2 levels and caloric consumption rates trended downwards in WT mice after four weeks of NR supplementation, potentially suggesting a decrease in activity (Figure 4-17). However, no significant differences in mean caloric consumption, energy expenditure, RER or VO_2 for both the light or dark phase, indicating that oral NR supplementation does not significantly affect basal metabolic parameters of aged WT mice (Figure 4-17). Similarly, no significant differences were observed across these parameters in NRK2.Tg mice, indicating that NRK2 enzyme levels within skeletal muscle are not relevant for driving metabolic adaptation or acute changes in metabolic phenotype in the presence of excess NR substrate administered orally (Figure 4-18).

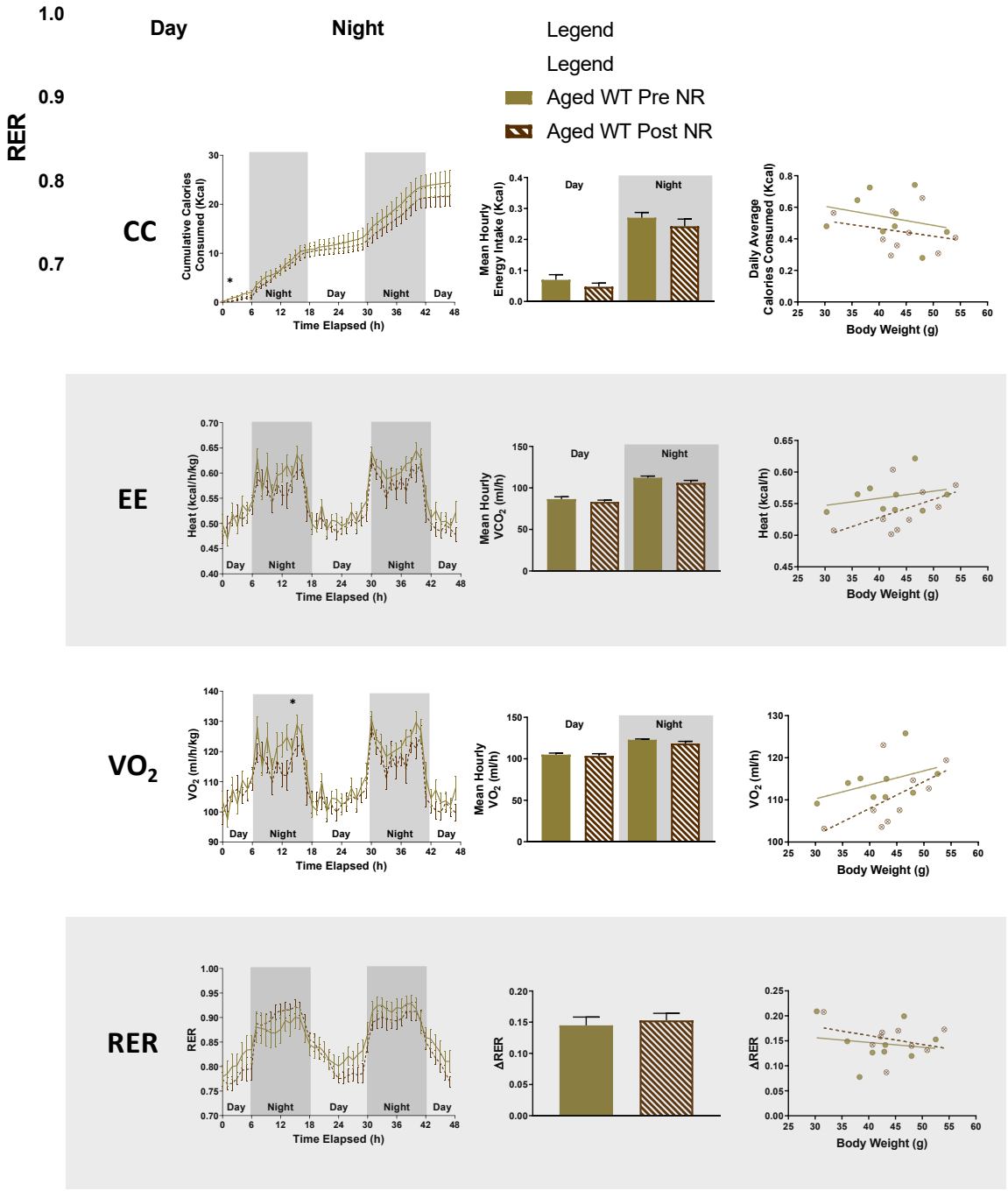

Figure 4-17 – Whole body basal metabolic phenotype is not affected by 4 weeks of oral NR supplementation in WT mice. Indirect calorimetric analysis of 18-20 month old female WT mice before and after 4 weeks of oral NR supplementation, quantifying caloric consumption (CC), energy expenditure (EE) and VO_2 presented as a trace of hourly averages, average day/night values and linear regression relative to body weight. RER is presented as a trace of hourly averages and ΔRER, a representation of metabolic flexibility which is calculated by subtracting the average of the 5 highest values during the night phase from the average of the 5 lowest values during the day phase. Data presented as mean ± SEM. Statistical significance of corresponding trace timepoints and average day/night values were determined by student's paired t test. Linear regression plots were analysed via ANCOVA. (* $p < 0.05$, ** $p < 0.01$, *** $p < 0.001$). n = 12.

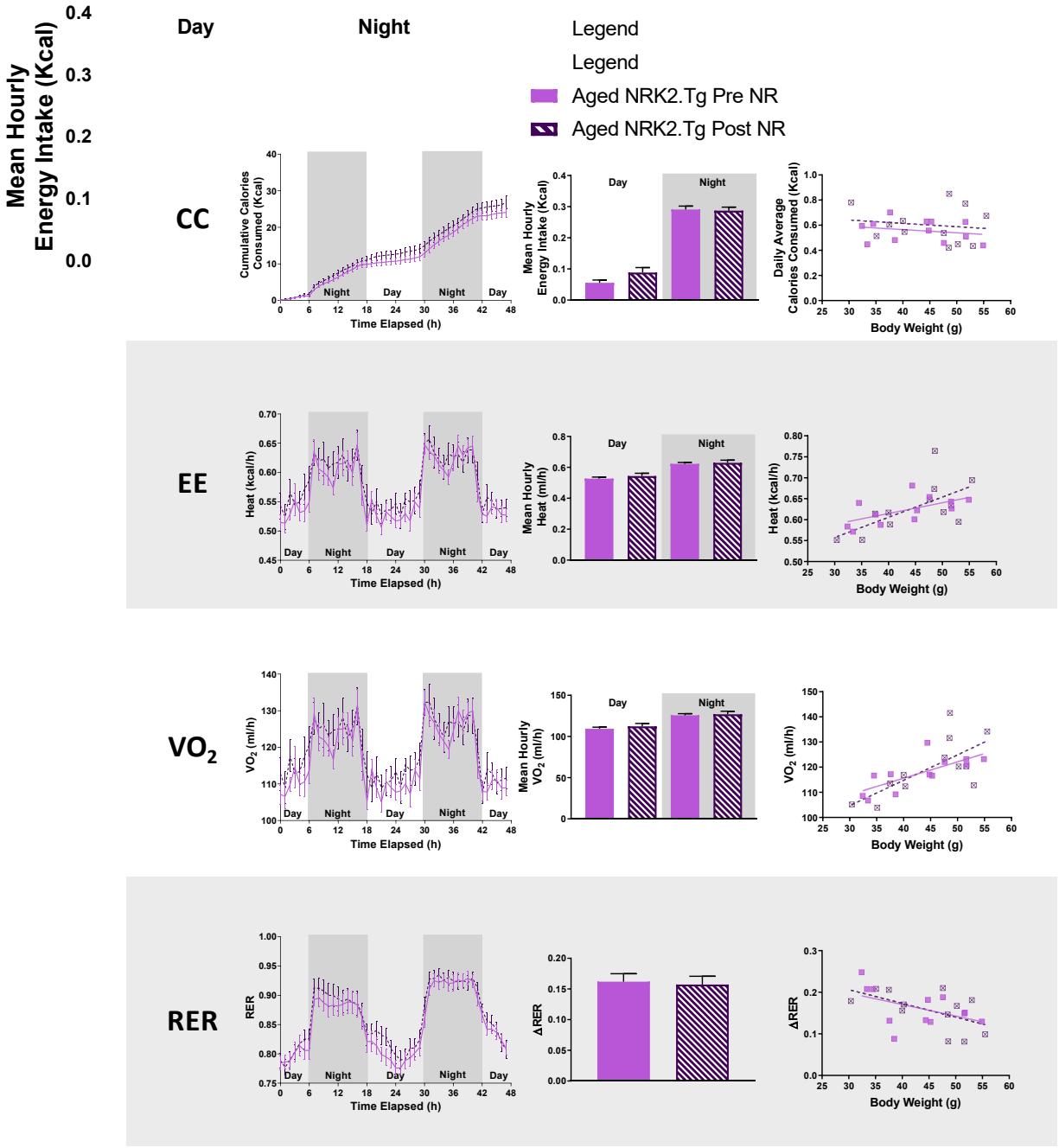

Figure 4-18 – Whole body basal metabolic phenotype is not affected by 4 weeks of oral NR supplementation in NRK2.Tg mice. Indirect calorimetric analysis of 18-20 month old female NRK2.Tg mice before and after 4 weeks of oral NR supplementation, quantifying caloric consumption (CC), energy expenditure (EE) and VO_2 presented as a trace of hourly averages, average day/night values and linear regression relative to body weight. RER is presented as a trace of hourly averages and ΔRER, a representation of metabolic flexibility which is calculated by subtracting the average of the 5 highest values during the night phase from the average of the 5 lowest values during the day phase. Data presented as mean ± SEM. Statistical significance of corresponding trace timepoints and average day/night values were determined by student's paired t test. Linear regression plots were analysed via ANCOVA. (* $p < 0.05$, ** $p < 0.01$, *** $p < 0.001$). n = 12.

Oral NR supplementation has also been reported to improve glucose tolerance under conditions of metabolic stress (165). IPGTTs were performed on aged WT and NRK2.Tg mice to establish any effects of NRK augmentation in skeletal muscle on glucose tolerance in aged animals. NR supplementation resulted in a significant yet small increase in blood glucose clearance efficiency independent of genotype (Figure 4-19). These data suggest that orally administered NR bestows a mild improvement on whole body glucose tolerance in aged mice, though skeletal muscle NRK2 expression levels do not modulate this effect.

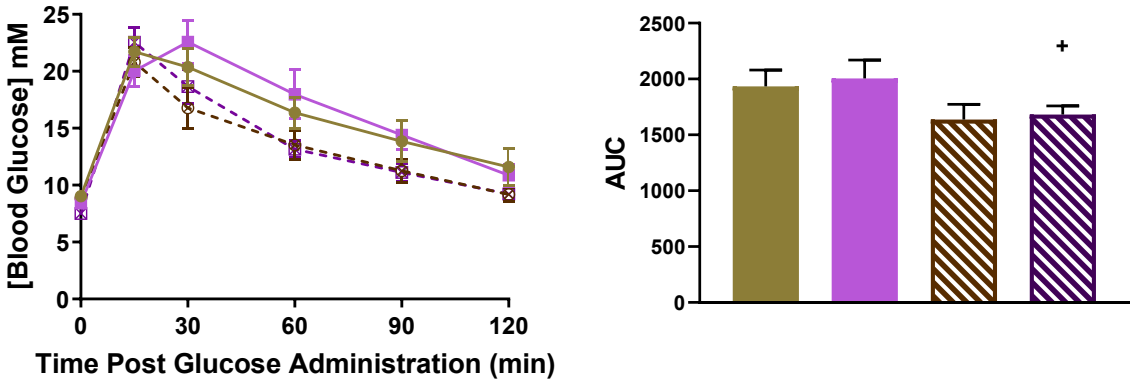

Figure 4-19 – Oral NR supplementation does not significantly affect glucose tolerance of aged WT and NRK2.Tg mice. Baseline blood glucose measurements followed by 15, 30, 60 and 90 minutes post glucose administration in 18-20 month old female WT and NRK2.Tg mice before and after 4 weeks of oral NR supplementation. Data presented as blood glucose concentration with time and AUC values (mean ± SEM). Statistical significance of corresponding trace timepoints and AUC were determined by student's unpaired t test (* $p < 0.05$, ** $p < 0.01$, *** $p < 0.001$). n = 6-8. # = statistically significant interaction between genotype and NR supplementation; + = statistically significant variation with NR supplementation; † = statistically significant variation between WT and NRK2.Tg mice.

4.4 Discussion

Healthy skeletal muscle is critical to metabolic homeostasis (18, 19). The loss of skeletal muscle mass and function with ageing and obesity is closely linked to whole body metabolic decline and evidence suggests a lack of bioavailable NAD^+ as a potentially reversible driving factor (11, 171, 180, 184, 284, 292, 387). Using an in vivo model of skeletal muscle specific NRK2 overexpression, this chapter characterised the metabolic consequences of constitutive skeletal muscle NAD^+ salvage pathway augmentation in the context of ageing. The key aims were to elucidate any specific functional metabolic roles of the NR/NRK salvage pathway in response to age related metabolic decline, as well as to further evaluate the potential of NAD^+ repletion strategies involving the NR/NRK pathway for improving metabolic health with age.

An age related decline in NAD^+ has been attributed to decreased expression and activity of key skeletal muscle NAD^+ repletion mechanisms, such as salvage from NAM via NAMPT (11, 104, 105) and increased activity of NAD^+ consuming enzymes such as PARPs and CD38 (261, 284). The resultant loss of bioavailable NAD^+ leads to decreased SIRT signalling and therefore diminished mitochondrial biogenesis and function (261, 284, 292). Conversely, both aged WT and NRK2.Tg mice had significantly increased skeletal muscle mRNA levels of Nampt and Nmrk1 relative to young mice along with a significant increase in Nmnat1 observed in aged NRK2.Tg muscle. Despite NAMPT upregulation, NAM levels were not perturbed in NRK2.Tg skeletal muscle as might be expected, though this was also reported in another study of NAMPT overexpression in skeletal muscle (315). Nmrk1 mRNA levels were also significantly increased, with a contrasting downregulation of Nmrk2 in both WT and

NRK2.Tg skeletal muscle. Nmrk2 overexpression was still present in aged NRK2.Tg muscle relative to aged WT though absolute mRNA levels had declined, likely as a result of endogenous Nmrk2 downregulation. These age related changes in skeletal muscle Nmrk1, Nmrk2 and Nmnat1 mRNA have not previously been observed, with one human study reporting no change with age in NRK1 and NRK2 expression (104). Though the NR kinase roles of NRK1 and NRK2 appear to be redundant (15), phosphorylation of NR by NRK is the rate limiting step for NAD^+ production (16), and thus differential endogenous regulation of NRKs could still have consequences on the applicability of NR as a skeletal muscle NAD^+ boosting supplement with age.

Expression levels of NAD^+ dependent enzymes were also modulated in aged and NRK2.Tg skeletal muscle. Parp1 mRNA was downregulated in aged WT muscle relative to young, agreeing with a previous human study which established a significant downregulation in PARP1 and PARP2 mRNA in 69-75 year old humans (399). Interestingly, mRNA encoding the nuclear deacetylase Sirt1 was significantly upregulated in aged NRK2.Tg skeletal muscle, with mRNA levels of the mitochondrial deacetylase Sirt3 showing a strong positive trend. SIRT signalling is NAD^+ dependent with SIRT1 being a potent inducer of mitochondrial biogenesis and potential mediator of skeletal muscle injury with age (234, 395, 400, 401), and Sirt3 implied a protective gene against mitochondrial ageing (239, 240, 402, 403). This upregulation has previously been observed in kidney, lung, spleen, adipose tissue and skin of aged mice (404) and SIRT1 expression was reported to be elevated in skeletal muscle of aged rats (105). SIRTs are upregulated in response to metabolic stressors such as exercise and caloric restriction, promoting a shift towards oxidative metabolism (245, 405-407). SIRT expression falls under the control of AMPK which is activated in times of energetic stress,

with NAMPT expression also under AMPK control to ensure NAD^+ bioavailability for SIRT signalling (405). As this was observed only in aged NRK2.Tg mice and not WT mice, SIRT upregulation may be a response to the metabolic stressors of aging amidst enhanced NAD^+ salvage from the NRK pathway. However in terms of functional metabolic relevance, it is important to note that mRNA abundance does not directly correlate with protein levels or enzyme activity levels, with one model reporting an upregulation of SIRT1 in aged rat skeletal muscle but a higher relative activity level despite downregulation following exercise (105).

Superficially, the concomitant upregulation of NAMPT and SIRTs alongside chronic NRK2 overexpression may suggest a general augmentation of skeletal muscle NAD^+ salvage pathways with age as well as an upregulation in oxidative metabolism exclusively in NRK2.Tg skeletal muscle. However, quantification of skeletal muscle NAD^+ using both colourimetric assays and LCMS revealed no significant differences in NAD^+ levels between aged WT and NRK2.Tg mice, and no significant differences in whole body metabolic phenotype were observed between WT and NRK2.Tg mice through indirect calorimetry. Furthermore, no significant elevations in mitochondrial capacity were observed in NRK2.Tg skeletal muscle despite some differential trends in TCA metabolite concentrations including increases in asparagine, fumarate, glutamine and malate with a concurrent decrease in aspartate. A non-significant upward trend in oxidative capacity was observed in NRK2 overexpressing TA, possibly suggesting type II fibre specific augmentation of oxidative capacity, though further investigations would be required to confirm this. Overall, the data suggests that the observed differences in expression levels of NAD^+ salvage and signalling genes are not functionally relevant, and lifetime augmentation of the NRK2 skeletal muscle NAD^+ salvage

pathway does not bolster skeletal muscle NAD^+ levels with age. Other models of amidated NAD^+ skeletal muscle salvage pathway augmentation have reported direct, significant NAD^+ boosting effects in the case of NAMPT overexpression (315) as well as the preservation of aged cellular NAD^+ levels with NAMPT (315) and NMNAT3 (408) overexpression, while knockout models of NRK2 have demonstrated that it is dispensable for general NAD^+ homeostasis in skeletal muscle (15). This comparative redundancy could be due to the relatively low circulatory availability of NR (164, 314) and the increased availability of NAM through production from NAD^+ consumption (139). Endogenous pools of NR and NAR have been identified within skeletal muscle (315) which are potentially generated through interconversion of NMN by 5' nucleotidases such as CD73 (162, 409), though this does not appear sufficient to generate an NAD^+ boosting effect upon augmentation of NRK2 enzyme levels with age. The data presented in this chapter therefore suggests that the NRK salvage pathway does not function as an auxiliary NAD^+ salvage mediator within skeletal muscle under metabolic decline as was hypothesised.

The previously observed increase in NRK2.Tg skeletal muscle NAD^+ during the active dark phase were not present in aged NRK2.Tg mice, and critically a young control cohort also did not present with elevated NAD^+ during night hours as previously observed in section 3.3.7, casting doubt on these initial observations. The initial circadian and acute exercise experiments were performed on male mice, but females were used for the remainder of the study due to an unforeseen occurrence of inflammation and stiffening of ankle joints in ageing male mice which was not genotype specific. It is therefore possible that this effect is sex linked, as transcriptional differences in NAD^+ dependent oxidative pathways are present between male and female skeletal muscle (410), with SIRT1 activity also having been linked

to androgen receptor (AR) regulation (411) which is a mediator of skeletal muscle hypertrophy (412). Furthermore, quadriceps was sampled throughout this chapter as a lack of time and resources meant that both TA and soleus could not be assessed. Given that quadriceps uniquely did not respond to IP NR+ supplementation in section 3.3.4, it is possible that NAD^+ boosting effects of NRK2 overexpression are muscle bed dependent, and this work should be followed up with thorough investigation into exclusively oxidative and glycolytic muscle.

The effects of NRK2 overexpression under conditions of chronic NAD^+ depletion were difficult to ascertain using this model, as though a significant decrease in total NAD levels was determined in aged skeletal muscle relative to young tissue during night hours, no significant decline in NAD^+ was detected in aged skeletal muscle in either WT or NRK2.Tg mice. Furthermore, an unanticipated upregulation in NAMPT with age was observed. These findings directly contradict a range of studies documenting a chronic decline in skeletal muscle NAD^+ decline with age (180, 184, 284, 292, 315). This thesis utilised mice at 18-20 months old as an ageing model for in vivo experimentation, with mice sacrificed for in vitro assessment of skeletal muscle at 21-23 months of age upon the conclusion of comprehensive metabolic assessment. This was decided due to project licence welfare restrictions imposing an age limit of 24 months alongside the high rate of comorbidities observed in mice of advanced age, further supported by evidence suggesting that the onset of age related skeletal muscle function and the resulting systemic metabolic decline occurs at 18 months of age (393-396).

It has been determined that age related skeletal muscle decline occurs in mid life prior to the full onset of sarcopenia in the context of mitochondrial and metabolic

dysfunction, with significantly reduced capacity for exercise and strength detectable as early as 10-14 months (394). As expected, in vivo metabolic phenotyping of mice aged 18-20 months revealed typical hallmarks of age related metabolic dysfunction including significant weight gain, impaired blood glucose clearance and impaired metabolic flexibility. However, it remains unclear as to whether these mice were aged sufficiently such that decreased skeletal NAD^+ levels were a major contributing factor to these observed metabolic deficiencies. The ages of mice utilised in prominent studies investigating age related decline of skeletal muscle NAD^+ have not been standardised, and the incidence of skeletal muscle NAD^+ decline relative to young muscle therefore varies between models. One study established a minor, non significant decrease in skeletal muscle NAD^+ in mice aged 18 months (184), while studies on 24 month old mice presented with a 50-70% depletion relative to young controls (11, 292). Further studies reported an 80-85% decline in mice aged between 25-31 months (180), a 45% decline at 30 months (184) and a 60-65% decrease at 32 months (284). Based on these data, mice aged between 18-20 months may not have constituted truly “old” mice with respect to skeletal muscle NAD^+ depletion, instead providing insight into the metabolic roles of NRK2 and NR supplementation for late middle age mice in vivo.

Despite this, a previous study identified a significant 35% decline in skeletal muscle NAD^+ in mice aged 22 months (184), which were comparable in age to the 21-23 month old skeletal muscle tissue utilised in this chapter in which a similar decline in NAD^+ could not be reproduced. Furthermore, a significant decline in muscle stem cell NAD^+ has been observed in mice aged 22-24 months, (171) though this may not have manifested in an observable decrease in NAD^+ due to the use of whole muscle lysate rather than quantification within

specific cell types. In all, while it is possible that the aged cohort was insufficiently aged for significant skeletal muscle NAD^+ depletion, the presented in vivo metabolic phenotyping data are still valuable in the context of age related metabolic decline through late middle age. Conversely, direct quantification of skeletal muscle NAD^+ was performed on muscle of an age in which significant NAD^+ decline has been previously confirmed (184), therefore constituting viable contradictory evidence for the concept of age related NAD^+ decline in skeletal muscle.

Such disparate results could also be linked to differences between rodent models. , . Several mouse studies cited utilised the C57BL/6J substrain (180, 184, 292), while the mice utilised for this study were C57Bl/6Ntac/J hybrids. C57BL/6J mice possess a mutant complete loss of function form of NNT gene, which encodes an integral inner mitochondrial membrane protein that catalyses the formation of NADPH from $NADP^+$ at the expense of NADH and translocation of an H+ ion into the matrix (413). In absence of NNT, NADPH levels within the mitochondrial matrix are insufficient resulting in impaired mitochondrial H_2O_2 detoxification which functionally manifests as mitochondrial redox abnormalities and impaired glucose tolerance (413). It could therefore be possible that such chronic metabolic stress may result in decreased NAD^+ levels with advancing age, though further studies would be required to support this explanation. In contrast, the mice bred for this study were genotyped as heterozygotes for the functional NNT allele, which is sufficient for normal NNT function (414).

Despite no significant changes to oxidised cellular NAD^+, there was a significant decrease in total NAD levels in aged skeletal muscle that was only present during the dark active phase. This suggests a general inability to maintain total NAD levels during periods of

heightened activity, which may also explain the observed decrease in metabolic flexibility and carbohydrate switching in aged mice. NRK2.Tg mice appeared to be more metabolically flexible when ΔRER was normalised to individual body weights, though no significant differences were observed between RER traces or absolute ΔRER, and it is therefore difficult to conclude that skeletal muscle overexpression improves metabolic flexibility with age Circadian NRK2 expression data discussed in section 3.3.7 indicated that endogenous NRK2 protein expression is lowest at this time, but constitutive skeletal muscle NRK2 overexpression did not ameliorate this decline in NAD or significantly alter the aged metabolic phenotype. Thus unlike NAMPT overexpression (11), NRK2 overexpression is not sufficient to ameliorate aged related changes to the NAD metabolome utilising endogenously produced and dietary NR alone.

Aged WT and NRK2.Tg mice were also supplemented with 325 mg/kg/day NR orally via drinking water to establish any metabolic effects of NRK2 overexpression in the presence of excess substrate. Orally administered NR is bioavailable (164) and several rodent studies have reported positive effects on systemic metabolic health in aged animals upon oral NR supplementation (11, 168) along with specific improvements within aged skeletal muscle metabolism and mitochondrial health (11, 171). Similar effects have been observed with exogenous NMN (180, 184, 415), with an acute increase in skeletal muscle NAD^+ upon gavage and improved mitochondrial oxidative capacity in aged mouse skeletal muscle upon chronic administration (181). Furthermore, despite questionable bioavailability of orally administered NR to skeletal muscle (314, 315), oral NR supplementation boosted NAD^+ levels in aged satellite cells, resulting in improved mitochondrial function and reduced senescence in aged mice and ultimately improving lifespan (171). However, no changes to skeletal

muscle NAD^+ levels were observed with NR supplementation in either aged WT or NRK2.Tg mice in this case. Furthermore, no such metabolic improvements were detected in NR supplemented mice via indirect calorimetry, with energy expenditure, VO_2 and metabolic flexibility following comparable patterns regardless of NR supplementation in both aged WT and NRK2.Tg mice. Additionally, despite an NR dependent increase in skeletal muscle lactate levels which could conversely suggest a shift towards anaerobic respiration (398), skeletal muscle mitochondrial oxidative capacity was not affected by chronic oral NR supplementation in either WT or NRK2.Tg skeletal muscle. NAD^+ and ATP levels were also unaffected indicating no effects of NR on cellular bioenergetics, though more detailed experiments into metabolic flux rates would be required to establish any potential differences in metabolite consumption and turnover.

Despite no skeletal muscle NAD^+ boosting or functional metabolic differences, NR supplementation significantly raised levels of the NAM clearance metabolite MeNAM. Skeletal muscle NAM levels remained comparable to unsupplemented mice suggesting that excess NAM is rapidly cleared to MeNAM, with excessive cellular NAM levels leading to SIRT inhibition (416). MeNAM has been suggested as a metabolic signalling mediator in skeletal muscle itself (417), though the lack of any observed metabolic changes implies that this is not biologically relevant in this context. MeNAM is produced and excreted under conditions of excess NAM via methylation of NAM through activity of NNMT (397), signifying that oral NR supplementation does augment the skeletal muscle NAD^+ metabolome, though no significant redox changes or functional metabolic improvements were noted. The oral bioavailability of NR to skeletal muscle is still unclear, with NR thought to be unstable in the bloodstream (375, 376) and a large proportion of orally administered NR is thought to be

degraded to NAM through first pass metabolism (314). Experiments utilising isotopically labelled NR also indicate that most exogenously derived NAD^+ within skeletal muscle following oral NR administration can be traced to NR-derived NAM (314, 315), whereas intravenous (IV) administration effectively delivered intact NR to skeletal muscle (314). The data presented within this chapter corroborates such observations in that orally administered NR did not directly affect skeletal muscle NAD^+ levels even in skeletal muscle overexpressing NRK2, which catalyses the rate limiting step for NR conversion to NAD^+ (16). Comparatively, an additive increase in skeletal muscle NAD^+ was observed with IP delivery in NRK2.Tg muscle in section 3.3.4, but intravenously administering NR to aged individuals is invasive and therefore potentially unsuitable as a chronic therapeutic strategy.

Similarly to these observations, an increase in skeletal muscle MeNAM was also observed in a concurrent study of oral NR supplementation in aged but otherwise healthy men (176). An increase in skeletal muscle NAAD was also detected, which signifies an increased rate of NAD^+ turnover and is produced in retrograde from exogenous NR (164, 176). Though this further supports the idea that orally administered exogenous NR does affect the skeletal muscle NAD^+ metabolome, no further improvements to skeletal muscle bioenergetics were identified and no differences were observed between young and aged skeletal muscle NAD^+ levels (176), as was also observed in this mouse study. Another recent human study reported no beneficial systemic metabolic effects in obese men (177), and it is important to note that the aged mice used for this study were sedentary and effectively obese. Taken together, it could be suggested that mammalian cellular NAD^+ levels remain unperturbed with “healthy” ageing in the absence of serious metabolic comorbidities such as type II diabetes or cardiovascular disease.

The data presented in this chapter indicates that skeletal muscle NRK2 overexpression is not sufficient to protect against ageing metabolic phenotypes, with no significant impact on the NAD^+ metabolome or functional alterations to whole body metabolism and skeletal muscle mitochondrial oxidative capacity. Furthermore, NR supplementation impacted upon the skeletal muscle NAD^+ metabolome but did not affect cellular redox status, absolute NAD^+ concentrations, metabolic phenotype or skeletal muscle oxidative capacity in either aged WT or NRK2.Tg mice. The absence of any effect on skeletal muscle NAD^+ levels in NRK2.Tg mice suggests that orally administered NR may not be functionally bioavailable as intact NR to skeletal muscle. These data suggest that NRK2 and the NRK salvage pathway do not constitute an endogenous metabolically relevant pathway in the context of metabolic stress induced by ageing. However, the unprecedented lack of skeletal muscle NAD^+ deficit in this aged model leaves the physiological role of NRK2 in this context unclear. Future experiments should prioritise investigations into states of severe metabolic stress coupled with ageing such as acute and endurance exercise, which was unsuccessfully attempted due to an inability to motivate the aged cohort to exercise.

CHAPTER 5 – STRUCTURAL AND FUNCTIONAL CONSEQUENCES OF NRK2 OVEREXPRESSION IN SKELETAL MUSCLE

5.1 Introduction

The previous chapter determined that skeletal muscle NRK2 overexpression has a minimal impact on aged metabolic phenotype. However, evidence suggests that the roles of NRK2 stretch beyond that of a rate limiting kinase in a seemingly redundant NAD^+ generating pathway for metabolic homeostasis. This chapter aimed to further clarify such potential roles through investigating the consequences of in vivo NRK2 skeletal muscle overexpression on muscle mass, structure and strength alongside the molecular mechanisms governing these processes.

The most prominent roles of NAD^+ are as a critical hydrogen and electron transfer molecule for glucose and fatty acid oxidation (106, 112), as well as a consumed cosubstrate for posttranslational modifications that influence metabolic adaptation (109, 118, 212, 230). However, NAD^+ dependent protein deacetylation and ADP-ribosylation events mediate a multitude of cellular processes alongside energy metabolism including transcription, cell cycle progression, apoptosis, DNA repair and regulation of cell adhesion (192, 418). This suggests that the biological influence of NAD^+ may be even more widespread than is currently established. NRK2 orthologs and splice variants have been specifically implicated as critical for zebrafish embryonic myogenesis (344), mouse myoblast differentiation (341) and the maintenance of skeletal muscle structural organisation (342), all of which processes are reliant on cell adhesion receptors such as integrins (341, 342, 419, 420). Such processes are also critical to skeletal muscle hypertrophy, remodelling and regeneration, implicating potential indirect roles of NRK2 in the homeostasis of skeletal muscle mass, structure and function.

5.1.1 Skeletal muscle hypertrophy and atrophy

Skeletal muscle mass is governed by several signalling pathways which modulate the balance between hypertrophy and atrophy (Figure 5-1). Upregulation of key skeletal muscle hypertrophy pathways are mediated by the growth hormones insulin growth factor 1 and 2 (IGF1/2) signalling through the insulin receptor (IR) which itself has two isoforms (421) (Figure 5-1). IGF1 is primarily active in adult muscle growth and regeneration, whereas IGF2 normally mediates skeletal muscle growth and development during embryonic myogenesis (422). IGF1 and IGF2 production are themselves regulated by mTOR signalling and nutritional status (423). IR receptor activation by IGF propagates signalling through the PI3K/AKT signalling pathway and the MAPK/ERK pathway, both of which ultimately result in mTOR activation and subsequent upregulation of transcription factors, such as eIF4E which promotes myofibrillar protein synthesis, and ribosomal protein S6 (rpS6) which promotes protein synthesis and ribosomal biogenesis (424, 425) (Figure 5-1).

Skeletal muscle hypertrophy pathways are counterbalanced by atrophic pathways, including transforming growth factor β (TGFβ) signalling through the p38 MAPK pathway (426), and the TGFβ related myostatin (MSTN) which binds the activin type II receptor (ACVR2) (427). MSTN induced signalling targets include the transcription factors FOXO and receptor mothers against decapentaplegic homologs 2 and 3 (R-SMAD2/3), which are phosphorylated and translocated to the nucleus (428), promoting expression of the ubiquitin E3 ligases Atrogin1 and muscle RING-finger protein 1 MuRF1 (Figure 5-1)(429). This leads to ubiquitination and subsequent proteasomal degradation of muscle proteins, reducing muscle mass (429, 430). Crosstalk between hypertrophy and atrophy signalling pathways serve as further regulatory mechanisms, with AKT inhibiting FOXO activity and SMAD2/3

inhibiting AKT activity, as well as activation of the MAPK/ERK pathway having downregulatory effects on TGFβ signalling (431, 432) (Figure 5-1).

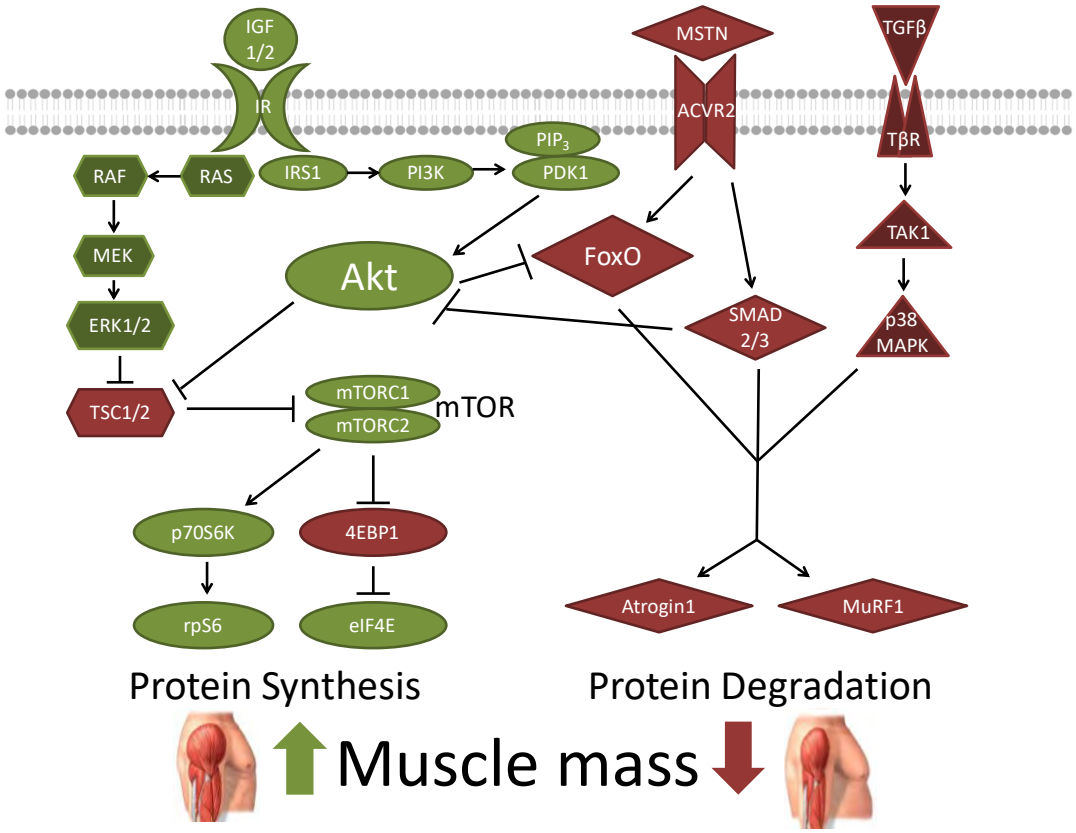

Figure 5-1 – Simplified Diagram of the major skeletal muscle hypertrophy/atrophy signalling pathways. Skeletal muscle hypertrophy is promoted through IGF mediated activation of the PI3K/AKT pathway, which inhibits tuber sclerosis complex 1 and 2 (TSC1/2) and stabilises the mTOR complex. The mTOR complex phosphorylates 4E binding protein 1 (4EBP1), releasing the protein synthesis inducing factor eIF4E, and p70S6K which itself phosphorylates rpS6, upregulating protein synthesis (light green). IGF signalling can also activate the MAPK/ERK pathway which also inhibits TSC2 (dark green). Conversely, skeletal muscle atrophy is promoted through myostatin (MSTN) signalling through FOXO and SMAD2/3 pathways (light red) and TGFβ signalling through the p38 MAPK pathway (dark red), upregulating the ubiquitin E3 ligases Atrogin1 and MuRF1 leading to protein degradation. Anabolic and catabolic homeostasis is also modulated through crosstalk between these pathways, with AKT having inhibitory effects on FOXO signalling and SMAD2/3 inhibiting AKT activity. IRS1: insulin receptor substrate 1; MEK: Mitogen-Activated protein kinase kinase; PIP_3: phosphatidylinositol (3,4,5)-trisphosphate; RAS: Ras GTPase; RAF: rapidly accelerated fibrosarcoma; TAK1: transforming growth factor beta activated kinase 1; TβR: transforming growth factor beta receptor.

Further to ligand/receptor mediated signalling, it important to note that physical activity can also modulate skeletal muscle mass. Short, intense exercise can induce skeletal muscle hypertrophy through mTOR complex stabilisation via mechanoreceptor signalling (433, 434), while AMPK can arrest hypertrophy in times of prolonged energetic stress through phosphorylation of RAPTOR and/or upregulation of TSC2 and subsequent inhibition of mTORC1 (435). AMPK can also promote skeletal muscle atrophy through activation of the p38 MAPK pathway, producing free amino acids which can be oxidised as fuel under conditions of starvation whilst also upregulating mitochondrial biogenesis pathways. Prolonged skeletal muscle disuse therefore results in increasingly diminished skeletal muscle health with age (436).

5.1.2 Regeneration of adult skeletal muscle

Skeletal muscle retains a remarkable capacity for regeneration after injury due to an extensive cohort of self-repopulating skeletal muscle stem cells, termed satellite cells (39, 437). Broadly, skeletal muscle regeneration can be split into three phases following injury. Firstly, an initial inflammatory reaction occurs which is characterised by infiltration of neutrophils and CD68+ proinflammatory macrophages, followed by an influx of CD163+ anti-inflammatory macrophages (438, 439). The second phase is characterised by activation, differentiation and subsequent fusion of satellite cells (439, 440). Quiescent Pax7 expressing satellite cells reside within their niche between the basal lamina and sarcolemma until proliferation is induced by cues which include sphingosine-1-phosphate generation on the inner plasma membrane (441), increased nitric oxide (NO) production (442) and subsequent hepatic growth factor (HGF) release from the ECM (443). Differentiation is then controlled by

Wnt and Notch signalling pathways, at which point the committed myogenic daughter cells express the MRFs MyoD, Myf5, Mrf4 and MyoG (439, 444). Subsequent differentiation to myoblasts is identified through expression of MyHC isoforms, dependent on their fibre type of origin, before fusion to multinucleated myotubes (439, 445). Lastly, further morphogenesis into mature muscle is dependent on re-establishment of blood supply and reformation of neuromuscular and myotendinous junctions (NMJs and MTJs), for which an intact basal lamina and proper myofibre/ECM interactions are critical (446-448). Growth factors such as IGF1 enhance the efficacy of skeletal muscle regeneration through activation of hypertrophic PI3K/AKT and ERK/MAPK pathways (449, 450), which are also required for myoblast fusion and differentiation (451). Terminally regenerated skeletal muscle fibres present with centrally located nuclei for 6-12 months post regeneration, with the likelihood of nuclei returning to the periphery thought to be influenced by localised factors such as proximity to NMJs and blood supply (452-454).

5.1.3 The satellite cell niche

Skeletal muscle homeostasis requires a fine balance between skeletal muscle atrophy, hypertrophy and retention of self renewal capacity. This is dynamically regulated by a highly specified satellite cell niche located between the basal lamina and sarcolemma, with niche/satellite cell interactions playing a major role ensuring specific regulation of satellite cell quiescence, self-renewal, proliferation and differentiation through structural and biochemical cues (43). Wnt and notch signalling pathways play major roles in regulating these processes (444, 455), with an exchange of diffusible signalling molecules including Wnt, IGF and FGF as well as cell-cell contact between adjacent satellite cells and/or

myofibres playing a major part (43). Sphingolipid signalling is also important, with sphingomyelin enrichment of quiescent satellite cell membrane diminishing upon activation in association with the biosynthesis of mitogenic S1P (43, 441, 456).

The satellite cell niche is located between the basal lamina and apical sarcolemma, separating satellite cells from muscle interstitium (457, 458). Direct interactions between the ECM of these interfaces and satellite cells are critical to regulation of satellite cell activity (43). The apical sarcolemma is covered with laminin while the ECM of the basal lamina consists mainly of type IV collagen, laminin, fibronectin, perlecan, entactin and decorin glycoproteins amongst other proteoglycans (457, 458). Though ECM is maintained primary by fibroblasts, it is also produced and remodelled by myoblasts upon skeletal muscle development and/or regeneration (43, 458).

Due to the two opposing microenvironments of the basal lamina and apical sarcolemma, quiescent satellite cells exhibit asymmetric distribution of regulatory cell surface proteins including M-cadherin and β-catenin which are enriched towards the myofibre, while ECM-interacting proteins such as integrin α7/β1 are concentrated towards the basal lamina (459). β-catenin is a potent driver of self renewal(460) while cadherins have been identified as critical regulators of satellite cell quiescence and the transition to activation (461). Physical tethering of the satellite cell actin cytoskeleton to the ECM via integrin α7/β1 allows for transduction of extracellular mechanical force through to intracellular chemical signalling, promoting satellite cell activation for repair of exercise induced damage (343, 462). Muscle specific laminin-2 and -4 associate with myofibres via integrin α7/β1 and dystroglycan (463), while satellite cell surface proteoglycans function as receptors for inactive growth factor precursors including Wnt glycoproteins, (444, 464)

hepatocyte growth factor (HGF)(465), basic fibroblast growth factor (bFGF) (466), epidermal growth factor (EGF) (467) and IGF1/2 (450). Upon muscle injury, proteolytic enzymes are released from serum or muscle interstitium, activating these precursors and eliciting a rapid proliferative response (43, 468).

Further to the immediate niche, the broader microenvironment is also critical to satellite cell regulation including blood vessels, neurons, interstitial cells and their associated secretable factors as well as systemic signalling from immune cells, androgens and nitric oxide signalling (43) altogether comprising a highly complex picture of regulation of skeletal muscle growth and regeneration.

5.1.4 Aged related skeletal muscle atrophy

From middle age, skeletal muscle mass is lost at a rate of 1% per year, reaching up to 50% by the 8^{th}-9^{th} decade, predisposing individuals to frailty, morbidity, metabolic decline and mortality (469). This age related decline in skeletal muscle mass can be attributed to many contributing factors besides that of insufficient NAD^+ for oxidative metabolism and metabolic adaptation, many of which are linked to imbalances between skeletal muscle protein synthesis and degradation (469). As well as a general decrease in physical activity with age (436), “Anabolic resistance” is a major factor, which is defined as an inability to respond to fundamental environmental cues that positively regulate muscle mass such as physical activity (470) and protein/amino acid intake (302, 469). The underlying molecular causes are not fully characterised but are thought to include impaired protein synthesis and ribosomal biogenesis due to impaired mTOR activation and p70S6K signalling (297, 469, 471), ROS accumulation and energetic stress from defective and inefficient mitochondria

(101, 102), increased lipid infiltration (305), increased inflammation (304) and impaired amino acid sensing (303, 469). Ageing muscle also presents with a greater proportion of denervated and therefore redundant fibres, indicating that defective neuromuscular remodelling could also be important (472).

Aged skeletal muscle also loses its capacity for regeneration due to reductions in satellite cell populations as a result of impaired self-renewal and increased senescence (299-301). Loss of skeletal muscle fibres, or hypoplasia, also contributes to skeletal muscle atrophy with age as well as a decrease in average fibre cross sectional area (469, 473), though this does not completely account for the loss of force (474, 475). Interestingly, satellite cell density remained stable between aged (20-24 month) and geriatric (28-32 month) old mice despite a further steep decline in myofibre number and size, implicating loss of intrinsic regenerative potential as the main driver of age related satellite cell dysfunction rather than an absolute decrease in satellite cell count (459). NR treatment has been shown to partially reverse age related satellite cell senescence through NAD^+ repletion (171). The metabolic rate of quiescent satellite cells is low, but dramatically increases upon activation which is characterised by a switch from oxidative to glycolytic metabolism (476). The resulting NAD^+ deficit decreases Sirt1 activity, in turn resulting in H4K16 hyperacetylation and increased transcription of skeletal muscle genes (476). Sirt1 driven autophagy has also been identified as critical for the provision of sufficient ATP under increased metabolic demand during satellite cell activation, with SIRT1KO mice showing impaired muscle regeneration and impaired satellite cell activation (477). These studies suggest that metabolic status directly influences satellite cell fate, highlighting loss of NAD^+

homeostasis as a major driver of age related satellite cell dysfunction and subsequent skeletal muscle incompetence.

5.1.5 NRK2 and myogenesis, differentiation and cell adhesion

Individual skeletal muscle fibres, fibre bundles and whole muscles are surrounded by ECM comprised of collagens, elastin, laminin, glycoproteins and proteoglycans (478), and the interaction between skeletal muscle cells and the basement membrane is critical to skeletal muscle morphogenesis and function (479). In skeletal muscle, two major membrane complexes mediate force transmission between the skeletal muscle cytoskeleton and the ECM: the dystroglycan/sarcoglycan complex and the integrin α7-laminin complex (480). Interestingly, a shortened splice variant of NRK2 termed MIBP binds to a shared membrane-proximal cytoplasmic region of β1A and β1D integrins which mediate skeletal muscle/ECM interaction (341). It was later determined that MIBP is a catalytically inactive splice variant of NRK2 lacking any affinity for NR phosphorylation (14). Further investigations determined that MIBP interacts specifically with the crucial α7β1 integrin subtype and is necessary for maintaining paxillin expression and phosphorylation levels, a protein essential for cell-ECM binding (342). More recent studies in zebrafish embryos have provided additional detail, reporting interactions of the NRK2 ortholog Nrk2b with integrins α6 (ITGA6) and α7 (ITGA7) and improper paxillin recruitment to cell matrix adhesion complexes (CMACs) upon knocking out Nrk2b (345). Furthermore, removal of Nrk2b leads to dysregulated cytoskeletal dynamics, defective laminin organisation, disrupted MTJ interactions and impaired myomere formation within developing skeletal muscle (344).

Crucially, such phenotypes could be rescued with the addition of NAD^+ (344, 345), suggesting a localised NAD^+ generating role of NRK2 for maintaining proper skeletal muscle/ECM interactions. One proposed model involves ADP-ribosyltransferases (ARTs), which are NAD^+ dependent mono-ADP ribosylases that are anchored to the surface of skeletal muscle cells (274, 277). EctoARTs are located on the plasma membrane with the catalytic site facing outwards, and are thought to mono-ADP ribosylate integrin α7β1 subtypes enabling skeletal muscle integrin/laminin binding, with ART1 being of particular importance (273, 274, 276, 277). Recruitment of NRK2 to integrin α7β1 may therefore ensure sufficient localised NAD^+ levels for integrin ADP-ribosylation via ARTs and subsequent recruitment of CMAC proteins such as paxillin, maintaining proper skeletal muscle/ECM binding dynamics (17) (Figure 5-2).

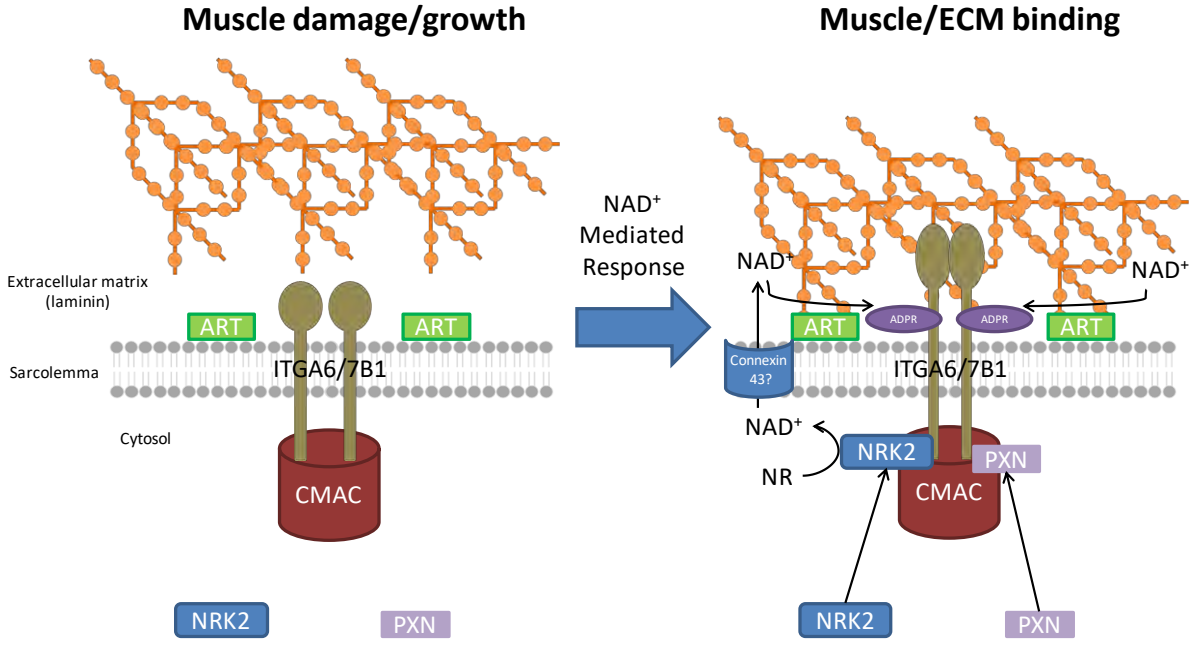

Figure 5-2 – The hypothesised role of NRK2 and NAD^+ in the maintenance of muscle-extracellular matrix (ECM) adhesion. In response to damage, muscle growth or development, NRK2 is recruited to the cytoplasmic tails of integrin receptors, where a membrane proximal cytosolic NAD^+ pool is generated. NAD^+ then crosses the sarcolemma into the ECM, possibly via the passive pyridine dinucleotide transporter connexin 43 (17, 481) or leaking through damaged sarcolemma in cases of localised injury (275). NAD^+ is then consumed by ADP-ribosyltransferases (ARTs) which mono ADP-ribosylate integrin receptors, promoting integrin/laminin binding and proper localisation of paxillin (PXN) to cell matrix adhesion complexes (CMACs).

Corroborating this, NRK2 is significantly upregulated in mammalian cells during conditions whereby skeletal muscle/ECM remodelling takes place, such as during myoblast fusion into myotubes (Figure 5-3) (15) and as a result of injury (326). Overexpression of the catalytically inactive MIBP isoform in C2C12 cells impaired myotube fusion and differentiation, also impairing cell adhesion to laminin as well as laminin deposition (341, 342). It is therefore likely that MIBP overexpression competitively inhibits the binding of catalytically active NRK2 to the integrin α7/β1 heterodimer, causing depletion of the membrane proximal NAD^+ pool and impairment of integrin/laminin binding integrity (Figure 5-3). Despite the apparent importance of NRK2 in this role, murine NRK2KO models did not

result in any structural abnormalities within skeletal muscle as was observed in zebrafish (15, 320). This suggests that the functional redundancy of NRK1 could compensate for the loss of NRK2 in mammals in this respect (15), although laminin/integrin integrity was not specifically investigated in these studies.

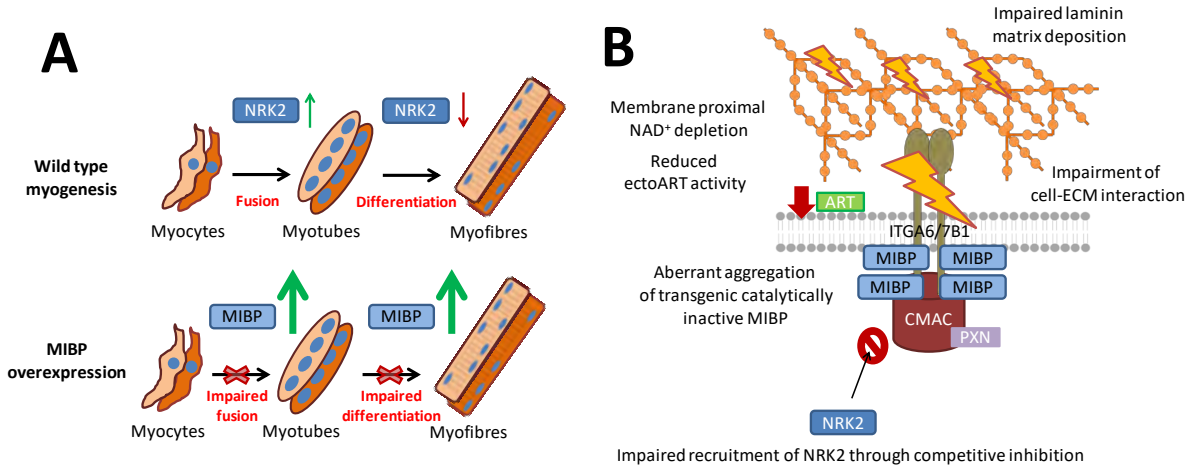

Figure 5-3 – Potential mechanism of constitutive MIBP overexpression causing impairment of myocyte fusion and differentiation. During normal myogenesis, NRK2 is upregulated during myocyte fusion then downregulated upon subsequent differentiation (15). Chronic overexpression of the catalytically inactive MIBP splice variant perturbs these expression dynamics, leading to impaired fusion and differentiation (A) (341, 342) as a result of competitive inhibition of catalytically active NRK2 binding to integrin α7β1 and subsequent depletion of the membrane proximal NAD^+ pool (B).

The data discussed indicate firstly that NRK2 retains a specific role concerning cell adhesion within mammals, and secondly that spatial and temporal expression levels of NRK2 are critical in this regard. Given the importance of cell-ECM interactions to skeletal muscle morphogenesis and regeneration, lifetime constitutive NRK2 overexpression may therefore influence the structural and functional properties of skeletal muscle with age as strength, regenerative capacity and metabolic health declines. The novel mouse strain validated for this thesis therefore provides an excellent opportunity to ascertain any effects of skeletal muscle NRK2 overexpression on skeletal muscle structure and function in vivo. The aim of

this chapter was to therefore establish the effects of lifetime constitutive NRK2 overexpression on aged skeletal muscle structure and function.

5.2 Materials and Methods

5.2.1 Tissue collection and weighing

Mice were culled via cervical dislocation and tissues weighed and snap frozen according to section 2.3. Unless otherwise stated, mice were culled between 10:00 and 12:00 to avoid circadian bias.

5.2.2 Grip Strength Tests

Grip strength tests are a technique for quantifying skeletal muscle strength in vivo on the basis that mice will instinctively grasp nearby surfaces tightly when suspended by the tail (482). Whole body grip strength tests were used because it allowed for quantification of total fore and hindlimb strength, and also because issues with differing animal compliance levels were mitigated using this method. The whole limb grip strength test was adapted from Castro and Kuang, 2017 (364). Grip strength tests were carried out using a Linton Grip Strength Meter (Linton Instrumentation, Norfolk, UK). Female WT and NRK2.Tg mice were held by the base of the tail and allowed to grip with all four limbs onto an angled mesh grid before being pulled away horizontally and peak grip force recorded. This was repeated 5 times with 1 minute of rest in between attempts. Results were normalised to mouse body weight and presented as peak force and average force from 5 attempts. All experiments

were carried out between 10:00-13:00 to minimise circadian bias and performed by the same experimenter blinded to mouse genotype to avoid interpersonal and genotype bias.

5.2.3 RNA extraction, reverse transcription and qPCR

RNA was extracted from mouse quadriceps samples using phenol/chloroform extraction (detailed in section 2.5.1) and reverse transcription was performed according to the protocol detailed in section 2.5.2. For qPCR analysis, all genes besides Nmrk2 were assayed using TaqMan probes following the protocol detailed in section 2.5.4. Nmrk2 was optimised and assayed using the SYBRGreen™ gene expression assay method to the protocol detailed in section 2.5.5. Table 5-1 contains the list of TaqMan™ probes used in chapter 5.

Table 5-1 – TaqMan™ probes used throughout chapter 5.

Gene	Accession Number
Act2	Mm00473658_m1
Act3	Mm00496495_m1
Acvr2b	Mm00431664_m1
Anxa1	Mm00440225_m1
Hspa5	Mm00517691_m1
Cav1	Mm00483057_m1
Col1a1	Mm00801666_g1
Ddit3	Mm01135937_g1
Gusb (reference gene)	Mm01197698_m1
Igf1	Mm00439560_m1
Igf2	Mm00439564_m1
Il6	Mm00446190_m1
Itga6	Mm00434375_m1
Itga7	Mm00434400_m1
Itgb1	Mm01253230_m1
Mrf4	Mm00435127_g1
Mstn	Mm01254559_m1
Myf5	Mm00435125_m1
Myod1	Mm00440387_m1
Myog	Mm00446194_m1
Plec	Mm01197443_m1
Pxn	Mm00448533_m1
Tnf	Mm00443258_m1
Trim63	Mm01185221_m1

5.2.4 Protein Analysis

5.2.4.1 Lysate preparation

Approximately 30 mg of three month and 22-24 month old female mouse quadriceps was prepared according to section 2.3.1 and placed into a 2 ml microfuge tube (Eppendorf UK Ltd, Stevenage, UK) along with 300 µl sucrose lysis buffer (50 mM Tris/HCl [pH 7.5], 250 mM sucrose, 10 mM Na-β-glycerophosphate, 5 mM Na-pyrophosphate, 1 mM benzamidine, 1mM EDTA, 1mM EGTA, 1% Triton X-100, 1mM Na_3VO_4, 50 mM NaF) and supplemented

with 1x protease and phosphatase inhibitor cocktail (Abcam, Cambridge, UK) on ice. A 5mm metal bead was added to the tube and homogenisation was performed using a TissueLyser II (QIAGEN, Germany) by shaking at a frequency of 30 cycles per second for 2 minutes. Lysates were centrifuged at 4 ^{o}C for 15 minutes to pellet debris. Protein concentration was determined using a Pierce^{TM} Coomassie Protein Assay Kit with BSA standards ranging from 0 -12.5 µg/ml (ThermoFisher Scientific, Massachusetts, USA).

5.2.4.2 **Immunoblotting**

Immunoblotting of prepared lysates was then performed collaboratively by Yu-Chiang Lai's group within the School of Sport, Exercise and Rehabilitation Sciences (University of Birmingham, UK). Lysate containing 15 µg total protein was loaded into 4-12% Bis-Tris precast gels (ThermoFisher Scientific, Massachusetts, USA) and ran for approximately 80 minutes at 140V in 200 mM 3-(N-morpholino)propanesulfonic acid/sodium acetate/sodium dehydrate (MOPS) buffer (pH 7). Proteins were transferred onto polyvinylidene difluoride (PVDF) membranes (GE Healthcare, USA) for 1h at 100 V. membranes were blocked in 5% milk in tris-buffered saline diluted with 150 mM sodium chloride/20 mM Tris-base/0.1% Tween-20 at pH 7.5 (TBS-T) for 1h then washed in TBS-T for 3 x 10 minutes before overnight incubation at 4 ^{o}C with primary antibody (Table 5-2) diluted in 3% BSA in TBS-T. Membranes were then washed for 3 x 10 minutes in TBS-T before incubation with species appropriate HRP-conjugated secondary antibody (Dako Laboratories, Denmark) at RT for 1h. 3 x 10 minute washes were performed again in TBS-T before antibody chemiluminescent detection (Enhanced Chemiluminescence HRP Substrate Detection Kit, Millipore, Massachusetts, USA). Imaging was performed directly using a G:Box Chemi-XR5 (Syngene, India). Densitometry was performed using ImageJ V1.48V.

Table 5-2 – Primary antibodies used for Immunoblotting in chapter 5.

Antibody Species/Specificity	Source	Product Code	Immunoblotting Dilution
Rabbit α eEF2	Cell Signalling Technology (USA)	#2332	1:1000
Rabbit α phospho-p44/42 MAPK (Erk1/2) (T202/Y204)	Cell Signalling Technology (USA)	#4370	1:1000
Rabbit α phospho-AKT (Thr308)	Cell Signalling Technology (USA)	#2965	1:1000
Rabbit α phospho-AKT (Ser473)	Cell Signalling Technology (USA)	#4060	1:1000
Rabbit α Phospho-4EBP1 (Thr37/46)	Cell Signalling Technology (USA)	#9459	1:1000
Rabbit α phospho-p70 S6 Kinase (Thr389)	Cell Signalling Technology (USA)	#9205	1:1000
Rabbit α phospho ribosomal protein -S6 (Ser240/244)	Cell Signalling Technology (USA)	#5364	1:1000
Mouse α MuRF1 (C11)	Santa Cruz Biotechnologies (USA)	sc-398608	1:1000

5.2.5 Immunohistochemistry

5.2.5.1 Formalin fixed paraffin embedding (FFPE) – tissue fixation, dehydration and clearing

Excised quadriceps from 22-24 month old female WT and NRK2.Tg mice were placed in 4% formaldehyde in PBS for at least 48 hours at RT to ensure complete tissue fixation. Before embedding, tissue must be dehydrated in order for the hydrophobic paraffin wax to infiltrate, which is achieved by exposure to increasing concentrations of alcohol. Samples were placed into plastic cassettes and submerged in 40% industrial methylated spirits (IMS) diluted in tap water for 1 hour, then transferred to 70% IMS for 1 hour, followed by 100% IMS for 1 hour then fresh 100% IMS for 1 hour. The tissue must next be cleared of alcohol before paraffin will infiltrate. This is achieved by exposure to xylene, which is miscible with

alcohols and once cleared turns the tissue samples translucent. Samples were placed in xylene for 3 hours at RT, being transferred to fresh xylene every hour. For paraffin infiltration, tissues were then placed into molten paraffin wax and incubated at 60 ^{o}C for one hour. This process was repeated twice more for a total of three hours.

5.2.5.2 **Tissue embedding and sectioning**

Tissues were embedded using an EG1150 H embedding workstation (Leica, Wetzlar, Germany). The tissue samples were placed into metal embedding moulds on a small volume of molten paraffin wax and promptly solidified whilst holding the sample in place, ensuring correct orientation was achieved. The mould was then filled with molten wax with care taken not to disturb the tissue sample. The cassette base was then placed onto the metal mould, topped up with more wax and allowed to solidify on a cold plate. Sections were then cut to a thickness of 5 µm using a Leica RM2125 RTS microtome (Leica, Wetzlar, Germany), floated on a 50 ^{o}C water bath to eliminate creases in the section and mounted on microscope slides (SuperFrost Plus, ThermoFisher Scientific, Massachusetts, USA). Mounted sections were incubated at 40 ^{o}C for an hour to ensure adhesion.

5.2.5.3 **Haematoxylin and eosin staining and microscopy**

To visualise tissue architecture, mounted sections must be treated with a tinctorial stain to provide contrast, in which two dyes are used in combination. Haematoxylin is a blue dye which is cationic when conjugated with metal salts, and will therefore bind to and stain negatively charged molecules such as nucleic acids, resulting in cell nuclei being dyed blue. Conversely, eosin is an anionic dye and will stain positively charged tissue components pink,

such as cytoplasmic protein groups. Other tissue components will take on variations and combinations of these colours.

Mounted tissue sections were placed in xylene for 15 minutes, changing the xylene every 5 minutes, then into 100% for 2 washes, 70% and 40% IMS for 2 minutes sequentially followed by dH_2O for 2 x 2 minutes. Sections were then stained in haematoxylin for 5 minutes before being transferred to Scott's tap water (50 µl 10 M NaOH in 400 ml tap water) for 2 minutes, turning the haematoxylin blue, followed by a brief dip in acid alcohol (0.5% conc. HCl in 70% ethanol) to prevent over staining (0.5% conc. HCl in 70% ethanol). Sections were then washed under running tap water for 5 minutes then stained with aqueous eosin for 5 minutes, followed by rinsing in 100% IMS prior to 2 washes in 100% IMS for 2 minutes, then cleared in xylene for 3 x 5 minutes. Sections were then mounted using a coverslip and Depex mounting medium (Vector Laboratories, California, USA). Images were obtained using a Leica DMIL Microscope and a Leica HI PLAN I objective at 10 x magnification.

5.2.5.4 **Antibody staining of FFPE sections**

Protein distribution can be visualised on FFPE sections by staining with a primary antibody specific to a protein of interest (Table 5-3) followed by a streptavidin/biotin HRP conjugated secondary antibody, before incubation with H_2O_2 and 3,3'-Diaminobenzidine (DAB). The peroxidase catalyses the conversion of H_2O_2 to water and oxygen, resulting in localised oxidation of DAB forming a brown precipitate in areas where the protein of interest is present. Before staining, FFPE sections must be rehydrated and the protein cross-linkages which form during formalin fixation must be reversed to allow the primary antibody to bind, in a process called antigen retrieval.

Table 5-3 – Primary antibodies used for immunohistochemistry in chapter 5.

Antibody Species/Specificity	Source	Product Code	IHC Dilution
Rabbit α laminin polyclonal	Abcam	ab11575	1/100
Rabbit α CD45 polyclonal	Abcam	ab10558	1/1000

All steps were performed at RT unless otherwise stated. Mounted FFPE Sections were dewaxed with 3 x 2 minute incubations in xylene then rehydrated with successive 2 minute incubations in serial dilutions of IMS (100%, 70% then 40%) followed by 2 x 2 minutes in ddH_2O. Antigen retrieval was performed by incubating the sections for 20 minutes at 95 ^{o}C in a sodium citrate buffer (4.7 g sodium citrate in 1.6 L ddH_2O, pH 6) then washing in ice cold PBS for 5 minutes. Sections were circled with an ImmEdge^{TM} hydrophobic barrier pen (Vector Laboratories, California, USA) and incubated with avidin for 15 minutes, rinsed with PBS-T and incubated in biotin for 15 minutes. Sections were then washed in PBS-T for 5 minutes followed by 1 hour incubation in blocking buffer (5% blocking serum [250 µl/1% BSA [50 µl] in 5 ml PBS-T) and overnight incubation at 4 ^{o}C with primary antibody (Table 5-3) diluted in blocking buffer. 3 x 2 minute washes in PBS-T were then performed before incubation with the species appropriate biotinylated secondary antibody in blocking buffer (5 µl antibody/1 ml buffer) (Vector Laboratories, California, USA). Sections were washed again in TBS-T as before and incubated for 30 minutes in ready to use avidin/biotin complex (ABC) reagent (Vector Laboratories, California, USA). PBS-T washes were repeated and the sections rinsed with ddH_2O then incubated in DAB solution (Vector Laboratories, California, USA). Sections were rinsed in tap water for 5 minutes followed by incubation with haemotoxylin for 5 minutes to counterstain, then transferred to Scott's tap water for 2 minutes and a brief dip in acid alcohol followed by 2 more minutes in Scott's tap water. Sections were then placed in

40%, 70% and 100% IMS successively for 2 minutes each, with the 100% step repeated once. Finally, sections were cleared in xylene for 3 x 2 minutes with fresh xylene for each repetition. Sections were then mounted using a coverslip and Depex mounting medium (Vector Laboratories, California, USA).

5.2.5.5 Quantification of fibre cross-sectional area (CSA) and centralised nuclei

Images were obtained from 5 µm laminin stained sections taken from female 22-24 month old WT and NRK2.Tg quadriceps using a Leica DMIL Microscope and a Leica HI PLAN I objective at 10 x magnification. Images were taken spanning the entire muscle section and analysed using ImageJ V1.48V. Fibre CSA was calculated in μm^2 for each fibre by manual outlining, and the presence or absence of central nuclei was noted as well as any incidence of multiple central nuclei being visible within one fibre.

5.2.5.6 Assessment of centralised nuclei fibre distribution

Images of a 5 µm quadriceps section from a 24 month old NRK2.Tg mouse were taken using a Leica DMIL Microscope and a Leica HI PLAN I objective at 10 x magnification, from which a composite image of the entire muscle section was created. The distribution of fibres featuring centralised nuclei was manually assessed by eye.

5.2.6 Proteomics

Proteomics is a method by which large scale quantification of proteins within biological samples can be achieved. Though post-translational modifications and relative activity levels of proteins cannot be quantified this way, the method is able to offer insight into differing protein expression levels between experimental cohorts and thus identify potentially

dysregulated cellular processes. Samples are first lysed and proteins are extracted then reduced and/or alkylated to facilitate peptide identification (483), before separation via mass spectrometry and identification using libraries of known peptide signatures. Specifically, the method used for this chapter utilised untargeted quantitative proteomics using sequential window acquisition of all theoretical mass spectra (SWATH-MS). Non-labelled protein samples are digested with trypsin and subjected to LCMS under data-independent acquisition (DIA) mode, resulting in unbiased and systematic fragmentation of all ionised compounds falling within a specific mass range (484). This also leads to co-fragmentation of many more eluting peptides within the precursor ion window, presenting complex fragment ion spectra (484). This multiplexed data is then analysed using peptide-centric scoring which utilises mass spectrometric and chromatographic coordinates of peptides of interest, termed Peptide Query Parameters (PQP), which are derived from pre-generated spectral libraries (484, 485). Identified proteins were then further analysed according to fold change using Reactome analysis to isolate potential pathways and ontological groups of importance in relation to any observed differences between aged WT and NRK2.Tg skeletal muscle.

5.2.6.1 **Protein extraction, purification and trypsinisation**

To extract protein, 50 mg of pulverised frozen quadriceps (prepared according to section 2.3.1) was homogenised in 500 µl CellLytic MT cell lysis buffer and 5 µl Halt Protease Inhibitor Cocktail (ThermoFisher Scientific, Massachusetts, USA) followed by centrifugation at 20,000 x g for 10 minutes. Lysate concentration was determined using the Pierce BCA Protein Assay Kit (ThermoFisher Scientific, Massachusetts, USA) according to manufacturer's protocol before storage at -80 ^{o}C. Protein (50 µg) was digested using sequencing grade

modified trypsin solution (Promega, Wisconsin, USA) and processed using S-trap^{TM} micro column methodology according to manufacturers protocol (ProtiFi, USA). Samples were dried and stored at -80°C until analysis. On the day of analysis, samples were resuspended in 5% acetonitrile and 0.1% formic acid prior to LCMS.

5.2.6.2 **Mass Spectrometry**

LCMS analysis was performed collaboratively by Dr David Boocock (Nottingham Trent University, UK). Samples (4 µl) were injected by Eksigent 425 LC system onto a trap column (Mobile Phase A; 0.1% formic acid, B; acetonitrile with 0.1% formic acid; YMC Triart C_{18} guard column 0.3 x 5 mm, 300 µm internal diameter) at 10 µl/min mobile phase A for 2 min before gradient elution onto the analytical column (YMC Triart C_{18} 150 x 0.3 mm internal diameter, 3 µm) in line to a Sciex TripleTOF 6600 Duospray Source using a 50 µm electrode, positive mode +5500V. Samples were analysed in two modes; information dependent acquisition (IDA) for the generation of a spectral library, and data independent acquisition (SWATH) to generate quantitative data. The following linear gradients were used: for IDA, mobile phase B increasing from 2% to 30% over 68 min; 40% B at 72 min followed by column wash at 80% B and re-equilibration (87 min total run time). For SWATH, 3-30% B over 38 min; 40% B at 43 min followed by wash and re-equilibration as before (57 min total run time). IDA acquisition mode was used with a top 30 ion fragmentation (Time of flight mass spectrometry (TOFMS) m/z 400-1250; product ion 100-1500) followed by 15 sec exclusion using rolling collision energy, 50 ms accumulation time; 1.8 s cycle. SWATH acquisition was using 100 variable windows (optimised on sample type) 25 ms accumulation time, 2.6 s cycle (m/z 400-1250). IDA data was searched using ProteinPilot 5.0.2, iodoacetamide alkylation, thorough search with emphasis on biological modifications (Swissprot mouse database, June

2018). SWATH data was analysed using Sciex OneOmics software extracted against the locally generated library to the following parameters: 12 peptides per protein, 6 transitions per peptide, extracted ion chromatogram (XIC) width 30 ppm, 5 min retention time window.

5.2.6.3 **Statistical Analysis**

Proteomic analysis was carried out using Advaita Bioinformatic iPathwayGuide software, identifying dysregulated proteins in NRK2.Tg quadriceps relative to WT quadriceps with a minimum of ± 0.5 fold change and a threshold of 0.25 for statistical significance (p value). Significantly dysregulated biological processes, pathways and molecular interactions were analysed using Gene Ontology (GO) terms in the context of pathways obtained from the Kyoto Encyclopedia of Genes and Genomes (KEGG) database (Release 84.0+/10-26, Oct 2017) (486, 487) and the Gene Ontology Consortium database (Nov 2017)(488). Differentially expressed genes are attributed to GO terms based on their function and further grouped according to known molecular functions, cellular components and biological processes. For a given GO term, the number of differentially expressed genes assigned to the term is compared with the number of differentially expressed genes which may be expected by chance, followed by an over-representation approach which computes the statistical chance of observing at least the given number of genes which were differentially expressed. To overcome the limitation of errors introduced by considering genes multiple times, the Elim pruning method is then used which iteratively removes genes mapped to a significant gene ontology (GO) term from more general (higher level) GO terms (489).

5.3 Results

5.3.1 NRK2.Tg mice present with significantly larger skeletal muscle beds

Despite few observable differences in metabolic parameters within aged NRK2.Tg skeletal muscle in the previous chapter, several skeletal muscle beds were significantly larger in aged NRK2.Tg animals when normalised to body weight. Female aged NRK2.Tg quadriceps, gastrocnemius and soleus were all significantly larger, though TA mass was comparable (Figure 5-4 A, B). In young female mice, this phenomenon was only present in soleus muscle (Figure 5-4C).

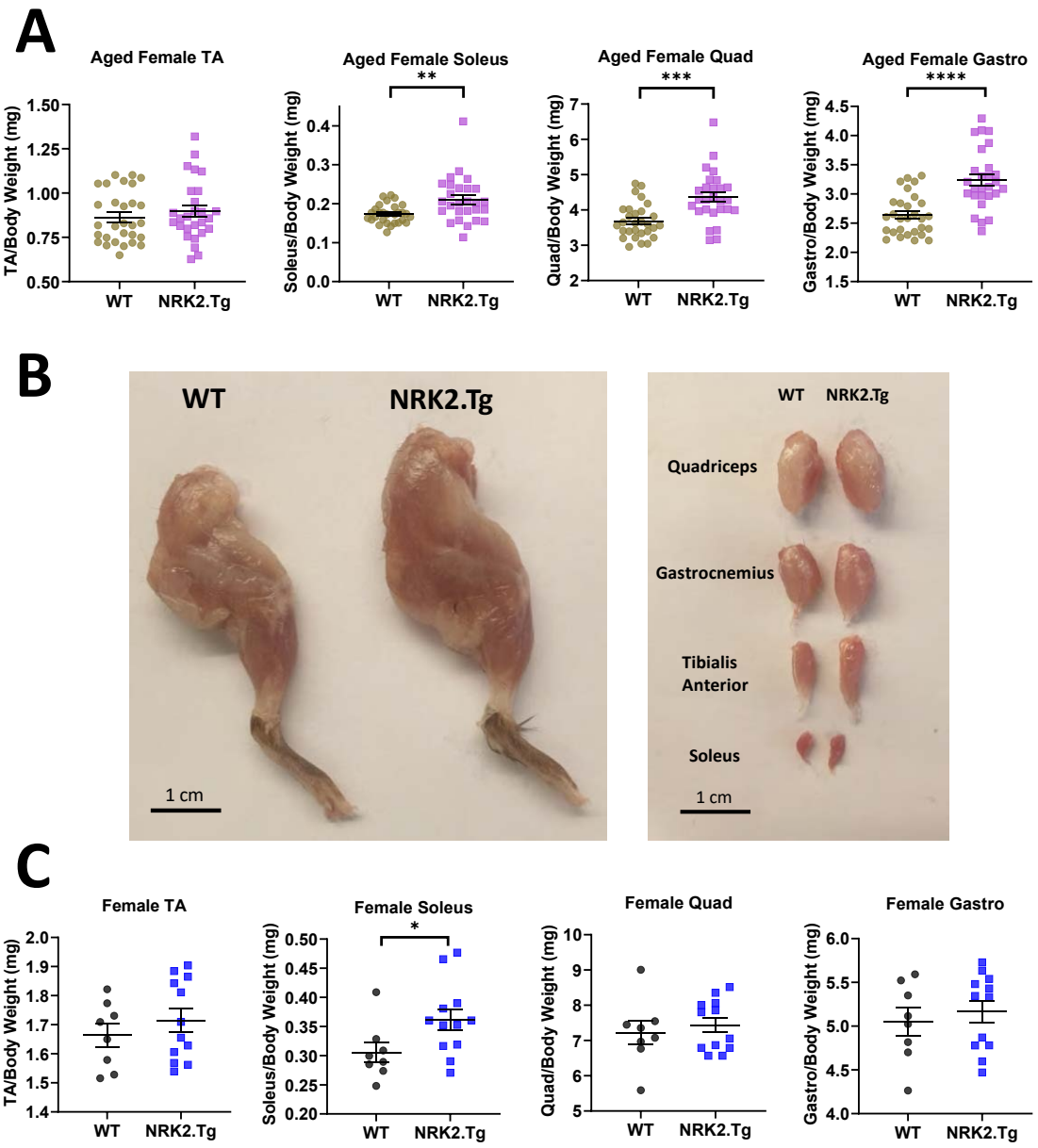

Figure 5-4 – Aged Female NRK2.Tg mice have significantly increased muscle mass relative to WT mice. A. Quantification of hindlimb skeletal muscle bed weights normalised to body weight from 22-24 month old (A) and 3-6 month old (B) WT and NRK2.Tg female mice. Data presented as mean ± SEM with individual data points representing one biological replicate. Statistical significance was determined by student's unpaired t test (* $p < 0.05$, ** $p < 0.01$, *** $p < 0.001$, **** $p < 0.0001$), n = 26-30. B. Representative photographs of litter-matched 22 month old female aged WT vs. NRK2.Tg mouse hindlimbs and excised muscle beds.

This phenotype was also present in aged overexpression male mice (Figure 5-5A), again with no significant difference in TA but significantly larger quadriceps, soleus and

gastrocnemius in NRK2.Tg mice (Figure 5-5). No differences in muscle mass relative to body weight were observed in young WT and NRK2.Tg mice (Figure 5-5B). These data indicate that NRK2 increases muscle mass in aged mice irrespective of sex.

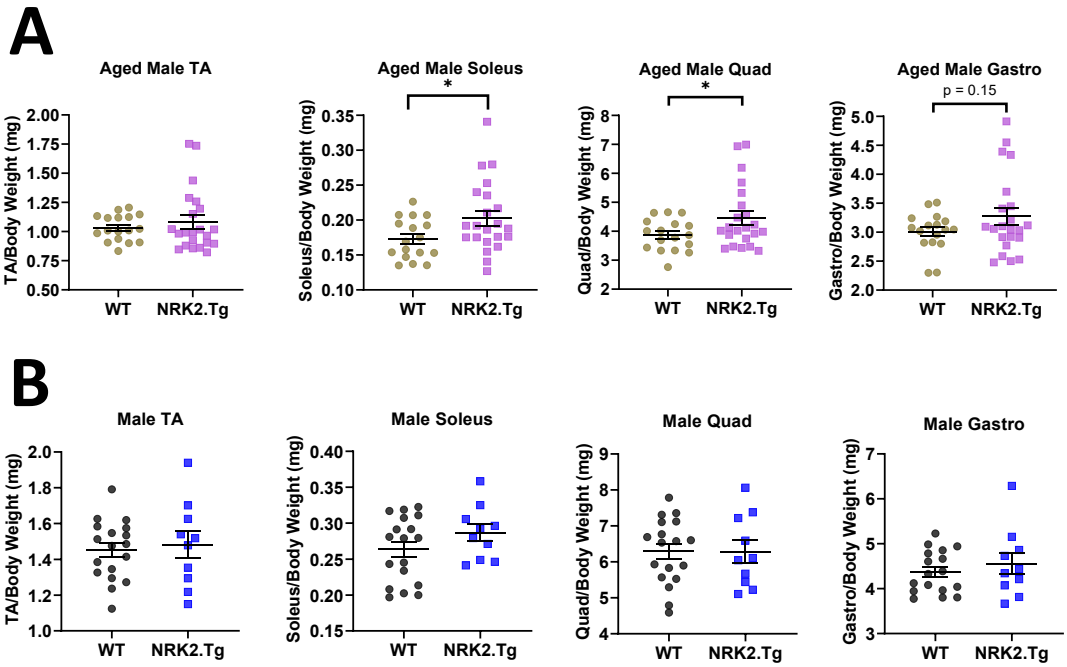

Figure 5-5 – Aged Male NRK2.Tg mice have significantly increased muscle mass relative to WT mice. Quantification of hindlimb skeletal muscle bed weights normalised to body weight from 22-24 month old (A) and 3-7 month old (B) WT and NRK2.Tg male mice. Data presented as mean ± SEM with individual data points representing one biological replicate. Statistical significance was determined by student's unpaired t test (* $p < 0.05$, ** $p < 0.01$, *** $p < 0.001$), n =9-21.

Absolute skeletal muscle weights were then compared between young and aged WT and NRK2Tg skeletal muscle to establish the effects of NRK2.Tg overexpression on age related decline of muscle mass. Soleus muscles of young NRK2.Tg mice were significantly larger relative to WT while TA, quadriceps and gastrocnemius were not significantly changed (Figure 5-6). Female aged mice presented with significantly larger skeletal muscle beds than young mice, which was not expected (4, 490). It is therefore possible that the female cohort had not yet attained full adult muscle mass at 3 months of age. However, the young male cohort ranged between 4-7 months with male muscle beds from 22-24 month old mice having significantly lower mass (Figure 5-6). The increased skeletal muscle mass in aged NRK2.Tg mice relative to aged WT mice could therefore indicate that skeletal muscle NRK2 overexpression bestows partial resistance to age associated sarcopenia.

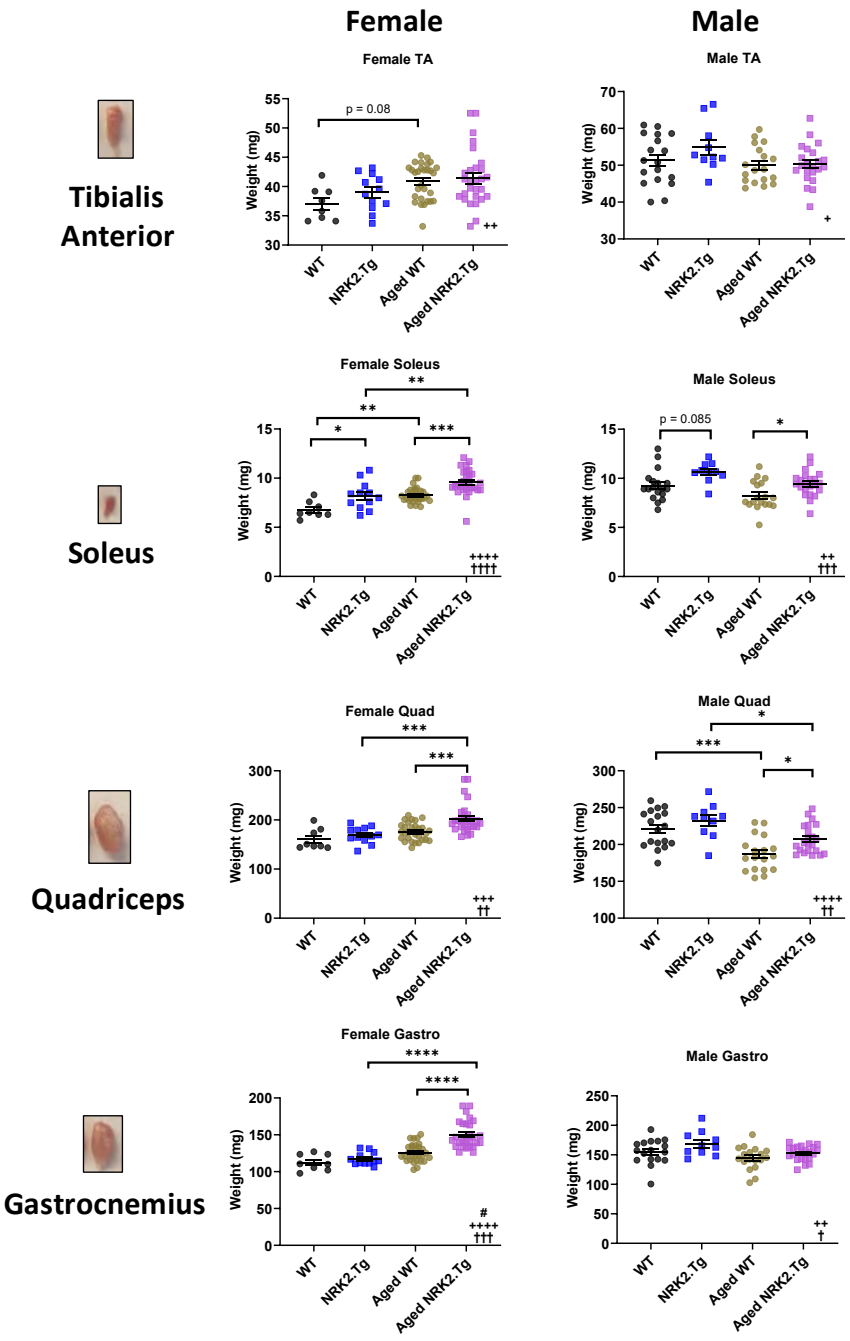

Figure 5-6 – Skeletal muscle beds in aged female and male NRK2.Tg mice are significantly larger, with soleus being significantly larger in young NRK2.Tg mice. Weights of female TA, soleus, quadriceps and gastrocnemius in young and aged WT and NRK2.Tg mice alongside age distributions of young and aged cohorts. Data presented as mean ± SEM with individual data points representing one biological replicate. Statistical significance was determined by ordinary two way ANOVA with Sidak's multiple comparison tests (* $p < 0.05$, ** $p < 0.01$, *** $p < 0.001$, **** $p < 0.0001$). # = statistically significant interaction between genotype and age; + = statistically significant variation between young and aged mice; † = statistically significant variation between WT and NRK2.Tg mice. n = 7-26.

Weights of other metabolic tissues including liver, gonadal white adipose tissue (WAT) and heart were also quantified, all of which were found to be significantly larger in aged mice relative to young mice independent of genotype. In both male and female mice, aged mouse livers were significantly larger than young mice though no weight differences between WT and NRK2.Tg livers were observed (Figure 5-7). Aged female mice presented with significantly larger gonadal WAT, though again no significant mass differences were observed between WT or NRK2.Tg mice in either the young or aged cohort (Figure 5-7). However, male aged NRK2.Tg mice trended towards larger gonadal WAT deposits than aged WT mice though this was not a significant observation (Figure 5-7). Interestingly, aged NRK2.Tg hearts were smaller than aged WT hearts, which was a significant observation in female mice (Figure 5-7). Given that that NRK2 was determined as overexpressed in NRK2.Tg heart as well as skeletal muscle in section 3.1.1, this may suggest that NRK2 overexpression could also confer resistance to age related cardiac hypertrophy (491), though this assertion would require further investigation.

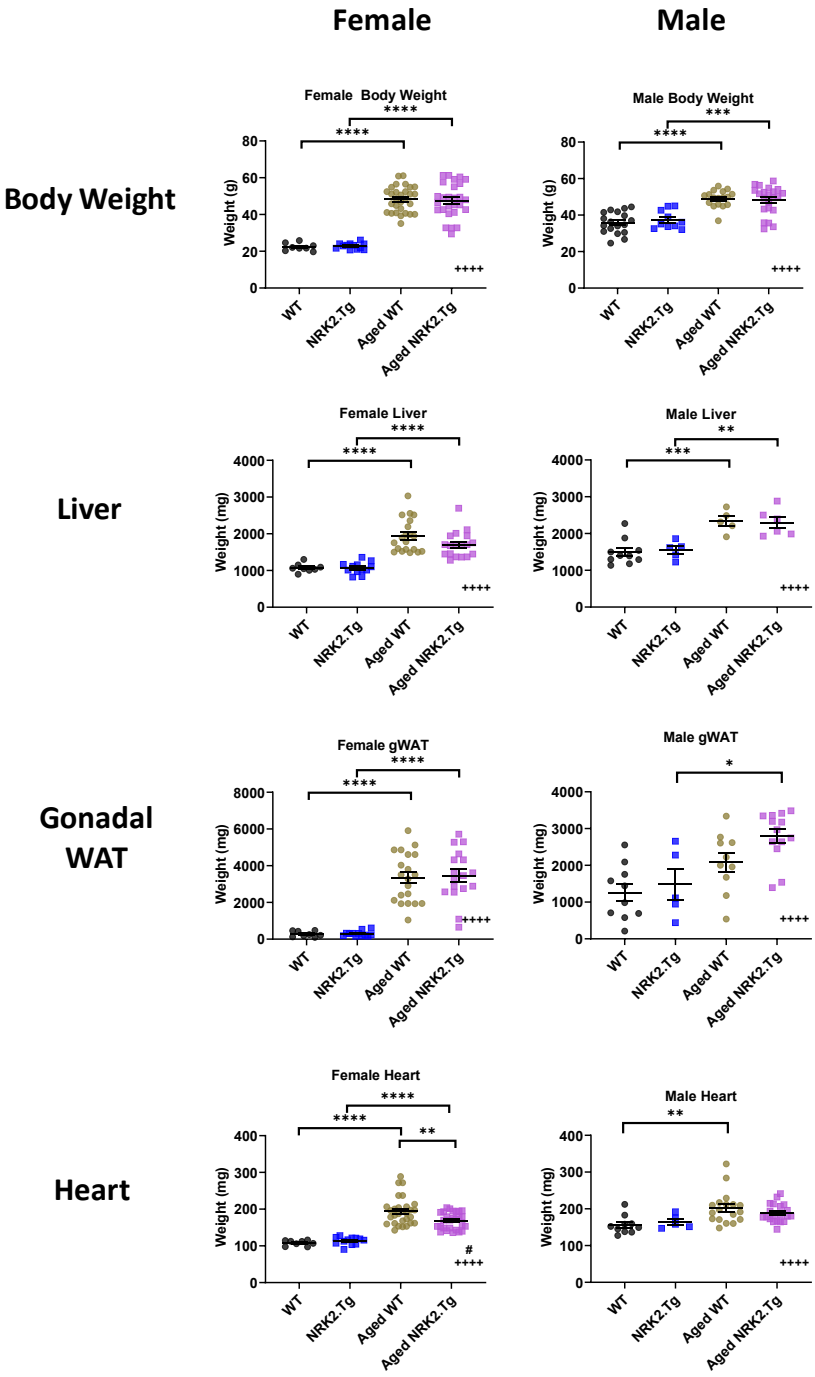

Figure 5-7 – Aged female NRK2.Tg hearts are significantly smaller than WT mice. Weight measurements of total body weight, liver, gonadal WAT and heart in male young and aged WT and NRK2.Tg mice. Data presented as mean ± SEM with individual data points representing one biological replicate. Statistical significance was determined by ordinary two way ANOVA with Sidak's multiple comparison tests (* $p < 0.05$, ** $p < 0.01$, *** $p < 0.001$, **** $p < 0.0001$). # = statistically significant interaction between genotype and age; + = statistically significant variation between young and aged mice; † = statistically significant variation between WT and NRK2.Tg mice. n = 8-26.

5.3.2 Aged NRK2.Tg mice are significantly stronger than aged WT mice

Grip strength tests were next performed on young and aged WT and NRK2.Tg mice to establish any functional consequences of increased aged NRK2.Tg skeletal muscle mass. Aged female NRK2.Tg mice generated significantly higher average and peak force values both when normalised to body weight (Figure 5-8A). These differences were not present within young mice (Figure 5-8B), indicating potential augmentation of skeletal muscle strength or ameliorated decline in weakness in NRK2 overexpressing skeletal muscle with age.

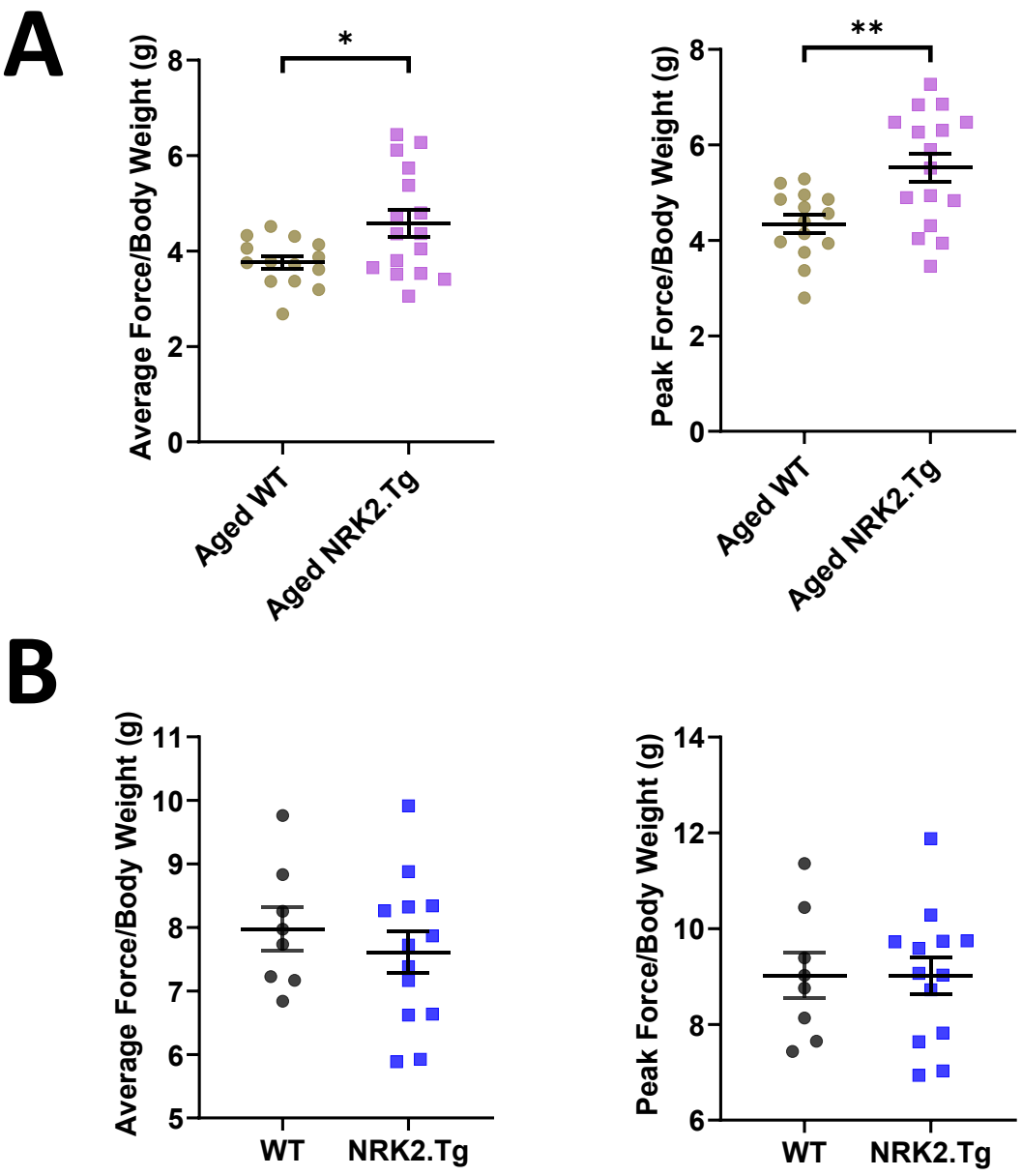

Figure 5-8 – Average and peak grip strength is significantly higher in aged NRK2.Tg mice. A. Quantification of average across 5 attempts and peak all-limb grip strength of female 18-22 month old WT and NRK2.Tg mice normalised to body weight. B. Absolute average and peak force of 3 month old WT and NRK2.Tg mice normalised to body weight. Data presented as mean ± SEM with individual data points representing one biological replicate. Statistical significance was determined by student's unpaired t test. (* $p < 0.05$, ** $p < 0.01$, *** $p < 0.001$, **** $p < 0.0001$), n = 8-16.

5.3.3 Skeletal muscle hypertrophic pathway growth factors are upregulated in NRK2.Tg skeletal muscle while atrophic ubiquitin E3 ligases are downregulated at mRNA level

Skeletal muscle mass and functional grip strength data suggested an augmentation of skeletal muscle with NRK2 overexpression. Potential molecular mechanisms behind such observations were next investigated, starting with expression levels of key skeletal muscle hypertrophy and atrophy markers. No significant changes were observed in expression levels of the MRFs Myf5, MyoD, Mrf4 and MyoG as well as the satellite cell quiescence marker Pax7 (Figure 5-9). Expression levels of the adult skeletal muscle hypertrophy marker insulin growth factor 1 (Igf1) and the skeletal muscle hypertrophy repressor myostatin (Mstn) were also unchanged between aged WT and NRK2.Tg skeletal muscle (Figure 5-9). However, expression levels of the hypertrophy promoting embryonic skeletal muscle growth factor insulin growth factor 2 (Igf2) were significantly upregulated with the skeletal muscle atrophy inducing ubiquitin E3 ligase muscle RING-finger protein-1 (Trim63) also being downregulated at transcript level (Figure 5-9). Taken together, it is possible that skeletal muscle NRK2 overexpression modulates skeletal muscle hypertrophy and atrophy signalling pathways with age, favouring skeletal muscle hypertrophy relative to WT muscle.

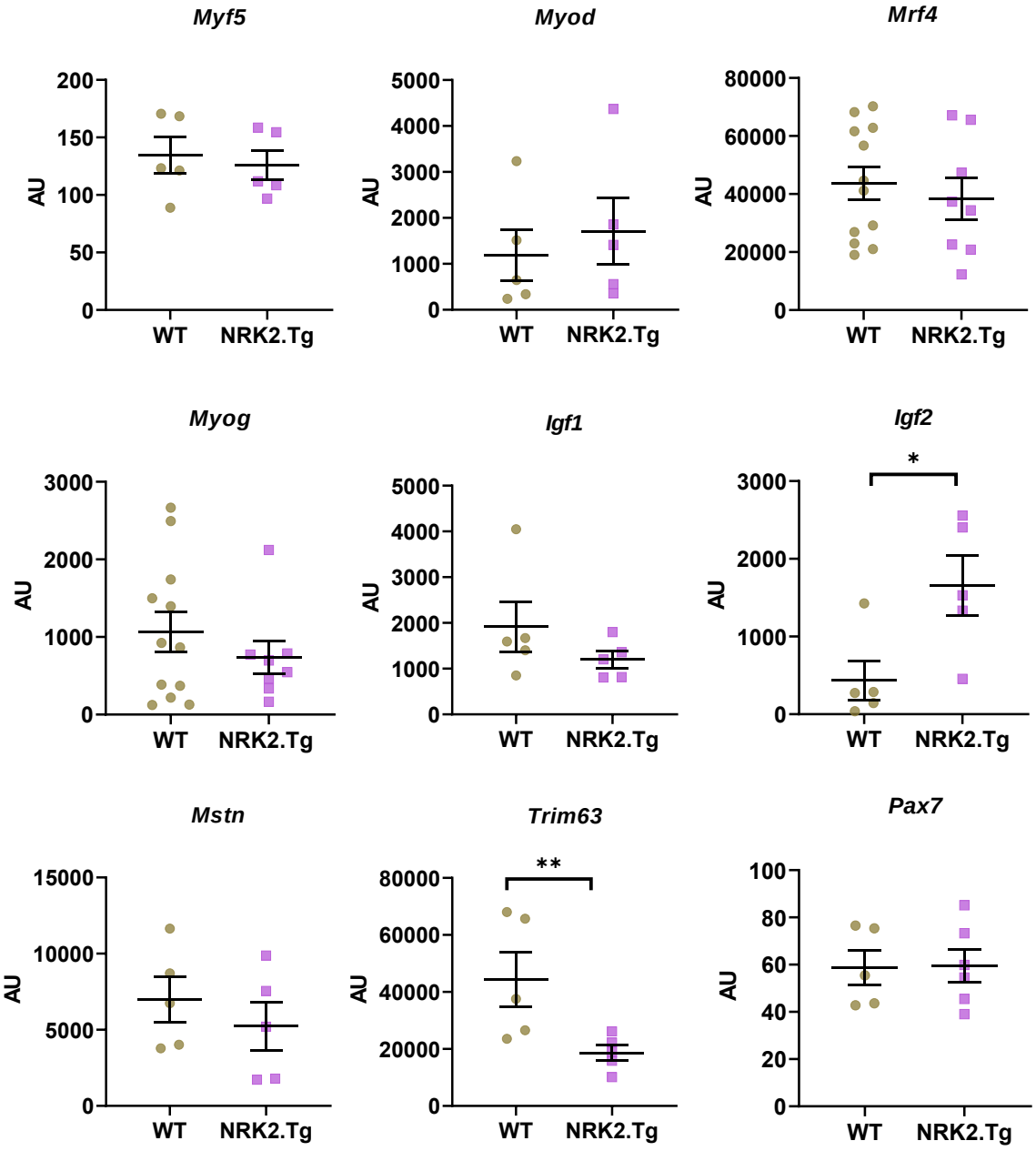

Figure 5-9 – Expression levels of myogenic regulatory factors and skeletal muscle atrophy markers in WT and NRK2.Tg quadriceps. Quantification of mRNA transcript levels in quadriceps from 3 month and 20-22 month old female mice. Data presented as mean ± SEM with individual data points representing one biological replicate. Statistical significance was determined by student's unpaired t test (* $p<0.05$, ** $p < 0.01$, *** $p < 0.001$, **** $p < 0.0001$). n = 5-8.

5.3.4 Hypertrophic signalling pathways are not significantly upregulated at protein level in aged NRK2.Tg skeletal muscle

To further investigate the cause of increased skeletal muscle mass in aged NRK2 overexpressing skeletal muscle in light of observed upregulation of Igf2 in NRK2.Tg skeletal muscle, activation levels of skeletal muscle hypertrophy pathways which are induced through IGF2 were next assessed. IGF1 and IGF2 stimulate skeletal muscle hypertrophy through binding the insulin receptor activating the PI3K/AKT/mTOR and MAPK/ERK signalling pathways, which in turn induce myofibrillar protein synthesis, cell growth pathways and inhibition of autophagy/skeletal muscle protein degradation (425, 492-494). The activation status of the PI3K/AKT/mTOR pathway can be assessed through phosphorylation status of AKT, for which partial and full activation requires phosphorylation of threonine 308 and serine 473 respectively. AKT is phosphorylated by mTORC2 at Ser473, which facilitates further phosphorylation by phosphoinositide-dependent kinase 1 (PDK1) at Thr308 forming a positive feedback loop promoting increased inhibition of TSC2 and therefore mTOR activation (495). Activation of skeletal muscle hypertrophy pathways can also be assessed through phosphorylation status of S6 kinase (S6K), its target rpS6 and 4E-BP1, which releases the transcription factor eIF-4E upon phosphorylation promoting protein synthesis (496). Activation of the alternative MAPK/ERK signalling pathway can also be assessed through levels of phosphorylated ERK1 and 2, which also promotes activation of the mTOR complex through phosphorylation and inhibition of TSC2 (497).

Quadriceps samples from young and aged WT and NRK2.Tg skeletal muscle were probed for levels of phosphorylated AKT at Thr308 and Ser473, p70S6K, rpS6, 4-EBP1 and

ERK1/2. A marked yet statistically insignificant decrease in AKT phosphorylated at Thr308 was observed between young and aged skeletal muscle for both WT and NRK2.Tg mice (Figure 5-10). A downward trend was also observed between young and aged WT skeletal muscle in AKT phosphorylated at Ser473 which was not present in young vs. aged NRK2.Tg mice (Figure 5-10). However, these observations were not significant and it is therefore unlikely that a reduced decline in AKT signalling is a major contributing factor to the observed preservation of skeletal muscle mass with age in NRK2.Tg mice. Furthermore, this relationship was not identified in any other of the assessed markers, and despite significant upregulation in Igf2 mRNA within aged NRK2.Tg skeletal muscle, no significant differences were identified directly between both young and aged WT and NRK2.Tg skeletal muscle (Figure 5-10).

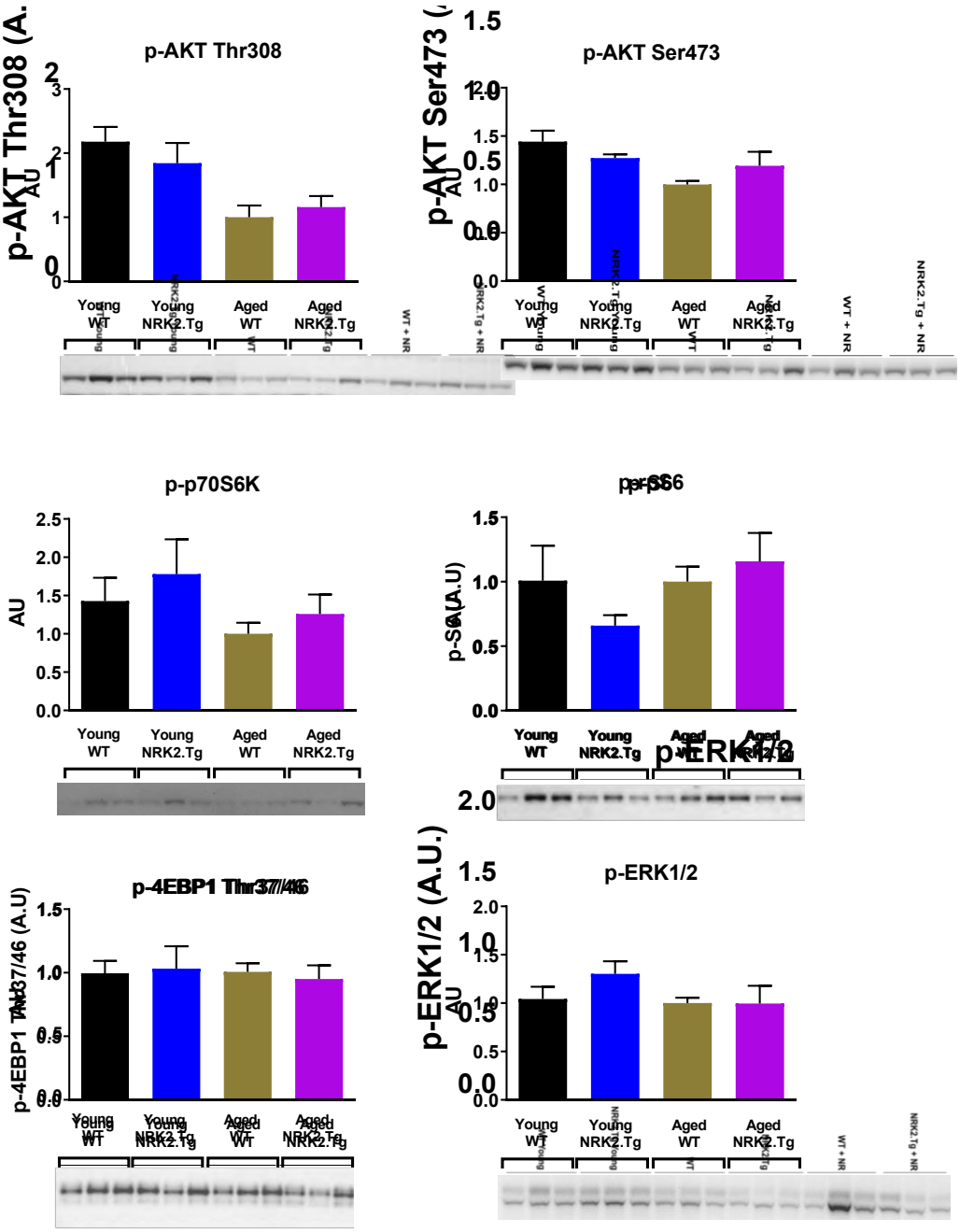

Figure 5-10 – Phosphorylated AKT levels are significantly lower in aged WT animals relative to WT, though no significant differences in mTOR activation markers are present in young or old WT and NRK2.Tg skeletal muscle. Densitometric analysis and representative immunoblots of phosphorylated (p-)AKT at threonine 308 or serine 473, p-ERK1/2, p-4EBP1 p-rpS6 and p-p70S6K levels in aged female quadriceps. Values were normalised to EEF2 loading control. Data presented as mean ± SEM. Statistical significance was determined by ordinary two way ANOVA with Sidak's multiple comparison tests (* $p < 0.05$, ** $p < 0.01$, *** $p < 0.001$, **** $p < 0.0001$). # = statistically significant interaction between genotype and age; + = statistically significant variation between young and aged mice; † = statistically significant variation between WT and NRK2.Tg mice. n = 3-6.

5.3.5 MuRF1 protein levels are downregulated in aged NRK2.Tg skeletal muscle relative to aged WT muscle

Given the observations of decreased Trim63 gene expression in aged NRK2.Tg mice, expression of the corresponding MuRF1 protein product was also quantified in quadriceps tissue. MuRF1 is an E3 ubiquitin ligase and a critical mediator of skeletal muscle remodelling and atrophic processes through ubiquitination, resulting in signal transduction and/or subsequent proteasomal degradation of target proteins (498). MuRF1 levels were similar between young WT and NRK2.Tg mice but elevated in aged WT mice, constituting a statistically significant difference across genotype means and a strong trend upon direct comparison of aged WT and NRK2.Tg muscle (Figure 5-11). Despite a lack of statistical significance upon direct comparison of aged WT and NRK2.Tg MuRF1 protein levels, these trends agreed with the significant decrease of Trim63 mRNA in aged NRK2.Tg quadriceps relative to WT tissue and indicate a decreased expression of MuRF1 in NRK2.Tg skeletal muscle. As no significant upregulation of the mTOR pathway was observed, these data suggest that the increased skeletal muscle mass in aged NRK2.Tg mice could be due to lower expression levels of MuRF1 with age and thus decreased skeletal muscle protein breakdown relative to normal ageing levels rather than any significant upregulation of hypertrophic pathways through IGF signalling.

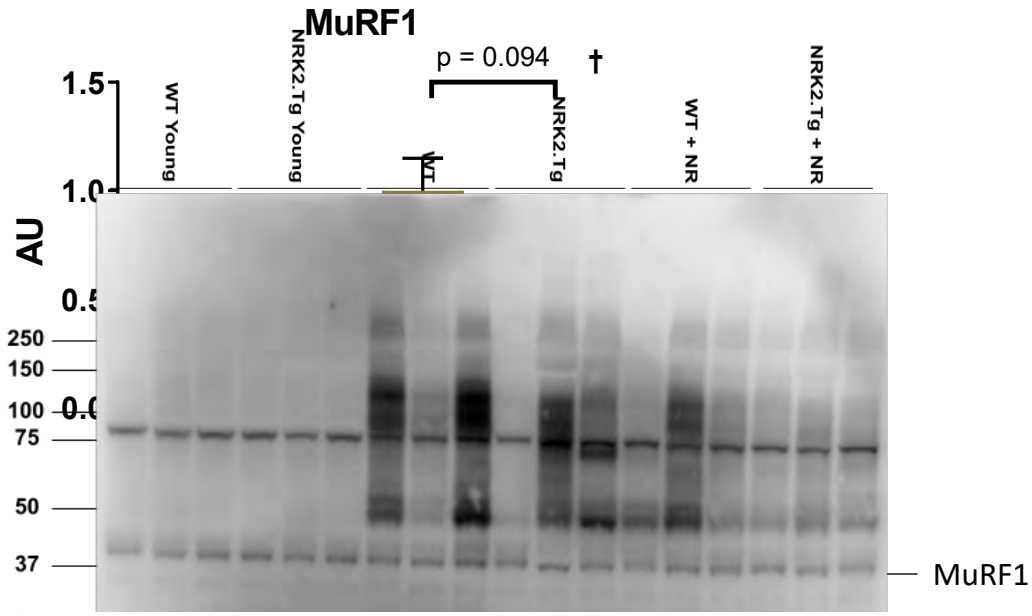

Figure 5-11 – MuRF1 protein levels are elevated in aged WT but not NRK2.Tg skeletal muscle. Densitometric analysis and representative immunoblot of MuRF1 in aged female quadriceps. Data presented as mean ± SEM. Statistical significance was determined by ordinary two way ANOVA with Sidak's multiple comparison tests (* $p < 0.05$, ** $p < 0.01$, *** $p < 0.001$, **** $p < 0.0001$). # = statistically significant interaction between genotype and age; + = statistically significant variation between young and aged mice; † = statistically significant variation between WT and NRK2.Tg mice. n =3.

5.3.6 Aged NRK2.Tg skeletal muscle fibres are larger with a significantly increased, peripherally located proportion possessing centralised nuclei

Given the hypothesised roles of NRK2 in skeletal muscle development and cell adhesion (Figure 5-12), histological analysis was performed on aged WT and aged NRK2.Tg quadriceps to establish any potential structural differences within skeletal muscle with NRK2 overexpression in light of the observed differences in mass. NRK2.Tg quadriceps had a significantly higher number of larger calibre fibres (Figure 5-12A).

Alongside increased skeletal muscle fibre CSA, there was also a significantly increased incidence of centralised nuclei within the fibres (Figure 5-12B, C). Furthermore, NRK2.Tg

skeletal muscle fibres had an increased incidence of several nuclei being present within the same 5 µm tissue section, implying that nuclei were in closer proximity or more numerous than in WT fibres. These observations were unexpected as nuclei within skeletal muscle fibres are typically peripheral, with centralised nuclei only being present within regenerating or previously regenerated adult skeletal muscle (452-454).

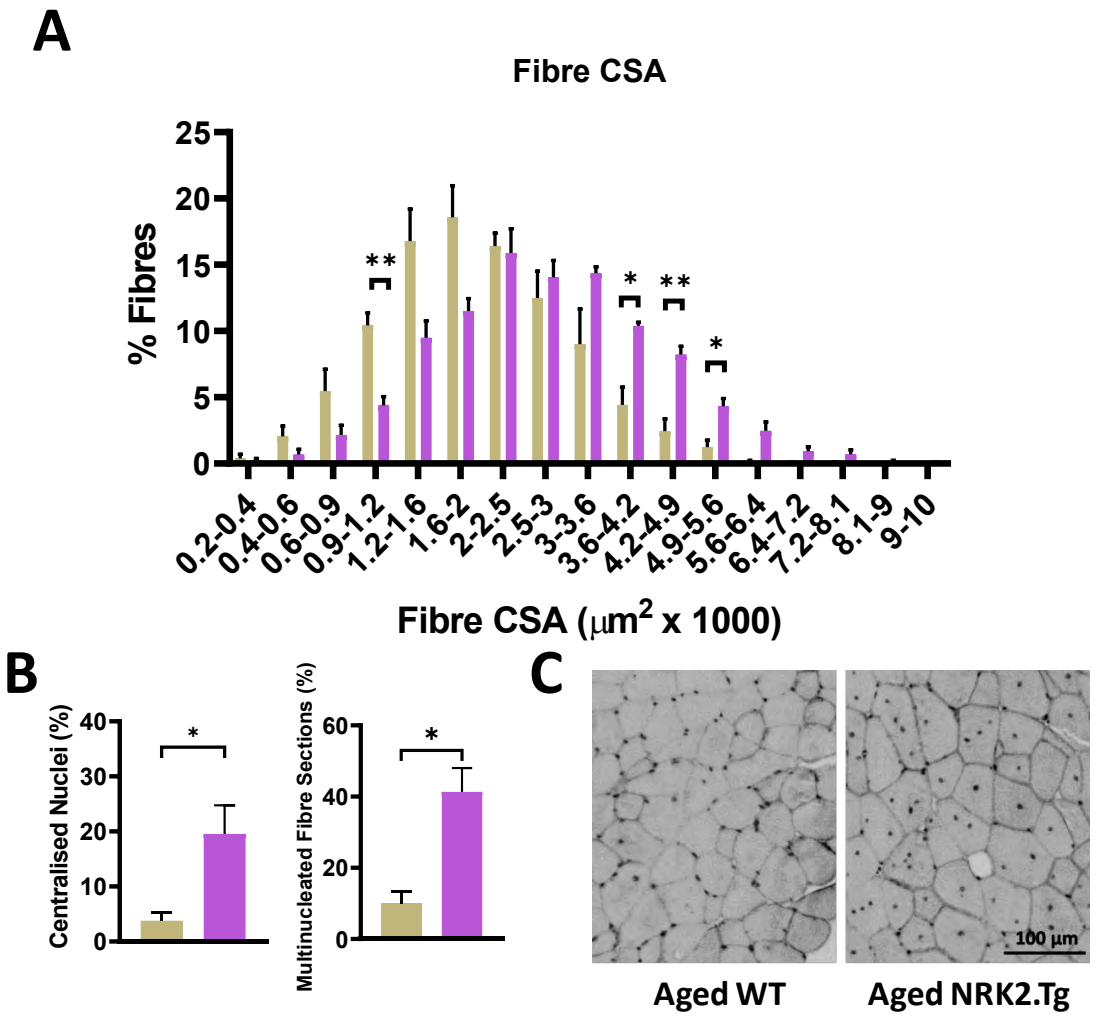

Figure 5-12 – Aged NRK2.Tg skeletal muscle fibres are larger with an increased proportion of fibres exhibiting centralised nuclei. A. Analysis of quadriceps muscle fibre cross-sectional area (CSA) in 24 month old female WT and NRK2.Tg mice. B. Analysis of proportion of fibres with centralised nuclei and multinucleated fibres. Data presented as mean ± SEM with individual data points representing one biological replicate. Statistical significance was determined by student's unpaired t test (* $p < 0.05$, ** $p < 0.01$, *** $p < 0.001$), n = 3. C. Representative image of 5 µm thick FFPE laminin stained quadriceps section of 24 month old WT and NRK2.Tg quadriceps.

A whole NRK2.Tg quadriceps section was imaged and subjective analysis of relative positioning of skeletal muscle fibres with centralised nuclei was performed. Generally, muscle fibres with centralised nuclei were concentrated at the periphery of the muscle bed (Figure 5-13).

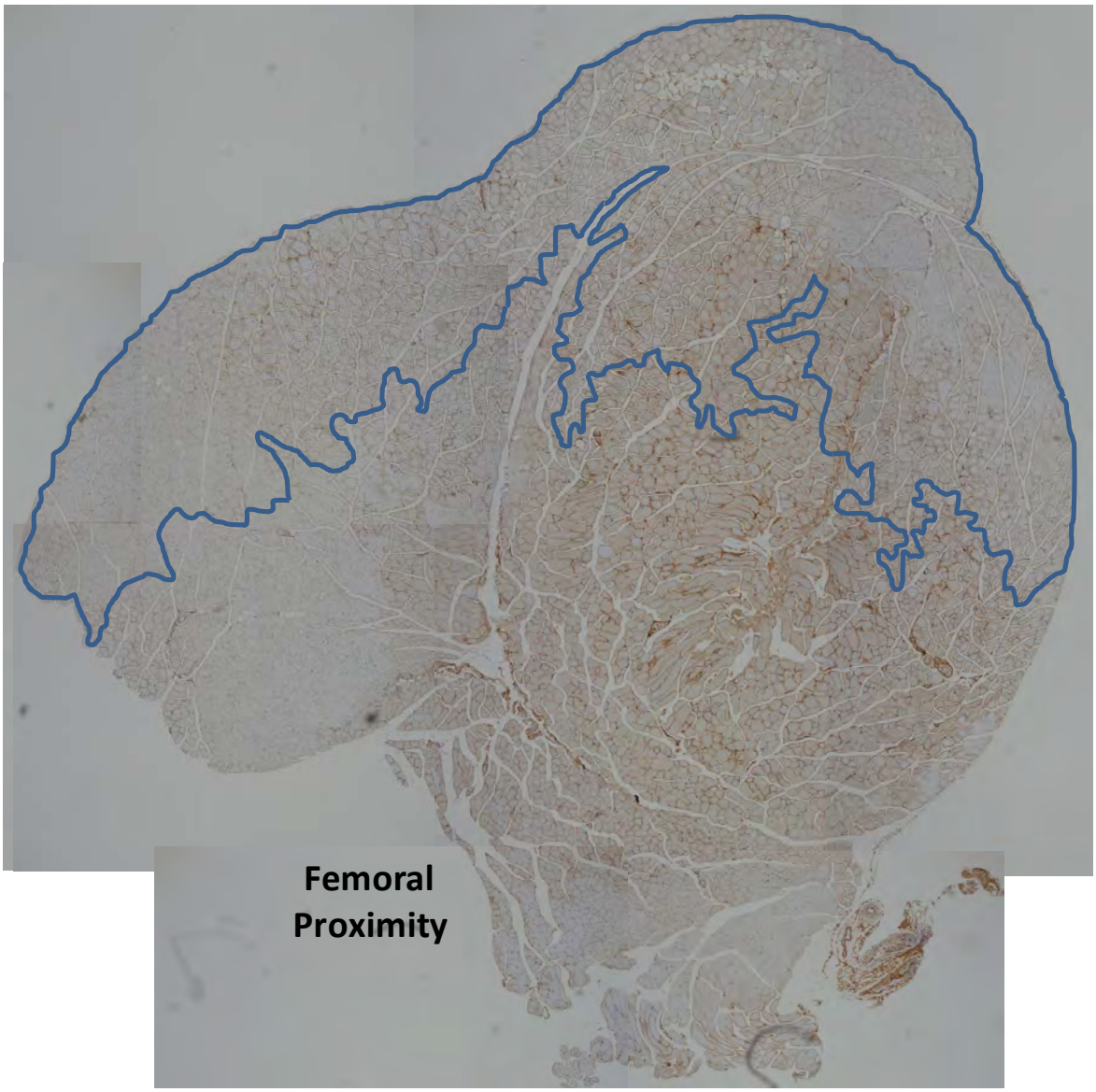

Figure 5-13 – Skeletal muscle fibres featuring centralised nuclei were subjectively determined to be more concentrated around the periphery of the muscle bed (outlined in blue). Mosaic Image of 5 µm thick, FFPE laminin stained 24 month old NRK2.Tg whole quadriceps section**.** n = 1.

5.3.7 Pro-inflammatory pathways and the UPR are not significantly induced in aged NRK2.Tg skeletal muscle relative to aged WT muscle

Centralised nuclei within myofibres can be indicative of skeletal muscle regeneration, and are a hallmark of pathological dystrophic disease states along with a decreased fibre CSA and skeletal muscle atrophy (499, 500). An active immune response is indicative of ongoing skeletal muscle regeneration (438, 439, 501), but chronic inflammation results in skeletal muscle atrophy and a loss of regenerative capacity (501), as is observed in aged skeletal muscle (304). Though aged NRK2.Tg skeletal muscle are hypertrophic and stronger despite increased levels of centralised nuclei, it was necessary to discount any pathological causes for these observations in NRK2.Tg skeletal muscle, such as a hyperactive UPR induced by misfolded transgenic NRK2 or immune cell infiltration and localised inflammation within NRK2.Tg skeletal muscle. No statistically significant upregulation of the putative UPR markers Hspa5, Hsp90 and Ddit3 was detected in aged NRK2.Tg skeletal muscle relative to aged WT muscle (Figure 5-14). The pro-apoptotic factor and UPR marker Ddit3 was significantly upregulated in aged NRK2.Tg skeletal muscle relative to young NRK2.Tg muscle, possibly suggesting some induction of the UPR with age in NRK2.Tg mice. However, this was not significantly higher than aged WT skeletal muscle levels (Figure 5-14), and therefore it could be concluded that the UPR is not significantly upregulated in aged NRK2.Tg muscle relative to aged WT muscle.

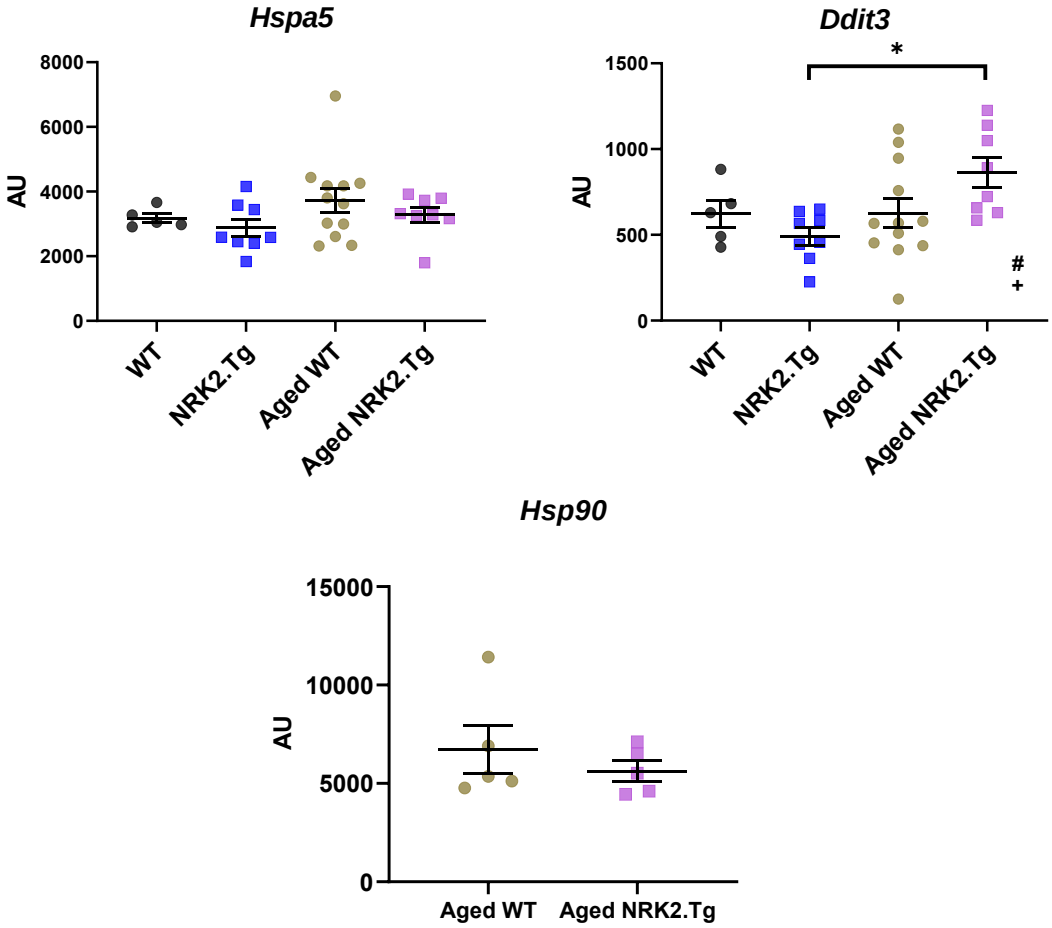

Figure 5-14 – The UPR is not significantly induced in aged NRK2.Tg mice relative to aged WT mice. Quantification of UPR marker mRNA transcript levels in WT and NRK2.Tg quadriceps in 3 month and 20-22 month old female mice. Data presented as mean ± SEM with individual data points representing one biological replicate. Statistical significance was determined by ordinary two way ANOVA with Sidak's multiple comparison tests (* $p<0.05$, ** $p < 0.01$, *** $p < 0.001$, **** $p < 0.0001$). # = statistically significant interaction between genotype and age; + = statistically significant variation between young and aged mice; † = statistically significant variation between WT and NRK2.Tg mice. n = 5-8.

To discount the possibility of inflammation being a contributory cause to the observed NRK2.Tg skeletal muscle phenotype and to determine the presence of ongoing skeletal muscle regeneration, mRNA transcript levels of pro-inflammatory cytokines Il6 and Tnf were quantified in young and aged WT and NRK2.Tg mice (Figure 5-15). Both Il6 and Tnf expression levels were significantly elevated in aged skeletal muscle with Il6 expression

being significantly higher in aged WT skeletal muscle upon direct comparison to young tissue, but no significant differences were observed between WT and NRK2.Tg skeletal muscle both in young and aged quadriceps (Figure 5-15A). No significant changes in mRNA levels of the macrophage marker F4/80 and the marker of NF-κB activity Hif1a were identified between aged WT and NRK2.Tg quadriceps, and immunohistochemical staining for the pan-leukocyte marker CD45 revealed no positive staining in either WT or NRK2.Tg quadriceps (Figure 5-15B). Together, these data imply that inflammation and leukocyte infiltration are not responsible for the observed structural differences and increased muscle mass in aged NRK2.Tg skeletal muscle, and a lack of macrophage markers suggests that ongoing skeletal muscle regeneration is not present.

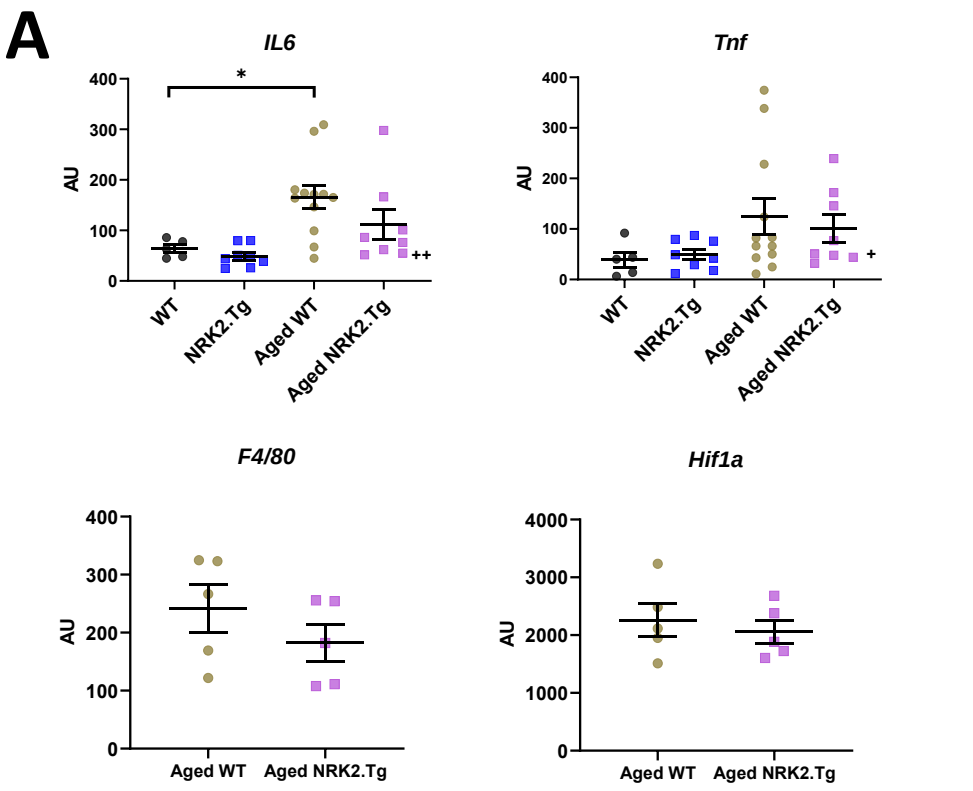

Figure 5-15 – Inflammatory Markers are not significantly upregulated in NRK2.Tg muscle. A. Quantification of immune cell infiltration marker mRNA transcript levels in WT and NRK2.Tg quadriceps in 3 month and 20-22 month old female mice. Data presented as mean ± SEM with individual data points representing one biological replicate. Statistical significance was determined by two way ANOVA with Sidak's multiple comparison tests (* $p < 0.05$, ** $p < 0.01$, *** $p < 0.001$). # = statistically significant interaction between genotype and age; + = statistically significant variation between young and aged mice; † = statistically significant variation between WT and NRK2.Tg mice. n = 5-12. B. Representative images of Immunohistochemical H + E staining along with staining of the leukocyte marker CD45 in steatotic liver positive control tissue, aged WT and NRK2.Tg quadriceps. CD45 positive cells are stained brown.

5.3.8 NRK2 is upregulated upon ITGA7 overexpression, though cytoskeletal and cell adhesion mediating proteins are not differentially regulated in aged NRK2.Tg skeletal muscle at the transcriptional level

NRK2 has previously been linked with skeletal muscle structural and cytoskeletal components and the regulation of muscle fibre/ECM interactions including integrins and paxillin (17, 344, 345). The skeletal muscle critical cell-ECM binding mediator integrin α7β1 subtype was shown to be of particular importance, with NRK2 overexpression disrupting C2C12 cell adhesion to laminin (342). Skeletal muscle regeneration and myonuclear positioning is also dependent on cell-ECM interactions (446, 502), and based on previous observations of centralised nuclei in NRK2.Tg skeletal muscle in section 5.3.6, expression levels of genes governing skeletal muscle cell adhesion were next assessed in the context of NRK2 overexpression.

Utilising publically available gene expression microarray data generated by Mahmassani et al., 2017 in which Itga7 was overexpressed in a mouse model (343), it was determined that Nmrk2 was significantly upregulated in response to Itga7 overexpression in mouse skeletal muscle (Figure 5-16), suggesting that NRK2 and ITGA7 expression levels are possibly co-regulated (Figure 5-16).

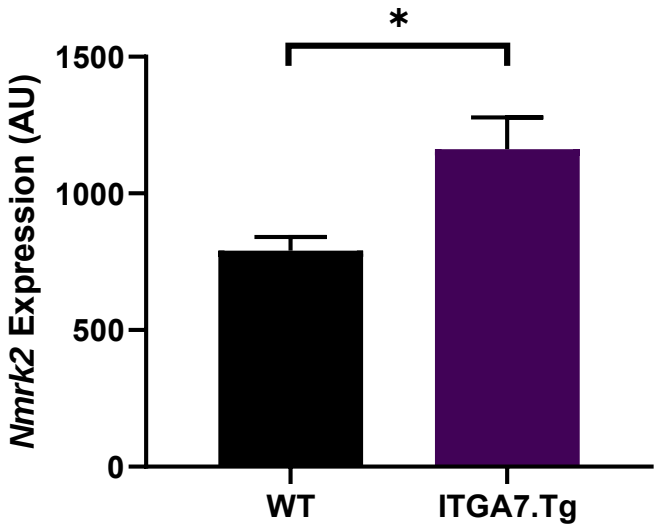

Figure 5-16 – Integrin α7 (ITGA7) overexpression results in significant upregulation of NRK2 in mouse gastrocnemius/soleus complex. Statistical significance was determined by student's unpaired t test (* $p < 0.05$), n=3. Data obtained from Mahmassani et al., 2017 (343).

To explore this interaction further and investigate the wider consequences of NRK2 overexpression for skeletal muscle cell adhesion, relative mRNA expression levels of critical cell adhesion and cytoskeletal components were therefore investigated in aged WT and NRK2.Tg quadriceps (Figure 5-17). Interestingly, subsequent Itga7 upregulation was not observed, together suggesting that NRK2 expression levels may be co-dependent on Itga7 but not vice versa (Figure 5-17). Furthermore, no significant differences were detected in the main collagen isoform (Col1a1), ECM binding integrin alpha subunit 6 (Itga6) or integrin subunit β1 (Itgb1), with paxillin (Pxn) expression levels also unchanged (Figure 5-17). Expression levels of Cytoskeletal actin isoforms 2 and 3 (Act2/3), the membrane scaffolding protein, mechanotransducer and satellite cell differentiation modulator annexin (Anxa1) (503) and the integral membrane protein, endocytic facilitator and satellite cell activator caveolin 1 (Cav1) (504) were downregulated in NRK2.Tg skeletal muscle, but not significantly so (Figure 5-17). Furthermore, expression levels of the cytoskeletal linker protein plectin

(Plec), which is essential to myonuclear architecture and positioning (505) were also unchanged (Figure 5-17). These data indicate that NRK2 overexpression does not affect skeletal muscle structural processes at the transcriptional level.

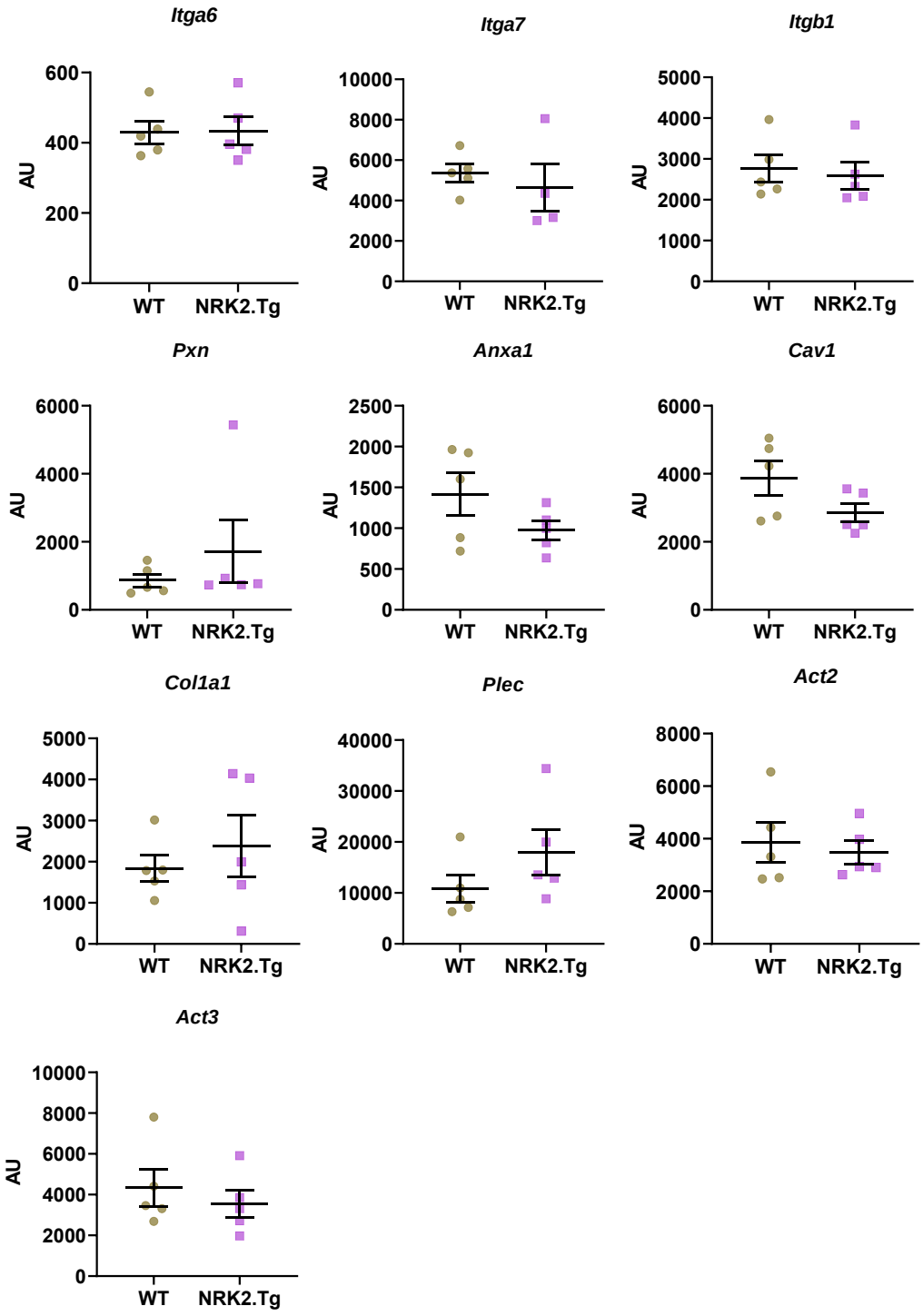

Figure 5-17 – Expression levels of ECM, cytoskeletal and cell adhesion facilitating genes in aged WT and NRK2.Tg mice. Quantification of mRNA transcript levels in WT and NRK2.Tg quadriceps in 3 month and 20-22 month old female mice. Data presented as mean ± SEM with individual data points representing one biological replicate. Statistical significance was determined by student's unpaired t test (* $p < 0.05$, ** $p < 0.01$, *** $p < 0.001$) n = 5.

5.3.9 Aged NRK2.Tg Skeletal Muscle Proteomics

Though NRK2 has been associated with cell adhesion and skeletal muscle development (17), the NRK2 interactome remains largely unclear. Previous experiments have determined aged NRK2 overexpressing skeletal muscle as hypertrophic and structurally distinct, though investigations into skeletal muscle hypertrophic and atrophic pathways and cytoskeletal gene expression levels yielded no clear mechanisms responsible for these observations. Untargeted quantitative proteomics using sequential window acquisition of all theoretical mass spectra (SWATH-MS) was therefore performed on aged WT and NRK2.Tg quadriceps tissue to isolate potential pathways and ontological groups of importance in relation to the observed differences in NRK2.Tg skeletal muscle.

Overall, 1606 proteins were detected of which 378 were differentially regulated in NRK2.Tg quadriceps according to analysis parameters detailed in section 5.2.6.3, including a 1.7 fold upregulation of NRK2 itself (Figure 5-18). Several key observations emerged from this analysis including significant changes in proteostasis, cytoskeletal and ECM protein dynamics, mono-ADP ribosylation, acyl-CoA metabolism and calcium signalling.

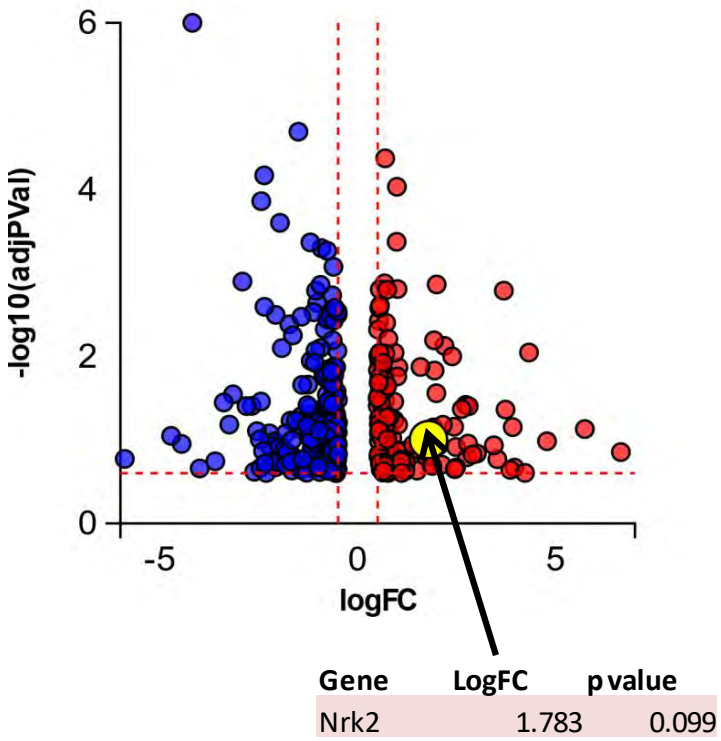

Figure 5-18 – Volcano Plot of differentially regulated proteins in NRK2.Tg quadriceps relative to WT, plotting adjusted p value (y axis) against log fold change (x axis). 1606 proteins were positively identified with 378 marked as dysregulated. Blue dots indicate downregulated proteins while red dots indicate upregulated proteins. The yellow dot represents NRK2.

5.3.10 Gene Ontology

Gene Ontology (GO) is a method of unbiased analysis for large protein expression datasets by which significantly dysregulated proteins are grouped into known biological processes, cellular components and molecular functions relative to control tissue, in this case allowing for insight into the cellular processes which are significantly affected by skeletal muscle NRK2 overexpression. In total, 104 GO terms were significantly enriched in NRK2.Tg quadriceps vs. WT quadriceps prior to correction for multiple comparisons via the elim pruning method (489).

5.3.10.1 Enriched biological processes

Interestingly, several GO terms within the top 20 most dysregulated biological processes involved cell-cell adhesion, adherens junction organisation and actin cytoskeletal organisation in NRK2.Tg skeletal muscle, further supporting the proposed regulatory role of NRK2 in cell adhesion (Table 5-4). "Negative regulation of mitochondrion regulation" was also significantly enriched, suggesting mitochondrial dysregulation (Table 5-4).

Table 5-4 – The top 20 most significantly dysregulated GO terms in the context of molecular functions. Red indicates involvement in energy metabolism, green indicates involvement in cell adhesion, ECM binding and cytoskeletal/contractile processes, and orange indicates involvement in skeletal muscle hypertrophy, atrophy and/or differentiation processes.

Top 20 dysregulated biological processes		
Rank	GO Term	Elim p value
1	organic anion transport	0.0073
2	cellular iron ion homeostasis	0.0094
3	neural tube closure	0.0123
4	cellular copper ion homeostasis	0.0152
5	negative regulation of embryonic development	0.0152
6	positive regulation of neural precursor cell proliferation	0.0152
7	organophosphate ester transport	0.0187
8	negative regulation of inflammatory response	0.0229
9	cell-cell adhesion via plasma-membrane adhesion molecules	0.0229
10	inorganic cation import across plasma membrane	0.0262
11	negative regulation of mitochondrion organization	0.0362
12	protein localization to endosome	0.0364
13	positive regulation of dendritic spine morphogenesis	0.0364
14	positive regulation of substrate adhesion-dependent cell spreading	0.0364
15	regulation of protein localization to plasma membrane	0.0382
16	digestive system process	0.0471
17	regulation of Rho protein signal transduction	0.0471
18	regulation of adherens junction organization	0.0471
19	regulation of actin cytoskeleton organization	0.0492
20	maturation of SSU-rRNA from tricistronic rRNA transcript (SSU-rRNA, 5.8S rRNA, LSU-rRNA)	0.0496

Additional analysis of significantly dysregulated biological processes outside of the top 20 revealed further enrichment of many GO terms concerning cell adhesion,

actin/myosin and sarcomere dynamics, adherens junction formation, focal adhesion assembly and vesicle trafficking, indicating widespread dysregulation of cytoskeletal dynamics and cell adhesion processes in NRK2.Tg skeletal muscle (Table 5-5). Crucially, "Positive regulation of myoblast fusion" and "positive regulation of substrate adhesion dependent cell spreading" were also enriched upon NRK2 overexpression, directly opposing the phenotype observed in MIBP overexpressing myocytes which demonstrate impaired fusion, differentiation and laminin binding/deposition (341, 342). Interestingly, " positive regulation of Ras protein signal transduction" and "positive regulation of insulin receptor signalling pathway" were also significantly enriched alongside "muscle hypertrophy" and striated muscle hypertrophy", reflecting the observed increase in NRK2.Tg skeletal muscle mass (Table 5-5). Several GO terms concerning mitochondrial dynamics were also enriched involving mitochondrial fusion, membrane permeability and intracellular distribution suggesting that NRK2 could be important for regulating the mitochondrial network within skeletal muscle (Table 5-5). Enrichment of "triglyceride homeostasis" and "regulation of lipid biosynthetic process" may also indicate dysregulated lipid dynamics in NRK2.Tg muscle, while enrichment of glucocorticoid and steroid biosynthetic processes could potentially suggest a role of NRK2 in endogenous corticosteroid processing (Table 5-5).

Table 5-5 – Selected significantly dysregulated GO terms in the context of molecular functions. Red indicates involvement in energy metabolism, green indicates involvement in cell adhesion, ECM binding and cytoskeletal/contractile processes, and orange indicates involvement in skeletal muscle hypertrophy, atrophy and/or differentiation processes.

Selected dysregulated biological processes (p < 0.1)		
Rank	**GO Term**	**Elim p value**
26	glucocorticoid metabolic process	0.0496
27	regulation of mitochondrial fusion	0.0496
29	negative regulation of mitochondrial membrane permeability	0.0496
30	positive regulation of Ras protein signal transduction	0.0496
31	positive regulation of insulin receptor signaling pathway	0.0496
32	intracellular distribution of mitochondria	0.0496
33	triglyceride homeostasis	0.0496
34	positive regulation of myoblast fusion	0.0496
35	negative regulation of cell adhesion	0.051
38	negative regulation of cell-cell adhesion	0.0521
39	negative regulation of actin filament depolymerization	0.0521
43	steroid biosynthetic process	0.0538
44	transmembrane receptor protein serine/threonine kinase signaling pathway	0.0538
45	muscle hypertrophy	0.0538
48	striated muscle hypertrophy	0.0538
47	negative regulation of actin filament polymerization	0.0538
48	regulation of actin filament organization	0.056
49	actomyosin structure organization	0.0606
53	positive regulation of adherens junction organization	0.0685
56	regulation of lipid biosynthetic process	0.0704
59	cell-substrate adherens junction assembly	0.0755
60	focal adhesion assembly	0.0755
61	actin filament depolymerization	0.076
62	regulation of actin filament depolymerization	0.076
64	contractile actin filament bundle assembly	0.077
65	regulation of actin filament bundle assembly	0.077
67	stress fiber assembly	0.077
68	vesicle-mediated transport to the plasma membrane	0.077

5.3.10.2 Enriched cellular components

Of the top 20 most significantly enriched GO terms for cellular components, many concerned clathrin mediated vesicle formation and vesicular transport indicating dysregulated membrane/cytoskeletal interactions, membrane vesicle formation and cell adhesion (506) (Table 5-6). Clathrin is also important in skeletal muscle for actin anchoring and sarcomere organisation (507). Furthermore, keratin and myosin filament proteins were dysregulated, which are critical to sarcomeric contractile function (Table 5-6), together

indicating potential dysregulation of sarcomeric integrity in NRK2.Tg skeletal muscle (Table 5-6). Enrichment of "mitochondrial outer membrane" and cAMP-dependent protein kinase complex" terms indicated potentially dysregulated mitochondrial function and substrate selection (Table 5-6). Furthermore, the small ribosomal subunit and eukaryotic translation initiation factor 3 complex (eIF3m) was significantly dysregulated indicating dysregulated protein translation in NRK2.Tg muscle (Table 5-6).

Table 5-6 – The top 20 most significantly dysregulated GO terms in the context of cellular components. Red indicates involvement in energy metabolism, green indicates involvement in cell adhesion, ECM binding and cytoskeletal/contractile processes, and orange indicates involvement in skeletal muscle hypertrophy, atrophy and/or differentiation processes.

Top 20 dysregulated cellular components		
Rank	GO Term	Elim p value
1	mitochondrial outer membrane	0.0041
2	clathrin-coated pit	0.0097
3	ciliary basal body	0.0154
4	Golgi apparatus	0.0171
5	cAMP-dependent protein kinase complex	0.0503
6	clathrin vesicle coat	0.0503
7	clathrin coat of coated pit	0.0503
8	trans-Golgi network transport vesicle	0.0503
9	clathrin-coated vesicle membrane	0.0503
10	keratin filament	0.0503
11	presynaptic endocytic zone	0.0503
12	presynaptic endocytic zone membrane	0.0503
13	coated vesicle membrane	0.0551
14	nuclear body	0.0629
15	plasma membrane protein complex	0.0661
16	clathrin-coated vesicle	0.0696
17	myosin filament	0.0696
18	eukaryotic translation initiation factor 3 complex, eIF3m	0.0696
19	cytosolic small ribosomal subunit	0.0723
20	extrinsic component of cytoplasmic side of plasma membrane	0.0777

5.3.10.3 Enriched molecular functions

Further GO analysis in the context of dysregulated molecular functions highlighted "ankyrin binding", and "fibronectin binding" and "clathrin binding". Ankyrins modulate attachment of

integral membrane proteins to the actin/β-spectrin based membrane cytoskeleton (508), while fibronectin is a key ECM protein which binds integrins mediating cell-ECM adhesion (509). Together these enriched GO terms imply dysregulated actin dynamics and cell adhesion in NRK2.Tg skeletal muscle, providing further support for the importance of NRK2 in these processes. Additional enrichment of GO terms concerning cellular ATP dynamics and protein kinase A (PKA) mediated signalling imply metabolic perturbations, while dysregulated growth factor receptor binding could relate to the observed hypertrophy of aged NRK2.Tg skeletal muscle (Table 5-7). “Calmodulin binding” and “potassium channel activity” were also highly enriched, suggesting perturbed skeletal muscle depolarisation and calcium signalling in NRK2.Tg muscle (Table 5-7).

Table 5-7 – The top 20 most significantly dysregulated GO terms in the context of molecular functions. Red indicates involvement in energy metabolism, green indicates involvement in cell adhesion, ECM binding and cytoskeletal/contractile processes, and orange indicates involvement in skeletal muscle hypertrophy, atrophy and/or differentiation processes.

Top 20 dysregulated molecular functions		
Rank	**GO Term**	**Elim p value**
1	symporter activity	0.0039
2	ankyrin binding	0.0046
3	steroid binding	0.0052
4	calmodulin binding	0.0103
5	potassium channel activity	0.0155
6	growth factor receptor binding	0.0155
7	exodeoxyribonuclease activity	0.0156
8	ATP transmembrane transporter activity	0.0156
9	ADP transmembrane transporter activity	0.0156
10	anion:anion antiporter activity	0.0156
11	protein kinase A regulatory subunit binding	0.0156
12	organic hydroxy compound transmembrane transporter activity	0.0156
13	transition metal ion binding	0.0156
14	clathrin binding	0.0156
15	organic anion transmembrane transporter activity	0.0256
16	ATP binding	0.0271
17	fibronectin binding	0.0475
18	arylesterase activity	0.0506
19	endodeoxyribonuclease activity	0.0507
20	transmembrane signaling receptor activity	0.0507

Further to the top 20 dysregulated molecular function GO terms, “dynein light intermediate chain binding” and “motor activity” were enriched indicating dysregulated intracellular trafficking, possibly relating to dysregulated cytoskeletal mechanics (510) (Table 5-8). “Lipid transporter activity” was also enriched, further indicating dysregulated fatty acid processing in NRK2.Tg skeletal muscle alongside “calmodulin-dependent protein kinase activity” which could suggest dysregulated calcium signalling (Table 5-8).

Table 5-8 – The top 20 most significantly dysregulated GO terms in the context of molecular functions. Red indicates involvement in energy metabolism, green indicates involvement in cell adhesion, ECM binding and cytoskeletal/contractile processes, and orange indicates involvement in skeletal muscle hypertrophy, atrophy and/or differentiation processes.

Selected dysregulated molecular functions (p < 0.1)		
Rank	GO Term	Elim p value
21	dynein light intermediate chain binding	0.0507
22	motor activity	0.054
27	calmodulin-dependent protein kinase activity	0.0704
31	lipid transporter activity	0.0798

Taken together, GO analysis indicates that NRK2 overexpression results in widespread dysregulation of skeletal muscle cytoskeletal dynamics and cell adhesion processes, protein translation, mitochondrial dynamics, fatty acid processing and calcium signalling, which could offer insight into the molecular causes of aberrant skeletal muscle structure, nuclear positioning and hypertrophy observed in aged NRK2.Tg skeletal muscle. The potential molecular mechanisms behind these enriched GO terms were therefore next investigated through interrogation of specific genes which were identified as significantly dysregulated.

5.3.11 NRK2 overexpressing skeletal muscle exhibits dysregulated proteostasis, acyl-CoA synthesis and calcium signalling proteins

Previous experiments suggested that the skeletal muscle mTOR pathway was not differentially activated in NRK2.Tg skeletal muscle while there was a downregulation of the ubiquitin E3 ligase MuRF1, and thus the observed hypertrophy in aged NRK2.Tg skeletal

muscle could be due to downregulated proteolysis pathways rather than increased protein synthesis. Conversely, SWATH-MS indicated that many proteasomal 20S core complex α and β subunit isoforms were upregulated in NRK2.Tg skeletal muscle, including proteasome subunits α2 (PSMA2), α4 (PSMA4), β3 (PSMB3), β4 (PSMB4), β5 (PSMB5) and β7 (PSMB7). The E2 ubiquitin conjugating enzyme ubiquitin conjugating enzyme E2 K (UBE2K) was also upregulated, though proteasome 26S subunits ATPase 1 (PSMC1) and 14 (PSMD14) were significantly downregulated (Figure 5-19), along with significant downregulation of the MyoD ubiquitinating E3 ligase HUWE1 (511).

Proteasomal Subunits/ Ub Enzymes

Gene	LogFC	p value
Psmb5	0.994	0.017
Psma2	0.766	0.248
Psmd1	0.751	0.243
Ube2k	0.688	0.224
Psmb7	0.621	0.078
Psma4	0.575	0.225
Psmb4	0.541	0.027
Psmb3	0.531	0.083
Psmc1	-0.540	0.054
Psmd14	-0.600	0.040
Huwe1	-1.407	0.022

Ribosomal subunits

Gene	LogFC	p value
Rps21	3.730	0.043
Rps16	2.783	0.110
Rps3a1	1.084	0.177
Rplp2	0.675	0.089
Rpl8	-0.518	0.009
Rps8	-0.548	0.052
Rpl6	-0.576	0.089
Rpl23a	-0.584	0.003
Rpl7a	-0.597	0.017
Rps5	-0.604	0.025
Rps26	-0.682	0.117
Rps6ka6	-0.720	0.111
Rps9	-0.761	0.125
Rps25	-0.777	0.195
Rps4x	-0.897	0.100
Mrpl49	-1.702	0.059

Translation Initiation

Gene	LogFC	p value
Eif4g2	-0.530	0.131
Eif3c	-0.618	0.001
Eif3i	-0.785	0.029
Eif3b	-0.826	0.077
Eif3e	-0.879	0.072
Eif3h	-1.860	0.131

Figure 5-19 – Significantly dysregulated proteins in NRK2.Tg quadriceps concerning proteostasis as determined through SWATH-MS. Red indicates an upregulation in log fold change (LogFC) relative to quadriceps while blue represents a downregulation. n=6.

Many proteins involved with ribosomal biogenesis and structure were downregulated, including many small 40s ribosomal subunit (RPS) and large 60s subunit (RPL) protein isoforms, as well as S6 kinase A6 (RPS6KA6) which is downstream of the mTOR skeletal muscle hypertrophy pathway and required for myoblast differentiation (512). A

concurrent upregulation in RPS21, 16, 3a1 and RPLP2 was also observed. Furthermore, several subunits of the eukaryotic translation initiation factor 3 (EIF3) complex were downregulated including EIF3b, EIF3c, EIF3e, EIF3h and EIF3i as well as the EIF4 subunit EIF4G2. Translational elongation is a critical step in protein production, and EIF3 deficiency causes a decline in mitochondrial capacity and skeletal muscle strength (513). Together, this suggests dysregulated protein translation and perturbations to proteostasis within NRK2.Tg skeletal muscle.

5.3.12 NRK2 overexpressing skeletal muscle exhibits dysregulated acyl-CoA synthesis and calcium signalling proteins

NRK2.Tg skeletal muscle also revealed a downregulation in enzymes that mediate the production of acyl-CoA from fatty acids, including acetyl-CoA acyltransferase (ACAA1) 1 and 2 (ACAA2), ATP citrate lyase (ACLY), acyl-CoA dehydrogenase medium chain (ACADM), long chain fatty acid CoA ligase 1 (ACSL1) and acyl-CoA thioesterase 9 (ACOT9), along with an upregulation in Acetyl-CoA carboxylation and dehydrogenation enzymes Acetyl-CoA carboxylase 2 (ACACB) short/branched chain acyl-CoA dehydrogenase (ACADSB) (Figure 5-20). Histidine triad nucleotide binding 2 (HINT2) was the most significantly dysregulated gene with a 4.2 fold downregulation, which has been found to be essential for mitochondrial function and glucose/lipid processing (514). These perturbations suggest a link between fatty acid oxidation and NRK2, although no significant differences were observed in mitochondrial FAO respiratory capacity in young, aged or NR supplemented NRK2.Tg mice, suggesting these observations may not be phenotypically relevant. An upregulation in calcium signalling proteins was also observed, including a 6.6 fold increase in

Calcium/calmodulin dependent protein kinase IIγ (CAMK2G) and a 4 fold upregulation of ryanodine receptor 1 (RYR1), though CAMK2D was significantly downregulated (Figure 5-20).

FA/Acyl-CoA Processing

Gene	LogFC	p value
Acadsb	3.524	0.170
Acacb	2.800	0.039
Hacd1	-0.707	0.226
Acaa1a	-0.607	0.004
Acaa2	-0.626	0.053
Acsl1	-0.809	0.018
Acadm	-1.179	0.049
Acot9	-1.502	0.001
Acly	-2.395	0.137
Hint2	-4.18185	0.001

Calcium Signalling

Gene	LogFC	p value
Camk2g	6.644	0.140
Ryr1	3.853	0.228
Camk2b	0.988	0.223
Camk2d	-0.729	0.014

Figure 5-20 – Significantly dysregulated proteins in NRK2.Tg quadriceps concerning fatty acid and acyl-CoA processing and calcium signalling as determined through SWATH-MS. Red indicates an upregulation in log fold change (LogFC) relative to quadriceps while blue represents a downregulation. n=6.

5.3.13 Aged NRK2.Tg skeletal muscle exhibits dysregulation of cytoskeletal, ECM, cell adhesion and organelle motility proteins

Many cytoskeletal proteins were downregulated in NRK2.Tg skeletal muscle despite few changes observed at mRNA level in section 5.3.8, including the actin associated proteins β-actin Like Protein 2 (ACTBL2), α-Actin Cardiac Muscle 1 (ACTC1), F-Actin-Capping Protein α2 (CAPZA2), and actin cap proteins tropomodulin 1 (TMOD1) and 4 (TMOD4). Myocilin (MYC) and the sarcomeric F-actin binding protein myotilin (MYOT) were also significantly downregulated, both of which are important for actin related sarcomeric organisation (515-517), as well as nebulin-related anchoring protein (NRAP) which anchors terminal actin filaments to the membrane and is enriched at MTJs (518, 519). Profilin1 (PFN1) was also downregulated ~4.5 fold. Profilins are critical actin binding proteins that modulate

cytoskeletal and sarcomeric integrity, though the PFN1 isoform is of more importance in cardiac muscle (520, 521). The critical myogenic differentiation and cytoarchitecture regulator cysteine and glycine-rich protein 3 (CSRP3) was also downregulated (522).

Alongside potentially dysregulated actin dynamics, a 2-3.4 fold downregulation in the fast twitch fibre associated myosin heavy chain isoforms 1 (MYH1) and the slow twitch associated myosin heavy chain isoform 7 (MYH7), as well as the embryonic myosin heavy chain isoform 3 (MYH3) alongside a 2.5 fold upregulation in MYH8, suggesting dysregulated actin/myosin dynamics within type I and type IIB fibres (Figure 5-21). The myosin chaperone UNC45B was also downregulated, which has been implicated as important for myofibrillar formation (523). Additionally, the cell adhesion associated protein cadherin EGF LAG seven-pass G-type receptor 3 (CELSR3) was also downregulated as well as ECM associated collagen subunits COL1A1 and the skeletal muscle specific type IV collagen subunit Collagen Type 6 α2 Chain (COL6A2), despite no previously observed differences in COL1A1 mRNA expression levels. A ~2 fold upregulation of keratin isoforms 1, 75 and 79 (KRT1, KRT75, KRT79) was also observed suggesting structural and compositional changes in intermediate filaments.

Actin/myosin Dynamics

Gene	LogFC	p value
Myh8	2.475	0.121
Cap1	-0.535	0.081
Actbl2	-0.550	0.013
Capza2	-0.637	0.220
Csrp3	-0.824	0.051
Tmod4	-0.865	0.080
Unc45b	-1.172	0.099
Myh4	-2.107	0.104
Actc1	-2.149	0.191
Tmod1	-2.460	0.216
Myh1	-3.154	0.028
Myh7	-3.389	0.036
Pfn1	-4.452	0.112

Intermediate Filaments

Gene	LogFC	p value
Krt75	2.625	0.043
Krt79	2.148	0.066
Krt1	2.121	0.198

Cytoskeletal Dynamics and Organelle Motility

Gene	LogFC	p value
Dynll2	1.983	0.028
Nrap	-0.505	0.033
Myot	-0.538	0.026
Col1a1	-0.792	0.016
Col6a2	-1.495	0.209
Dync1h1	-1.657	0.156
Myoc	-2.078	0.212
Celsr3	-4.719	0.089

Figure 5-21 – Significantly dysregulated proteins in NRK2.Tg quadriceps concerning actin/myosin dynamics, intermediate filaments and cytoskeletal dynamics/organelle motility as determined through SWATH-MS. Red indicates an upregulation in log fold change (LogFC) relative to quadriceps while blue represents a downregulation. n=6.

Interestingly, the dynein protein subunit Dynein Cytoplasmic 1 Heavy Chain 1 (DYNC1H11) was downregulated with Dynein Light Chain LC8-type 2 (DYNLL2) significantly upregulated in NRK2.Tg skeletal muscle. Dynein is a microtubule associated motor protein which is essential for movement and positioning of organelles, including the positioning of nuclei within myofibres (524). It is therefore possible that cytoskeletal defects coupled with dysregulated dynein mediated nuclear locomotion are contributing factors in the aberrant centrally located nuclei observed in NRK2.Tg skeletal muscle fibres. In all, such widespread differences at the protein level could indicate major dysregulation of cytoskeletal integrity and function as well as disruptions to cell adhesion and ECM remodelling.

5.3.14 Aged NRK2.Tg skeletal muscle has dysregulated cell-ECM adhesion proteins including NAD$^+$ dependent ARTs

Differential expressions of proteins which mediate the formation of ECM and cell-ECM interactions were also identified in NRK2.Tg skeletal muscle. The basement membrane component laminin α4 chain (LAMA4), a component of laminin 8, 9 and 14 (525) was identified as significantly upregulated alongside a downregulation in fibromodulin (FMOD) which is required for ECM assembly and can modulate myostatin signalling during myoblast differentiation (526) (Figure 5-22). The critical skeletal muscle fibre sarcolemmal/plasma membrane stabilising, cell-ECM adhesion anchoring and signalling protein dystrophin (DMD) was also significantly downregulated (527). Furthermore, an upregulation in Cavin4 was identified. Cavin4 is a muscle specific protein that is thought to promote formation of caveolae at the plasma membrane (528). Caveolae are thought to be important for cell adhesion signalling (528), and Cavin4 has also been implicated as important for sarcolemmal stability and myogenesis in zebrafish (529).

Cell adhesion/ECM Proteins

Gene	LogFC	p value
Lama4	1.820	0.154
Cavin4	0.690	0.001
Fmod	-0.512	0.110
Dmd	-0.650	0.002

Mono-ADP ribosyltransferases

Gene	LogFC	p value
Arl3	0.733	0.095
Art1	0.655	0.123
Art3	0.639	0.012
Arl6ip5	0.565	0.069
Arf1	-0.543	0.228
Arf5	-1.733	0.004

Figure 5-22 – Significantly dysregulated proteins in NRK2.Tg quadriceps concerning cell-ECM adhesion as determined through SWATH-MS. Red indicates an upregulation in log fold change (LogFC) relative to quadriceps while blue represents a downregulation. n=6.

Alongside these changes, ADP-ribosyltransferase 1 (ART1) and 3 (ART3) were upregulated in NRK2.Tg skeletal muscle alongside ADP-Ribosylation Factor-Like 6 Interacting Protein 5 (ARL6IP5 and ADP-Ribosylation Factor-Like 3 (ARL3) as well as subsequent downregulation of ADP-ribosylation factor 1 (ARF1) and 5 (ARF5). ARFs are small, membrane localised G proteins that regulate cell membrane structure and vesicle formation and also influence phospholipid dynamics, with ARF6 being critical for myoblast fusion (530). A proposed role of NRK2 in cell adhesion and skeletal muscle/ECM binding involves the generation of a membrane localised NAD^+ pool, allowing NAD^+ dependent ARTs to catalyse the mono-ADP ribosylation of integrins which facilitates integrin/laminin binding (17, 344, 345), with the membrane tethered extracellular ART1 isoform being required for mono-ADP ribosylation of integrin α7 (273, 274, 276, 277).These observations may therefore indicate an NAD^+ salvage specific consequence of NRK2 overexpression associated with cell adhesion dynamics, further implying an intrinsic link between NRK2 and ARTs in skeletal muscle.

Taken together, these observations suggest that NRK2 overexpression results in widespread changes to the skeletal muscle proteome, particularly concerning proteostasis, cytoskeletal/sarcomeric regulation and cell adhesion/ECM binding. Though this data cannot determine whether such changes are as a direct or indirect result of NRK2 overexpression, it can serve to highlight potential areas which are worthy of further scrutiny to further clarify the causes of skeletal muscle hypertrophy and altered histological structure within aged NRK2.Tg skeletal muscle.

5.4 Discussion

This chapter determined that NRK2 overexpression increases muscle mass and physical strength, particularly within aged skeletal muscle. Significant mRNA upregulation of the skeletal muscle hypertrophy inducing growth factor Igf2 was identified in NRK2.Tg skeletal muscle, implying upregulated hypertrophy signalling as a potential cause alongside significant downregulation of skeletal muscle atrophy as indicated by significantly lower mRNA levels of the ubiquitin E3 ligase Trim63. Key markers of mTOR pathway activation were comparable between both young and aged WT and NRK2.Tg muscle, though levels of the Trim63 protein product MuRF1 were strongly trending downwards in aged NRK2.Tg skeletal muscle relative to aged WT muscle, reflecting Trim63 mRNA levels. Further histological analysis revealed an increase in skeletal muscle fibre CSA alongside evidence of fibre regeneration in the form of centralised nuclei concentrated around the muscle bed periphery, and activation of the UPR and chronic inflammation were discounted as potentially confounding pathological causes. NRK2 has been implicated as a critical mediator of skeletal muscle development, differentiation and cell-ECM adhesion (341, 342, 344, 345), but NRK2 overexpression did not affect mRNA levels of critical skeletal muscle cell adhesion genes. However, subsequent analysis of the NRK2.Tg proteome indicated widespread dysregulation of these processes in NRK2.Tg skeletal muscle alongside potential perturbations to skeletal muscle proteostasis, fatty acid processing and calcium signalling.

IGF2 is a critical activator of skeletal muscle growth pathways during embryonic myogenesis (531), and is also induced during regeneration and differentiation of adult skeletal muscle (423). Autocrine and paracrine activity through insulin receptor binding of

IGF2 is necessary for satellite cell differentiation, resulting in expression of MRF genes such as Myog (532). IGF2 mediated signalling subsequently induces skeletal muscle differentiation though PI3K/AKT (533) with the induction of the Igf2 gene itself governed by mTOR signalling and amino acid availability (423), which may possibly relate to the dysregulated proteostasis implied by proteomics analysis within NRK2.Tg skeletal muscle. Interestingly, an association between NRK2 and IGF2 has been identified through a high throughput protein interaction screen (534). Furthermore, overexpression of the catalytically inactive NRK2 isoform MIBP impairs myoblast differentiation (341) indicating a role for NRK2 in this process, for which IGF2 is also a critical mediator (532). Though the specific dynamics of this interaction are unknown, this study provides further evidence for the importance of NRK2 and IGF2 in skeletal muscle and also implies that Nmrk2 and Igf2 could be co-regulated.

Upregulation of IGF2 could therefore be considered as a molecular mechanism responsible for the increased muscle mass and evidence of myofibre regeneration upon overexpression of NRK2 in aged muscle, with IGF signalling being capable of driving skeletal muscle hypertrophy, regeneration and differentiation (532, 535-537). However, though Igf2 mRNA was significantly upregulated, levels of phosphorylated AKT, p70S6K and rpS6 were not increased implying no significant upregulation of mTOR and PI3K/AKT signalling. Alongside the insulin receptor, IGF2 also has a high affinity for the IGF2 receptor (IGF2R), which serves to sequester and degrade IGF2 attenuating IGF2/IR driven hypertrophic signalling (538). IGF2R is upregulated in Duchenne muscular dystrophy (DMD) and mdx mice, contributing to the atrophic phenotype (539). The pathology of DMD is driven by mutated dystrophin, which disrupts cytoskeletal and ECM interactions (527, 540). Dystrophic muscle is also characterised by increased centralised nuclei due to constant regeneration (527, 540),

drawing parallels with the observed NRK2.Tg histological phenotype, though paradoxically NRK2.Tg skeletal muscle fibres were larger and conferred greater grip strength in aged NRK2.Tg mice. Given the evidence that constitutive NRK2 overexpression causes dysregulated skeletal muscle cell-ECM adhesion, IGF2R may also be upregulated and thus partially attenuating IGF driven hypertrophic pathways, which further experiments must determine.

It is also possible that the misplaced nuclei in NRK2.Tg skeletal muscle are due to impaired cytoskeletal dynamics, with untargeted proteomics identifying potentially widespread dysregulation of cytoskeletal integrity and organelle trafficking motor proteins such as dynein. After myoblast fusion, myofibrillar nuclei are centralised by dynein transport along microtubules and spread out along the length of the myotube by the kinesin-1 motor protein before migrating and anchoring to the periphery by desmin and nesprin (453). Significantly increased incidences of multiple nuclei within the same 5 μm section could indicate a failure at the nuclear spreading phase in regenerated NRK2.Tg myofibres, though no significant dysregulation of the microtubule network, kinesins, nesprin or desmin were identified. Peripheral nuclear positioning is thought to influence skeletal muscle function through regulation of myonuclear domains, and different subsets of myonuclei exist which preferentially localise to cell-cell junctions including NMJs and MTJs (541). Though the functional relevance of these precisely positioned nuclei remains unclear, it is remarkable that aged NRK2.Tg mice appear stronger despite possessing a significantly elevated proportion of fibres with aberrantly positioned myonuclei, coupled with potential disruptions to cytoskeletal and sarcolemmal organisation.

Another possibility is that the cytoskeletal and sarcolemmal perturbations were secondary features of impaired cell-ECM adhesion, as significant dysregulation of ART and ARF enzymes in NRK2.Tg skeletal muscle was also detected. Importantly, the critical ectoART ART1 was significantly dysregulated, which is required for NAD^+ dependent mono-ADP ribosylation of integrin α7 facilitating skeletal muscle/laminin binding (274-277). Furthermore, dysregulation of the laminin 8, 9 and 14 component laminin α4 and the ECM assembly facilitator fibromodulin implied perturbed laminin organisation (525) alongside significant dysregulation of the cytoskeletal/ECM binding mediators dystrophin and cavin4. In support of these observations, a recently published study found that NRK2KO mice developed dilated cardiomyopathy with age and were vulnerable to injury through pressure overload (374). Disordered laminin deposition between cardiomyocytes and a loss of integrin α7 expression with age was found to be a driving mechanism alongside depleted cardiomyocyte NAD^+ levels (374), drawing remarkable parallels with the effects of catalytically inactive MIBP overexpression in skeletal muscle which likely arose due to competitive inhibition of NRK2/integrin α7β1 binding and subsequent local NAD^+ depletion (341, 342). Together, these observations corroborate previously hypothesised models in which NRK2 is required for the dynamic generation of a membrane proximal NAD^+ pool which maintains laminin organisation and muscle/ECM binding in response to muscle growth and regeneration (17, 344, 345), further implicating NRK2 as an important regulator of cell/ECM adhesion.

NAD^+ dynamics are clearly important during skeletal muscle development, with a detectable decrease in NAD^+ in fully differentiated myotubes relative to myoblasts (542) which closely follows the pattern of NRK2 expression during myogenesis (15, 341). However,

changes to the NAD^+ metabolome induced through NRK2 may be subtle and highly compartmentalised, and may therefore be undetectable using whole cell quantification methods. Further experiments could spatially visualise membrane proximal NAD^+ pools using sarcolemma and/or ECM targeted NAD^+ biosensors (201, 209, 210) with concurrent visualisation of spatial and temporal NRK2 expression levels throughout skeletal muscle remodelling. Furthermore, relative ADP-ribosylation status of the critical integrin receptor subunits α6 and α7 could also be assessed in NRK2.Tg skeletal muscle, offering valuable insight into the relationship between NRK2, NAD^+ and skeletal muscle cell adhesion.

Despite few differences in mTOR and AKT activation levels, aged NRK2.Tg skeletal muscle beds were significantly larger and aged NRK2.Tg mice were stronger implying that NRK2.Tg skeletal muscle at least partially resists age related sarcopenia. The observed downregulation in both Trim63 mRNA and MuRF1 protein levels in aged NRK2.Tg muscle could therefore constitute an alternative mechanism of hypertrophy. MuRF1 levels in aged WT mice were elevated relative to young WT mice while aged NRK2.Tg remained comparable to young mice, implying that downregulated atrophic pathways could be responsible for the observed resistance of NRK2.Tg mice to sarcopenia. However, age related skeletal muscle loss is mainly thought to be driven by resistance to anabolic signals rather than upregulated atrophy pathways (297). Furthermore, previous studies have determined that Atrogin1 and MuRF1 are counterintuitively downregulated in ageing skeletal muscle, implying that the molecular mechanisms of sarcopenia are distinct from drivers of acute atrophy (543). This suggests that decreased MuRF1 expression is unlikely to be behind the observed sarcopenic resistance of NRK2.Tg skeletal muscle. However, skeletal muscle hypertrophy has also been associated with increased proteasomal activity driven by

FOXO1 and FOXO3a independently of Atrogin1 and MuRF1 (544), indicating that hypertrophy involves an increase in both protein synthesis and degradation. Indeed, untargeted proteomics determined that proteasomal dynamics were significantly dysregulated in aged NRK2.Tg skeletal muscle alongside ribosomal dynamics and protein elongation, thus constituting an area in which further targeted analysis is required to fully elucidate the molecular mechanisms behind increased muscle mass in aged NRK2.Tg muscle.

Increased skeletal muscle mass with age was not consistent across all muscle beds assessed within NRK2.Tg mice. Significant hypertrophy was not present in the predominantly glycolytic TA muscle bed in either young or aged NRK2.Tg mice of both sexes, while conversely the predominantly oxidative soleus muscle was significantly larger in young NRK2.Tg mice despite no other muscle beds being relative enlarged at a young age. Comparatively, mixed fibre type quadriceps and gastrocnemius muscles were only significantly larger with advancing age. Disparate endogenous NRK2 expression levels between TA and soleus allude to the varying importance of this pathway depending on skeletal muscle type (15), and these observations could imply that the hypertrophic effects of NRK2 overexpression may be specific to type I muscle fibres. It is possible that any augmentation of the NAD^+ metabolome by NRK2 overexpression could augment type I fibres more than type II fibres due to their increased reliance on NAD^+ for oxidative metabolism. Elevated NRK2.Tg skeletal muscle NAD^+ levels were only observed in young male animals during night hours, but NRK2 overexpression could influence NAD^+ flux rates which cannot be detected by absolute quantification methods, thereby requiring more detailed analysis utilising isotopically labelled precursors.

Though NRK2.Tg muscle fibres appeared regenerative, mTOR/AKT signalling pathways were not significantly upregulated in NRK2.Tg skeletal muscle and the pro-regenerative MRF genes Myf5, MyoD, Mrf4 and Myog (439, 545) were not elevated relative to WT levels despite an increase in Igf2 mRNA, the expression of which is closely linked to MRF expression (537, 546, 547). Furthermore, no evidence of an active immune response was detected including an absence of infiltrating leukocytes and comparable levels of pro-inflammatory cytokines and macrophage markers between WT and NRK2.Tg muscle (439). It is therefore possible that the increased incidence of fibres containing centralised nuclei is indicative of historic regeneration, though further quantification of quiescent and activated satellite cell markers within aged NRK2.Tg skeletal muscle is required to confirm this, such as through immunostaining for satellite cell activation status in whole muscle sections or gene expression levels in isolated satellite cell populations. The predominantly peripheral location of centrally nucleated fibres is also indicative of past regeneration, as centralised nuclei return to the periphery more quickly in regenerated skeletal muscle fibres with greater innervation and blood supply (454), and capillary density is higher in the deep sections of rodent muscle relative to superficial white regions of larger mixed fibre type muscles such as the quadriceps and gastrocnemius (548, 549).

Future experiments must therefore determine the point at which this regeneration occurs in the lifecycle of the animal across different skeletal muscle beds. The zebrafish NRK2 ortholog Nrk2b is critical for embryonic myomere development resulting in improper laminin polymerisation and disrupted cell-ECM binding at MTJs when knocked out (344), but skeletal muscle NRK2 expression levels may be comparable to WT during embryogenesis in this model given low Acta1 expression levels in embryonic muscle stem cells (373) and initial

ACTA1-Cre mouse embryo validation experiments only detecting strong cre expression in somites with differentiated embryonic muscle (352). It is however clear from the untargeted proteomics analysis that NRK2 overexpression results in widespread dysregulation of cell adhesion and cytoskeletal integrity in adult skeletal muscle.

Endogenous NRK2 is strongly expressed prior to myoblast fusion, falling dramatically upon differentiation to myotubes (15, 341). This temporal modulation of NRK2 expression appears critical, with constitutive overexpression of the catalytically inactive NRK2 splice variant MIBP impairing myoblast differentiation, cell adhesion and laminin deposition in C2C12s (341, 342), likely through competitive inhibition of NRK2 binding to integrin α7β1. Interestingly, no perturbations to mRNA levels of the myogenic differentiation signalling protein paxillin were observed in NRK2.Tg muscle despite MIBP/NRK2 levels having been reported to directly influence paxillin protein levels and phosphorylation status, constituting a potential mechanism by which NRK2 affects myogenic differentiation (342, 344, 345). It is possible that this effect was present but not reflected at the transcriptional level, and future experiments should seek to quantify paxillin protein levels and phosphorylation status in NRK2.Tg muscle.

The presented data indicate that constitutive skeletal muscle NRK2 overexpression causes dysregulation of myoblast differentiation in vivo, which is of particular importance during periods of intense skeletal muscle remodelling and growth such as during adolescence (550, 551). Given the inhibitory effect of MIBP overexpression on myoblast fusion and differentiation (341, 342), it is possible that constitutive overexpression of NRK2 dysregulates these processes through specific augmentation of membrane proximal NAD^+ pools during phases where endogenous NRK2 is downregulated (15), enabling increased

levels of integrin α7β1 ADP-ribosylation through elevated ART activity. Significant enrichment of protein pathways mediating positive regulation of myoblast fusion and substrate adhesion in NRK2.Tg muscle alongside widespread dysregulation of cell adhesion processes supports this assertion, though it should be noted that markers of active skeletal muscle regeneration were not significantly upregulated. This suggests that a transient, hyper-regenerative phenotype may be induced during incidences of upregulated skeletal muscle hypertrophy (537). This augmented hypertrophy could persist with age, particularly as regenerating and undamaged fibres within injured muscle are protected against apoptosis (552) and further damage by genes such as Zeb1 (553). Similarly, NAD^+ dependent cell-ECM interactions are critical to skeletal muscle regeneration and repair (275, 439) with NRK2 upregulation identified post skeletal muscle injury (326). Experiments assessing the in vivo response of NRK2 overexpressing skeletal muscle to injury would therefore provide further insight as to this assertion and the role of NRK2 in skeletal muscle regeneration as a whole, establishing whether the observed regenerative phenotype corresponds with increased regenerative capacity upon acute injury.

Alternatively, it is possible that low levels of regeneration and myofibre turnover remain active within aged NRK2.Tg skeletal muscle, where upregulation of MRFs may be subtle and restricted to satellite cells and therefore undetectable in mRNA derived from whole muscle lysate. Interestingly, the observed NRK2.Tg myofibre phenotype bears a striking resemblance to a recent study which noted a significant increase in centrally nucleated skeletal muscle myofibres upon conditional knockout of N- and M-Cadherin, crucially without acute injury as was observed in this case (461). Cadherins are adhesion proteins which mediate interactions between stem cells and niche cells at adhesive junctions

(AJs) between satellite cells and myofibres (461), with known roles in myogenesis (554, 555) and regulation of satellite cell activation, commitment and differentiation (556, 557). N and M cadherin was determined to be inessential for skeletal muscle development but critical to the maintenance of satellite cell quiescence in adult muscle (461). Conditional removal of N- and both N- and M-Cadherin resulted in a non-pathological, pseudo-regenerative response due to expansion of a partially activated population of $Pax7^{+}/MyoD^{+}/Myf5^{-}$ satellite cells, resulting in hyperactivation of muscle fibre regeneration without stimulus from acute injury (461). Further analysis identified disruption to AJs through aberrant localisation of β-catenin at the cell periphery and nucleus rather than the apical membrane, which was identified as a driver for self renewal of the partially activated satellite cell population due to upregulation of axin2, a positive regulator of β-catenin signalling (461). M- and N-Cadherin KO myoblasts failed to fuse in vitro drawing further parallels with the proposed function of NRK2 as evidenced by fusion inhibition upon overexpression of catalytically inactive MIBP (341, 342).

Though MyoD mRNA expression levels were not significantly elevated in NRK2.Tg skeletal muscle and no differences in cadherin, β-axin2 expression were detected with untargeted proteomics from whole muscle lysate, the observed disruptions to cell adhesion and cytoskeletal organisation processes could have an indirect effect on the stability of the satellite cell niche in NRK2.Tg skeletal muscle through perturbations to the basal lamina and/or apical membrane. It is important to note that the expression levels of endogenous NRK2 are linked to levels of integrin α7β1, which mediates important physical interactions between the satellite cell actin cytoskeleton and laminin within the basal lamina (343, 462). NRK2 may therefore indirectly regulate the transduction of physical signals promoting satellite cell activation, with overexpression resulting in satellite cell hyperactivation and the

observed regenerative phenotype. In this context, upregulation of IGF2 may therefore constitute a secondary autocrine/paracrine driver of satellite cell differentiation as a result of aberrant satellite cell activation due to niche instability (423, 532, 536, 547, 558), ultimately resulting in continuous regeneration and hypertrophy of skeletal muscle which directly opposes age related sarcopenia. Notably, adult soleus muscle has a two- to fourfold higher proportion of satellite cells than TA and EDL muscle which also exhibit greater regeneration capacity (60), with more satellite cells localised to type I fibres relative to type II (43, 559). The fact that the hypertrophic phenotype was more prominent in NRK2.Tg soleus and mixed muscle beds over predominantly fast twitch TA supports this satellite cell driven hypothesis. This concept therefore remains an interesting possibility, necessitating further targeted investigations across all muscle bed types including quantification of niche and AJ morphology, satellite cell numbers, subpopulations and activation status through immunofluorescence staining of specific markers including Pax7, MyoD, MyoG, Mrf5, β-catenin and axin2.

Importantly, ageing increases satellite cell senescence and decreases overall satellite cell numbers, impairing the ability of aged muscle to regenerate (171). Interestingly, repletion of NAD^+ via oral NR supplementation resulted in renewal of regenerative capacity through restored mitochondrial function, significantly increasing the lifespan of mice (171). Stem cells are thought to primarily rely on glycolysis to meet energetic requirements, imposing further demand on cellular NAD^+ levels (560). A significant decline in NAD^+ levels was indeed identified within satellite cell populations from 22-24 month old mouse muscle, with NR supplementation effectively replenishing aged satellite cell NAD^+ levels back to levels found within satellite cells derived from young mice (171, 476, 477). Based on this

evidence, it is also possible that NRK2 overexpression could replicate this effect through increased capacity of NAD^+ repletion via NR in satellite cells, contributing towards the regenerative phenotype.

If dysregulated regeneration is a contributing factor, it is important to consider the nature of regeneration. Satellite cells can differentiate and fuse to pre-existing fibres as well as form entirely new myofibres (50, 61, 461). Newly derived fibres are characterised by long strings of central nuclei, while fusion of satellite cells to pre-existing fibres results in widely dispersed central nuclei along the longitudinal plane (461). Determination of this would allow for insight into the specific mechanisms of regeneration which are involved, highlighting satellite cell subsets which may be relevant to the phenotype (50, 61). Longitudinal or serial transverse myofibre sectioning and subsequent visualisation of nuclear positioning and the cytoskeleton is therefore required to further investigate these possibilities and define any potential mechanisms.

In all, there is significant evidence to suggest that the NRK2.Tg regenerative phenotype is driven by dysregulation of satellite cell activation. However, the activation state of the NRK2.Tg transgene within satellite cells remains unclear throughout embryonic myogenesis, juvenile and adult muscle development and repair. As ACTA1 is a major component of the sarcolemma (561), strong overexpression of NRK2 may only occur upon fusion and differentiation into striated muscle. Absent Acta1 expression within embryonic muscle progenitor cells suggests that NRK2 overexpression is minimal within embryonic myogenic precursors in this model (373). However, within adult mouse satellite cells, absolute levels of Acta1 mRNA were observed to be low relative to differentiated muscle yet still detectible (562). Furthermore, the actin cytoskeleton plays an important part in

activation of satellite cells in response to physical signals (343, 462) and sarcomeric α-actin has been detected in activated satellite cells within adult skeletal muscle (563) suggesting some degree of Acta1 transcription. NRK2 may therefore be overexpressed sufficiently within satellite cells to drive such a phenotype within this model, particularly if a "pseudo-activated" population of satellite cells is present due to disrupted niche/ECM interaction (461). It is also possible that overexpression of NRK2 in striated muscle causes dysregulation of laminin deposition which would cause inherent niche instability without NRK2 overexpression within satellite cells (342). Direct quantification of spatiotemporal NRK2 expression levels within satellite cells across all stages of quiescence, activation, proliferation, fusion and differentiation with assessment of satellite cell niche integrity is therefore required to further investigate this hypothesis.

In all, the data presented in this chapter describes an unforeseen consequence of skeletal muscle NRK2 overexpression in the form of augmented skeletal muscle mass. This effect was more pronounced in aged mice and accompanied with functional improvements in grip strength, strongly suggesting that NRK2 overexpression confers at least partial resistance to age related skeletal muscle loss. Histological analysis of NRK2.Tg skeletal muscle revealed an increase in average myofibre CSA alongside an elevated proportion of fibres featuring centralised nuclei. Despite significantly increased skeletal muscle Igf2 levels, skeletal muscle hypertrophic pathways driven by mTOR and PI3K/AKT signalling were not definitively activated, while skeletal muscle Murf1 levels were attenuated. Though the specific molecular mechanisms driving this phenotype remain elusive, the specific importance of NRK2 mediated NAD^+ salvage for cell adhesion and therefore skeletal muscle regeneration and differentiation was reinforced. The experimental evidence presented in

this chapter suggests periods of historic muscle fibre regeneration and hypertrophy, which may have occurred as a result of ongoing regeneration due to disrupted cell-ECM adhesion during periods of elevated skeletal muscle growth (537, 550) and/or in response to a loss of function of other muscle groups, which could be more widely affected at this stage than others (564) (Figure 5-23). There is also strong evidence to suggest satellite cell hyperactivation through niche disruption as a potential driver given the similarities of the NRK2.Tg phenotype to such a model (461) and the roles of NRK2 in regulating integrin/laminin interactions and laminin deposition (341, 342, 344, 345, 374) (Figure 5-23)Targeted experiments are required to further define this phenotype, particularly concerning the age of onset and the status of skeletal muscle hypertrophic and atrophic pathways at this time, any potential bias between fibre types, and the specific molecular perturbations which occur as a result of NRK2 overexpression in the context of basal lamina organisation and integrity, muscle/ECM interactions and satellite cell properties.

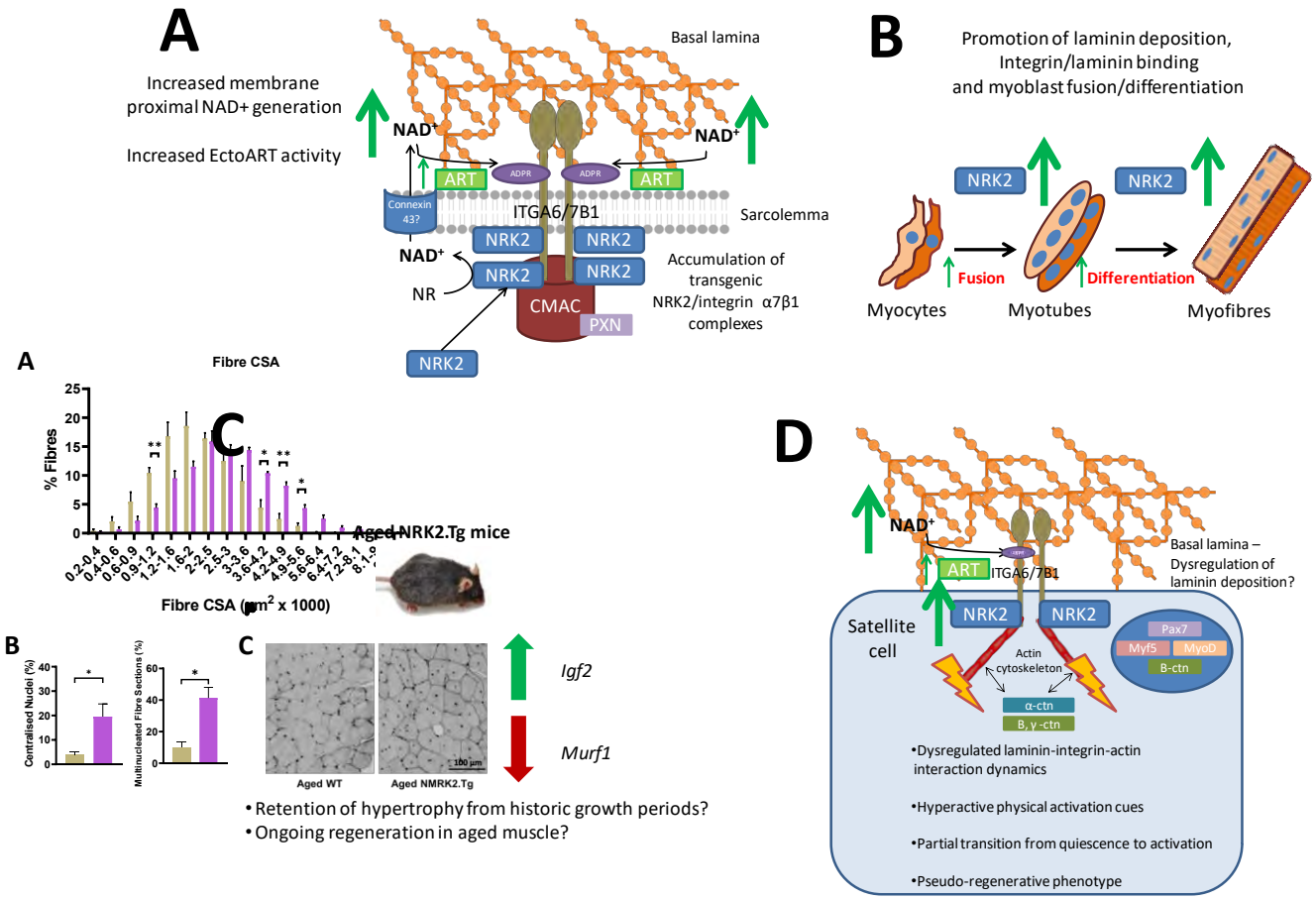

Figure 5-23 – Potential molecular, cellular and phenotypic consequences of constitutive skeletal muscle NRK2 overexpression. NRK2 overexpression promotes cell-ECM adhesion processes (A) which leads to dysregulated myogenesis and remodelling through overpromotion of integrin/laminin binding (B). This could result in hyperactive skeletal muscle regeneration and hypertrophy during periods of muscle remodelling which persists with age or ongoing regeneration in aged muscle without acute injury, which would need to be defined with further experiments (C). If NRK2 overexpression is also present within satellite cells or significant dysregulation of ECM protein organisation is present, dysregulated laminin-integrin-actin cytoskeleton interactions could promote a partially activated subset of satellite cells as described in Goel et al., 2017 (461) which drive the observed regenerative NRK2.Tg phenotype (D). Future work should prioritise investigating these potential mechanisms in developing animals across all ages and across different muscle bed types.

CHAPTER 6 – FINAL DISCUSSION

The importance of NAD^+ in metabolism is now widely appreciated as both a redox cofactor and a consumed substrate for signalling processes governing metabolic homeostasis and adaptation. As the mediator of locomotion and the largest and most metabolically flexible site of energy metabolism in the body, the status of the skeletal muscle NAD^+ metabolome is intrinsically linked to skeletal muscle health (11). Skeletal muscle health is essential for physical strength and whole body metabolic health. This is of particular importance amidst an increasingly sedentary and ageing world population in which sarcopenia is becoming increasingly common, bringing with it a range of clinically demanding comorbidities and significant curtailment of healthspan (1, 4-7, 9, 10).

Recent research strongly suggests an age related decline in skeletal muscle NAD^+ levels to which age related metabolic decline and sarcopenia is at least partly attributable (11, 171, 180, 184, 284, 292, 315, 387), prompting widespread research into endogenous skeletal muscle NAD^+ repletion mechanisms and potential therapeutic strategies concerning NAD supplementation. Skeletal muscle homeostasis is primarily reliant on NAD^+ salvage from NAM via NAMPT (11, 15). However, salvage from the alternative dietary precursor NR (160) via NRK2 constitutes an auxiliary route to NAD^+, which is dispensable for general NAD^+ homeostasis but significantly more efficacious for cellular NAD^+ boosting upon exogenous substrate supplementation (15). Furthermore, exploitation of the NR/NRK pathway is a more viable option with regards to age related NAD^+ decline due to downregulation of NAMPT with age (104, 105), inhibition of SIRTs via NAM (132, 140, 141) and self regulation of NAMPT by NAD^+ (142).

Of late, several highly informative skeletal muscle NRK gain and loss of function studies have been performed (15, 16, 320), identifying the NRKs as rate limiting for the

production of NAD^+ from NR, their necessity for exogenous NMN processing and the functional redundancy between NRK1 and NRK2 in this regard (15, 16). However, the in vivo metabolic and functional consequences of NRK augmentation in skeletal muscle were poorly understood. Skeletal muscle NRK2 upregulation has been observed in conditions of chronic redox stress (325) and has a varied circadian expression pattern, suggesting that it is induced as a compensatory response during periods of high metabolic demand. The primary objective of this thesis was therefore to define the metabolic consequences of chronic lifetime NRK2 overexpression in skeletal muscle, further defining the metabolic niche of the NR/NRK salvage pathway and assessing its relevance as a therapeutic target in combating age related metabolic decline. Furthermore, NRK2 is also upregulated in skeletal muscle injury (326) and has hypothesised roles in skeletal muscle cell adhesion involving the generation of a cell membrane proximal NAD^+ pool required for ADP-ribosylation of integrins to facilitate cell/ECM binding (17, 341, 342, 344, 345, 374). Based on such evidence, this thesis also sought to further define these potential specific roles of NRK2 in the context of chronic NRK2 overexpression.

Young NRK2.Tg mice developed normally and had a similar capacity for acute exercise compared to WT mice, indicating that NRK2 overexpression did not impair skeletal muscle development and growth despite the perturbations to cell adhesion proteins identified within aged NRK2.Tg skeletal muscle. Though NRK2 overexpression did not significantly affect the NAD^+ metabolome during periods of inactivity, Phosphorylation of NR to NMN via NRK2 was determined as the rate limiting step in the production of skeletal muscle NAD^+ in both TA and soleus muscle, manifesting as an additive increase in total NAD^+

levels in NRK2.Tg mice upon IP administration of NR and agreeing with current knowledge derived from in vitro assessments (15, 16).

Evidence was also presented for elevated skeletal muscle NAD^+ levels during night hours in male NRK2.Tg mice, though this was subsequently re-assessed in females and not determined to be present, suggesting potential sex differences in the metabolic relevance of individual NAD^+ salvage routes. Ultimately, this suggests that metabolic quantification should be repeated in male mice alongside females, but it was identified early in the study that the ankle joints of male NRK2.Tg mice were significantly enlarged, enflamed and stiffened as the mice aged irrespective of WT or NRK2.Tg genotype. The cause of these observations remained unknown, but would have significantly confounded any home cage metabolic assessment due to abnormal behaviour and rendered any exercise and grip strength studies on aged mice impossible, constituting a study limitation.

Skeletal muscle specific NRK2 overexpression did not significantly affect the oxidative metabolic phenotype of young mice both basally and in response to acute exercise. Augmentation of the NAD^+ metabolome through skeletal muscle NAMPT overexpression in young mice was previously determined to be ineffectual due to pre-existing NAD^+ sufficiency (315), explaining these observations. This also indicated that nullifying NRK2 circadian expression dynamics through constitutive overexpression did not affect metabolic phenotype, implying that circadian variations of NRK2 expression levels are not metabolically relevant in the context of young and healthy animals. This study was limited in that NAD^+ and TCA cycle metabolites could only be determined as a snapshot of absolute whole tissue levels. Further assessment of metabolic flux rates within the skeletal muscle NAD^+ metabolome, endogenous NR and NMN levels and central carbon metabolite flux

using isotopically labelled tracers would therefore be beneficial for increasing confidence in these observations.

NRK2 overexpression did not significantly affect the functional metabolic phenotype of aged mice, with few differences present in whole body metabolic phenotype upon assessment via indirect calorimetry. However, aged NRK2.Tg mice had significantly higher ΔRER values when normalised to body weight relative to aged WT mice, suggesting that NRK2.Tg mice are more metabolically flexible. This was interesting given the significantly increased skeletal muscle mass in aged NRK2.Tg mice observed in chapter 5, which may have shifted the lean mass of NRK2.Tg mice upwards relative to WT mice, increasing the proportion of metabolically plastic skeletal muscle and therefore impacting on metabolic phenotype. Though subsequent increases in body weight and gonadal fat mass were discounted, precise lean body mass measurements were not available, and utilising equipment such as a dual energy x-ray absorptiometer (DEXA) could provide further confidence in these observations going forward. No other whole body metabolic parameters were significantly different in NRK2.Tg mice, though a recent study which reported protection against sarcopenia and an improvement in endurance exercise capacity in aged male PGC1-α overexpressing mice also did not identify a subsequent improvement in whole body metabolism (565), implying that increased skeletal muscle mass is not always associated with significant metabolic improvements that are detectible with traditional methods.

PGC1-α is a target of SIRT1 and induces mitochondrial biogenesis (234, 389, 566), with the same study also reporting an increase in endurance capacity. Given the upwards but non-significant trend in FAO capacity in aged NRK2.Tg TA, assessment of acute and

endurance exercise capacity in aged NRK2.Tg mice would have been informative as to the relevance of NRK2 during exercise in a suboptimal metabolic model, but this was hampered by an inability to motivate aged mice to run as well as an inability to exercise mice to exhaustion within the guidelines of the current project licence. The lack of significant metabolic differences in aged NRK2.Tg muscle was interesting given that untargeted proteomics flagged up significant dysregulation of fatty acid processing and calcium signalling, though it is possible that the functional impact of such dysregulation may have been compensated by other undetected genes or simply have been too subtle to detect with the assay methods utilised.

Contrary to recent research (11, 171, 180, 184, 284, 292, 315, 387), the aged mice in this study did not present with significantly depleted skeletal muscle NAD^+ besides a significant decline in total NAD^+ levels during the night which was not improved in NRK2.Tg mice. Due to licence restrictions, aged mice were metabolically assessed in vivo at 18-20 months of age and sacrificed for skeletal muscle NAD^+ quantification between 21-23 months old. Though the majority of cited studies which noted a decline in skeletal muscle NAD^+ levels used mouse models aged 24 months or older, there is evidence for a significant decline at 22 months of age (184) which was not replicated in this study. This suggests that the intended aim of examining the metabolic consequences of NRK2 augmentation in a system of NAD^+ deficit was not achieved, though a recent study in humans has suggested that skeletal muscle NAD^+ may not decline significantly under “normal” ageing (176). Though skeletal muscle NAD^+ repletion through oral NR has shown to improve severely impaired metabolic phenotypes due to critical depletion of NAD^+ (11), NAD^+ boosting may therefore not be an effective strategy for combating age related metabolic decline under normal

conditions in humans, and efforts should be refocused on metabolic disease states in this regard. The same study observed significant increases in the NAM clearance metabolite MeNAM but ultimately no increase in skeletal muscle NAD^+ levels upon oral NR supplementation (176), as was also identified in both WT and NRK2.Tg aged mice. This corroborates studies suggesting that exogenous NR may not be available to skeletal muscle in its original form but as NAM derived from degradation of the exogenous NR through first pass metabolism and/or in the bloodstream (314, 315), indicating that oral administration of NR may not be optimal for boosting skeletal muscle NAD^+ levels outside of the NAM/NAMPT salvage pathway due to degradation of NR to NAM.

The increase in aged NRK2.Tg skeletal muscle mass was not expected, and could not be explained simply by a general augmentation of NAD^+ salvage pathways and thus improved muscle metabolism with age, especially given that aged WT and NRK2.Tg skeletal muscle NAD^+ levels were comparable. Furthermore, studies using skeletal muscle overexpressing NAMPT models have reported an improved oxidative phenotype with age and greater endurance capacity following training, but not increased muscle bed weights (11, 315, 316) indicating that this effect is directly associated with NRK2 rather than general NAD^+ augmentation. Conversely, the mice used in this study were sedentary, and soleus muscles were significantly larger in NRK2.Tg mice even at a young age. This early onset of soleus augmentation and lack of mass increase at any stage in TA could indicate a skeletal muscle fibre type specific effect of NRK2 overexpression, which requires further clarification through identifying any potential correlations between fibre type and regeneration status as well as any potential fibre type switching. As has previously been noted (15), endogenous NRK2 levels were higher in the predominantly glycolytic TA relative to the oxidative soleus

implying that NRK2 may be of more importance in glycolytic muscle. However, this could also mean that NRK2 overexpression produces a more significant effect where levels are usually low. Comprehensive assessment of this phenotype within fast twitch TA and slow twitch soleus muscle alongside the previous analysis of quadriceps is required going forward to establish this.

A more widespread increase across all muscle beds assessed was noted in aged animals as well as increased grip strength, suggesting that NRK2.Tg mice partially resist age related loss of skeletal muscle mass and function. Induction of the UPR and chronic inflammation were discounted as potential confounding causes, and further controls will be assessed to increase confidence in these observations including ACTA1-cre only control mice. Though the skeletal muscle growth factor Igf2 was significantly upregulated alongside a downregulation in the atrophy promoting ubiquitin E3 ligase MuRF1 in aged skeletal muscle, no significant upregulation of skeletal muscle hypertrophy signalling was observed. Histological analysis of aged muscle revealed a high incidence of centrally nucleated myofibres in NRK2.Tg skeletal muscle, though inflammatory pathways and skeletal muscle regeneration markers were not significantly upregulated, which together imply historic regeneration. However, striking parallels can be drawn between the NRK2.Tg phenotype and M- and N- cadherin KO mice in which the regenerative phenotype is driven by a subset of pseudo-activated satellite cells due to niche instability (461), constituting a potential driving mechanism which requires further investigation. Though the specific molecular mechanisms could not yet be determined due to time constraints, untargeted proteomics indicated widespread disruption to cell adhesion processes and cytoskeletal dynamics as well as positive regulation of fibroblast fusion and substrate binding in aged NRK2.Tg skeletal

muscle, further highlighting the importance of NRK2 in this role (344, 345) and implying persistent regeneration in aged NRK2.Tg muscle. This phenomenon has also not been reported in other models involving manipulation of other skeletal muscle NAD^+ salvage mechanisms, suggesting that this role is specific to NRK2 (11, 15, 16, 315, 316). Future work should consider investigations into NRK2.Tg satellite cell dynamics and longitudinal sectioning of NRK2.Tg skeletal muscle to visualise sarcomeric structure, nuclear positioning across the long axis, positioning of structural/regenerative proteins including NRK2, and the appearance of NMJs/MTJs and further myofibrillar ultrastructure to determine key areas of dysregulation.

Some of the data presented appears paradoxical, and it is not clear whether the observed phenotype in aged NRK2.Tg mice is benign, beneficial, or even potentially deleterious. The NRK2.Tg phenotype is not outwardly obvious at any stage of the life cycle, with young mice developing normally and presenting no metabolic or behavioural differences. The sarcopenic resistance and increased grip strength in aged NRK2.Tg animals would appear beneficial, though no overt metabolic benefits or changes to the NAD^+ metabolome were observed. Regenerated fibres can be indicative of skeletal muscle malfunction as is apparent within dystrophic phenotypes (499, 500) and Igf2 is upregulated in response to muscle injury (537, 567), though regenerated fibres within healthy muscle are protected from apoptosis and further inflammatory damage induced by nearby damaged fibres (552, 553). Assessment of NRK2.Tg mouse lifespan via Kaplan-Meier survival curves would provide more information regarding this, but was not possible due to the constraints of the project licence.

Considering the data presented, it is possible that in H6PDKO muscle, NRK2 is not upregulated to alleviate severe metabolic and redox stress (325) but indirectly induced as a result of the extensive pathological skeletal muscle remodelling which follows (324), particularly given that NRK2 is strongly upregulated in response to skeletal muscle injury (326) and the fact that NRK2 induction and association with integrins is necessary for myoblast fusion (341, 342). Under normal conditions, the specific role of NRK2 in generating a membrane proximal NAD^+ pool to maintain skeletal muscle cell/ECM cohesion may be of more prominence than NAD^+ generation for metabolic homeostasis in skeletal muscle, which is mainly perpetuated by NAM recycling via NAMPT (15) (Figure 6-1). Use of NAD^+ biosensors to determine spatially distinct NAD^+ pools could serve to further determine this (201, 209, 210).

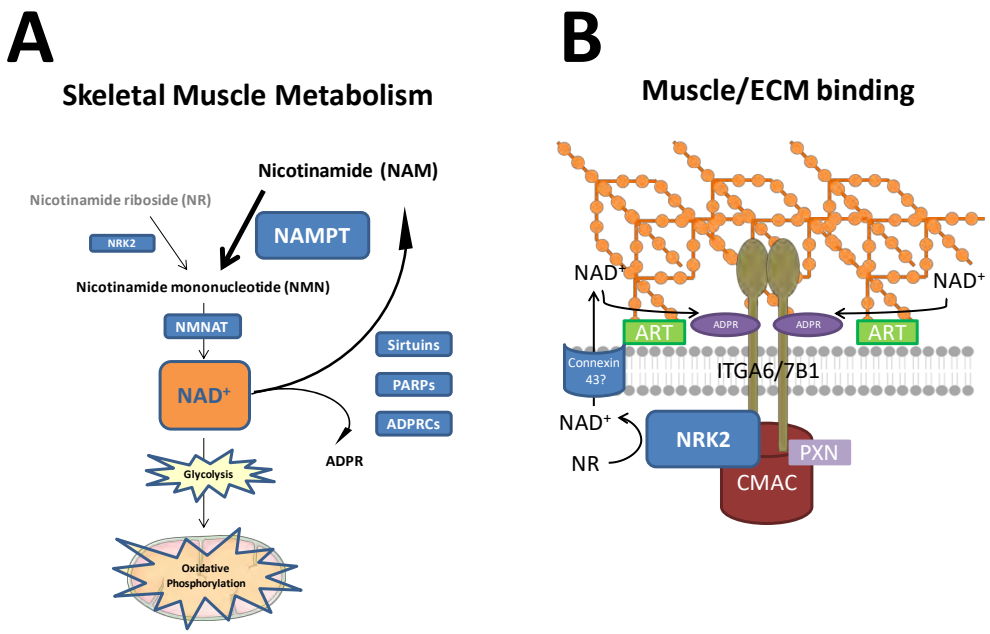

Figure 6-1 – Proposed roles of NRK2 in skeletal muscle. NRK2 mediated NAD+ salvage from NR is dispensable for endogenous skeletal muscle metabolic homeostasis, but the contribution of NR to the metabolic NAD^+ pool could be increased if NR can be effectively delivered intact to skeletal muscle (A). However, NRK2 generates a membrane proximal pool of NAD+ facilitating cell-ECM adhesion, dynamically regulating structural homeostasis (B).

Based on this model, chronic overexpression of NRK2 may disrupt the stoichiometric balance of CMAC complex assembly and/or NRK2 and paxillin recruitment as well as the temporal NRK2 induction patterns which appear functionally relevant (341, 342), causing dysregulated skeletal muscle cell/ECM adhesion towards a more pro-adhesive phenotype. Constitutive NRK2 overexpression may also perturb myoblast differentiation due to the observed downregulation of endogenous NRK2 at this point (15). Such dysregulation may manifest critically during periods of increased skeletal muscle remodelling such as during adolescence or in response to injury, resulting in compensatory upregulation of myofibrillar hypertrophy as is observed during regeneration (537, 550) and in models of depleted muscle function (564). The effects of this hypothetical model are apparent upon examination of histological examination of aged NRK2.Tg skeletal muscle, which could also be initially driven and perpetuated with age through satellite niche instability favouring a pro-regenerative phenotype in absence of acute injury (461).

In summary, this thesis has supplemented current knowledge of the metabolic relevance of the NR/NRK2 route to NAD^+ in skeletal muscle, reinforced the specific importance of NRK2 in skeletal muscle structure and function, and identified that NRK2 overexpression may potentially alleviate age related skeletal muscle loss. The evidence presented suggests that augmentation of skeletal muscle NRK mediated NAD^+ salvage via overexpression of NRK2 does not increase skeletal muscle NAD^+ levels with age and that oral NR supplementation may not be an optimal strategy for raising skeletal muscle NAD^+ levels. Despite this, NRK2 has specific and compartmentalised roles within skeletal muscle which lead to increased skeletal muscle mass and strength when it is constitutively overexpressed, potentially prolonging healthspan in aged individuals. Future research should seek to further

clarify the specific molecular mechanisms by which this phenomenon initially occurs and is maintained with age.

REFERENCES

1. Christensen K, Doblhammer G, Rau R, Vaupel JW. Ageing populations: the challenges ahead. Lancet (London, England). 2009;374(9696):1196-208.
2. How to cope with an ageing population. Lancet. 2013;382(9900):1225.
3. Huber M, Knottnerus JA, Green L, Horst Hvd, Jadad AR, Kromhout D, et al. How should we define health? BMJ. 2011;343:d4163.
4. Keller K, Engelhardt M. Strength and muscle mass loss with aging process. Age and strength loss. Muscles Ligaments Tendons J. 2013;3(4):346-50.
5. Cartee GD, Hepple RT, Bamman MM, Zierath JR. Exercise Promotes Healthy Aging of Skeletal Muscle. Cell Metab. 2016;23(6):1034-47.
6. Santilli V, Bernetti A, Mangone M, Paoloni M. Clinical definition of sarcopenia. Clin Cases Miner Bone Metab. 2015;11(3):177-80.
7. Yazar T, Olgun Yazar H. Prevalance of sarcopenia according to decade. Clin Nutr ESPEN. 2019;29:137-41.
8. Pugh TD, Conklin MW, Evans TD, Polewski MA, Barbian HJ, Pass R, et al. A shift in energy metabolism anticipates the onset of sarcopenia in rhesus monkeys. Aging Cell. 2013;12(4):672-81.
9. Mesinovic J, Zengin A, De Courten B, Ebeling PR, Scott D. Sarcopenia and type 2 diabetes mellitus: a bidirectional relationship. Diabetes Metab Syndr Obes. 2019;12:1057-72.
10. Reginster J-Y, Beaudart C, Buckinx F, Bruyère O. Osteoporosis and sarcopenia: two diseases or one? Curr Opin Clin Nutr Metab Care. 2016;19(1):31-6.
11. Frederick DW, Loro E, Liu L, Davila A, Jr., Chellappa K, Silverman IM, et al. Loss of NAD Homeostasis Leads to Progressive and Reversible Degeneration of Skeletal Muscle. Cell Metab. 2016;24(2):269-82.
12. Aman Y, Qiu Y, Tao J, Fang EF. Therapeutic potential of boosting NAD+ in aging and age-related diseases. Translational Medicine of Aging. 2018;2:30-7.
13. Yoshino J, Baur JA, Imai SI. NAD(+) Intermediates: The Biology and Therapeutic Potential of NMN and NR. Cell Metab. 2018;27(3):513-28.
14. Bieganowski P, Brenner C. Discoveries of nicotinamide riboside as a nutrient and conserved NRK genes establish a Preiss-Handler independent route to NAD+ in fungi and humans. Cell. 2004;117(4):495-502.
15. Fletcher RS, Ratajczak J, Doig CL, Oakey LA, Callingham R, Da Silva Xavier G, et al. Nicotinamide riboside kinases display redundancy in mediating nicotinamide mononucleotide and nicotinamide riboside metabolism in skeletal muscle cells. Mol Metab. 2017;6(8):819-32.
16. Ratajczak J, Joffraud M, Trammell SA, Ras R, Canela N, Boutant M, et al. NRK1 controls nicotinamide mononucleotide and nicotinamide riboside metabolism in mammalian cells. Nat Commun. 2016;7:13103.
17. Goody MF, Henry CA. A need for NAD+ in muscle development, homeostasis, and aging. Skelet Muscle. 2018;8(1):9.
18. Frontera WR, Ochala J. Skeletal muscle: a brief review of structure and function. Calcif Tissue Int. 2015;96(3):183-95.
19. Zurlo F, Larson K, Bogardus C, Ravussin E. Skeletal muscle metabolism is a major determinant of resting energy expenditure. J Clin Invest. 1990;86(5):1423-7.
20. Webb RC. Smooth muscle contraction and relaxation. Adv Physiol Educ. 2003;27(1-4):201-6.

21. Rossi AE, Dirksen RT. Sarcoplasmic reticulum: the dynamic calcium governor of muscle. Muscle Nerve. 2006;33(6):715-31.
22. Calderon JC, Bolanos P, Caputo C. The excitation-contraction coupling mechanism in skeletal muscle. Biophys Rev. 2014;6(1):133-60.
23. Ebashi S. Regulatory mechanism of muscle contraction with special reference to the Ca-troponin-tropomyosin system. Essays Biochem. 1974;10:1-36.
24. Huxley HE. The mechanism of muscular contraction. Science. 1969;164(3886):1356-65.
25. Talbot J, Maves L. Skeletal muscle fiber type: using insights from muscle developmental biology to dissect targets for susceptibility and resistance to muscle disease. Wiley Interdiscip Rev Dev Biol. 2016;5(4):518-34.
26. Schiaffino S, Reggiani C. Fiber types in mammalian skeletal muscles. Physiol Rev. 2011;91(4):1447-531.
27. Bourdeau Julien I, Sephton CF, Dutchak PA. Metabolic Networks Influencing Skeletal Muscle Fiber Composition. Front Cell Dev Biol. 2018;6:125.
28. Zierath JR, Hawley JA. Skeletal muscle fiber type: influence on contractile and metabolic properties. PLoS Biol. 2004;2(10):e348.
29. Szent-Gyorgyi AG. The early history of the biochemistry of muscle contraction. J Gen Physiol. 2004;123(6):631-41.
30. Lee SH, Kim BJ, Park DR, Kim UH. Exercise induces muscle fiber type switching via transient receptor potential melastatin 2-dependent Ca(2+) signaling. J Appl Physiol (1985). 2018;124(2):364-73.
31. Chal J, Pourquie O. Making muscle: skeletal myogenesis in vivo and in vitro. Development. 2017;144(12):2104-22.
32. White RB, Ziman MR. Genome-wide discovery of Pax7 target genes during development. Physiol Genomics. 2008;33(1):41-9.
33. Roy SD, Williams VC, Pipalia TG, Li K, Hammond CL, Knappe S, et al. Myotome adaptability confers developmental robustness to somitic myogenesis in response to fibre number alteration. Dev Biol. 2017;431(2):321-35.
34. Francetic T, Li Q. Skeletal myogenesis and Myf5 activation. Transcription. 2011;2(3):109-14.
35. Abmayr SM, Pavlath GK. Myoblast fusion: lessons from flies and mice. Development. 2012;139(4):641-56.
36. Gros J, Manceau M, Thome V, Marcelle C. A common somitic origin for embryonic muscle progenitors and satellite cells. Nature. 2005;435(7044):954-8.
37. Mansouri A, Stoykova A, Torres M, Gruss P. Dysgenesis of cephalic neural crest derivatives in Pax7-/- mutant mice. Development. 1996;122(3):831-8.
38. Hood DA, Irrcher I, Ljubicic V, Joseph AM. Coordination of metabolic plasticity in skeletal muscle. J Exp Biol. 2006;209(Pt 12):2265-75.
39. Buckingham M. Skeletal muscle progenitor cells and the role of Pax genes. C R Biol. 2007;330(6-7):530-3.
40. Kitajima Y, Ono Y. Visualization of PAX7 protein dynamics in muscle satellite cells in a YFP knock-in-mouse line. Skelet Muscle. 2018;8(1):26.
41. Zammit PS, Relaix F, Nagata Y, Ruiz AP, Collins CA, Partridge TA, et al. Pax7 and myogenic progression in skeletal muscle satellite cells. J Cell Sci. 2006;119(Pt 9):1824-32.

42. Wozniak AC, Kong J, Bock E, Pilipowicz O, Anderson JE. Signaling satellite-cell activation in skeletal muscle: markers, models, stretch, and potential alternate pathways. Muscle Nerve. 2005;31(3):283-300.
43. Yin H, Price F, Rudnicki MA. Satellite cells and the muscle stem cell niche. Physiol Rev. 2013;93(1):23-67.
44. Kuang S, Kuroda K, Le Grand F, Rudnicki MA. Asymmetric self-renewal and commitment of satellite stem cells in muscle. Cell. 2007;129(5):999-1010.
45. Relaix F, Montarras D, Zaffran S, Gayraud-Morel B, Rocancourt D, Tajbakhsh S, et al. Pax3 and Pax7 have distinct and overlapping functions in adult muscle progenitor cells. J Cell Biol. 2006;172(1):91-102.
46. Gunther S, Kim J, Kostin S, Lepper C, Fan CM, Braun T. Myf5-positive satellite cells contribute to Pax7-dependent long-term maintenance of adult muscle stem cells. Cell Stem Cell. 2013;13(5):590-601.
47. Lepper C, Partridge TA, Fan CM. An absolute requirement for Pax7-positive satellite cells in acute injury-induced skeletal muscle regeneration. Development. 2011;138(17):3639-46.
48. Sambasivan R, Yao R, Kissenpfennig A, Van Wittenberghe L, Paldi A, Gayraud-Morel B, et al. Pax7-expressing satellite cells are indispensable for adult skeletal muscle regeneration. Development. 2011;138(17):3647-56.
49. von Maltzahn J, Jones AE, Parks RJ, Rudnicki MA. Pax7 is critical for the normal function of satellite cells in adult skeletal muscle. Proc Natl Acad Sci U S A. 2013;110(41):16474-9.
50. Knappe S, Zammit PS, Knight RD. A population of Pax7-expressing muscle progenitor cells show differential responses to muscle injury dependent on developmental stage and injury extent. Front Aging Neurosci. 2015;7:161.
51. Murray IR, Baily JE, Chen WCW, Dar A, Gonzalez ZN, Jensen AR, et al. Skeletal and cardiac muscle pericytes: Functions and therapeutic potential. Pharmacol Ther. 2017;171:65-74.
52. Dellavalle A, Sampaolesi M, Tonlorenzi R, Tagliafico E, Sacchetti B, Perani L, et al. Pericytes of human skeletal muscle are myogenic precursors distinct from satellite cells. Nat Cell Biol. 2007;9(3):255-67.
53. Liu N, Garry GA, Li S, Bezprozvannaya S, Sanchez-Ortiz E, Chen B, et al. A Twist2-dependent progenitor cell contributes to adult skeletal muscle. Nat Cell Biol. 2017;19(3):202-13.
54. Tamaki T, Akatsuka A, Ando K, Nakamura Y, Matsuzawa H, Hotta T, et al. Identification of myogenic-endothelial progenitor cells in the interstitial spaces of skeletal muscle. J Cell Biol. 2002;157(4):571-7.
55. Mitchell KJ, Pannerec A, Cadot B, Parlakian A, Besson V, Gomes ER, et al. Identification and characterization of a non-satellite cell muscle resident progenitor during postnatal development. Nat Cell Biol. 2010;12(3):257-66.
56. Gussoni E, Soneoka Y, Strickland CD, Buzney EA, Khan MK, Flint AF, et al. Dystrophin expression in the mdx mouse restored by stem cell transplantation. Nature. 1999;401(6751):390-4.
57. Negroni E, Riederer I, Chaouch S, Belicchi M, Razini P, Di Santo J, et al. In vivo myogenic potential of human CD133+ muscle-derived stem cells: a quantitative study. Mol Ther. 2009;17(10):1771-8.
58. Sacco A, Doyonnas R, Kraft P, Vitorovic S, Blau HM. Self-renewal and expansion of single transplanted muscle stem cells. Nature. 2008;456(7221):502-6.

59. Beauchamp JR, Heslop L, Yu DS, Tajbakhsh S, Kelly RG, Wernig A, et al. Expression of CD34 and Myf5 defines the majority of quiescent adult skeletal muscle satellite cells. J Cell Biol. 2000;151(6):1221-34.
60. Collins CA, Olsen I, Zammit PS, Heslop L, Petrie A, Partridge TA, et al. Stem cell function, self-renewal, and behavioral heterogeneity of cells from the adult muscle satellite cell niche. Cell. 2005;122(2):289-301.
61. Pipalia TG, Koth J, Roy SD, Hammond CL, Kawakami K, Hughes SM. Cellular dynamics of regeneration reveals role of two distinct Pax7 stem cell populations in larval zebrafish muscle repair. Dis Model Mech. 2016;9(6):671-84.
62. Schultz E. Satellite cell proliferative compartments in growing skeletal muscles. Dev Biol. 1996;175(1):84-94.
63. Egan B, Zierath JR. Exercise metabolism and the molecular regulation of skeletal muscle adaptation. Cell Metab. 2013;17(2):162-84.
64. Baker JS, McCormick MC, Robergs RA. Interaction among Skeletal Muscle Metabolic Energy Systems during Intense Exercise. J Nutr Metab. 2010;2010:905612.
65. Romijn JA, Coyle EF, Sidossis LS, Gastaldelli A, Horowitz JF, Endert E, et al. Regulation of endogenous fat and carbohydrate metabolism in relation to exercise intensity and duration. Am J Physiol. 1993;265(3 Pt 1):E380-91.
66. Jensen J, Rustad PI, Kolnes AJ, Lai YC. The role of skeletal muscle glycogen breakdown for regulation of insulin sensitivity by exercise. Front Physiol. 2011;2:112.
67. Goodpaster BH, Sparks LM. Metabolic Flexibility in Health and Disease. Cell Metab. 2017;25(5):1027-36.
68. Baird MF, Graham SM, Baker JS, Bickerstaff GF. Creatine-kinase- and exercise-related muscle damage implications for muscle performance and recovery. J Nutr Metab. 2012;2012:960363.
69. Bonora M, Patergnani S, Rimessi A, De Marchi E, Suski JM, Bononi A, et al. ATP synthesis and storage. Purinergic Signal. 2012;8(3):343-57.
70. Mookerjee SA, Gerencser AA, Nicholls DG, Brand MD. Quantifying intracellular rates of glycolytic and oxidative ATP production and consumption using extracellular flux measurements. J Biol Chem. 2018;293(32):12649-52.
71. Kennedy EP, Lehninger AL. Oxidation of fatty acids and tricarboxylic acid cycle intermediates by isolated rat liver mitochondria. J Biol Chem. 1949;179(2):957-72.
72. Lundsgaard AM, Fritzen AM, Kiens B. Molecular Regulation of Fatty Acid Oxidation in Skeletal Muscle during Aerobic Exercise. Trends Endocrinol Metab. 2018;29(1):18-30.
73. Smith RL, Soeters MR, Wust RCI, Houtkooper RH. Metabolic Flexibility as an Adaptation to Energy Resources and Requirements in Health and Disease. Endocr Rev. 2018;39(4):489-517.
74. Osellame LD, Blacker TS, Duchen MR. Cellular and molecular mechanisms of mitochondrial function. Best Pract Res Clin Endocrinol Metab. 2012;26(6):711-23.
75. Jagoe RT, Engelen MP. Muscle wasting and changes in muscle protein metabolism in chronic obstructive pulmonary disease. Eur Respir J Suppl. 2003;46:52s-63s.
76. Simonson DC, DeFronzo RA. Indirect calorimetry: methodological and interpretative problems. Am J Physiol. 1990;258(3 Pt 1):E399-412.
77. Horowitz JF, Klein S. Lipid metabolism during endurance exercise. Am J Clin Nutr. 2000;72(2 Suppl):558s-63s.

78. Ko K, Woo J, Bae JY, Roh HT, Lee YH, Shin KO. Exercise training improves intramuscular triglyceride lipolysis sensitivity in high-fat diet induced obese mice. Lipids in Health and Disease. 2018;17(1):81.
79. Ramos-Jimenez A, Hernandez-Torres RP, Torres-Duran PV, Romero-Gonzalez J, Mascher D, Posadas-Romero C, et al. The Respiratory Exchange Ratio is Associated with Fitness Indicators Both in Trained and Untrained Men: A Possible Application for People with Reduced Exercise Tolerance. Clin Med Circ Respirat Pulm Med. 2008;2:1-9.
80. Warburton DE, Nicol CW, Bredin SS. Health benefits of physical activity: the evidence. CMAJ. 2006;174(6):801-9.
81. Ito N, Ruegg UT, Takeda S. ATP-Induced Increase in Intracellular Calcium Levels and Subsequent Activation of mTOR as Regulators of Skeletal Muscle Hypertrophy. Int J Mol Sci. 2018;19(9).
82. Friedrichsen M, Mortensen B, Pehmoller C, Birk JB, Wojtaszewski JF. Exercise-induced AMPK activity in skeletal muscle: role in glucose uptake and insulin sensitivity. Mol Cell Endocrinol. 2013;366(2):204-14.
83. Graham ZA, Gallagher PM, Cardozo CP. Focal adhesion kinase and its role in skeletal muscle. J Muscle Res Cell Motil. 2015;36(4-5):305-15.
84. McGee SL, Walder KR. Exercise and the Skeletal Muscle Epigenome. Cold Spring Harb Perspect Med. 2017;7(9).
85. Fernandez-Marcos PJ, Auwerx J. Regulation of PGC-1alpha, a nodal regulator of mitochondrial biogenesis. Am J Clin Nutr. 2011;93(4):884S-90.
86. Lundell LS, Massart J, Altintas A, Krook A, Zierath JR. Regulation of glucose uptake and inflammation markers by FOXO1 and FOXO3 in skeletal muscle. Mol Metab. 2019;20:79-88.
87. Furuyama T, Kitayama K, Yamashita H, Mori N. Forkhead transcription factor FOXO1 (FKHR)-dependent induction of PDK4 gene expression in skeletal muscle during energy deprivation. Biochem J. 2003;375(Pt 2):365-71.
88. Richter EA, Hargreaves M. Exercise, GLUT4, and skeletal muscle glucose uptake. Physiol Rev. 2013;93(3):993-1017.
89. Berry NT, Hubal M, Wideman L. The effects of an acute exercise bout on GH and IGF-1 in prediabetic and healthy African Americans: A pilot study investigating gene expression. PLoS One. 2018;13(1):e0191331.
90. Perez-Schindler J, Hamilton DL, Moore DR, Baar K, Philp A. Nutritional strategies to support concurrent training. Eur J Sport Sci. 2015;15(1):41-52.
91. Melanson EL, MacLean PS, Hill JO. Exercise improves fat metabolism in muscle but does not increase 24-h fat oxidation. Exercise and sport sciences reviews. 2009;37(2):93-101.
92. Friedman JR, Nunnari J. Mitochondrial form and function. Nature. 2014;505(7483):335-43.
93. Ploumi C, Daskalaki I, Tavernarakis N. Mitochondrial biogenesis and clearance: a balancing act. FEBS J. 2017;284(2):183-95.
94. McCommis KS, Finck BN. Mitochondrial pyruvate transport: a historical perspective and future research directions. Biochem J. 2015;466(3):443-54.
95. Nakamoto RK, Baylis Scanlon JA, Al-Shawi MK. The rotary mechanism of the ATP synthase. Arch Biochem Biophys. 2008;476(1):43-50.
96. Houten SM, Violante S, Ventura FV, Wanders RJ. The Biochemistry and Physiology of Mitochondrial Fatty Acid beta-Oxidation and Its Genetic Disorders. Annu Rev Physiol. 2016;78:23-44.

97. Glatz JF, Luiken JJ, Bonen A. Membrane fatty acid transporters as regulators of lipid metabolism: implications for metabolic disease. Physiol Rev. 2010;90(1):367-417.
98. Monné M, Vozza A, Lasorsa FM, Porcelli V, Palmieri F. Mitochondrial Carriers for Aspartate, Glutamate and Other Amino Acids: A Review. International journal of molecular sciences. 2019;20(18):4456.
99. Hood DA, Memme JM, Oliveira AN, Triolo M. Maintenance of Skeletal Muscle Mitochondria in Health, Exercise, and Aging. Annu Rev Physiol. 2019;81:19-41.
100. Madreiter-Sokolowski CT, Sokolowski AA, Waldeck-Weiermair M, Malli R, Graier WF. Targeting Mitochondria to Counteract Age-Related Cellular Dysfunction. Genes (Basel). 2018;9(3).
101. Ljubicic V, Hood DA. Diminished contraction-induced intracellular signaling towards mitochondrial biogenesis in aged skeletal muscle. Aging Cell. 2009;8(4):394-404.
102. Diot A, Morten K, Poulton J. Mitophagy plays a central role in mitochondrial ageing. Mamm Genome. 2016;27(7-8):381-95.
103. Scarpulla RC, Vega RB, Kelly DP. Transcriptional integration of mitochondrial biogenesis. Trends Endocrinol Metab. 2012;23(9):459-66.
104. de Guia RM, Agerholm M, Nielsen TS, Consitt LA, Sogaard D, Helge JW, et al. Aerobic and resistance exercise training reverses age-dependent decline in NAD(+) salvage capacity in human skeletal muscle. Physiol Rep. 2019;7(12):e14139.
105. Koltai E, Szabo Z, Atalay M, Boldogh I, Naito H, Goto S, et al. Exercise alters SIRT1, SIRT6, NAD and NAMPT levels in skeletal muscle of aged rats. Mech Ageing Dev. 2010;131(1):21-8.
106. Pollak N, Dolle C, Ziegler M. The power to reduce: pyridine nucleotides--small molecules with a multitude of functions. Biochem J. 2007;402(2):205-18.
107. Hegyi J, Schwartz RA, Hegyi V. Pellagra: dermatitis, dementia, and diarrhea. Int J Dermatol. 2003;43(1):1-5.
108. Manchester KL. Arthur Harden: an unwitting pioneer of metabolic control analysis. Trends Biochem Sci. 2000;25(2):89-92.
109. Yang Y, Sauve AA. NAD(+) metabolism: Bioenergetics, signaling and manipulation for therapy. Biochim Biophys Acta. 2016;1864(12):1787-800.
110. Meyerhof O, Oesper P. The oxidative reaction of fermentation. Fed Proc. 1947;6(1 Pt 2):278.
111. Yang H, Yang T, Baur JA, Perez E, Matsui T, Carmona JJ, et al. Nutrient-sensitive mitochondrial NAD+ levels dictate cell survival. Cell. 2007;130(6):1095-107.
112. Stein LR, Imai S. The dynamic regulation of NAD metabolism in mitochondria. Trends Endocrinol Metab. 2012;23(9):420-8.
113. Agledal L, Niere M, Ziegler M. The phosphate makes a difference: cellular functions of NADP. Redox Rep. 2010;15(1):2-10.
114. Liu CL, Hsu YC, Lee JJ, Chen MJ, Lin CH, Huang SY, et al. Targeting the pentose phosphate pathway increases reactive oxygen species and induces apoptosis in thyroid cancer cells. Mol Cell Endocrinol. 2020;499:110595.
115. Ho HY, Lin YT, Lin G, Wu PR, Cheng ML. Nicotinamide nucleotide transhydrogenase (NNT) deficiency dysregulates mitochondrial retrograde signaling and impedes proliferation. Redox Biol. 2017;12:916-28.
116. Rechsteiner M, Catanzarite V. The biosynthesis and turnover of nicotinamide adenine dinucleotide in enucleated culture cells. J Cell Physiol. 1974;84(3):409-22.

117. Rechsteiner M, Hillyard D, Olivera BM. Turnover at nicotinamide adenine dinucleotide in cultures of human cells. J Cell Physiol. 1976;88(2):207-17.
118. Canto C, Menzies KJ, Auwerx J. NAD(+) Metabolism and the Control of Energy Homeostasis: A Balancing Act between Mitochondria and the Nucleus. Cell Metab. 2015;22(1):31-53.
119. Chiarugi A, Dölle C, Felici R, Ziegler M. The NAD metabolome--a key determinant of cancer cell biology. Nat Rev Cancer. 2012;12(11):741-52.
120. Davila A, Liu L, Chellappa K, Redpath P, Nakamaru-Ogiso E, Paolella LM, et al. Nicotinamide adenine dinucleotide is transported into mammalian mitochondria. Elife. 2018;7.
121. Mori V, Amici A, Mazzola F, Di Stefano M, Conforti L, Magni G, et al. Metabolic profiling of alternative NAD biosynthetic routes in mouse tissues. PLoS One. 2014;9(11):e113939.
122. Zamporlini F, Ruggieri S, Mazzola F, Amici A, Orsomando G, Raffaelli N. Novel assay for simultaneous measurement of pyridine mononucleotides synthesizing activities allows dissection of the NAD(+) biosynthetic machinery in mammalian cells. FEBS J. 2014;281(22):5104-19.
123. Nikiforov A, Dolle C, Niere M, Ziegler M. Pathways and subcellular compartmentation of NAD biosynthesis in human cells: from entry of extracellular precursors to mitochondrial NAD generation. J Biol Chem. 2011;286(24):21767-78.
124. Ruggieri S, Orsomando G, Sorci L, Raffaelli N. Regulation of NAD biosynthetic enzymes modulates NAD-sensing processes to shape mammalian cell physiology under varying biological cues. Biochim Biophys Acta. 2015;1854(9):1138-49.
125. Bender DA, Olufunwa R. Utilization of tryptophan, nicotinamide and nicotinic acid as precursors for nicotinamide nucleotide synthesis in isolated rat liver cells. Br J Nutr. 1988;59(2):279-87.
126. Terakata M, Fukuwatari T, Sano M, Nakao N, Sasaki R, Fukuoka S, et al. Establishment of true niacin deficiency in quinolinic acid phosphoribosyltransferase knockout mice. J Nutr. 2012;142(12):2148-53.
127. Mielgo-Ayuso J, Aparicio-Ugarriza R, Olza J, Aranceta-Bartrina J, Gil Á, Ortega RM, et al. Dietary Intake and Food Sources of Niacin, Riboflavin, Thiamin and Vitamin B_6 in a Representative Sample of the Spanish Population. The Anthropometry, Intake, and Energy Balance in Spain (ANIBES) Study †. Nutrients. 2018;10(7).
128. Fricker RA, Green EL, Jenkins SI, Griffin SM. The Influence of Nicotinamide on Health and Disease in the Central Nervous System. Int J Tryptophan Res. 2018;11:1178646918776658.
129. Preiss J, Handler P. Biosynthesis of diphosphopyridine nucleotide. I. Identification of intermediates. J Biol Chem. 1958;233(2):488-92.
130. Houtkooper RH, Canto C, Wanders RJ, Auwerx J. The secret life of NAD+: an old metabolite controlling new metabolic signaling pathways. Endocr Rev. 2010;31(2):194-223.
131. Hara N, Yamada K, Terashima M, Osago H, Shimoyama M, Tsuchiya M. Molecular identification of human glutamine- and ammonia-dependent NAD synthetases. Carbon-nitrogen hydrolase domain confers glutamine dependency. J Biol Chem. 2003;278(13):10914-21.
132. Hara N, Yamada K, Shibata T, Osago H, Hashimoto T, Tsuchiya M. Elevation of cellular NAD levels by nicotinic acid and involvement of nicotinic acid phosphoribosyltransferase in human cells. J Biol Chem. 2007;282(34):24574-82.

133. Vogt A, Kassner U, Hostalek U, Steinhagen-Thiessen E. Prolonged-release nicotinic acid for the management of dyslipidemia: an update including results from the NAUTILUS study. Vasc Health Risk Manag. 2007;3(4):467-79.
134. Hanson J, Gille A, Offermanns S. Role of HCA(2) (GPR109A) in nicotinic acid and fumaric acid ester-induced effects on the skin. Pharmacol Ther. 2012;136(1):1-7.
135. Otto C, Parhofer KG, Ritter MM, Richter WO, Schwandt P. Effects of acipimox on haemorheology and plasma lipoproteins in patients with mixed hyperlipoproteinaemia. Br J Clin Pharmacol. 1998;46(5):473-8.
136. van de Weijer T, Phielix E, Bilet L, Williams EG, Ropelle ER, Bierwagen A, et al. Evidence for a direct effect of the NAD+ precursor acipimox on muscle mitochondrial function in humans. Diabetes. 2015;64(4):1193-201.
137. Benyó Z, Gille A, Kero J, Csiky M, Suchánková M, Nüsing R, et al. GPR109A (PUMA-G/HM74A) mediates nicotinic acid-induced flushing. The Journal of clinical investigation. 2006;115:3634-40.
138. Garten A, Petzold S, Korner A, Imai S, Kiess W. Nampt: linking NAD biology, metabolism and cancer. Trends Endocrinol Metab. 2009;20(3):130-8.
139. Burgos ES, Vetticatt MJ, Schramm VL. Recycling nicotinamide. The transition-state structure of human nicotinamide phosphoribosyltransferase. J Am Chem Soc. 2013;135(9):3485-93.
140. Dietrich LS, Muniz O, Powanda M. NAD synthesis in animal tissues. J Vitaminol (Kyoto). 1968;14:Suppl:123-9.
141. Dietrich LS, Muniz O. Inhibition of nicotinamide phosphoribosyltransferase by pyridine nucleotides. Biochemistry. 1972;11(9):1691-5.
142. Wang T, Cui H, Ma N, Jiang Y. Nicotinamide-mediated inhibition of SIRT1 deacetylase is associated with the viability of cancer cells exposed to antitumor agents and apoptosis. Oncol Lett. 2013;6(2):600-4.
143. Sauve AA, Schramm VL. Sir2 regulation by nicotinamide results from switching between base exchange and deacetylation chemistry. Biochemistry. 2003;42(31):9249-56.
144. Bitterman KJ, Anderson RM, Cohen HY, Latorre-Esteves M, Sinclair DA. Inhibition of silencing and accelerated aging by nicotinamide, a putative negative regulator of yeast sir2 and human SIRT1. J Biol Chem. 2002;277(47):45099-107.
145. Jackson MD, Schmidt MT, Oppenheimer NJ, Denu JM. Mechanism of nicotinamide inhibition and transglycosidation by Sir2 histone/protein deacetylases. J Biol Chem. 2003;278(51):50985-98.
146. Sun Z, Lei H, Zhang Z. Pre-B cell colony enhancing factor (PBEF), a cytokine with multiple physiological functions. Cytokine Growth Factor Rev. 2013;24(5):433-42.
147. Harasim E, Chabowski A, Gorski J. Lack of downstream insulin-mimetic effects of visfatin/eNAMPT on glucose and fatty acid metabolism in skeletal muscles. Acta Physiol (Oxf). 2011;202(1):21-8.
148. Wang T, Zhang X, Bheda P, Revollo JR, Imai S, Wolberger C. Structure of Nampt/PBEF/visfatin, a mammalian NAD+ biosynthetic enzyme. Nat Struct Mol Biol. 2006;13(7):661-2.
149. Revollo JR, Korner A, Mills KF, Satoh A, Wang T, Garten A, et al. Nampt/PBEF/Visfatin regulates insulin secretion in beta cells as a systemic NAD biosynthetic enzyme. Cell Metab. 2007;6(5):363-75.

150. Kieswich J, Sayers SR, Silvestre MF, Harwood SM, Yaqoob MM, Caton PW. Monomeric eNAMPT in the development of experimental diabetes in mice: a potential target for type 2 diabetes treatment. Diabetologia. 2016;59(11):2477-86.
151. Dall M, Trammell SAJ, Asping M, Hassing AS, Agerholm M, Vienberg SG, et al. Mitochondrial function in liver cells is resistant to perturbations in NAD(+) salvage capacity. J Biol Chem. 2019;294(36):13304-26.
152. Zhang LQ, Van Haandel L, Xiong M, Huang P, Heruth DP, Bi C, et al. Metabolic and molecular insights into an essential role of nicotinamide phosphoribosyltransferase. Cell death & disease. 2017;8(3):e2705-e.
153. Hasmann M, Schemainda I. FK866, a highly specific noncompetitive inhibitor of nicotinamide phosphoribosyltransferase, represents a novel mechanism for induction of tumor cell apoptosis. Cancer Res. 2003;63(21):7436-42.
154. Tan B, Dong S, Shepard RL, Kays L, Roth KD, Geeganage S, et al. Inhibition of Nicotinamide Phosphoribosyltransferase (NAMPT), an Enzyme Essential for NAD+ Biosynthesis, Leads to Altered Carbohydrate Metabolism in Cancer Cells. J Biol Chem. 2015;290(25):15812-24.
155. Mitchell SJ, Bernier M, Aon MA, Cortassa S, Kim EY, Fang EF, et al. Nicotinamide Improves Aspects of Healthspan, but Not Lifespan, in Mice. Cell Metab. 2018;27(3):667-76 e4.
156. Klaidman LK, Mukherjee SK, Hutchin TP, Adams JD. Nicotinamide as a precursor for NAD+ prevents apoptosis in the mouse brain induced by tertiary-butylhydroperoxide. Neurosci Lett. 1996;206(1):5-8.
157. Liu D, Gharavi R, Pitta M, Gleichmann M, Mattson MP. Nicotinamide prevents NAD+ depletion and protects neurons against excitotoxicity and cerebral ischemia: NAD+ consumption by SIRT1 may endanger energetically compromised neurons. Neuromolecular Med. 2009;11(1):28-42.
158. Tempel W, Rabeh WM, Bogan KL, Belenky P, Wojcik M, Seidle HF, et al. Nicotinamide riboside kinase structures reveal new pathways to NAD+. PLoS Biol. 2007;5(10):e263.
159. Gingrich W, Schlenk F. Codehydrogenase I and Other Pyridinium Compounds as V-Factor for Hemophilus influenzae and H. parainfluenzae. J Bacteriol. 1944;47(6):535-50.
160. Trammell SA, Yu L, Redpath P, Migaud ME, Brenner C. Nicotinamide Riboside Is a Major NAD+ Precursor Vitamin in Cow Milk. J Nutr. 2016;146(5):957-63.
161. Belenky P, Bogan KL, Brenner C. NAD+ metabolism in health and disease. Trends Biochem Sci. 2007;32(1):12-9.
162. Grozio A, Sociali G, Sturla L, Caffa I, Soncini D, Salis A, et al. CD73 protein as a source of extracellular precursors for sustained NAD+ biosynthesis in FK866-treated tumor cells. The Journal of biological chemistry. 2013;288(36):25938-49.
163. Kulikova V, Shabalin K, Nerinovski K, Dölle C, Niere M, Yakimov A, et al. Generation, Release, and Uptake of the NAD Precursor Nicotinic Acid Riboside by Human Cells. The Journal of biological chemistry. 2015;290(45):27124-37.
164. Trammell SA, Schmidt MS, Weidemann BJ, Redpath P, Jaksch F, Dellinger RW, et al. Nicotinamide riboside is uniquely and orally bioavailable in mice and humans. Nat Commun. 2016;7:12948.
165. Canto C, Houtkooper RH, Pirinen E, Youn DY, Oosterveer MH, Cen Y, et al. The NAD(+) precursor nicotinamide riboside enhances oxidative metabolism and protects against high-fat diet-induced obesity. Cell Metab. 2012;15(6):838-47.

166. Shi W, Hegeman MA, van Dartel DAM, Tang J, Suarez M, Swarts H, et al. Effects of a wide range of dietary nicotinamide riboside (NR) concentrations on metabolic flexibility and white adipose tissue (WAT) of mice fed a mildly obesogenic diet. Molecular Nutrition & Food Research. 2017;61(8):1600878.
167. Trammell SA, Weidemann BJ, Chadda A, Yorek MS, Holmes A, Coppey LJ, et al. Nicotinamide Riboside Opposes Type 2 Diabetes and Neuropathy in Mice. Sci Rep. 2016;6:26933.
168. Zhou CC, Yang X, Hua X, Liu J, Fan MB, Li GQ, et al. Hepatic NAD(+) deficiency as a therapeutic target for non-alcoholic fatty liver disease in ageing. Br J Pharmacol. 2016;173(15):2352-68.
169. Khan NA, Auranen M, Paetau I, Pirinen E, Euro L, Forsstrom S, et al. Effective treatment of mitochondrial myopathy by nicotinamide riboside, a vitamin B3. EMBO Mol Med. 2014;6(6):721-31.
170. Fang EF, Kassahun H, Croteau DL, Scheibye-Knudsen M, Marosi K, Lu H, et al. NAD(+) Replenishment Improves Lifespan and Healthspan in Ataxia Telangiectasia Models via Mitophagy and DNA Repair. Cell Metab. 2016;24(4):566-81.
171. Zhang H, Ryu D, Wu Y, Gariani K, Wang X, Luan P, et al. NAD(+) repletion improves mitochondrial and stem cell function and enhances life span in mice. Science. 2016;352(6292):1436-43.
172. Gong B, Pan Y, Vempati P, Zhao W, Knable L, Ho L, et al. Nicotinamide riboside restores cognition through an upregulation of proliferator-activated receptor-gamma coactivator 1alpha regulated beta-secretase 1 degradation and mitochondrial gene expression in Alzheimer's mouse models. Neurobiol Aging. 2013;34(6):1581-8.
173. Gariani K, Menzies KJ, Ryu D, Wegner CJ, Wang X, Ropelle ER, et al. Eliciting the mitochondrial unfolded protein response by nicotinamide adenine dinucleotide repletion reverses fatty liver disease in mice. Hepatology. 2016;63(4):1190-204.
174. Brown KD, Maqsood S, Huang JY, Pan Y, Harkcom W, Li W, et al. Activation of SIRT3 by the NAD^+ precursor nicotinamide riboside protects from noise-induced hearing loss. Cell Metab. 2014;20(6):1059-68.
175. Martens CR, Denman BA, Mazzo MR, Armstrong ML, Reisdorph N, McQueen MB, et al. Chronic nicotinamide riboside supplementation is well-tolerated and elevates NAD(+) in healthy middle-aged and older adults. Nat Commun. 2018;9(1):1286.
176. Elhassan YS, Kluckova K, Fletcher RS, Schmidt MS, Garten A, Doig CL, et al. Nicotinamide Riboside Augments the Aged Human Skeletal Muscle NAD(+) Metabolome and Induces Transcriptomic and Anti-inflammatory Signatures. Cell Rep. 2019;28(7):1717-28 e6.
177. Dollerup OL, Christensen B, Svart M, Schmidt MS, Sulek K, Ringgaard S, et al. A randomized placebo-controlled clinical trial of nicotinamide riboside in obese men: safety, insulin-sensitivity, and lipid-mobilizing effects. Am J Clin Nutr. 2018;108(2):343-53.
178. Giroud-Gerbetant J, Joffraud M, Giner MP, Cercillieux A, Bartova S, Makarov MV, et al. A reduced form of nicotinamide riboside defines a new path for NAD(+) biosynthesis and acts as an orally bioavailable NAD(+) precursor. Mol Metab. 2019;30:192-202.
179. Caton PW, Kieswich J, Yaqoob MM, Holness MJ, Sugden MC. Nicotinamide mononucleotide protects against pro-inflammatory cytokine-mediated impairment of mouse islet function. Diabetologia. 2011;54(12):3083-92.

180. Yoshino J, Mills KF, Yoon MJ, Imai S. Nicotinamide mononucleotide, a key NAD(+) intermediate, treats the pathophysiology of diet- and age-induced diabetes in mice. Cell Metab. 2011;14(4):528-36.
181. Mills KF, Yoshida S, Stein LR, Grozio A, Kubota S, Sasaki Y, et al. Long-Term Administration of Nicotinamide Mononucleotide Mitigates Age-Associated Physiological Decline in Mice. Cell Metab. 2017;24(6):795-806.
182. Ramsey KM, Mills KF, Satoh A, Imai S. Age-associated loss of Sirt1-mediated enhancement of glucose-stimulated insulin secretion in beta cell-specific Sirt1-overexpressing (BESTO) mice. Aging Cell. 2008;7(1):78-88.
183. Peek CB, Affinati AH, Ramsey KM, Kuo HY, Yu W, Sena LA, et al. Circadian clock NAD+ cycle drives mitochondrial oxidative metabolism in mice. Science. 2013;342(6158):1243417.
184. Gomes AP, Price NL, Ling AJ, Moslehi JJ, Montgomery MK, Rajman L, et al. Declining NAD(+) induces a pseudohypoxic state disrupting nuclear-mitochondrial communication during aging. Cell. 2013;155(7):1624-38.
185. Sims CA, Guan Y, Mukherjee S, Singh K, Botolin P, Davila A, Jr., et al. Nicotinamide mononucleotide preserves mitochondrial function and increases survival in hemorrhagic shock. JCI Insight. 2018;3(17).
186. Lin JB, Kubota S, Ban N, Yoshida M, Santeford A, Sene A, et al. NAMPT-Mediated NAD(+) Biosynthesis Is Essential for Vision In Mice. Cell Rep. 2016;17(1):69-85.
187. Tarantini S, Valcarcel-Ares MN, Toth P, Yabluchanskiy A, Tucsek Z, Kiss T, et al. Nicotinamide mononucleotide (NMN) supplementation rescues cerebromicrovascular endothelial function and neurovascular coupling responses and improves cognitive function in aged mice. Redox Biol. 2019;24:101192.
188. Wang P, Li CG, Qi Z, Cui D, Ding S. Acute exercise stress promotes Ref1/Nrf2 signalling and increases mitochondrial antioxidant activity in skeletal muscle. Exp Physiol. 2016;101(3):410-20.
189. Irie J, Inagaki E, Fujita M, Nakaya H, Mitsuishi M, Yamaguchi S, et al. Effect of oral administration of nicotinamide mononucleotide on clinical parameters and nicotinamide metabolite levels in healthy Japanese men. Endocr J. 2019.
190. Felici R, Lapucci A, Cavone L, Pratesi S, Berlinguer-Palmini R, Chiarugi A. Pharmacological NAD-Boosting Strategies Improve Mitochondrial Homeostasis in Human Complex I-Mutant Fibroblasts. Mol Pharmacol. 2015;87(6):965-71.
191. Felici R, Lapucci A, Ramazzotti M, Chiarugi A. Insight into molecular and functional properties of NMNAT3 reveals new hints of NAD homeostasis within human mitochondria. PLoS One. 2013;8(10):e76938.
192. Nikiforov A, Kulikova V, Ziegler M. The human NAD metabolome: Functions, metabolism and compartmentalization. Crit Rev Biochem Mol Biol. 2015;50(4):284-97.
193. Grozio A, Mills KF, Yoshino J, Bruzzone S, Sociali G, Tokizane K, et al. Slc12a8 is a nicotinamide mononucleotide transporter. Nat Metab. 2019;1(1):47-57.
194. Schmidt MS, Brenner C. Absence of evidence that Slc12a8 encodes a nicotinamide mononucleotide transporter. Nature Metabolism. 2019;1(7):660-1.
195. Nakagawa T, Lomb DJ, Haigis MC, Guarente L. SIRT5 Deacetylates carbamoyl phosphate synthetase 1 and regulates the urea cycle. Cell. 2009;137(3):560-70.

196. Fjeld CC, Birdsong WT, Goodman RH. Differential binding of NAD+ and NADH allows the transcriptional corepressor carboxyl-terminal binding protein to serve as a metabolic sensor. Proc Natl Acad Sci U S A. 2003;100(16):9202-7.
197. Zhang T, Berrocal JG, Frizzell KM, Gamble MJ, DuMond ME, Krishnakumar R, et al. Enzymes in the NAD+ salvage pathway regulate SIRT1 activity at target gene promoters. J Biol Chem. 2009;284(30):20408-17.
198. Alano CC, Tran A, Tao R, Ying W, Karliner JS, Swanson RA. Differences among cell types in NAD(+) compartmentalization: a comparison of neurons, astrocytes, and cardiac myocytes. J Neurosci Res. 2007;85(15):3378-85.
199. Ryu KW, Nandu T, Kim J, Challa S, DeBerardinis RJ, Kraus WL. Metabolic regulation of transcription through compartmentalized NAD(+) biosynthesis. Science. 2018;360(6389).
200. Pittelli M, Formentini L, Faraco G, Lapucci A, Rapizzi E, Cialdai F, et al. Inhibition of nicotinamide phosphoribosyltransferase: cellular bioenergetics reveals a mitochondrial insensitive NAD pool. J Biol Chem. 2010;285(44):34106-14.
201. Cambronne XA, Stewart ML, Kim D, Jones-Brunette AM, Morgan RK, Farrens DL, et al. Biosensor reveals multiple sources for mitochondrial NAD(+). Science. 2016;352(6292):1474-7.
202. Dash RK, Li Y, Kim J, Beard DA, Saidel GM, Cabrera ME. Metabolic dynamics in skeletal muscle during acute reduction in blood flow and oxygen supply to mitochondria: in-silico studies using a multi-scale, top-down integrated model. PLoS One. 2008;3(9):e3168.
203. VanLinden MR, Dolle C, Pettersen IK, Kulikova VA, Niere M, Agrimi G, et al. Subcellular Distribution of NAD+ between Cytosol and Mitochondria Determines the Metabolic Profile of Human Cells. J Biol Chem. 2015;290(46):27644-59.
204. Veech RL, Eggleston LV, Krebs HA. The redox state of free nicotinamide-adenine dinucleotide phosphate in the cytoplasm of rat liver. Biochem J. 1969;115(4):609-19.
205. Mracek T, Drahota Z, Houstek J. The function and the role of the mitochondrial glycerol-3-phosphate dehydrogenase in mammalian tissues. Biochim Biophys Acta. 2013;1827(3):401-10.
206. McReynolds MR, Chellappa K, Baur JA. Age-related NAD(+) decline. Exp Gerontol. 2020;134:110888.
207. Dölle C, Niere M, Lohndal E, Ziegler M. Visualization of subcellular NAD pools and intra-organellar protein localization by poly-ADP-ribose formation. Cell Mol Life Sci. 2010;67(3):433-43.
208. VanLinden MR, Niere M, Nikiforov AA, Ziegler M, Dolle C. Compartment-Specific Poly-ADP-Ribose Formation as a Biosensor for Subcellular NAD Pools. Methods Mol Biol. 2017;1608:45-56.
209. Yu Q, Pourmandi N, Xue L, Gondrand C, Fabritz S, Bardy D, et al. A biosensor for measuring NAD+ levels at the point of care. Nature Metabolism. 2019;1(12):1219-25.
210. Sallin O, Reymond L, Gondrand C, Raith F, Koch B, Johnsson K. Semisynthetic biosensors for mapping cellular concentrations of nicotinamide adenine dinucleotides. eLife. 2018;7:e32638.
211. Elhassan YS, Philp AA, Lavery GG. Targeting NAD+ in Metabolic Disease: New Insights Into an Old Molecule. J Endocr Soc. 2017;1(7):816-35.
212. Imai S, Armstrong CM, Kaeberlein M, Guarente L. Transcriptional silencing and longevity protein Sir2 is an NAD-dependent histone deacetylase. Nature. 2000;403(6771):795-800.

213. Tissenbaum HA, Guarente L. Increased dosage of a sir-2 gene extends lifespan in Caenorhabditis elegans. Nature. 2001;410(6825):227-30.
214. Viswanathan M, Kim SK, Berdichevsky A, Guarente L. A role for SIR-2.1 regulation of ER stress response genes in determining C. elegans life span. Dev Cell. 2005;9(5):605-15.
215. Rogina B, Helfand SL. Sir2 mediates longevity in the fly through a pathway related to calorie restriction. Proc Natl Acad Sci U S A. 2004;101(45):15998-6003.
216. Burnett C, Valentini S, Cabreiro F, Goss M, Somogyvari M, Piper MD, et al. Absence of effects of Sir2 overexpression on lifespan in C. elegans and Drosophila. Nature. 2011;477(7365):482-5.
217. Kilic U, Gok O, Erenberk U, Dundaroz MR, Torun E, Kucukardali Y, et al. A remarkable age-related increase in SIRT1 protein expression against oxidative stress in elderly: SIRT1 gene variants and longevity in human. PLoS One. 2015;10(3):e0117954.
218. Grabowska W, Sikora E, Bielak-Zmijewska A. Sirtuins, a promising target in slowing down the ageing process. Biogerontology. 2017;18(4):447-76.
219. Li X. SIRT1 and energy metabolism. Acta biochimica et biophysica Sinica. 2013;45(1):51-60.
220. Canto C, Gerhart-Hines Z, Feige JN, Lagouge M, Noriega L, Milne JC, et al. AMPK regulates energy expenditure by modulating NAD+ metabolism and SIRT1 activity. Nature. 2009;458(7241):1056-60.
221. Erion DM, Yonemitsu S, Nie Y, Nagai Y, Gillum MP, Hsiao JJ, et al. SirT1 knockdown in liver decreases basal hepatic glucose production and increases hepatic insulin responsiveness in diabetic rats. Proc Natl Acad Sci U S A. 2009;106(27):11288-93.
222. Raynes R, Brunquell J, Westerheide SD. Stress Inducibility of SIRT1 and Its Role in Cytoprotection and Cancer. Genes Cancer. 2013;4(3-4):172-82.
223. Vazquez BN, Thackray JK, Simonet NG, Kane-Goldsmith N, Martinez-Redondo P, Nguyen T, et al. SIRT7 promotes genome integrity and modulates non-homologous end joining DNA repair. EMBO J. 2016;35(14):1488-503.
224. Inoue T, Hiratsuka M, Osaki M, Oshimura M. The molecular biology of mammalian SIRT proteins: SIRT2 in cell cycle regulation. Cell Cycle. 2007;6(9):1011-8.
225. Zhang W, Feng Y, Guo Q, Guo W, Xu H, Li X, et al. SIRT1 modulates cell cycle progression by regulating CHK2 acetylation-phosphorylation. Cell Death Differ. 2019.
226. Nakamura K, Kageyama S, Ke B, Fujii T, Sosa RA, Reed EF, et al. Sirtuin 1 attenuates inflammation and hepatocellular damage in liver transplant ischemia/Reperfusion: From mouse to human. Liver Transpl. 2017;23(10):1282-93.
227. Nakahata Y, Sahar S, Astarita G, Kaluzova M, Sassone-Corsi P. Circadian control of the NAD+ salvage pathway by CLOCK-SIRT1. Science. 2009;324(5927):654-7.
228. Ou X, Lee MR, Huang X, Messina-Graham S, Broxmeyer HE. SIRT1 positively regulates autophagy and mitochondria function in embryonic stem cells under oxidative stress. Stem Cells. 2014;32(5):1183-94.
229. Tong L, Denu JM. Function and metabolism of sirtuin metabolite O-acetyl-ADP-ribose. Biochim Biophys Acta. 2010;1804(8):1617-25.
230. Kupis W, Palyga J, Tomal E, Niewiadomska E. The role of sirtuins in cellular homeostasis. J Physiol Biochem. 2016;72(3):371-80.
231. Cuyas E, Verdura S, Llorach-Pares L, Fernandez-Arroyo S, Joven J, Martin-Castillo B, et al. Metformin Is a Direct SIRT1-Activating Compound: Computational Modeling and Experimental Validation. Front Endocrinol (Lausanne). 2018;9:657.

232. Caton PW, Nayuni NK, Kieswich J, Khan NQ, Yaqoob MM, Corder R. Metformin suppresses hepatic gluconeogenesis through induction of SIRT1 and GCN5. J Endocrinol. 2010;205(1):97-106.
233. Banks AS, Kon N, Knight C, Matsumoto M, Gutierrez-Juarez R, Rossetti L, et al. SirT1 gain of function increases energy efficiency and prevents diabetes in mice. Cell Metab. 2008;8(4):333-41.
234. Vila L, Roca C, Elias I, Casellas A, Lage R, Franckhauser S, et al. AAV-mediated Sirt1 overexpression in skeletal muscle activates oxidative capacity but does not prevent insulin resistance. Mol Ther Methods Clin Dev. 2016;5:16072.
235. Pfluger PT, Herranz D, Velasco-Miguel S, Serrano M, Tschop MH. Sirt1 protects against high-fat diet-induced metabolic damage. Proc Natl Acad Sci U S A. 2008;105(28):9793-8.
236. Nassir F, Arndt JJ, Johnson SA, Ibdah JA. Regulation of mitochondrial trifunctional protein modulates nonalcoholic fatty liver disease in mice. J Lipid Res. 2018;59(6):967-73.
237. Gerhart-Hines Z, Rodgers JT, Bare O, Lerin C, Kim SH, Mostoslavsky R, et al. Metabolic control of muscle mitochondrial function and fatty acid oxidation through SIRT1/PGC-1alpha. EMBO J. 2007;26(7):1913-23.
238. Lee D, Goldberg AL. SIRT1 protein, by blocking the activities of transcription factors FoxO1 and FoxO3, inhibits muscle atrophy and promotes muscle growth. J Biol Chem. 2013;288(42):30515-26.
239. Hirschey MD, Shimazu T, Huang JY, Schwer B, Verdin E. SIRT3 regulates mitochondrial protein acetylation and intermediary metabolism. Cold Spring Harb Symp Quant Biol. 2011;76:267-77.
240. Jing E, O'Neill BT, Rardin MJ, Kleinridders A, Ilkeyeva OR, Ussar S, et al. Sirt3 regulates metabolic flexibility of skeletal muscle through reversible enzymatic deacetylation. Diabetes. 2013;62(10):3404-17.
241. Cheng Y, Ren X, Gowda AS, Shan Y, Zhang L, Yuan YS, et al. Interaction of Sirt3 with OGG1 contributes to repair of mitochondrial DNA and protects from apoptotic cell death under oxidative stress. Cell Death Dis. 2013;4:e731.
242. Sundaresan NR, Gupta M, Kim G, Rajamohan SB, Isbatan A, Gupta MP. Sirt3 blocks the cardiac hypertrophic response by augmenting Foxo3a-dependent antioxidant defense mechanisms in mice. J Clin Invest. 2009;119(9):2758-71.
243. Giovannini L, Bianchi S. Role of nutraceutical SIRT1 modulators in AMPK and mTOR pathway: Evidence of a synergistic effect. Nutrition. 2017;34:82-96.
244. Palacios OM, Carmona JJ, Michan S, Chen KY, Manabe Y, Ward JL, 3rd, et al. Diet and exercise signals regulate SIRT3 and activate AMPK and PGC-1alpha in skeletal muscle. Aging. 2009;1(9):771-83.
245. Huang CC, Wang T, Tung YT, Lin WT. Effect of Exercise Training on Skeletal Muscle SIRT1 and PGC-1alpha Expression Levels in Rats of Different Age. Int J Med Sci. 2016;13(4):260-70.
246. Hou X, Xu S, Maitland-Toolan KA, Sato K, Jiang B, Ido Y, et al. SIRT1 regulates hepatocyte lipid metabolism through activating AMP-activated protein kinase. The Journal of biological chemistry. 2008;283(29):20015-26.
247. Lan F, Cacicedo JM, Ruderman N, Ido Y. SIRT1 modulation of the acetylation status, cytosolic localization, and activity of LKB1. Possible role in AMP-activated protein kinase activation. The Journal of biological chemistry. 2008;283(41):27628-35.

248. Canto C, Jiang LQ, Deshmukh AS, Mataki C, Coste A, Lagouge M, et al. Interdependence of AMPK and SIRT1 for metabolic adaptation to fasting and exercise in skeletal muscle. Cell Metab. 2010;11(3):213-9.
249. Boily G, Seifert EL, Bevilacqua L, He XH, Sabourin G, Estey C, et al. SirT1 regulates energy metabolism and response to caloric restriction in mice. PLoS One. 2008;3(3):e1759.
250. Kitada M, Ogura Y, Monno I, Koya D. Sirtuins and Type 2 Diabetes: Role in Inflammation, Oxidative Stress, and Mitochondrial Function. Front Endocrinol (Lausanne). 2019;10:187.
251. Bartoli-Leonard F, Wilkinson FL, Schiro A, Inglott FS, Alexander MY, Weston R. Suppression of SIRT1 in Diabetic Conditions Induces Osteogenic Differentiation of Human Vascular Smooth Muscle Cells via RUNX2 Signalling. Sci Rep. 2019;9(1):878.
252. Wu T, Liu YH, Fu YC, Liu XM, Zhou XH. Direct evidence of sirtuin downregulation in the liver of non-alcoholic fatty liver disease patients. Ann Clin Lab Sci. 2014;44(4):410-8.
253. Cerutti R, Pirinen E, Lamperti C, Marchet S, Sauve AA, Li W, et al. NAD(+)-dependent activation of Sirt1 corrects the phenotype in a mouse model of mitochondrial disease. Cell Metab. 2014;19(6):1042-9.
254. Canto C, Sauve AA, Bai P. Crosstalk between poly(ADP-ribose) polymerase and sirtuin enzymes. Mol Aspects Med. 2013;34(6):1168-201.
255. Morales J, Li L, Fattah FJ, Dong Y, Bey EA, Patel M, et al. Review of poly (ADP-ribose) polymerase (PARP) mechanisms of action and rationale for targeting in cancer and other diseases. Crit Rev Eukaryot Gene Expr. 2014;24(1):15-28.
256. Liu Y, Xu X, Yang H, Xu E, Wu S, Wei W, et al. Analysis of poly(ADP-ribose) polymerase-1 by enzyme-initiated auto-PARylation-controlled aggregation of hemin-graphene nanocomposites. Analyst. 2018;143(11):2501-7.
257. Bai P, Canto C, Oudart H, Brunyanszki A, Cen Y, Thomas C, et al. PARP-1 inhibition increases mitochondrial metabolism through SIRT1 activation. Cell Metab. 2011;13(4):461-8.
258. Pillai JB, Isbatan A, Imai S, Gupta MP. Poly(ADP-ribose) polymerase-1-dependent cardiac myocyte cell death during heart failure is mediated by NAD+ depletion and reduced Sir2alpha deacetylase activity. J Biol Chem. 2005;280(52):43121-30.
259. Kolthur-Seetharam U, Dantzer F, McBurney MW, de Murcia G, Sassone-Corsi P. Control of AIF-mediated cell death by the functional interplay of SIRT1 and PARP-1 in response to DNA damage. Cell Cycle. 2006;5(8):873-7.
260. Szanto M, Rutkai I, Hegedus C, Czikora A, Rozsahegyi M, Kiss B, et al. Poly(ADP-ribose) polymerase-2 depletion reduces doxorubicin-induced damage through SIRT1 induction. Cardiovasc Res. 2011;92(3):430-8.
261. Guarente L. Linking DNA damage, NAD(+)/SIRT1, and aging. Cell Metab. 2014;20(5):706-7.
262. Braidy N, Guillemin GJ, Mansour H, Chan-Ling T, Poljak A, Grant R. Age related changes in NAD+ metabolism oxidative stress and Sirt1 activity in wistar rats. PLoS One. 2011;6(4):e19194.
263. Massudi H, Grant R, Braidy N, Guest J, Farnsworth B, Guillemin GJ. Age-associated changes in oxidative stress and NAD+ metabolism in human tissue. PLoS One. 2012;7(7):e42357.
264. Pirinen E, Canto C, Jo YS, Morato L, Zhang H, Menzies KJ, et al. Pharmacological Inhibition of poly(ADP-ribose) polymerases improves fitness and mitochondrial function in skeletal muscle. Cell Metab. 2014;19(6):1034-41.

265. Rajamohan SB, Pillai VB, Gupta M, Sundaresan NR, Birukov KG, Samant S, et al. SIRT1 promotes cell survival under stress by deacetylation-dependent deactivation of poly(ADP-ribose) polymerase 1. Mol Cell Biol. 2009;29(15):4116-29.
266. Ito S, Murphy CG, Doubrovina E, Jasin M, Moynahan ME. PARP Inhibitors in Clinical Use Induce Genomic Instability in Normal Human Cells. PLoS One. 2016;11(7):e0159341.
267. Palazzo L, Mikolčević P, Mikoč A, Ahel I. ADP-ribosylation signalling and human disease. Open Biol. 2019;9(4):190041.
268. Leutert M, Menzel S, Braren R, Rissiek B, Hopp AK, Nowak K, et al. Proteomic Characterization of the Heart and Skeletal Muscle Reveals Widespread Arginine ADP-Ribosylation by the ARTC1 Ectoenzyme. Cell Rep. 2018;24(7):1916-29.e5.
269. Hong S, Schwarz N, Brass A, Seman M, Haag F, Koch-Nolte F, et al. Differential regulation of P2X7 receptor activation by extracellular nicotinamide adenine dinucleotide and ecto-ADP-ribosyltransferases in murine macrophages and T cells. J Immunol. 2009;183(1):578-92.
270. Fabrizio G, Di Paola S, Stilla A, Giannotta M, Ruggiero C, Menzel S, et al. ARTC1-mediated ADP-ribosylation of GRP78/BiP: a new player in endoplasmic-reticulum stress responses. Cellular and Molecular Life Sciences. 2015;72(6):1209-25.
271. Martello R, Leutert M, Jungmichel S, Bilan V, Larsen SC, Young C, et al. Proteome-wide identification of the endogenous ADP-ribosylome of mammalian cells and tissue. Nature Communications. 2016;7(1):12917.
272. Matic I, Ahel I, Hay RT. Reanalysis of phosphoproteomics data uncovers ADP-ribosylation sites. Nat Methods. 2012;9(8):771-2.
273. Zolkiewska A, Moss J. Processing of ADP-ribosylated integrin alpha 7 in skeletal muscle myotubes. J Biol Chem. 1995;270(16):9227-33.
274. Zolkiewska A, Moss J. The alpha 7 integrin as a target protein for cell surface mono-ADP-ribosylation in muscle cells. Adv Exp Med Biol. 1997;419:297-303.
275. Zolkiewska A. Ecto-ADP-ribose transferases: cell-surface response to local tissue injury. Physiology (Bethesda). 2005;20:374-81.
276. Zhao Z, Gruszczynska-Biegala J, Zolkiewska A. ADP-ribosylation of integrin alpha7 modulates the binding of integrin alpha7beta1 to laminin. Biochem J. 2005;385(Pt 1):309-17.
277. Zolkiewska A, Moss J. Integrin alpha 7 as substrate for a glycosylphosphatidylinositol-anchored ADP-ribosyltransferase on the surface of skeletal muscle cells. J Biol Chem. 1993;268(34):25273-6.
278. Quarona V, Zaccarello G, Chillemi A, Brunetti E, Singh VK, Ferrero E, et al. CD38 and CD157: a long journey from activation markers to multifunctional molecules. Cytometry B Clin Cytom. 2013;84(4):207-17.
279. De Flora A, Guida L, Franco L, Zocchi E, Bruzzone S, Benatti U, et al. CD38 and ADP-ribosyl cyclase catalyze the synthesis of a dimeric ADP-ribose that potentiates the calcium-mobilizing activity of cyclic ADP-ribose. J Biol Chem. 1997;272(20):12945-51.
280. de Toledo FG, Cheng J, Liang M, Chini EN, Dousa TP. ADP-Ribosyl cyclase in rat vascular smooth muscle cells: properties and regulation. Circ Res. 2000;86(11):1153-9.
281. Chini EN. CD38 as a regulator of cellular NAD: a novel potential pharmacological target for metabolic conditions. Curr Pharm Des. 2009;15(1):57-63.
282. Escande C, Nin V, Price NL, Capellini V, Gomes AP, Barbosa MT, et al. Flavonoid apigenin is an inhibitor of the NAD+ ase CD38: implications for cellular NAD+ metabolism, protein acetylation, and treatment of metabolic syndrome. Diabetes. 2013;62(4):1084-93.

283. Barbosa MT, Soares SM, Novak CM, Sinclair D, Levine JA, Aksoy P, et al. The enzyme CD38 (a NAD glycohydrolase, EC 3.2.2.5) is necessary for the development of diet-induced obesity. FASEB J. 2007;21(13):3629-39.
284. Camacho-Pereira J, Tarrago MG, Chini CCS, Nin V, Escande C, Warner GM, et al. CD38 Dictates Age-Related NAD Decline and Mitochondrial Dysfunction through an SIRT3-Dependent Mechanism. Cell Metab. 2016;23(6):1127-39.
285. Sauve AA, Schramm VL. SIR2: the biochemical mechanism of NAD(+)-dependent protein deacetylation and ADP-ribosyl enzyme intermediates. Curr Med Chem. 2004;11(7):807-26.
286. Jin J, Bai L, Johnson DS, Fulbright RM, Kireeva ML, Kashlev M, et al. Synergistic action of RNA polymerases in overcoming the nucleosomal barrier. Nat Struct Mol Biol. 2010;17(6):745-52.
287. DiLoreto R, Murphy CT. The cell biology of aging. Mol Biol Cell. 2015;26(25):4524-31.
288. Trounce I, Byrne E, Marzuki S. Decline in skeletal muscle mitochondrial respiratory chain function: possible factor in ageing. Lancet. 1989;1(8639):637-9.
289. Okabe K, Yaku K, Tobe K, Nakagawa T. Implications of altered NAD metabolism in metabolic disorders. J Biomed Sci. 2019;26(1):34-.
290. Dominguez LJ, Barbagallo M. The biology of the metabolic syndrome and aging. Curr Opin Clin Nutr Metab Care. 2016;19(1):5-11.
291. Gong H, Pang J, Han Y, Dai Y, Dai D, Cai J, et al. Age-dependent tissue expression patterns of Sirt1 in senescence-accelerated mice. Mol Med Rep. 2014;10(6):3296-302.
292. Mouchiroud L, Houtkooper RH, Moullan N, Katsyuba E, Ryu D, Canto C, et al. The NAD(+)/Sirtuin Pathway Modulates Longevity through Activation of Mitochondrial UPR and FOXO Signaling. Cell. 2013;154(2):430-41.
293. Aksoy P, White TA, Thompson M, Chini EN. Regulation of intracellular levels of NAD: a novel role for CD38. Biochem Biophys Res Commun. 2006;345(4):1386-92.
294. Deschenes MR. Effects of aging on muscle fibre type and size. Sports Med. 2004;34(12):809-24.
295. Brown JC, Harhay MO, Harhay MN. Sarcopenia and mortality among a population-based sample of community-dwelling older adults. J Cachexia Sarcopenia Muscle. 2016;7(3):290-8.
296. Hunter GR, Singh H, Carter SJ, Bryan DR, Fisher G. Sarcopenia and Its Implications for Metabolic Health. J Obes. 2019;2019:8031705-.
297. Brook MS, Wilkinson DJ, Mitchell WK, Lund JN, Phillips BE, Szewczyk NJ, et al. Synchronous deficits in cumulative muscle protein synthesis and ribosomal biogenesis underlie age-related anabolic resistance to exercise in humans. J Physiol. 2016;594(24):7399-417.
298. Altun M, Besche HC, Overkleeft HS, Piccirillo R, Edelmann MJ, Kessler BM, et al. Muscle wasting in aged, sarcopenic rats is associated with enhanced activity of the ubiquitin proteasome pathway. J Biol Chem. 2010;285(51):39597-608.
299. Chakkalakal JV, Jones KM, Basson MA, Brack AS. The aged niche disrupts muscle stem cell quiescence. Nature. 2012;490(7420):355-60.
300. Bernet JD, Doles JD, Hall JK, Kelly Tanaka K, Carter TA, Olwin BB. p38 MAPK signaling underlies a cell-autonomous loss of stem cell self-renewal in skeletal muscle of aged mice. Nat Med. 2014;20(3):265-71.
301. Brack AS, Bildsoe H, Hughes SM. Evidence that satellite cell decrement contributes to preferential decline in nuclear number from large fibres during murine age-related muscle atrophy. J Cell Sci. 2005;118(Pt 20):4813-21.

302. Atherton PJ, Etheridge T, Watt PW, Wilkinson D, Selby A, Rankin D, et al. Muscle full effect after oral protein: time-dependent concordance and discordance between human muscle protein synthesis and mTORC1 signaling. Am J Clin Nutr. 2010;92(5):1080-8.
303. Moro T, Ebert SM, Adams CM, Rasmussen BB. Amino Acid Sensing in Skeletal Muscle. Trends Endocrinol Metab. 2016;27(11):796-806.
304. Wahlin-Larsson B, Wilkinson DJ, Strandberg E, Hosford-Donovan A, Atherton PJ, Kadi F. Mechanistic Links Underlying the Impact of C-Reactive Protein on Muscle Mass in Elderly. Cell Physiol Biochem. 2017;44(1):267-78.
305. Marcus RL, Addison O, Kidde JP, Dibble LE, Lastayo PC. Skeletal muscle fat infiltration: impact of age, inactivity, and exercise. J Nutr Health Aging. 2010;14(5):362-6.
306. Carter HN, Kim Y, Erlich AT, Zarrin-Khat D, Hood DA. Autophagy and mitophagy flux in young and aged skeletal muscle following chronic contractile activity. J Physiol. 2018;596(16):3567-84.
307. Joseph AM, Malamo AG, Silvestre J, Wawrzyniak N, Carey-Love S, Nguyen LM, et al. Short-term caloric restriction, resveratrol, or combined treatment regimens initiated in late-life alter mitochondrial protein expression profiles in a fiber-type specific manner in aged animals. Exp Gerontol. 2013;48(9):858-68.
308. Dirks AJ, Leeuwenburgh C. Aging and lifelong calorie restriction result in adaptations of skeletal muscle apoptosis repressor, apoptosis-inducing factor, X-linked inhibitor of apoptosis, caspase-3, and caspase-12. Free Radic Biol Med. 2004;36(1):27-39.
309. Hepple RT, Qin M, Nakamoto H, Goto S. Caloric restriction optimizes the proteasome pathway with aging in rat plantaris muscle: implications for sarcopenia. Am J Physiol Regul Integr Comp Physiol. 2008;295(4):R1231-7.
310. White AT, Schenk S. NAD(+)/NADH and skeletal muscle mitochondrial adaptations to exercise. Am J Physiol Endocrinol Metab. 2012;303(3):E308-21.
311. Price NL, Gomes AP, Ling AJY, Duarte FV, Martin-Montalvo A, North BJ, et al. SIRT1 is required for AMPK activation and the beneficial effects of resveratrol on mitochondrial function. Cell Metab. 2012;15(5):675-90.
312. Rezende LFMd, Rey-López JP, Matsudo VKR, Luiz OdC. Sedentary behavior and health outcomes among older adults: a systematic review. BMC Public Health. 2014;14(1):333.
313. Han TS, Tajar A, Lean ME. Obesity and weight management in the elderly. Br Med Bull. 2011;97:169-96.
314. Liu L, Su X, Quinn WJ, 3rd, Hui S, Krukenberg K, Frederick DW, et al. Quantitative Analysis of NAD Synthesis-Breakdown Fluxes. Cell Metab. 2018;27(5):1067-80 e5.
315. Frederick DW, Davis JG, Davila A, Jr., Agarwal B, Michan S, Puchowicz MA, et al. Increasing NAD synthesis in muscle via nicotinamide phosphoribosyltransferase is not sufficient to promote oxidative metabolism. J Biol Chem. 2015;290(3):1546-58.
316. Brouwers B, Stephens NA, Costford SR, Hopf ME, Ayala JE, Yi F, et al. Elevated Nicotinamide Phosphoribosyl Transferase in Skeletal Muscle Augments Exercise Performance and Mitochondrial Respiratory Capacity Following Exercise Training. Frontiers in physiology. 2018;9:704-.
317. Kim JS, Yoon CS, Park DR. NAMPT regulates mitochondria biogenesis via NAD metabolism and calcium binding proteins during skeletal muscle contraction. J Exerc Nutrition Biochem. 2014;18(3):259-66.

318. Costford SR, Brouwers B, Hopf ME, Sparks LM, Dispagna M, Gomes AP, et al. Skeletal muscle overexpression of nicotinamide phosphoribosyl transferase in mice coupled with voluntary exercise augments exercise endurance. Mol Metab. 2017.
319. Costford SR, Bajpeyi S, Pasarica M, Albarado DC, Thomas SC, Xie H, et al. Skeletal muscle NAMPT is induced by exercise in humans. Am J Physiol Endocrinol Metab. 2010;298(1):E117-26.
320. Deloux R, Tannous C, Ferry A, Li Z, Mericskay M. Aged Nicotinamide Riboside Kinase 2 Deficient Mice Present an Altered Response to Endurance Exercise Training. Front Physiol. 2018;9:1290.
321. Ryu D, Zhang H, Ropelle ER, Sorrentino V, Mazala DA, Mouchiroud L, et al. NAD+ repletion improves muscle function in muscular dystrophy and counters global PARylation. Sci Transl Med. 2016;8(361):361ra139.
322. Dolle C, Ziegler M. Application of a coupled enzyme assay to characterize nicotinamide riboside kinases. Anal Biochem. 2009;385(2):377-9.
323. Sambeat A, Ratajczak J, Joffraud M, Sanchez-Garcia JL, Giner MP, Valsesia A, et al. Endogenous nicotinamide riboside metabolism protects against diet-induced liver damage. Nature Communications. 2019;10(1):4291.
324. Lavery GG, Walker EA, Turan N, Rogoff D, Ryder JW, Shelton JM, et al. Deletion of hexose-6-phosphate dehydrogenase activates the unfolded protein response pathway and induces skeletal myopathy. J Biol Chem. 2008;283(13):8453-61.
325. Doig CL, Zelinska AE, Oakey LA, Fletcher RS, El Hassan Y, Garten A, et al. Induction of the nicotinamide riboside kinase NAD⁺ salvage pathway in skeletal muscle of H6PDH KO mice. bioRxiv. 2019:567297.
326. Aguilar CA, Shcherbina A, Ricke DO, Pop R, Carrigan CT, Gifford CA, et al. In vivo Monitoring of Transcriptional Dynamics After Lower-Limb Muscle Injury Enables Quantitative Classification of Healing. Sci Rep. 2015;5:13885.
327. Xu W, Barrientos T, Mao L, Rockman HA, Sauve AA, Andrews NC. Lethal Cardiomyopathy in Mice Lacking Transferrin Receptor in the Heart. Cell Rep. 2015;13(3):533-45.
328. Diguet N, Trammell SAJ, Tannous C, Deloux R, Piquereau J, Mougenot N, et al. Nicotinamide Riboside Preserves Cardiac Function in a Mouse Model of Dilated Cardiomyopathy. Circulation. 2018;137(21):2256-73.
329. Sasaki Y, Araki T, Milbrandt J. Stimulation of nicotinamide adenine dinucleotide biosynthetic pathways delays axonal degeneration after axotomy. J Neurosci. 2006;26(33):8484-91.
330. Imai S. "Clocks" in the NAD World: NAD as a metabolic oscillator for the regulation of metabolism and aging. Biochim Biophys Acta. 2010;1804(8):1584-90.
331. Menet JS, Pescatore S, Rosbash M. CLOCK:BMAL1 is a pioneer-like transcription factor. Genes Dev. 2014;28(1):8-13.
332. Nakahata Y, Kaluzova M, Grimaldi B, Sahar S, Hirayama J, Chen D, et al. The NAD+-dependent deacetylase SIRT1 modulates CLOCK-mediated chromatin remodeling and circadian control. Cell. 2008;134(2):329-40.
333. Ramsey KM, Yoshino J, Brace CS, Abrassart D, Kobayashi Y, Marcheva B, et al. Circadian clock feedback cycle through NAMPT-mediated NAD+ biosynthesis. Science. 2009;324(5927):651-4.
334. Trott AJ, Menet JS. Regulation of circadian clock transcriptional output by CLOCK:BMAL1. PLoS Genet. 2018;14(1):e1007156.

335. Eckel-Mahan KL, Patel VR, de Mateo S, Orozco-Solis R, Ceglia NJ, Sahar S, et al. Reprogramming of the circadian clock by nutritional challenge. Cell. 2013;155(7):1464-78.
336. Mauvoisin D, Atger F, Dayon L, Nunez Galindo A, Wang J, Martin E, et al. Circadian and Feeding Rhythms Orchestrate the Diurnal Liver Acetylome. Cell Rep. 2017;20(7):1729-43.
337. Schiaffino S, Blaauw B, Dyar KA. The functional significance of the skeletal muscle clock: lessons from Bmal1 knockout models. Skelet Muscle. 2016;6:33.
338. Liu C, Li S, Liu T, Borjigin J, Lin JD. Transcriptional coactivator PGC-1alpha integrates the mammalian clock and energy metabolism. Nature. 2007;447(7143):477-81.
339. Yang G, Jia Z, Aoyagi T, McClain D, Mortensen RM, Yang T. Systemic PPARgamma deletion impairs circadian rhythms of behavior and metabolism. PLoS One. 2012;7(8):e38117.
340. Dyar KA, Ciciliot S, Wright LE, Bienso RS, Tagliazucchi GM, Patel VR, et al. Muscle insulin sensitivity and glucose metabolism are controlled by the intrinsic muscle clock. Mol Metab. 2014;3(1):29-41.
341. Li J, Mayne R, Wu C. A novel muscle-specific beta 1 integrin binding protein (MIBP) that modulates myogenic differentiation. J Cell Biol. 1999;147(7):1391-8.
342. Li J, Rao H, Burkin D, Kaufman SJ, Wu C. The muscle integrin binding protein (MIBP) interacts with alpha7beta1 integrin and regulates cell adhesion and laminin matrix deposition. Dev Biol. 2003;261(1):209-19.
343. Mahmassani ZS, Son K, Pincu Y, Munroe M, Drnevich J, Chen J, et al. alpha7beta1 Integrin regulation of gene transcription in skeletal muscle following an acute bout of eccentric exercise. Am J Physiol Cell Physiol. 2017;312(5):C638-c50.
344. Goody MF, Kelly MW, Lessard KN, Khalil A, Henry CA. Nrk2b-mediated NAD+ production regulates cell adhesion and is required for muscle morphogenesis in vivo: Nrk2b and NAD+ in muscle morphogenesis. Dev Biol. 2010;344(2):809-26.
345. Goody MF, Kelly MW, Reynolds CJ, Khalil A, Crawford BD, Henry CA. NAD plus Biosynthesis Ameliorates a Zebrafish Model of Muscular Dystrophy. Plos Biol. 2012;10(10).
346. Hamilton DL, Abremski K. Site-specific recombination by the bacteriophage P1 lox-Cre system. Cre-mediated synapsis of two lox sites. J Mol Biol. 1984;178(2):481-6.
347. Feil S, Valtcheva N, Feil R. Inducible Cre mice. Methods Mol Biol. 2009;530:343-63.
348. Van Deursen J, Fornerod M, Van Rees B, Grosveld G. Cre-mediated site-specific translocation between nonhomologous mouse chromosomes. Proc Natl Acad Sci U S A. 1995;92(16):7376-80.
349. Sternberg N, Hamilton D, Austin S, Yarmolinsky M, Hoess R. Site-specific recombination and its role in the life cycle of bacteriophage P1. Cold Spring Harb Symp Quant Biol. 1981;45 Pt 1:297-309.
350. Kim H, Kim M, Im SK, Fang S. Mouse Cre-LoxP system: general principles to determine tissue-specific roles of target genes. Lab Anim Res. 2018;34(4):147-59.
351. Brennan KJ, Hardeman EC. Quantitative analysis of the human alpha-skeletal actin gene in transgenic mice. J Biol Chem. 1993;268(1):719-25.
352. Miniou P, Tiziano D, Frugier T, Roblot N, Le Meur M, Melki J. Gene targeting restricted to mouse striated muscle lineage. Nucleic Acids Res. 1999;27(19):e27.
353. Lanza IR, Nair KS. Functional assessment of isolated mitochondria in vitro. Methods Enzymol. 2009;457:349-72.
354. Doerrier C, Garcia-Souza LF, Krumschnabel G, Wohlfarter Y, Mészáros AT, Gnaiger E. High-Resolution FluoRespirometry and OXPHOS Protocols for Human Cells, Permeabilized Fibers

from Small Biopsies of Muscle, and Isolated Mitochondria. Methods Mol Biol. 2018;1782:31-70.
355. Jamur MC, Oliver C. Permeabilization of cell membranes. Methods Mol Biol. 2010;588:63-6.
356. Grivennikova VG, Kapustin AN, Vinogradov AD. Catalytic activity of NADH-ubiquinone oxidoreductase (complex I) in intact mitochondria. evidence for the slow active/inactive transition. J Biol Chem. 2001;276(12):9038-44.
357. Portoles T, Pitarch E, Lopez FJ, Hernandez F, Niessen WM. Use of soft and hard ionization techniques for elucidation of unknown compounds by gas chromatography/time-of-flight mass spectrometry. Rapid Commun Mass Spectrom. 2011;25(11):1589-99.
358. Beale DJ, Pinu FR, Kouremenos KA, Poojary MM, Narayana VK, Boughton BA, et al. Review of recent developments in GC–MS approaches to metabolomics-based research. Metabolomics. 2018;14(11):152.
359. Perez ER, Knapp JA, Horn CK, Stillman SL, Evans JE, Arfsten DP. Comparison of LC-MS-MS and GC-MS Analysis of Benzodiazepine Compounds Included in the Drug Demand Reduction Urinalysis Program. J Anal Toxicol. 2016;40(3):201-7.
360. Mtaweh H, Tuira L, Floh AA, Parshuram CS. Indirect Calorimetry: History, Technology, and Application. Front Pediatr. 2018;6:257-.
361. Andrikopoulos S, Blair AR, Deluca N, Fam BC, Proietto J. Evaluating the glucose tolerance test in mice. Am J Physiol Endocrinol Metab. 2008;295(6):E1323-32.
362. Fernandez-Verdejo R, Ravussin E, Speakman JR, Galgani JE. Progress and challenges in analyzing rodent energy expenditure. Nat Methods. 2019.
363. Song AJ, Palmiter RD. Detecting and Avoiding Problems When Using the Cre-lox System. Trends Genet. 2018;34(5):333-40.
364. Castro B, Kuang S. Evaluation of Muscle Performance in Mice by Treadmill Exhaustion Test and Whole-limb Grip Strength Assay. Bio Protoc. 2017;7(8).
365. Conner JD, Wolden-Hanson T, Quinn LS. Assessment of murine exercise endurance without the use of a shock grid: an alternative to forced exercise. J Vis Exp. 2014(90):e51846.
366. Reneker LW, Chen H, Overbeek PA. Activation of unfolded protein response in transgenic mouse lenses. Invest Ophthalmol Vis Sci. 2011;52(5):2100-8.
367. Cai Y, Arikkath J, Yang L, Guo ML, Periyasamy P, Buch S. Interplay of endoplasmic reticulum stress and autophagy in neurodegenerative disorders. Autophagy. 2016;12(2):225-44.
368. Chen Y, Liang Y, Hu T, Wei R, Cai C, Wang P, et al. Endogenous Nampt upregulation is associated with diabetic nephropathy inflammatory-fibrosis through the NF-kappaB p65 and Sirt1 pathway; NMN alleviates diabetic nephropathy inflammatory-fibrosis by inhibiting endogenous Nampt. Exp Ther Med. 2017;14(5):4181-93.
369. Augusto V, Padovani C, Eduardo G, Campos R. Skeletal muscle fiber types in C57BL6J mice. J morphol Sci. 2004;21:89-94.
370. Oakey LA, Fletcher RS, Elhassan YS, Cartwright DM, Doig CL, Garten A, et al. Metabolic tracing reveals novel adaptations to skeletal muscle cell energy production pathways in response to NAD (+) depletion. Wellcome Open Res. 2018;3:147.
371. Owen OE, Kalhan SC, Hanson RW. The key role of anaplerosis and cataplerosis for citric acid cycle function. J Biol Chem. 2002;277(34):30409-12.
372. Vandekerckhove J, Bugaisky G, Buckingham M. Simultaneous expression of skeletal muscle and heart actin proteins in various striated muscle tissues and cells. A quantitative determination of the two actin isoforms. J Biol Chem. 1986;261(4):1838-43.

373. Al Tanoury Z, Rao J, Tassy O, Gobert B, Gapon S, Garnier JM, et al. Differentiation of the human PAX7-positive myogenic precursors/satellite cell lineage in vitro. Development. 2020;147(12).
374. Tannous C, Deloux R, Karoui A, Mougenot N, Burkin D, Blanc J, et al. NMRK2 Gene Is Upregulated in Dilated Cardiomyopathy and Required for Cardiac Function and NAD Levels during Aging. Int J Mol Sci. 2021;22(7).
375. Airhart SE, Shireman LM, Risler LJ, Anderson GD, Nagana Gowda GA, Raftery D, et al. An open-label, non-randomized study of the pharmacokinetics of the nutritional supplement nicotinamide riboside (NR) and its effects on blood NAD+ levels in healthy volunteers. PLoS One. 2017;12(12):e0186459.
376. Rowen JW, Kornberg A. The phosphorolysis of nicotinamide riboside. J Biol Chem. 1951;193(2):497-507.
377. Graham TE, Sinclair DG, Chapler CK. Metabolic intermediates and lactate diffusion in active dog skeletal muscle. Am J Physiol. 1976;231(3):766-71.
378. Schiotz Thorud HM, Lunde PK, Nicolaysen G, Nicolaysen A, Helge JW, Nilsson GE, et al. Muscle dysfunction during exercise of a single skeletal muscle in rats with congestive heart failure is not associated with reduced muscle blood supply. Acta Physiol Scand. 2004;181(2):173-81.
379. Sahlin K, Katz A, Henriksson J. Redox state and lactate accumulation in human skeletal muscle during dynamic exercise. The Biochemical journal. 1987;245(2):551-6.
380. Moxnes JF, Sandbakk Ø. The kinetics of lactate production and removal during whole-body exercise. Theor Biol Med Model. 2012;9:7-.
381. Cynamon MH, Sorg TB, Patapow A. Utilization and metabolism of NAD by Haemophilus parainfluenzae. J Gen Microbiol. 1988;134(10):2789-99.
382. Palacios OM, Carmona JJ, Michan S, Chen KY, Manabe Y, Ward JL, 3rd, et al. Diet and exercise signals regulate SIRT3 and activate AMPK and PGC-1alpha in skeletal muscle. Aging (Albany NY). 2010;1(9):771-83.
383. Bournat JC, Brown CW. Mitochondrial dysfunction in obesity. Curr Opin Endocrinol Diabetes Obes. 2010;17(5):446-52.
384. Chung HY, Kim DH, Lee EK, Chung KW, Chung S, Lee B, et al. Redefining Chronic Inflammation in Aging and Age-Related Diseases: Proposal of the Senoinflammation Concept. Aging Dis. 2019;10(2):367-82.
385. Kaila B, Raman M. Obesity: a review of pathogenesis and management strategies. Can J Gastroenterol. 2008;22(1):61-8.
386. Stenholm S, Harris TB, Rantanen T, Visser M, Kritchevsky SB, Ferrucci L. Sarcopenic obesity: definition, cause and consequences. Curr Opin Clin Nutr Metab Care. 2008;11(6):693-700.
387. Yaku K, Okabe K, Nakagawa T. Simultaneous measurement of NAD metabolome in aged mice tissue using liquid chromatography tandem-mass spectrometry. Biomed Chromatogr. 2018;32(6):e4205.
388. Tang BL. Sirt1 and the Mitochondria. Mol Cells. 2016;39(2):87-95.
389. Fang EF, Scheibye-Knudsen M, Brace LE, Kassahun H, SenGupta T, Nilsen H, et al. Defective mitophagy in XPA via PARP-1 hyperactivation and NAD(+)/SIRT1 reduction. Cell. 2014;157(4):882-96.
390. Lagouge M, Larsson NG. The role of mitochondrial DNA mutations and free radicals in disease and ageing. J Intern Med. 2013;273(6):529-43.

391. Langelier MF, Pascal JM. PARP-1 mechanism for coupling DNA damage detection to poly(ADP-ribose) synthesis. Curr Opin Struct Biol. 2013;23(1):134-43.
392. Hocsak E, Szabo V, Kalman N, Antus C, Cseh A, Sumegi K, et al. PARP inhibition protects mitochondria and reduces ROS production via PARP-1-ATF4-MKP-1-MAPK retrograde pathway. Free Radic Biol Med. 2017;108:770-84.
393. Jackson JR, Ryan MJ, Alway SE. Long-term supplementation with resveratrol alleviates oxidative stress but does not attenuate sarcopenia in aged mice. J Gerontol A Biol Sci Med Sci. 2011;66(7):751-64.
394. Del Campo A, Contreras-Hernandez I, Castro-Sepulveda M, Campos CA, Figueroa R, Tevy MF, et al. Muscle function decline and mitochondria changes in middle age precede sarcopenia in mice. Aging (Albany NY). 2018;10(1):34-55.
395. Myers MJ, Shepherd DL, Durr AJ, Stanton DS, Mohamed JS, Hollander JM, et al. The role of SIRT1 in skeletal muscle function and repair of older mice. J Cachexia Sarcopenia Muscle. 2019;10(4):929-49.
396. Graber TG, Kim JH, Grange RW, McLoon LK, Thompson LV. C57BL/6 life span study: age-related declines in muscle power production and contractile velocity. Age (Dordr). 2015;37(3):9773.
397. Felsted RL, Chaykin S. N1-methylnicotinamide oxidation in a number of mammals. J Biol Chem. 1967;242(6):1274-9.
398. Rogatzki MJ, Ferguson BS, Goodwin ML, Gladden LB. Lactate is always the end product of glycolysis. Frontiers in neuroscience. 2015;9:22-.
399. Chevanne M, Calia C, Zampieri M, Cecchinelli B, Caldini R, Monti D, et al. Oxidative DNA damage repair and parp 1 and parp 2 expression in Epstein-Barr virus-immortalized B lymphocyte cells from young subjects, old subjects, and centenarians. Rejuvenation Res. 2007;10(2):191-204.
400. Elibol B, Kilic U. High Levels of SIRT1 Expression as a Protective Mechanism Against Disease-Related Conditions. Front Endocrinol (Lausanne). 2018;9:614.
401. Gurd BJ, Yoshida Y, McFarlan JT, Holloway GP, Moyes CD, Heigenhauser GJ, et al. Nuclear SIRT1 activity, but not protein content, regulates mitochondrial biogenesis in rat and human skeletal muscle. Am J Physiol Regul Integr Comp Physiol. 2011;301(1):R67-75.
402. Kincaid B, Bossy-Wetzel E. Forever young: SIRT3 a shield against mitochondrial meltdown, aging, and neurodegeneration. Frontiers in Aging Neuroscience. 2013;5(48).
403. Hirschey MD, Shimazu T, Jing E, Grueter CA, Collins AM, Aouizerat B, et al. SIRT3 deficiency and mitochondrial protein hyperacetylation accelerate the development of the metabolic syndrome. Mol Cell. 2011;44(2):177-90.
404. Kwon Y, Kim J, Lee CY, Kim H. Expression of SIRT1 and SIRT3 varies according to age in mice. Anat Cell Biol. 2015;48(1):54-61.
405. Guarente L. Calorie restriction and sirtuins revisited. Genes Dev. 2013;27(19):2072-85.
406. Vargas-Ortiz K, Pérez-Vázquez V, Macías-Cervantes MH. Exercise and Sirtuins: A Way to Mitochondrial Health in Skeletal Muscle. International journal of molecular sciences. 2019;20(11):2717.
407. Chen D, Bruno J, Easlon E, Lin SJ, Cheng HL, Alt FW, et al. Tissue-specific regulation of SIRT1 by calorie restriction. Genes Dev. 2008;22(13):1753-7.

408. Gulshan M, Yaku K, Okabe K, Mahmood A, Sasaki T, Yamamoto M, et al. Overexpression of Nmnat3 efficiently increases NAD and NGD levels and ameliorates age-associated insulin resistance. Aging cell. 2018;17(4):e12798-e.
409. Kulikova V, Shabalin K, Nerinovski K, Dolle C, Niere M, Yakimov A, et al. Generation, Release, and Uptake of the NAD Precursor Nicotinic Acid Riboside by Human Cells. J Biol Chem. 2015;290(45):27124-37.
410. Yoshioka M, Boivin A, Bolduc C, St-Amand J. Gender difference of androgen actions on skeletal muscle transcriptome. J Mol Endocrinol. 2007;39(2):119-33.
411. Fu M, Liu M, Sauve AA, Jiao X, Zhang X, Wu X, et al. Hormonal control of androgen receptor function through SIRT1. Mol Cell Biol. 2006;26(21):8122-35.
412. Chambon C, Duteil D, Vignaud A, Ferry A, Messaddeq N, Malivindi R, et al. Myocytic androgen receptor controls the strength but not the mass of limb muscles. Proceedings of the National Academy of Sciences. 2010;107(32):14327.
413. Ronchi JA, Figueira TR, Ravagnani FG, Oliveira HC, Vercesi AE, Castilho RF. A spontaneous mutation in the nicotinamide nucleotide transhydrogenase gene of C57BL/6J mice results in mitochondrial redox abnormalities. Free Radic Biol Med. 2013;63:446-56.
414. Ronchi JA, Francisco A, Passos LA, Figueira TR, Castilho RF. The Contribution of Nicotinamide Nucleotide Transhydrogenase to Peroxide Detoxification Is Dependent on the Respiratory State and Counterbalanced by Other Sources of NADPH in Liver Mitochondria. J Biol Chem. 2016;291(38):20173-87.
415. de Picciotto NE, Gano LB, Johnson LC, Martens CR, Sindler AL, Mills KF, et al. Nicotinamide mononucleotide supplementation reverses vascular dysfunction and oxidative stress with aging in mice. Aging Cell. 2016;15(3):522-30.
416. Avalos JL, Bever KM, Wolberger C. Mechanism of Sirtuin Inhibition by Nicotinamide: Altering the NAD+ Cosubstrate Specificity of a Sir2 Enzyme. Molecular Cell. 2005;17(6):855-68.
417. Strom K, Morales-Alamo D, Ottosson F, Edlund A, Hjort L, Jorgensen SW, et al. N(1)-methylnicotinamide is a signalling molecule produced in skeletal muscle coordinating energy metabolism. Sci Rep. 2018;8(1):3016.
418. Cohen MS, Chang P. Insights into the biogenesis, function, and regulation of ADP-ribosylation. Nat Chem Biol. 2018;14(3):236-43.
419. McClure MJ, Clark NM, Hyzy SL, Chalfant CE, Olivares-Navarrete R, Boyan BD, et al. Role of integrin α7β1 signaling in myoblast differentiation on aligned polydioxanone scaffolds. Acta Biomater. 2016;39:44-54.
420. Liu H, Niu A, Chen SE, Li YP. Beta3-integrin mediates satellite cell differentiation in regenerating mouse muscle. Faseb j. 2011;25(6):1914-21.
421. Andersen M, Nørgaard-Pedersen D, Brandt J, Pettersson I, Slaaby R. IGF1 and IGF2 specificities to the two insulin receptor isoforms are determined by insulin receptor amino acid 718. PloS one. 2017;12(6):e0178885-e.
422. Kadakia R, Josefson J. The Relationship of Insulin-Like Growth Factor 2 to Fetal Growth and Adiposity. Hormone Research in Paediatrics. 2016;85(2):75-82.
423. Erbay E, Park I-H, Nuzzi PD, Schoenherr CJ, Chen J. IGF-II transcription in skeletal myogenesis is controlled by mTOR and nutrients. The Journal of cell biology. 2003;163(5):931-6.
424. Marabita M, Baraldo M, Solagna F, Ceelen JJM, Sartori R, Nolte H, et al. S6K1 Is Required for Increasing Skeletal Muscle Force during Hypertrophy. Cell Rep. 2016;17(2):501-13.

425. Egerman MA, Glass DJ. Signaling pathways controlling skeletal muscle mass. Crit Rev Biochem Mol Biol. 2014;49(1):59-68.
426. Mendias CL, Gumucio JP, Davis ME, Bromley CW, Davis CS, Brooks SV. Transforming growth factor-beta induces skeletal muscle atrophy and fibrosis through the induction of atrogin-1 and scleraxis. Muscle & nerve. 2012;45(1):55-9.
427. Lee S-J, Reed LA, Davies MV, Girgenrath S, Goad MEP, Tomkinson KN, et al. Regulation of muscle growth by multiple ligands signaling through activin type II receptors. Proceedings of the National Academy of Sciences of the United States of America. 2005;102(50):18117-22.
428. Tando T, Hirayama A, Furukawa M, Sato Y, Kobayashi T, Funayama A, et al. Smad2/3 Proteins Are Required for Immobilization-induced Skeletal Muscle Atrophy. The Journal of biological chemistry. 2016;291(23):12184-94.
429. Gumucio JP, Mendias CL. Atrogin-1, MuRF-1, and sarcopenia. Endocrine. 2013;43(1):12-21.
430. Heras G, Namuduri AV, Traini L, Shevchenko G, Falk A, Bergstrom Lind S, et al. Muscle RING-finger protein-1 (MuRF1) functions and cellular localization are regulated by SUMO1 post-translational modification. J Mol Cell Biol. 2019;11(5):356-70.
431. Hay N. Interplay between FOXO, TOR, and Akt. Biochimica et biophysica acta. 2011;1813(11):1965-70.
432. Luo K. Signaling Cross Talk between TGF-β/Smad and Other Signaling Pathways. Cold Spring Harbor perspectives in biology. 2017;9(1):a022137.
433. Marcotte GR, West DWD, Baar K. The molecular basis for load-induced skeletal muscle hypertrophy. Calcified tissue international. 2015;96(3):196-210.
434. Philp A, Schenk S. Unraveling the complexities of SIRT1-mediated mitochondrial regulation in skeletal muscle. Exerc Sport Sci Rev. 2013;41(3):174-81.
435. Gwinn DM, Shackelford DB, Egan DF, Mihaylova MM, Mery A, Vasquez DS, et al. AMPK phosphorylation of raptor mediates a metabolic checkpoint. Mol Cell. 2008;30(2):214-26.
436. McPhee JS, French DP, Jackson D, Nazroo J, Pendleton N, Degens H. Physical activity in older age: perspectives for healthy ageing and frailty. Biogerontology. 2016;17(3):567-80.
437. Mauro A. Satellite cell of skeletal muscle fibers. J Biophys Biochem Cytol. 1961;9:493-5.
438. Dort J, Fabre P, Molina T, Dumont NA. Macrophages Are Key Regulators of Stem Cells during Skeletal Muscle Regeneration and Diseases. Stem Cells International. 2019;2019:4761427.
439. Ciciliot S, Schiaffino S. Regeneration of mammalian skeletal muscle. Basic mechanisms and clinical implications. Curr Pharm Des. 2010;16(8):906-14.
440. Relaix F, Zammit PS. Satellite cells are essential for skeletal muscle regeneration: the cell on the edge returns centre stage. Development. 2012;139(16):2845.
441. Nagata Y, Kobayashi H, Umeda M, Ohta N, Kawashima S, Zammit PS, et al. Sphingomyelin levels in the plasma membrane correlate with the activation state of muscle satellite cells. J Histochem Cytochem. 2006;54(4):375-84.
442. Anderson JE. A role for nitric oxide in muscle repair: nitric oxide-mediated activation of muscle satellite cells. Mol Biol Cell. 2000;11(5):1859-74.
443. Miller KJ, Thaloor D, Matteson S, Pavlath GK. Hepatocyte growth factor affects satellite cell activation and differentiation in regenerating skeletal muscle. Am J Physiol Cell Physiol. 2000;278(1):C174-81.
444. Brack AS, Conboy IM, Conboy MJ, Shen J, Rando TA. A Temporal Switch from Notch to Wnt Signaling in Muscle Stem Cells Is Necessary for Normal Adult Myogenesis. Cell Stem Cell. 2008;2(1):50-9.

445. Bryla K, Karasinski J. Diversity of myosin heavy chain expression in satellite cells from mouse soleus and EDL muscles. Folia Histochem Cytobiol. 2001;39(4):295-300.
446. Gillies AR, Lieber RL. Structure and function of the skeletal muscle extracellular matrix. Muscle & nerve. 2011;44(3):318-31.
447. Goddeeris MM, Wu B, Venzke D, Yoshida-Moriguchi T, Saito F, Matsumura K, et al. LARGE glycans on dystroglycan function as a tunable matrix scaffold to prevent dystrophy. Nature. 2013;503(7474):136-40.
448. Balius R, Alomar X, Pedret C, Blasi M, Rodas G, Pruna R, et al. Role of the Extracellular Matrix in Muscle Injuries: Histoarchitectural Considerations for Muscle Injuries. Orthop J Sports Med. 2018;6(9):2325967118795863-.
449. Zhang L, Wang XH, Wang H, Du J, Mitch WE. Satellite cell dysfunction and impaired IGF-1 signaling cause CKD-induced muscle atrophy. J Am Soc Nephrol. 2010;21(3):419-27.
450. Machida S, Booth FW. Insulin-like growth factor 1 and muscle growth: implication for satellite cell proliferation. Proc Nutr Soc. 2004;63(2):337-40.
451. Gredinger E, Gerber AN, Tamir Y, Tapscott SJ, Bengal E. Mitogen-activated protein kinase pathway is involved in the differentiation of muscle cells. J Biol Chem. 1998;273(17):10436-44.
452. Cadot B, Gache V, Gomes ER. Moving and positioning the nucleus in skeletal muscle - one step at a time. Nucleus. 2015;6(5):373-81.
453. Roman W, Gomes ER. Nuclear positioning in skeletal muscle. Seminars in Cell & Developmental Biology. 2018;82:51-6.
454. Ralston E, Lu Z, Biscocho N, Soumaka E, Mavroidis M, Prats C, et al. Blood vessels and desmin control the positioning of nuclei in skeletal muscle fibers. J Cell Physiol. 2006;209(3):874-82.
455. Conboy IM, Rando TA. The regulation of Notch signaling controls satellite cell activation and cell fate determination in postnatal myogenesis. Dev Cell. 2002;3(3):397-409.
456. Nagata Y, Partridge TA, Matsuda R, Zammit PS. Entry of muscle satellite cells into the cell cycle requires sphingolipid signaling. J Cell Biol. 2006;174(2):245-53.
457. Sanes JR. The basement membrane/basal lamina of skeletal muscle. J Biol Chem. 2003;278(15):12601-4.
458. Kovanen V. Intramuscular extracellular matrix: complex environment of muscle cells. Exerc Sport Sci Rev. 2002;30(1):20-5.
459. Dumont NA, Wang YX, Rudnicki MA. Intrinsic and extrinsic mechanisms regulating satellite cell function. Development. 2015;142(9):1572-81.
460. Perez-Ruiz A, Ono Y, Gnocchi VF, Zammit PS. beta-Catenin promotes self-renewal of skeletal-muscle satellite cells. J Cell Sci. 2008;121(Pt 9):1373-82.
461. Goel AJ, Rieder MK, Arnold HH, Radice GL, Krauss RS. Niche Cadherins Control the Quiescence-to-Activation Transition in Muscle Stem Cells. Cell Rep. 2017;21(8):2236-50.
462. Boppart MD, Burkin DJ, Kaufman SJ. Alpha7beta1-integrin regulates mechanotransduction and prevents skeletal muscle injury. Am J Physiol Cell Physiol. 2006;290(6):C1660-5.
463. Gullberg D, Tiger CF, Velling T. Laminins during muscle development and in muscular dystrophies. Cell Mol Life Sci. 1999;56(5-6):442-60.
464. Le Grand F, Jones AE, Seale V, Scimè A, Rudnicki MA. Wnt7a activates the planar cell polarity pathway to drive the symmetric expansion of satellite stem cells. Cell Stem Cell. 2009;4(6):535-47.

465. Tatsumi R, Anderson JE, Nevoret CJ, Halevy O, Allen RE. HGF/SF is present in normal adult skeletal muscle and is capable of activating satellite cells. Dev Biol. 1998;194(1):114-28.
466. DiMario J, Buffinger N, Yamada S, Strohman RC. Fibroblast growth factor in the extracellular matrix of dystrophic (mdx) mouse muscle. Science. 1989;244(4905):688-90.
467. Golding JP, Calderbank E, Partridge TA, Beauchamp JR. Skeletal muscle stem cells express anti-apoptotic ErbB receptors during activation from quiescence. Exp Cell Res. 2007;313(2):341-56.
468. Yamada M, Tatsumi R, Kikuiri T, Okamoto S, Nonoshita S, Mizunoya W, et al. Matrix metalloproteinases are involved in mechanical stretch-induced activation of skeletal muscle satellite cells. Muscle Nerve. 2006;34(3):313-9.
469. Wilkinson DJ, Piasecki M, Atherton PJ. The age-related loss of skeletal muscle mass and function: Measurement and physiology of muscle fibre atrophy and muscle fibre loss in humans. Ageing Res Rev. 2018;47:123-32.
470. Cuthbertson DJ, Babraj J, Smith K, Wilkes E, Fedele MJ, Esser K, et al. Anabolic signaling and protein synthesis in human skeletal muscle after dynamic shortening or lengthening exercise. Am J Physiol Endocrinol Metab. 2006;290(4):E731-8.
471. Fry CS, Drummond MJ, Glynn EL, Dickinson JM, Gundermann DM, Timmerman KL, et al. Aging impairs contraction-induced human skeletal muscle mTORC1 signaling and protein synthesis. Skelet Muscle. 2011;1(1):11.
472. Spendiff S, Vuda M, Gouspillou G, Aare S, Perez A, Morais JA, et al. Denervation drives mitochondrial dysfunction in skeletal muscle of octogenarians. J Physiol. 2016;594(24):7361-79.
473. Lexell J, Taylor CC, Sjostrom M. What is the cause of the ageing atrophy? Total number, size and proportion of different fiber types studied in whole vastus lateralis muscle from 15- to 83-year-old men. J Neurol Sci. 1988;84(2-3):275-94.
474. Jubrias SA, Odderson IR, Esselman PC, Conley KE. Decline in isokinetic force with age: muscle cross-sectional area and specific force. Pflugers Arch. 1997;434(3):246-53.
475. Ochala J, Frontera WR, Dorer DJ, Van Hoecke J, Krivickas LS. Single skeletal muscle fiber elastic and contractile characteristics in young and older men. J Gerontol A Biol Sci Med Sci. 2007;62(4):375-81.
476. Ryall JG, Dell'Orso S, Derfoul A, Juan A, Zare H, Feng X, et al. The NAD(+)-dependent SIRT1 deacetylase translates a metabolic switch into regulatory epigenetics in skeletal muscle stem cells. Cell Stem Cell. 2015;16(2):171-83.
477. Tang AH, Rando TA. Induction of autophagy supports the bioenergetic demands of quiescent muscle stem cell activation. EMBO J. 2014;33(23):2782-97.
478. Csapo R, Gumpenberger M, Wessner B. Skeletal Muscle Extracellular Matrix - What Do We Know About Its Composition, Regulation, and Physiological Roles? A Narrative Review. Frontiers in physiology. 2020;11:253-.
479. Goody MF, Sher RB, Henry CA. Hanging on for the ride: adhesion to the extracellular matrix mediates cellular responses in skeletal muscle morphogenesis and disease. Dev Biol. 2015;401(1):75-91.
480. Grounds MD, Sorokin L, White J. Strength at the extracellular matrix-muscle interface. Scand J Med Sci Sports. 2005;15(6):381-91.
481. Bruzzone S, Guida L, Zocchi E, Franco L, De Flora A. Connexin 43 hemi channels mediate Ca2+-regulated transmembrane NAD+ fluxes in intact cells. Faseb j. 2001;15(1):10-2.

482. Deacon RM. Measuring the strength of mice. J Vis Exp. 2013(76).
483. Suttapitugsakul S, Xiao H, Smeekens J, Wu R. Evaluation and optimization of reduction and alkylation methods to maximize peptide identification with MS-based proteomics. Mol Biosyst. 2017;13(12):2574-82.
484. Ludwig C, Gillet L, Rosenberger G, Amon S, Collins BC, Aebersold R. Data-independent acquisition-based SWATH-MS for quantitative proteomics: a tutorial. Mol Syst Biol. 2018;14(8):e8126.
485. Gillet LC, Navarro P, Tate S, Rost H, Selevsek N, Reiter L, et al. Targeted data extraction of the MS/MS spectra generated by data-independent acquisition: a new concept for consistent and accurate proteome analysis. Mol Cell Proteomics. 2012;11(6):O111.016717.
486. Kanehisa M, Goto S, Kawashima S, Nakaya A. The KEGG databases at GenomeNet. Nucleic acids research. 2002;30(1):42-6.
487. Kanehisa M, Goto S. KEGG: kyoto encyclopedia of genes and genomes. Nucleic acids research. 2000;28(1):27-30.
488. Ashburner M, Ball CA, Blake JA, Botstein D, Butler H, Cherry JM, et al. Gene ontology: tool for the unification of biology. The Gene Ontology Consortium. Nat Genet. 2000;25(1):25-9.
489. Alexa A, Rahnenführer J, Lengauer T. Improved scoring of functional groups from gene expression data by decorrelating GO graph structure. Bioinformatics. 2006;22(13):1600-7.
490. Uchitomi R, Hatazawa Y, Senoo N, Yoshioka K, Fujita M, Shimizu T, et al. Metabolomic Analysis of Skeletal Muscle in Aged Mice. Sci Rep. 2019;9(1):10425.
491. Chiao YA, Rabinovitch PS. The Aging Heart. Cold Spring Harbor perspectives in medicine. 2015;5(9):a025148-a.
492. Welle S, Burgess K, Mehta S. Stimulation of skeletal muscle myofibrillar protein synthesis, p70 S6 kinase phosphorylation, and ribosomal protein S6 phosphorylation by inhibition of myostatin in mature mice. Am J Physiol Endocrinol Metab. 2009;296(3):E567-72.
493. Magnuson B, Ekim B, Fingar DC. Regulation and function of ribosomal protein S6 kinase (S6K) within mTOR signalling networks. Biochem J. 2012;441(1):1-21.
494. Yoon MS. mTOR as a Key Regulator in Maintaining Skeletal Muscle Mass. Front Physiol. 2017;8:788.
495. Sarbassov DD, Guertin DA, Ali SM, Sabatini DM. Phosphorylation and regulation of Akt/PKB by the rictor-mTOR complex. Science. 2005;307(5712):1098-101.
496. Gingras AC, Raught B, Gygi SP, Niedzwiecka A, Miron M, Burley SK, et al. Hierarchical phosphorylation of the translation inhibitor 4E-BP1. Genes & development. 2001;15(21):2852-64.
497. Roux PP, Ballif BA, Anjum R, Gygi SP, Blenis J. Tumor-promoting phorbol esters and activated Ras inactivate the tuberous sclerosis tumor suppressor complex via p90 ribosomal S6 kinase. Proc Natl Acad Sci U S A. 2004;101(37):13489-94.
498. Bodine SC, Baehr LM. Skeletal muscle atrophy and the E3 ubiquitin ligases MuRF1 and MAFbx/atrogin-1. Am J Physiol Endocrinol Metab. 2014;307(6):E469-84.
499. Folker ES, Baylies MK. Nuclear positioning in muscle development and disease. Frontiers in physiology. 2013;4:363-.
500. Watkins SC, Cullen MJ. Muscle fibre size and shape in Duchenne muscular dystrophy. Neuropathol Appl Neurobiol. 1982;8(1):11-7.
501. Howard EE, Pasiakos SM, Blesso CN, Fussell MA, Rodriguez NR. Divergent Roles of Inflammation in Skeletal Muscle Recovery From Injury. Frontiers in physiology. 2020;11:87-.

502. Wang N, Tytell JD, Ingber DE. Mechanotransduction at a distance: mechanically coupling the extracellular matrix with the nucleus. Nat Rev Mol Cell Biol. 2009;10(1):75-82.
503. Bizzarro V, Belvedere R, Dal Piaz F, Parente L, Petrella A. Annexin A1 induces skeletal muscle cell migration acting through formyl peptide receptors. PloS one. 2012;7(10):e48246-e.
504. Volonte D, Liu Y, Galbiati F. The modulation of caveolin-1 expression controls satellite cell activation during muscle repair. Faseb j. 2005;19(2):237-9.
505. Staszewska I, Fischer I, Wiche G. Plectin isoform 1-dependent nuclear docking of desmin networks affects myonuclear architecture and expression of mechanotransducers. Human Molecular Genetics. 2015;24(25):7373-89.
506. Lock JG, Baschieri F, Jones MC, Humphries JD, Montagnac G, Strömblad S, et al. Clathrin-containing adhesion complexes. The Journal of cell biology. 2019;218(7):2086-95.
507. Vassilopoulos S, Gentil C, Lainé J, Buclez P-O, Franck A, Ferry A, et al. Actin scaffolding by clathrin heavy chain is required for skeletal muscle sarcomere organization. The Journal of cell biology. 2014;205(3):377-93.
508. Cunha SR, Mohler PJ. Ankyrin protein networks in membrane formation and stabilization. J Cell Mol Med. 2009;13(11-12):4364-76.
509. Danen EH, Yamada KM. Fibronectin, integrins, and growth control. J Cell Physiol. 2001;189(1):1-13.
510. Disanza A, Scita G. Cytoskeletal regulation: coordinating actin and microtubule dynamics in membrane trafficking. Curr Biol. 2008;18(18):R873-5.
511. Noy T, Suad O, Taglicht D, Ciechanover A. HUWE1 ubiquitinates MyoD and targets it for proteasomal degradation. Biochemical and biophysical research communications. 2012;418:408-13.
512. Jia L, Li Y-F, Wu G-F, Song Z-Y, Lu H-Z, Song C-C, et al. MiRNA-199a-3p regulates C2C12 myoblast differentiation through IGF-1/AKT/mTOR signal pathway. International journal of molecular sciences. 2013;15(1):296-308.
513. Lin Y, Li F, Huang L, Duan H, Fang J, Sun L, et al. eIF3 promotes early translation elongation to ensure mitochondrial homeostasis and skeletal muscle health. bioRxiv. 2019:651240.
514. Martin J, Maurhofer O, Bellance N, Benard G, Graber F, Hahn D, et al. Disruption of the histidine triad nucleotide-binding hint2 gene in mice affects glycemic control and mitochondrial function. Hepatology. 2013;57(5):2037-48.
515. Lynch JM, Dolman AJ, Guo C, Dolan K, Xiang C, Reda S, et al. Mutant myocilin impacts sarcomere ultrastructure in mouse gastrocnemius muscle. PLoS One. 2018;13(11):e0206801.
516. Selcen D, Engel AG. Mutations in myotilin cause myofibrillar myopathy. Neurology. 2004;62(8):1363-71.
517. Kwon H-S, Lee H-S, Ji Y, Rubin JS, Tomarev SI. Myocilin is a modulator of Wnt signaling. Molecular and cellular biology. 2009;29(8):2139-54.
518. Luo G, Zhang JQ, Nguyen TP, Herrera AH, Paterson B, Horowits R. Complete cDNA sequence and tissue localization of N-RAP, a novel nebulin-related protein of striated muscle. Cell Motil Cytoskeleton. 1997;38(1):75-90.
519. Lu S, Borst DE, Horowits R. Expression and alternative splicing of N-RAP during mouse skeletal muscle development. Cell Motil Cytoskeleton. 2008;65(12):945-54.
520. Kooij V, Viswanathan MC, Lee DI, Rainer PP, Schmidt W, Kronert WA, et al. Profilin modulates sarcomeric organization and mediates cardiomyocyte hypertrophy. Cardiovascular research. 2016;110(2):238-48.

521. Ding Z, Bae YH, Roy P. Molecular insights on context-specific role of profilin-1 in cell migration. Cell Adhesion & Migration. 2012;6(5):442-534.
522. Vafiadaki E, Arvanitis DA, Sanoudou D. Muscle LIM Protein: Master regulator of cardiac and skeletal muscle functions. Gene. 2015;566(1):1-7.
523. Myhre JL, Hills JA, Jean F, Pilgrim DB. Unc45b is essential for early myofibrillogenesis and costamere formation in zebrafish. Developmental Biology. 2014;390(1):26-40.
524. Wilson MH, Holzbaur EL. Opposing microtubule motors drive robust nuclear dynamics in developing muscle cells. J Cell Sci. 2012;125(Pt 17):4158-69.
525. Thorsteinsdóttir S, Deries M, Cachaço AS, Bajanca F. The extracellular matrix dimension of skeletal muscle development. Developmental Biology. 2011;354(2):191-207.
526. Lee EJ, Jan AT, Baig MH, Ashraf JM, Nahm SS, Kim YW, et al. Fibromodulin: a master regulator of myostatin controlling progression of satellite cells through a myogenic program. Faseb j. 2016;30(8):2708-19.
527. Gao QQ, McNally EM. The Dystrophin Complex: Structure, Function, and Implications for Therapy. Compr Physiol. 2015;5(3):1223-39.
528. Echarri A, Del Pozo MA. Caveolae. Curr Biol. 2012;22(4):R114-6.
529. Housley MP, Njaine B, Ricciardi F, Stone OA, Hölper S, Krüger M, et al. Cavin4b/Murcb Is Required for Skeletal Muscle Development and Function in Zebrafish. PLoS genetics. 2016;12(6):e1006099-e.
530. Bach A-S, Enjalbert S, Comunale F, Bodin S, Vitale N, Charrasse S, et al. ADP-ribosylation factor 6 regulates mammalian myoblast fusion through phospholipase D1 and phosphatidylinositol 4,5-bisphosphate signaling pathways. Mol Biol Cell. 2010;21(14):2412-24.
531. Younis S, Schonke M, Massart J, Hjortebjerg R, Sundstrom E, Gustafson U, et al. The ZBED6-IGF2 axis has a major effect on growth of skeletal muscle and internal organs in placental mammals. Proc Natl Acad Sci U S A. 2018;115(9):E2048-E57.
532. Florini JR, Magri KA, Ewton DZ, James PL, Grindstaff K, Rotwein PS. "Spontaneous" differentiation of skeletal myoblasts is dependent upon autocrine secretion of insulin-like growth factor-II. J Biol Chem. 1991;266(24):15917-23.
533. Ge Y, Chen J. Mammalian target of rapamycin (mTOR) signaling network in skeletal myogenesis. The Journal of biological chemistry. 2012;287(52):43928-35.
534. Vinayagam A, Stelzl U, Foulle R, Plassmann S, Zenkner M, Timm J, et al. A directed protein interaction network for investigating intracellular signal transduction. Sci Signal. 2011;4(189):rs8.
535. Levinovitz A, Jennische E, Oldfors A, Edwall D, Norstedt G. Activation of insulin-like growth factor II expression during skeletal muscle regeneration in the rat: correlation with myotube formation. Mol Endocrinol. 1992;6(8):1227-34.
536. Ge Y, Sun Y, Chen J. IGF-II is regulated by microRNA-125b in skeletal myogenesis. J Cell Biol. 2011;192(1):69-81.
537. Zanou N, Gailly P. Skeletal muscle hypertrophy and regeneration: interplay between the myogenic regulatory factors (MRFs) and insulin-like growth factors (IGFs) pathways. Cell Mol Life Sci. 2013;70(21):4117-30.
538. Frago S, Nicholls RD, Strickland M, Hughes J, Williams C, Garner L, et al. Functional evolution of IGF2:IGF2R domain 11 binding generates novel structural interactions and a specific IGF2 antagonist. Proceedings of the National Academy of Sciences. 2016;113(20):E2766-E75.

539. Bella P, Farini A, Banfi S, Parolini D, Tonna N, Meregalli M, et al. Blockade of IGF2R improves muscle regeneration and ameliorates Duchenne muscular dystrophy. EMBO molecular medicine. 2020;12(1):e11019-e.
540. Pastoret C, Sebille A. Age-related differences in regeneration of dystrophic (mdx) and normal muscle in the mouse. Muscle Nerve. 1995;18(10):1147-54.
541. Perillo M, Folker ES. Specialized Positioning of Myonuclei Near Cell-Cell Junctions. Frontiers in Physiology. 2018;9(1531).
542. Fulco M, Schiltz RL, Iezzi S, King MT, Zhao P, Kashiwaya Y, et al. Sir2 regulates skeletal muscle differentiation as a potential sensor of the redox state. Mol Cell. 2003;12(1):51-62.
543. Edström E, Altun M, Hägglund M, Ulfhake B. Atrogin-1/MAFbx and MuRF1 Are Downregulated in Aging-Related Loss of Skeletal Muscle. The Journals of Gerontology: Series A. 2006;61(7):663-74.
544. Baehr LM, Tunzi M, Bodine SC. Muscle hypertrophy is associated with increases in proteasome activity that is independent of MuRF1 and MAFbx expression. Frontiers in physiology. 2014;5:69-.
545. Wei X, Luo L, Chen J. Roles of mTOR Signaling in Tissue Regeneration. Cells. 2019;8(9):1075.
546. Schultz E, Jaryszak DL. Effects of skeletal muscle regeneration on the proliferation potential of satellite cells. Mech Ageing Dev. 1985;30(1):63-72.
547. Wilson EM, Hsieh MM, Rotwein P. Autocrine growth factor signaling by insulin-like growth factor-II mediates MyoD-stimulated myocyte maturation. J Biol Chem. 2003;278(42):41109-13.
548. Hudlicka O. Microcirculation in skeletal muscle. Muscles, ligaments and tendons journal. 2011;1(1):3-11.
549. Wüst RC, Gibbings SL, Degens H. Fiber capillary supply related to fiber size and oxidative capacity in human and rat skeletal muscle. Adv Exp Med Biol. 2009;645:75-80.
550. Schiaffino S, Dyar KA, Ciciliot S, Blaauw B, Sandri M. Mechanisms regulating skeletal muscle growth and atrophy. Febs j. 2013;280(17):4294-314.
551. Bachman JF, Klose A, Liu W, Paris ND, Blanc RS, Schmalz M, et al. Prepubertal skeletal muscle growth requires Pax7-expressing satellite cell-derived myonuclear contribution. Development (Cambridge, England). 2018;145(20):dev167197.
552. Borselli C, Storrie H, Benesch-Lee F, Shvartsman D, Cezar C, Lichtman JW, et al. Functional muscle regeneration with combined delivery of angiogenesis and myogenesis factors. Proceedings of the National Academy of Sciences. 2010;107(8):3287-92.
553. Siles L, Ninfali C, Cortés M, Darling DS, Postigo A. ZEB1 protects skeletal muscle from damage and is required for its regeneration. Nature Communications. 2019;10(1):1364.
554. Cifuentes-Diaz C, Nicolet M, Goudou D, Rieger F, Mege RM. N-cadherin and N-CAM-mediated adhesion in development and regeneration of skeletal muscle. Neuromuscul Disord. 1993;3(5-6):361-5.
555. Krauss RS, Joseph GA, Goel AJ. Keep Your Friends Close: Cell-Cell Contact and Skeletal Myogenesis. Cold Spring Harb Perspect Biol. 2017;9(2).
556. George-Weinstein M, Gerhart J, Blitz J, Simak E, Knudsen KA. N-cadherin promotes the commitment and differentiation of skeletal muscle precursor cells. Dev Biol. 1997;185(1):14-24.

557. Hatoko M, Niitsuma K, Tanaka A, Kuwahara M, Iioka H. Expression of N-cadherin by skeletal muscle in the degeneration and the degeneration/regeneration processes after nerve injury. Scand J Plast Reconstr Surg Hand Surg. 2004;38(4):198-203.
558. Alzhanov D, Rotwein P. Characterizing a distal muscle enhancer in the mouse Igf2 locus. Physiol Genomics. 2016;48(2):167-72.
559. Gibson MC, Schultz E. The distribution of satellite cells and their relationship to specific fiber types in soleus and extensor digitorum longus muscles. Anat Rec. 1982;202(3):329-37.
560. Ito K, Suda T. Metabolic requirements for the maintenance of self-renewing stem cells. Nat Rev Mol Cell Biol. 2014;15(4):243-56.
561. Lyons GE, Ontell M, Cox R, Sassoon D, Buckingham M. The expression of myosin genes in developing skeletal muscle in the mouse embryo. J Cell Biol. 1990;111(4):1465-76.
562. De Micheli AJ, Laurilliard EJ, Heinke CL, Ravichandran H, Fraczek P, Soueid-Baumgarten S, et al. Single-Cell Analysis of the Muscle Stem Cell Hierarchy Identifies Heterotypic Communication Signals Involved in Skeletal Muscle Regeneration. Cell Rep. 2020;30(10):3583-95 e5.
563. Lancioni H, Lucentini L, Palomba A, Fulle S, Micheli MR, Panara F. Muscle actin isoforms are differentially expressed in human satellite cells isolated from donors of different ages. Cell Biol Int. 2007;31(2):180-5.
564. Gutmann E, Schiaffino S, Hanzliková V. Mechanism of compensatory hypertrophy in skeletal muscle of the rat. Experimental Neurology. 1971;31(3):451-64.
565. Yang S, Loro E, Wada S, Kim B, Tseng W-J, Li K, et al. Functional effects of muscle PGC-1alpha in aged animals. Skeletal Muscle. 2020;10(1):14.
566. Amat R, Planavila A, Chen SL, Iglesias R, Giralt M, Villarroya F. SIRT1 controls the transcription of the peroxisome proliferator-activated receptor-gamma Co-activator-1alpha (PGC-1alpha) gene in skeletal muscle through the PGC-1alpha autoregulatory loop and interaction with MyoD. J Biol Chem. 2009;284(33):21872-80.
567. Jiao S, Ren H, Li Y, Zhou J, Duan C, Lu L. Differential regulation of IGF-I and IGF-II gene expression in skeletal muscle cells. Mol Cell Biochem. 2013;373(1-2):107-13.

List of Publications

Cartwright DM, Oakey L**,** Fletcher S, Doig CL, Heaselgrave S, Berry C, Heising S, Larner DP, Nasteska D, Ludwig C, Hodson DJ, Lavery GG, Garten A. **Nicotinamide riboside has minimal impact on energy metabolism in mouse models of mild obesity.** 2021 **Under review.**

Seranova E, Chipara M, Palhegyi AM, Cohen MA, Acharjee A, Panda PK, Sedlackova L, Silva LFS, Torresi J, Kaufman KJ, Sun C, Zhang S, Varga TG, Ward C, **Cartwright DM**, Trushina E, Sahay G, Buganim Y, Lavery GG, Angerson DG, Maddocks ODK, Wang H, Rosenstock TR, Jaenisch R, Korolchuk VI, Sarkar S. **Metabolic defect mediates cytotoxicity in human neurons with autophagy deficiency.** 2020 **Under review.**

Doig CL, Zelinska AE, Oakey LA, Fletcher RS, Elhassan YS, Garten A, **Cartwright DM**, Heising S, Tennant DA, Watson D, Adamski J, Lavery GG. **Induction of the nicotinamide riboside kinase NAD$^+$ salvage pathway in skeletal muscle of H6PDH KO mice.** 2019 bioRxiv 567297; doi: https://doi.org/10.1101/567297

Elhassan YS, Kluckova K, Fletcher RS, Schmidt M, Garten A, Doig CL, **Cartwright DM**, Oakey LA, Burley CV, Jenkinson N, Wilson M, Lucas SJE, Akerman I, Seabright A, Lai YC, Tennant DA, Nightingale P, Wallis GA, Manolopoulos KN, Brenner C, Philp A, Lavery GG. **Nicotinamide riboside augments the human skeletal muscle NAD$^+$ metabolome and induces transcriptomic and anti-inflammatory signatures in aged subjects: a placebo-controlled, randomized trial.** Cell Rep. 2019 Aug 13;28(7):1717-1728.e6. PMID 31412242.

Oakey LA, Fletcher RS, Elhassan YS, **Cartwright DM**, Doig CL, Garten A, Thakker A, Maddocks ODK, Zhang T, Tennant DA, Ludwig C, Lavery GG. **Metabolic tracing reveals novel adaptations to skeletal muscle cell energy production pathways in response to NAD$^+$ depletion**. Wellcome Open Res. 2018 Nov 15;3:147. PMID 30607371.